Oxidation of the amyloid-beta peptide and consequences on the etiology of Alzheimer's disease

Clémence Cheignon

Université Fédérale

Toulouse Midi-Pyrénées

THÈSE

En vue de l'obtention du

DOCTORAT DE L'UNIVERSITÉ DE TOULOUSE

Délivré par :

Université Toulouse 3 Paul Sabatier (UT3 Paul Sabatier)

Présentée et soutenue par :

Clémence Cheignon

le lundi 28 novembre 2016

Titre :

Oxidation of the Amyloid-Beta peptide and consequences on the etiology of Alzheimer's Disease

---

École doctorale et discipline ou spécialité :

ED SDM : Chimie, Biologie, Santé - CO 042

Unité de recherche :

Pharma-DEV / Laboratoire de Chimie de Coordination

Directeur/trice(s) de Thèse :

Dr. Fabrice Collin

Dr. Christelle Hureau

Jury :

Pr. François Couderc, IMRCP, Toulouse, Président

Dr. Marius Réglier, iSm2, Marseille, Rapporteur

Dr. Jérôme Santolini, I2BC, Gif-sur-Yvette, Rapporteur

Pr. Dominique Bonnefont-Rousselot, Université Paris Descartes, Examinatrice

Dr. Fabrice Collin, LCC, Toulouse, Directeur de thèse

Dr. Christelle Hureau, LCC, Toulouse, Co-directrice de thèse

Pr. Peter Faller, Institut de Strasbourg, Membre invité

Remerciements

La thèse est une grande aventure faite de rencontres, d'opportunités et de nouveautés. C'est un tout nouveau monde qui s'ouvre à soi, inconnu, inconfortable mais exaltant. Au cours de mon parcours de thèse parfois tumultueux, j'ai eu la chance de faire de belles rencontres scientifiques et humaines. Je souhaiterais remercier toutes ces personnes et espère n'oublier personne.

J'ai accompli ce travail de thèse au Laboratoire de Pharmacologie et Biologie pour le Développement (Pharma-DEV) ainsi qu'au Laboratoire de Chimie de Coordination (LCC). Je remercie le Pr. Nicolas Fabre et le Dr. Azzedine Bousseksou pour leur accueil au sein de ces deux laboratoires.

Je souhaiterais adresser mes remerciements aux Dr. Marius Réglier et Dr. Jérôme Santolini qui ont référé ce travail avec beaucoup d'attention et d'intérêt. Je tiens également à remercier les différents membres du jury pour leur présence ainsi que pour les discussions scientifiques qui ont eu lieu au cours de ma soutenance et qui m'ont beaucoup apporté.

Pendant ces trois années de thèse, j'ai eu la chance d'être encadrée par des personnes exceptionnelles, scientifiquement et humainement. Je tiens à remercier très chaleureusement Fabrice Collin, Christelle Hureau et Peter Faller qui m'ont apporté leur confiance, leur soutien et m'ont appris tellement… Je n'aurais pas pu être mieux encadrée qu'avec vous ! Merci aussi de m'avoir donné l'opportunité de faire des activités « extra-labos » comme les enseignements, la vulgarisation scientifique, le club jeunes SCF, toutes ces conférences auxquelles j'ai pu assister et présenter, et les sessions à l'ESRF. Ce n'est pas donné à tous les doctorants d'avoir autant d'opportunités et de liberté, et je vous remercie de m'avoir donné cette chance.

Fabrice, tout d'abord merci de m'avoir donné ma chance en me choisissant pour ce projet de thèse. Merci pour ta disponibilité, tes précieux conseils et pour ton optimisme contagieux. Tu as toujours su partager ta passion pour la chimie mais aussi ta bonne humeur, même quand j'étais au fond du trou, notamment quand le peptide oxydé n'en faisait qu'à sa tête. Je te remercie également pour ta patience et ta pédagogie. Corriger mon premier article en « franglais » tout en faisant attention de ne pas me vexer n'a pas dû être une mince affaire !! Merci pour les longues discussions scientifiques, pour le temps que tu as passé avec moi quand les manips ne fonctionnaient pas (masse ou autre). J'ai passé des supers moments avec toi en conf' et à l'ESRF en mode 007 !

Christelle, je souhaiterais te remercier pour (i) la générosité et la passion avec laquelle tu partages ton savoir scientifique, (ii) ta disponibilité pour discuter de chimie ou de choses plus personnelles et ce, même dans les moments où tu as déjà accordé 110% de ton temps à l'ERC et 90% à l'équipe, (iii) avoir été une super coloc de bureau prête à dégainer du chocolat à tout moment et enfin (iv) ne pas m'avoir viré quand j'ai cassé ta voiture ! Je te remercie de m'avoir fait me sentir comme ton égale lors de nos longues conversations scientifiques pendant lesquelles j'ai pu développer mon sens critique et proposer toutes les idées (quelquefois farfelues) qui me venaient à l'esprit, sans peur du ridicule. Merci également de montrer à toutes les femmes de l'équipe qu'on peut être une super chercheuse et une super maman de 4 bambins en même temps !

Peter, tout d'abord je te remercie de m'avoir accueillie dans ton équipe. Merci pour tes précieux conseils, pour les discussions scientifiques qui m'ont beaucoup apporté mais aussi pour ton enthousiasme permanent. Un grand merci aussi pour la confiance que tu m'as accordée et pour ta disponibilité, même après ton départ pour Strasbourg. Ta passion pour les sciences est vraiment contagieuse, alors propage la autant que tu peux !

Cette thèse n'aurait pu se faire sans l'aide précieuse de :

- Emilien Jamin pour la HRMS, je te remercie pour tes précieux conseils et pour le temps que tu m'as accordé. Et désolée pour la poisse que j'emmenais (souvent) avec moi à l'orbitrap !
- Christian Bijani pour les spectres RMN, merci de ne pas t'être lassé de voir des RMN avec des pics super larges tout le temps !! Et merci d'avoir pris le temps de regarder la partie RMN du manuscrit.
- Lionel Rechignat pour la RPE, merci pour les conseils et pour la conversation sur la théorie de la RPE (toujours aussi obscure pour moi !!).
- Vanessa Soldan pour le TEM, je tiens à te remercier pour les précieux conseils et le temps que tu as passé avec moi à sonder l'échantillon à la recherche de fibres (ou d'absence de fibres !).
- Toute l'équipe FAME de l'ESRF. Merci à Isabelle Kieffer pour toutes les explications sur le XAS et pour la visite guidée de la nouvelle ligne. Merci à Denis Testemale pour sa disponibilité et sa patience quand la ligne plantait en notre présence (juré c'est pas de notre faute !) et pour les précieux conseils prodigués en somnambule à toute heure de la nuit !!
- Stéphanie Sayen et Emmanuel Guillon lors des sessions à l'ESRF. Merci pour l'aide précieuse apportée, pour toutes les réponses à mes questions floues sur le XANES. Merci aussi d'avoir partagé les sessions blind-test et les bonbons avec moi !
- Petit Poney qui a subi nos expériences plus ou moins douteuses avec l'azote liquide. Merci pour les photos souvenirs !

Coté Pharma-DEV, je remercie Françoise Nepveu, Karine Reybier, Paul-Louis Fabre, Mohamed Haddad, Marieke Vansteelandt, Geneviève Bourdy ainsi que tous les autres membres des équipes Redstress et PEPS, avec qui j'ai eu la chance de travailler, de partager un repas ou bien un café. Merci à Pierre pour sa gentillesse et sa bonne humeur quotidienne, ainsi que pour l'aide précieuse et les bons conseils qu'il m'a apporté. Merci également à Franck qui a toujours le sourire et qui m'a beaucoup aidé pour les questions administratives. Franck, ton punch est à tomber par terre ! Il me faut la recette ! Merci à tous les stagiaires, doctorants et post-doc de Pharma-DEV qui m'ont permis de travailler dans une super ambiance : Ennaji, Nambinina, Rémi, Thi Thu, Luyen, Solomiia, Filip, Marion, Lucie, Mireia, Laure-Estelle (LEC), Cynthia. Malgré le froid glacial l'hiver, j'ai adoré partager les repas du midi avec vous dans le « couloir-cantine ». Et j'aurais bien besoin de me remettre aux mots croisés du midi !! Un énormissime merci à LEC et Cynthia pour l'accueil très chaleureux que vous m'avez fait à mon arrivée au laboratoire, je me suis sentie bien tout de suite et c'est grâce à vous. Merci pour vos encouragements au quotidien, pour les discussions scientifiques (ou pas !) et pour tous les bons moments passés ensemble. Vous avez été mes modèles de réussite !

Coté LCC, je remercie toute l'équipe F qui m'a chaleureusement accueillie et m'a fait mourir de faim jusqu'à 13h30 pendant mes deux premières années de thèse ! Merci à Manu pour sa bonne humeur et ses super blagues, mais aussi pour les discussions autour des sciences, de l'administration (et des mouches !), de la musique et de l'œnologie ! Merci à Béatrice qui a toujours le sourire, pour sa gentillesse et ses conseils. Laurent, je te remercie de ne pas m'avoir détesté d'office quand j'ai cassé ta voiture ! Je suis très contente d'avoir pu te connaître ces derniers mois et je te remercie pour l'aide et le soutien que tu m'as apporté. Viviane, merci pour ton rire contagieux, ta bonne humeur quotidienne et ta gentillesse ! Je tiens également à remercier tous les étudiants / postdoc actuels ou anciens de l'équipe : Olivia, Hélène, Adam, Olena, Carine, Melisa, Daniel (bon aprèm les garces !), Mireia (mais c'est vrai ça ?!), Megan (so cute !), Gabriel (Mr Marcel), Rufus (c'est qui Clémence ?!), Sara (à ne pas confondre avec Sara !), Marie, Alex (petit puits), Omar (Ahomalll), Elena (a fare l'amore, encore merci pour la chanson !), Valentina (la mammmmmmmma) et Amandine (ACDC <3). Merci pour la super ambiance que vous apportez dans l'équipe, pour les discussions scientifiques qui permettent de faire avancer nos manips qui rament, mais aussi un grand merci pour les nombreux moments passés ensemble à l'extérieur du labo, les soirées mojitos / danses tahitiennes à La Plage… Le labo a été un super endroit pour se faire des amis !

Mes remerciements s'adressent ensuite à toute l'équipe pédagogique Chimie pharmaceutique aux cotés desquels j'ai eu le plaisir de découvrir l'enseignement pendant mes deux années de DCE : Geneviève Baziard, Salomé El Hage, Barbora Lajoie, Jean-Luc Stigliani, Fatima El Garah,

Christelle Recoche-Gueriot et Laurent Amielet. J'ai beaucoup appris auprès de vous et je tiens à vous remercier pour votre accueil et votre bienveillance.

Je tiens à remercier tout le bureau jeune de la SCF Midi-Py avec qui j'ai eu la chance d'animer des ateliers scientifiques et de monter des projets sympas : Claudia, Cécile, Alix, Morgane, Jérémy, Stéphane, et tous les étudiants de l'équipe F. Les sessions Chimie & Terroir vont me manquer, mais pas les ventes des kits chimistes ! Merci aussi à Lydie Valade et plus largement à Chimie et Société de m'avoir fait partager leur passion pour la vulgarisation scientifique.

Je remercie les organisatrices des fameux et très sélects « Zumbapéro » qui m'ont permis de garder la forme pendant ces années de dur labeur ! Julie, merci d'avoir toujours la pêche et d'avoir été là pour les sessions papotage nécessaires à la survie de la thèse ! Amandine, je ne sais même pas quoi dire… Merci d'avoir été là pour moi pendant les bons mais aussi les mauvais moments, de m'avoir fait rire à en pleurer, d'avoir fait mon copilote pendant les missions… et tant d'autres choses ! Bref, merci d'être toi !! Merci aussi à Laurent de nous avoir supporté toutes les deux, je sais qu'on peut être intenables parfois !!

Léa, mon petit, merci d'être là pour moi, avec ta pêche d'enfer et ton hyperactivité !! Merci aussi à ma Flow qui est dans un pays lointain (une fois !). Votre amitié m'a beaucoup aidé à traverser cette thèse.

Merci à mes deux petites angevines Noémie et Marine que j'ai le plaisir de revoir quand je remonte dans le grand nord ! Merci d'être toujours là pour moi après toutes ces années…

Pierre, cette thèse est aussi la tienne. Je n'aurais jamais pu aller au bout sans toi. Merci d'avoir été là pendant toutes ces années, de m'avoir soutenu, nourri (j'ai fait des envieux au labo avec mes gamelles du midi !!), remis sur les rails quand je perdais toute motivation. Tu as été d'une patience à toute épreuve et un vrai roc pour moi.

Enfin, un grand merci à toute ma famille qui m'a toujours soutenu pendant mes longues années d'études et m'a encouragé dans les moments de doute. Je sais que je ne suis pas toujours facile à suivre quand je parle de mon travail, c'est comme si je vous parlais chinois, mais vous êtes toujours intéressés et ça me fait très plaisir. Bref, tout ça pour vous dire : 我愛你 (et cette fois-ci c'est vraiment du chinois, pas du langage de chimiste !).

List of abbreviations

A

AD: Alzheimer's Disease

AFM: Atomic Force Microscopy

AICD: Amino-Terminal APP Intracellular Domain

Ala: Alanine

APP: Amyloid Precursor Protein

Arg: Arginine

Asc: Ascorbate

Asn; Asparagine

Asp: Aspartate

Aβ: Amyloid-β peptide

AβDPs: Aβ-degrading proteases

Aβox: Oxidized Amyloid-β Peptide

C

CCA: Coumarin-3-Carboxylic Acid

CID: Collision Induced Dissociation

CNS: Central Nervous System

CTF: Carboxyterminal Fragments

Cu(I): Cuprous ion

Cu(II): Cupric ion

Cu: Copper

D

Da: Dalton

E

EDTA: Ethylenediaminetetraacetic acid

ENDOR: Electron Nuclear Double Resonance

EPR: Electron Paramagnetic Resonance

ESI: Electrospray ionization

F

FDA: Food and Drug Administration

FDG: Fluoro-deoxy-D-glucose

Fe : Iron

FID: Free Induction Decay

FPLC: Fast Protein Liquid Chromatography

G

G: Gauss

Gln: Glutamine

Glu: Glutamate

Gly: Glycine

GSH: Glutathione

GS-SG: Glutathione disulfide

H

H_2O_2: Hydrogen peroxide

H_2SO_4: Sulfuric acid

His: Histidine

$HO^{\bullet}$: Hydroxyl radical

HPLC: High Performance Liquid Chromatography

HRMS: High-Resolution Mass Spectrometry

HYSCORE: Hyperfine Sublevel Correlation

I

IBS: "In-between" state

L

LC: Liquid Chromatography

Leu: Leucine

Lys: Lysine

M

m/z: Mass to charge ratio

MCO: Metal-catalyzed oxidation

Met: Methionine

MRI: Magnetic Resonance Imaging

MS/MS: Tandem Mass Spectrometry

MS: Mass Spectrometry

N

NaOH: Sodium Hydroxide

NMDA: *N*-Methyl-D-Aspartate

NMR: Nuclear Magnetic Resonance

O

O_2: Dioxygen

$O_2^{\bullet-}$: Superoxide anion

P

PD: Parkinson's Disease

PDA: Photodiode array

PET: Positron Emission Tomography

Phe: Phenylalanine

PSEN1: Presenilin 1

PSEN2: Presenilin 2

R

ROS: Reactive Oxygen Species

RS: Resting State

S

sAPP: Secreted Amyloid Precursor Protein

Ser: Serine

SOD: Superoxide Dismutase

T

TEM: Transmission Electron Microscopy

ThT: Thioflavin T

TIC: Total ion current

TMS: Tetramethylsilane

Tyr: Tyrosine

U

UV-Vis: Ultraviolet-Visible Spectroscopy

V

Val : Valine

X

XANES: X-Ray Absorption Near Edge Structure

XAS: X-Ray Absorption Spectroscopy

Z

Zn: Zinc

Greek letters

ε : Molar Attenuation Coefficient

λ : Wavelength

Numbers

7-OH-CCA: 7-Hydroxycoumarin-3-carboxylic acid

Table of Contents

General introduction

General introduction

Le cerveau humain est un organe très surprenant. Alors qu'il ne pèse que 2 % du poids total du corps et qu'il est constitué majoritairement d'eau (75%), il assure les fonctions cognitives et motrices du corps et traite les informations provenant de la vue, de l'ouïe, de l'odorat, du toucher et du goût. Il est l'une des parties du corps dont l'activité métabolique est la plus intense, et utilise au repos, à lui tout seul, 20% de l'oxygène consommé par l'organisme entier. Il est constitué de 100 milliards de neurones qui communiquent entre eux grâce aux neurotransmetteurs, messagers chimiques qui traversent les synapses. Le cerveau étant un organe extrêmement complexe et multitâche, les origines biologiques et chimiques de ses nombreuses fonctions ne sont pas encore toutes parfaitement connues.

De nombreuses pathologies sont liées à un dysfonctionnement métabolique du cerveau, mais pour la plupart d'entre elles, leur étiologie est inconnue. C'est le cas des maladies neurodégénératives, ou démences, qui touchent actuellement plus de 45 millions de personnes à travers le monde. En raison de l'augmentation de l'espérance de vie liée aux avancées de la médecine, le nombre de personnes atteintes de démence ne fait que s'accroître. Parmi les différentes maladies neurodégénératives, la maladie d'Alzheimer, découverte il y a plus d'un siècle, est la plus répandue. Bien que la cause de son développement soit encore inconnue à l'heure actuelle, deux types de lésions cérébrales sont observés chez les patients : (i) les enchevêtrements neurofibrillaires, ayant pour origine l'hyperphosphorylation de la protéine Tau et (ii) la formation de plaques amyloïdes extracellulaires. Les recherches scientifiques sont donc principalement dirigées vers l'étude de ces deux caractéristiques de la maladie, que ce soit d'un point de vue mécanistique, pour comprendre l'étiologie de la maladie, ou d'un point de vue thérapeutique, pour tenter de trouver un médicament efficace.

Dans ce cadre global, le travail présenté ici s'est focalisé sur la problématique des plaques amyloïdes – appelées aussi plaques séniles – et plus précisément sur son composant principal, le peptide amyloïde-bêta (Aβ). Aβ est un peptide composé de 40 à 42 acides aminés, naturellement présent sous forme monomérique dans le cerveau. Dans le cas de la maladie d'Alzheimer, il est retrouvé sous forme agrégée dans les plaques amyloïdes. Ces dernières peuvent être formées dans l'espace inter-synaptique et empêcher le bon fonctionnement des neurones en obstruant le passage des neurotransmetteurs entre les synapses de deux cellules

nerveuses. Un lien entre maladie d'Alzheimer et stress oxydant a également été démontré. En plus de sa capacité d'agrégation dans des conditions spécifiques à la maladie d'Alzheimer, Aβ est également à l'origine de la production d'espèces réactives de l'oxygène (ROS) car il est capable de chélater des ions métalliques ayant des propriétés oxydo-réductrices, ions cuivre ou fer par exemple. En présence d'un agent réducteur tel que l'ascorbate, naturellement présent dans le cerveau à des concentrations pouvant être localement importantes, le complexe Cu-Aβ formé peut catalyser la production de l'anion superoxyde ($O_2^{\bullet -}$), du peroxyde d'hydrogène (H_2O_2) et du radical hydroxyle ($HO^{\bullet}$) à partir du dioxygène. Ces ROS, et plus spécifiquement le radical hydroxyle, sont des espèces oxydantes réactives qui peuvent endommager les biomolécules environnantes (lipides, protéines, ADN). Lors de la production de ROS, le peptide Aβ, lié au cuivre, subit également des attaques oxydantes. Dans ce contexte général, le projet de thèse a consisté à caractériser l'oxydation du peptide Aβ lors de la production de ROS, catalysée par le cuivre, et en l'étude des conséquences des dommages d'oxydation subis par Aβ sur la coordination d'ions métalliques, la production de ROS et l'agrégation du peptide oxydé.

Le premier chapitre situe le contexte du projet de thèse. La maladie d'Alzheimer y est décrite avec les différentes étapes connues de son développement, ainsi que quelques approches diagnostiques et thérapeutiques. Les lésions cérébrales associées à la maladie sont présentées et une attention particulière est portée aux plaques amyloïdes et à la caractérisation du peptide Aβ qui fait l'objet de notre étude. Les différents événements impliquant le peptide Aβ y sont décrits : la formation des plaques amyloïdes, la production d'espèces réactives de l'oxygène (ROS) en présence d'ions métalliques pouvant entrainer l'oxydation des biomolécules et du peptide Aβ. Enfin, les sites d'oxydation du peptide Aβ décrits dans la littérature sont présentés.

Le second chapitre expose la méthodologie du projet de thèse. La préparation d'échantillons, étape essentielle pour l'étude des peptides, y est présentée. Différentes techniques spectroscopies ont été utilisées : la Spectrométrie de Masse (MS), les spectroscopies UV-Visible et de fluorescence, la Résonance Magnétique Nucléaire du proton (^{1}H RMN) ainsi que la Résonance Paramagnétique Electronique (RPE) et l'absorption des rayons X (XANES). Les principes généraux de chaque technique sont rappelés, et les conditions d'utilisation (matériel et méthodes) pour notre sujet d'étude sont présentées.

L'oxydation du peptide $A\beta_{40}$ catalysée par le cuivre est étudiée dans le chapitre III par MS haute résolution et MS en tandem. Les acides aminés oxydés sont identifiés et la cinétique

d'oxydation de chacun d'eux est présentée. Une étude du peptide oxydé est également réalisée par ^{1}H RMN.

Le chapitre IV se concentre sur l'étude des conséquences de l'oxydation de Aβ. Le mode de coordination du peptide oxydé (Aβox) avec les ions métalliques Cu(I) et Cu(II), catalyseurs de la production de ROS, est étudié par XANES et RPE respectivement, et l'effet de l'oxydation de Aβ sur la production de ROS est étudié par spectroscopie de fluorescence. La coordination du peptide Aβox avec l'ion Zn(II) est également étudiée par XANES et les conséquences de l'oxydation de Aβ sur le phénomène d'agrégation sont investiguées par spectroscopie de fluorescence et par microscopie électronique à transmission (TEM).

Dans le chapitre V, la production de ROS catalysée par le cuivre est étudiée par spectroscopie de fluorescence, avec une série de peptides Aβ ayant subi des modifications (troncation, mutation d'un acide aminé, blocage de l'amine N-terminale), afin de déterminer quels acides aminés sont liés au cuivre pendant la production de ROS.

Enfin, le chapitre VI se focalise sur l'ascorbate, molécule connue pour ses propriétés antioxydantes, mais qui participe également à la production de ROS catalysée par un métal. Afin d'évaluer ses effets pro- et anti-oxydants dans le cadre de la maladie d'Alzheimer, les oxydations des molécules environnantes et du peptide Aβ lors de la production de ROS catalysée par le cuivre sont évaluées par spectroscopie de fluorescence et MS respectivement, pour différentes concentrations d'ascorbate.

Chapter I

Chapter I: Context of the project

I.A. Alzheimer's Disease

In 1907, Aloïs Alzheimer related in the article "Über eine eigenartige Erkankung der Hirnrinde" ("On an unusual Illness of the Cerebral Cortex") the uncommon case of a 51-year-old patient who was suffering from memory loss, disorientation, hallucinations and cognitive impairment. After the death of the patient, the post-mortem examination showed an atrophic brain with "striking changes of the neurofibrils" and "minute military foci" caused by the "deposition of a special substance in the cortex".[1] One century later, this "unusual illness" named Alzheimer's Disease (AD) has become the most widespread neurodegenerative disease whose etiology is still unknown.[2]

I.A.1. Prevalence

According to the World Alzheimer Report,[3] 46.8 million people were suffering from dementia worldwide in 2015 and this number is expected to almost double every 20 years. Approximately 5% - 8% of individuals over age 65, 15% - 20% of individuals over age 75, and 25% - 50% of individuals over age 85 are affected by dementia.[4] Figure I.A-1 shows the repartition of the 46.8 million people living with dementia. In Europe, 10.5 million people are estimated to suffer from a neurodegenerative disease.

Alzheimer's disease is the most common form of dementia, accounting for 50% - 75% of all dementias.[4]

Figure I.A-1: Estimated number of people suffering from dementia in each continent in 2015.[3]

I.A.2. Clinical signs

AD is characterized by a progressive deterioration of cognitive functions and progresses in three stages: mild, moderate and severe.[5]

At the early-stage of AD, the patient can have memory lapse, difficulties to complete familiar tasks and be confused with time or place. New problems with words in speaking or writing can arise, and the possible changes in mood can be misinterpreted as depression.

At the middle-stage, the symptoms become stronger, the patient can get frustrated or angry and the personality and behavior are impacted. The memory troubles worsen: the patient can have forgotten events or parts of his personal history.

At the severe stage, the patient requires around-the-clock assistance. He loses the ability to carry on a conversation and to control movement and can be bedbound. Individual is then vulnerable to infections (especially pneumonia) and the cause of death is usually external to the disease.

I.A.3. Histopathological signs

a. Brain size [6]

In AD, the volume of the brain is significantly reduced compared to normal brain (Figure I.A-2). This atrophy results from the degeneration of synapses and the death of neurons. Hippocampus, the brain region playing a role in memory and spatial orientation, is particularly affected. The reduction of brain size and the progression of AD are related.

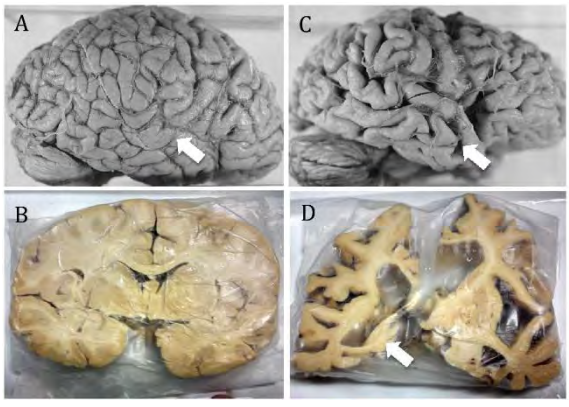

Figure I.A-2: Neuroanatomical comparison of normal brain (A, B) and AD brain (C, D). Prominent atrophy in C compared with A (arrows). B, D: Coronal plane of A and C respectively. Arrow on D shows an enlargement of the ventricles and a selective hippocampal atrophy.[7]

b. Amyloid plaques

The first hallmarks of AD described by Aloïs Alzheimer in 1907 [1] as "minute military foci" caused by the "deposition of a special substance in the cortex" are amyloid plaques (Figure I.A-3a). They are composed of deposits of a peptide named Amyloid-β peptide (Aβ) in aggregated forms [8] mostly fibrils. Those plaques, also named senile plaques, are found in the extracellular media of AD brain and more especially located in the hippocampus region. Aβ is mainly a 40 to 42-amino acid residues peptide originating from the cleavage of Amyloid Precursor Protein (APP) by two enzymes: β- and γ-secretases (see Section I.B for more details).

c. Neurofibrillary tangles

The other hallmarks of the disease are intracellular neurofibrillary tangles (Figure I.A-3b). Those tangles are also observed in Parkinson's disease (PD)[9] and are composed of hyper-phosphorylated Tau proteins.[10] This microtubule-associated protein interacts with tubulin to stabilize microtubules. In AD and PD, the abnormal phosphorylation of Tau induces accumulation as paired helical filaments that aggregate inside neurons in neurofibrillary tangles, making unstable the microtubules. Since microtubules are essential to preserve the structure of the neuron, the neuron loses its functionality.

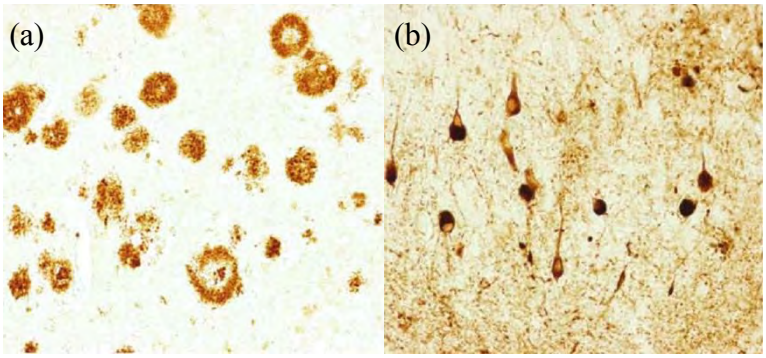

Figure I.A-3: Neuropathological lesions revealed by immunohistochemistry. (a) Senile plaques observed by immunohistochemistry with antibodies against Aβ. (b) Neurofibrillary tangles observed by immunohistochemistry with antibodies against phosphorylated Tau (Pictures from reference [11])

I.A.4. Risk factors

a. Age

The age is the higher risk factor: the more aged the individuals, the higher the risk to develop AD. Indeed, around 5% of 65 years old individuals suffer from dementia and the risk

of developing the disease reaches 50% for individuals beyond age 85.[4] As the life expectancy increases with the medicine advances, more and more people are likely to develop AD.

b. Gender

Women are known to have a higher life expectancy than men, thus being more susceptible to suffer from AD. Furthermore, studies suggest that the decrease in estrogen levels due to menopause could increase the risk of having AD. Indeed, clinical trials have shown that women who had been treated with hormone therapy have a lower risk of AD.[12]

c. Genetic mutations

There are two major forms of AD: the sporadic or late-onset form that is the most common, and the familial or early-onset form, representing less than 5 % of the cases. [13]

Individuals living with Down's syndrome (also called trisomy 21) have an increased risk of early-onset AD. Indeed, they carry an extra copy of chromosome 21 in which is located the gene that is responsible for the APP formation.[14]

Mutations in genes coding for APP, Presenilin 1 and Presenilin 2 (parts of the γ-secretase which is responsible for cleavage of APP in Aβ) and ApoE (involved in Aβ clearance) genes increase the risk of developing AD as these proteins are involved in Aβ regulation in the brain.[13, 15]

I.A.5. Diagnosis

The diagnosis of AD is realized at 70% accuracy with clinical examination and neuropsychological assessment of the patient combined with brain imaging techniques.[7] However, the definitive diagnosis of AD requires histopathologic confirmation and is made post-mortem, based on the observation of specific pathological lesions: intracellular neurofibrillary tangles and senile plaques.[11]

a. Clinical diagnosis

In 1984, the National Institute of Neurological and Communicative Disorders and Stroke–Alzheimer's Disease and Related Disorders Association (NINCDS-ADRDA) has proposed diagnostic criteria for dementia and for AD.[16] Medical history, clinical examination,

neuropsychological testing and laboratory assessment are the recommended standard methods of examination. Criteria are made for several stages: probable AD dementia, possible AD dementia and probable or possible AD dementia with evidence of the AD pathophysiological process. The diagnostic criteria have been revised in 2011[17] and are still used as no specific marker for AD is known. However, they are realized in combination with brain imaging techniques.

b. Neuroimaging [18]

Structural magnetic resonance imaging (MRI) and positron emission tomography (PET) are two brain imaging techniques clinically used for the detection of abnormalities in the brain.[19] Structural MRI is commonly used to visualize brain atrophy caused by neuronal and dendritic losses. However, the cerebral atrophy is not specific to AD and can be the result of another pathology. Structural MRI has thus limitations in AD recognition as it cannot detect the histopathological hallmarks of AD (amyloid plaques and neurofibrillary tangles).

Fluoro-deoxy-D-glucose (FDG) PET is used as an indicator of brain metabolism by measuring the synaptic activity. Nevertheless, as metabolism can be disrupted for different reasons, FDG is not a specific marker for AD either.

Specific biomarkers of AD hallmarks are now under focus. Recently, the European Medicines Agency granted marketing authorization for the Florbetapir F18 (^{18}F-AV-45) (also called Amyvid), a PET marker with a good affinity for Aβ plaques (K_d = 3.7 nM[20]). This active substance can be used to detect amyloid plaques on living patient. [20-21] This is a great advance for AD diagnosis.

I.A.6. Current treatments

There is currently no cure for AD, only symptomatic treatments. The U.S Food and Drug Administration (FDA) has approved four medications that are marketed in France and classified in two groups: acetylcholinesterase inhibitors (Donepezil, Rivastigmine and Galantamine) and *N*-Methyl-D-Aspartate (NMDA) receptor antagonists (Memantine).

Apart from amyloid plaques and neurofibrillary tangles, AD is characterized by a deficit of acetylcholine, a neurotransmitter that diffuses signal across the synapse, between two neurons. Acetylcholinesterase inhibitors avoid acetylcholine degradation by inhibiting

acetylcholinesterase, an enzyme that catalyzes the breakdown of acetylcholine. The level of acetylcholine thus remains stable, allowing neurotransmission.

An over-concentration of glutamate is also observed in synaptic clefts of AD patients. This molecule is an excitatory neurotransmitter that plays a role in neural activation but it can also lead to neuronal death if physiologically over-concentrated. NMDA receptor antagonists block the glutamate receptors to avoid the loss of neurons.

These symptomatic treatments only slow down the cognitive deterioration and have no effect on patients in the severe stage of AD. Researchers particularly focus on amyloid plaques and neurofibrillary tangles to find new therapeutic pathways that could prevent or stop the progression of the disease.[22]

I.B. Aβ and the amyloid plaques formation

I.B.1. Aβ: Structure and formation

Aβ is a 38 to 43 amino acid residue peptide (Figure I.B-1) derived from the enzymatic cleavage of APP. Depending on the exact location of the cleavage on the C-terminal part, several lengths can be formed, from $A\beta_{1-38}$ to $A\beta_{1-43}$. However, the most abundant species produced in the brain are $A\beta_{1-40}$ and to a lesser extent $A\beta_{1-42}$. Aβ is amphiphilic: the N-terminal moiety is hydrophilic while the C-terminal one is hydrophobic.

Figure I.B-1: Amino acid sequence of $A\beta_{1-43}$ (1-letter code)

APP is a type-1 trans-membrane protein expressed in various tissues of the organism, especially in the central nervous system (CNS).[23] Its major neuronal isoform encompasses 695 amino acid residues. [24] Although its physiological function is still unclear, APP would play an important role in brain development, memory and synaptic plasticity.[24]

Two different pathways of APP metabolism can occur, as shown in Figure I.B-2. In the non-amyloidogenic pathway, the predominant one, APP is first cleaved by α-secretase and then by γ-secretase to form truncated $A\beta_{17-40/42}$ (P3) peptides or by β-secretase leading to the formation of the truncated $A\beta_{1-16}$. In the amyloidogenic pathway that occurs to a minor extent, APP is cleaved consecutively by β- and γ-secretases leading to the formation of full-length Aβ

peptides (mainly $A\beta_{1-40/42}$). Both pathways also lead first to the formation of amino terminal fragments (secreted APP (sAPP) α or β) and carboxyterminal fragments (CTF83 or CTF99) and then to the formation of the amino-terminal APP intracellular domain (AICD).[25]

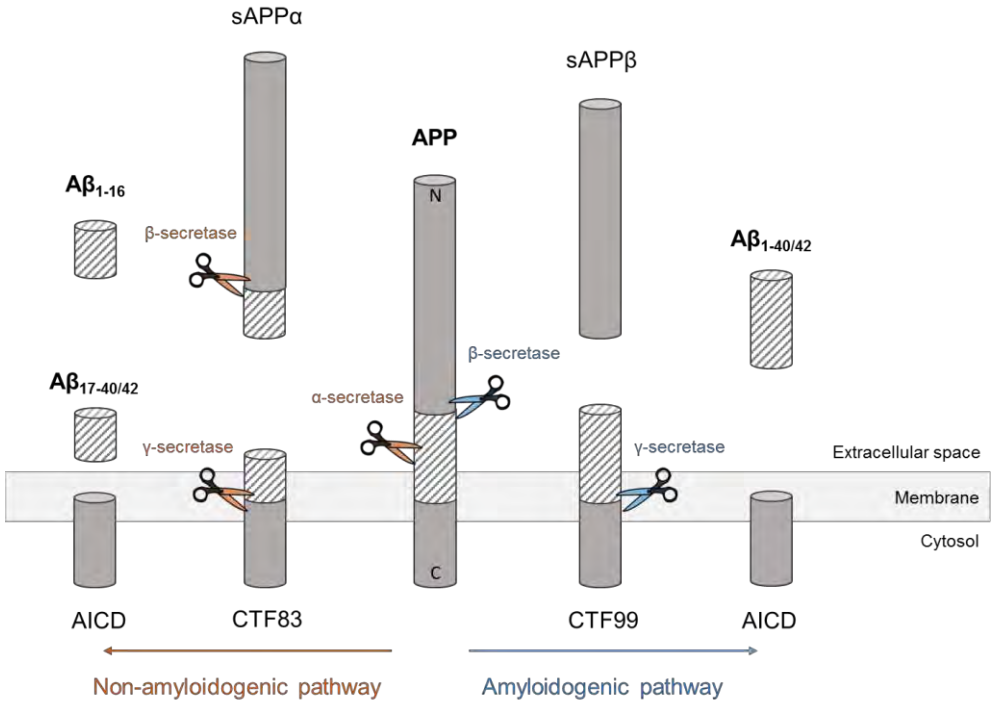

Figure I.B-2: A schematic view of APP proteolytic cleavage. In the non-amyloidogenic pathway, APP is first cleaved by α-secretase and then by γ-secretase to form truncated $A\beta_{17-40/42}$ peptides or by β-secretase leading to the formation of the truncated $A\beta_{1-16}$. In the amyloidogenic pathway, APP is cleaved consecutively by the β- and γ-secretases leading to the formation of full-length $A\beta_{1-40/42}$ peptides.

Thus, Aβ peptides are the product of a minor pathway of APP metabolism,[26] released in the extracellular space of healthy brain during neuronal activity, without leading necessarily to Alzheimer's pathology. Aβ is subject to a proteolytic degradation by Aβ-degrading proteases (AβDPs), which regulates Aβ levels in the brain.[27] Its functions in the brain are still unknown, although Aβ could play a role in the synaptic plasticity and the memory.[28]

I.B.2. APP and Aβ mutations

Familial AD are caused by mutations on a gene of APP, Presenilin 1 (PSEN1) or Presenilin 2 (PSEN2). PSEN1 and PSEN2 are two subunits of γ-secretase. The mutations on both PSEN1 and PSEN2 lead to a higher Aβ production, PSEN1 mutations specifically conducting to an increased $A\beta_{1-42}$ formation.[13]

For APP, 65 mutations are indexed in the Alzheimer Disease & Frontotemporal Dementia Mutation Database, with only 15 being non-pathogenic.[29] The mutations are divided in three categories: mutations at the β-secretase cleavage site, at the γ-secretase cleavage site and in the mild-domain amyloid-β region.[30] The mutations at the γ-secretase cleavage site can alter the cleavage position and lead to an increase of the $A\beta_{1-42}/A\beta_{1-40}$ ratio. The mutations at the β-secretase cleavage site increase the rate of APP proteolysis by the β-secretase. The mutations in the mild-domain of Aβ region in APP alters Aβ assembly by increasing the propensity of Aβ to form oligomers and fibrils.[31] As APP mutations can occur in the Aβ domain, APP proteolysis by both β- and γ-secretases leads to the formation of a mutated peptide. The possible mutations are shown in Figure I.B-3.

Figure I.B-3: Familial AD mutations on $A\beta_{1-43}$. The amino acid residues mutated and the names of the mutations are colored. (1-letter code). [13]

I.B.3. Amyloid cascade hypothesis

AD is a multifactorial disease and the multiple mechanisms related to the disease are unclear. However, since Aβ has been found in healthy brain on soluble form but on aggregated form in AD patient's brain,[8] a hypothesis has been proposed to explain the formation of senile plaques composed of aggregated Aβ. The amyloid cascade hypothesis (Figure I.B-4) formulated in the early 1990s [32-35] has become the dominant model for AD pathogenesis,[36] although still controversial.[37-38]

It is proposed that an abnormal extracellular increase of Aβ levels in brain could lead to its aggregation in β-sheet rich structures.[39] The aggregation starts with the formation of oligomers species that are reorganized into protofibrils and fibrils, which are found in amyloid plaques, a hallmark of AD. In particular, oligomers accumulated in AD patient brains [40] are proposed to be the more toxic species for cells [41-42] as they can permeabilize cellular membranes, thus initiating a series of events leading to cell dysfunction and death.[43] According to this hypothesis, the others events such as the intracellular formation of neurofibrillary tangles and the disruption of synaptic functions would ensue from this early and key event.

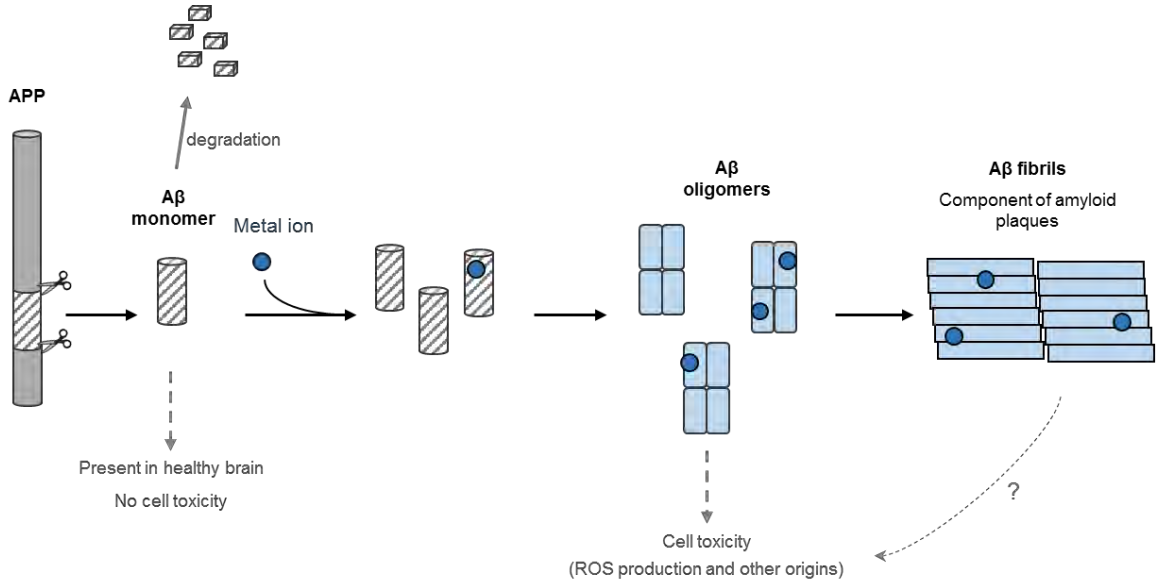

Figure I.B-4: Schematic representation of the amyloid cascade hypothesis with the intervention of metal ions.

Metal ions such as zinc, iron and copper ions have been found in amyloid plaques.[44] In addition, Cu and Zn are exchanged within the synaptic cleft of some neurons. They are supposed to play an important role in the aggregation according to the amyloid cascade hypothesis.[45] Actually, metal ions can bind Aβ and thus modulate the aggregation process. They act either on the kinetics or on the thermodynamics by impacting the morphology of the formed aggregates.[46] Furthermore, amyloid aggregates with entrapped redox-active metal ions such as copper ions are considered as more toxic since they can produce Reactive Oxygen Species (ROS), deleterious for the biomolecules.[47]

I.B.4. Aggregation

Aβ is a natively unfolded peptide with no defined 3D structure. As this peptide is highly flexible and unstructured, it can easily undergo aggregation to amorphous or ordered structures (Figure I.B-5, green and blue pathways respectively), the β-sheet rich structures being thermodynamically the most stable.[48-49]

The fibrils formed during the aggregation process are organized in stacked parallel or anti-parallel β-sheets structures. In $A\beta_{40}$ fibrils, the 12-24 and 30-40 residues would be responsible for β-sheet formation.[50] The aggregation process of Aβ in β-sheet structures is dynamic and complex, consisting in multiple self-assembly steps. Two different steps are observed over time: nucleation and elongation.

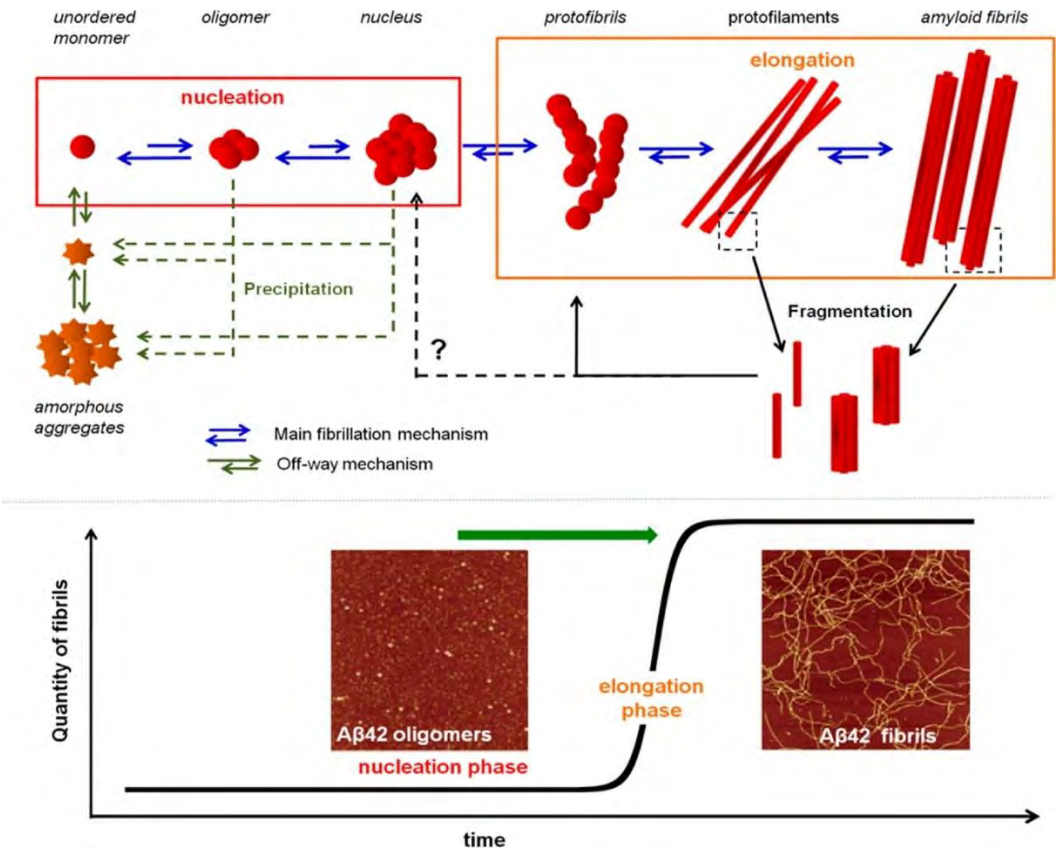

Figure I.B-5: Schematic representation of amyloid aggregation (top section) and AFM images (2 × 2 µM) of the Aβ peptide at the oligomeric and fibrillary stages superimposed with the typical sigmoid curve of fibril formation (bottom section). Picture from reference [46].

During nucleation, the unstructured monomers in solution cluster in small aggregates called oligomers that further form nuclei (red pathway in Figure I.B-5). Nucleation is the slower and limiting step of aggregation since association of monomers that occurs during nucleation is not thermodynamically favorable.[46] The nucleation phase is then followed by a rapid elongation phase in which protofibrils and finally fibrils are formed from nuclei (orange pathway in Figure I.B-5).

Several techniques have been developed to monitor Aβ aggregation.[46, 51] Among them, fluorescence of Thioflavin T (ThT) dye is widely used. ThT interacts with β-sheet and upon interaction undergoes a strong fluorescence enhancement.[52] This allows to monitor the aggregation kinetics. Atomic force microscopy (AFM) and transmission electron microscopy (TEM) give information about the size and shape of aggregates (see AFM images in Figure I.B-5).

I.C. Aβ, metal ions and Reactive Oxygen Species

I.C.1. Coordination of Aβ with metal ions

Metal ions such as zinc, iron and copper are present in the brain. They are necessary and required to regulate the neuronal activity in the synapses and involved in biological functions of metallo-proteins. In several diseases such as AD, the metal ion homeostasis is disrupted and the concentration is very far from the physiological one, with Cu and Zn levels that can reach up to three times the control levels.[53] Moreover, high content of these metal ions is found in amyloid plaques extracted from AD brains. [44] In addition, such ions can bind to Aβ under physiological concentrations. Thus, knowing the coordination mode of these metal ions with Aβ is a pre-requisite to understand their role in AD.

a. Zn(II) coordination to the Aβ peptide

Zn ion exists only as Zn(II) and its coordination to Aβ is still not well-established.[54-55] Although it is consensual that a complex 1:1 is formed,[55] the nature of the amino acid residues involved in the coordination sphere is still under debate. A novel binding model has been recently proposed, based on Nuclear Magnetic Resonance (NMR) and X-ray Absorption Spectroscopy (XAS) studies of Zn coordination with mutated and N-terminal acetylated peptides (Figure I.C-1).[56] In this model, Zn(II) would be bound by imidazole rings of His6 and either His13 or His14 residues, the carboxylate group of Glu11 and the carboxylate group of Asp1, Glu3 or Asp7.

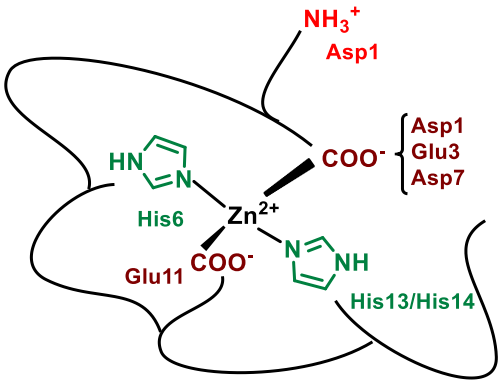

Figure I.C-1: Proposed coordination sites of Zn(II) to the Aβ peptide at pH 7.4.[56]

b. Cu(II) coordination to the Aβ peptide

The Cu(II) coordination to Aβ has been widely studied for years and is challenging as several species are formed depending on the pH. Numerous studies have been realized in the past decade and the results have been recently reviewed,[54, 57-59] leading to a consensual model with different Cu(II) binding modes depending on the pH. The four binding modes observed for pH values higher than 6.5 are shown in Figure I.C-2.

For component I, it is now established that Cu(II) is bound to the NH_2 terminus, the adjacent CO function from Asp1-Ala2 and to imidazole rings of His6 and either His13 or His14.[60-64]

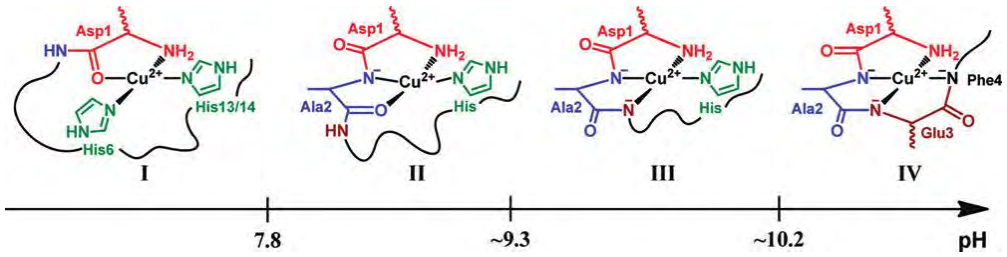

Figure I.C-2: Schematic representation of equatorial Cu(II)-Aβ binding sites depending on the pH. The pKa of the different components are indicated in the pH scale (Picture from reference [65]).

For component II, two distinct models have been proposed. In the first one, Cu(II) is bound *via* the carbonyl function from Ala2-Glu3 and the imidazole rings of the three His. [62, 64] In the second one, Cu(II) is bound to the N-terminal amine of Asp1, the amidyl function of Asp1-Ala2, the carboxylate group of Ala2 and the imidazole ring of one His. [60-61, 65] The first model does not explain the effect of pH on the coordination as all the residues involved in Cu(II) coordination that can undergo deprotonation are already deprotonated. The second model explains the change of Cu(II) binding mode that occurs around pH 7.8 with the deprotonation of the Asp1-Ala2 amide function, leading to its coordination. Furthermore, Electron Nuclear Double Resonance (ENDOR), Hyperfine Sublevel Correlation (HYSCORE) and NMR studies highlight the involvement of both the NH_2 terminus of Asp1 and the deprotonated Asp1-Ala2 amide bond, favoring the second model.[57] Thus, the second proposed model (illustrated in Figure I.C-2) is the most accepted model and it will be used as the component II model thereafter.

The other two components (called III and IV) are formed at higher pH with the deprotonation of the Ala2-Glu3 and Glu3-Phe4 amide functions, respectively.[65] Cu(II) is bound *via* the -NH_2 terminus, the two amidyl functions between Asp1 and Glu3 and one His

residue in component III and *via* the NH_2 terminus and the three amidyl functions between Asp1 and Phe4 in component IV.

A carboxylate group has also been proposed to be involved in apical position for several components, coming from Asp1[60-62] or from Glu3, Asp7 and Glu11 carboxylates in equilibrium with Asp1 for component I.[61]

c. Cu(I) coordination to the Aβ peptide

Copper is a redox-active ion which is present physiologically in two redox states: Cu(I) and Cu(II). Cu(I) coordination with Aβ has been investigated more recently than Cu(II) coordination and the involvement of histidine residues is now consensual. Several binding models are suggested, two of them being most populated (Figure I.C-3).

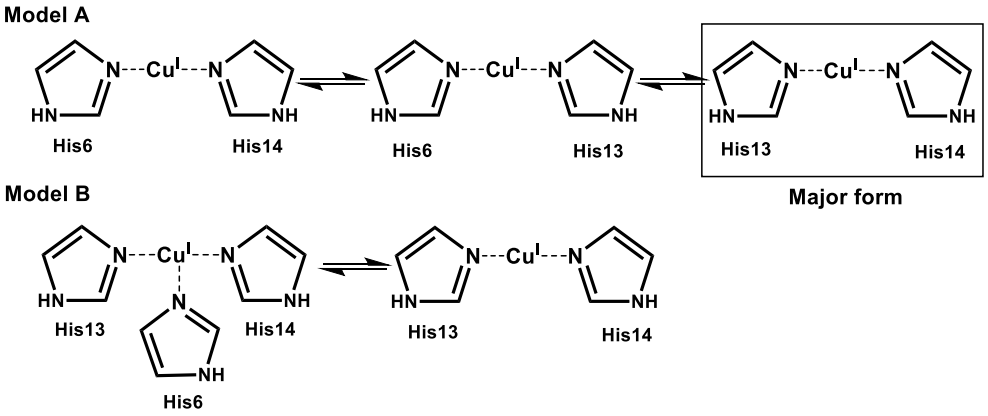

Figure I.C-3: Schematic view of the two proposed models for Cu(I) coordination in the Aβ peptide. Adapted from reference [66].

Model A proposes a linear binding of histidines with a dynamic exchange between His6, His13 and His14. Model B involves an equilibrium between the His dyad and the His triad. NMR studies have shown the implication of the three histidines in the Cu(I) coordination with a dynamic exchange, in line with the two proposed models.[66] However, XAS studies [66-67] and a comparison of synthetized Cu(I) complexes HisHis dipeptides and Cu(I) complexes with truncated $A\beta_{6-14}$ and $A\beta_{10-14}$ peptides [68-69] highlight a linear binding mode with 2 histidines, corroborating the model A.

In addition, according to a tandem mass spectrometry (MS/MS) study on Cu(I)-Aβ structure, the two histidines mostly involved in Cu(I) coordination would be His13 and His14 [70]. Thus, evidences suggest that Aβ is bound to Cu(I) by histidine residues in a linear fashion with a dynamic exchange between His6, His13 and His14, the major form being His13 and

His14 dyad. This is in line with affinity studies realized on three Cu(I) complexes with one His-Ala mutation on Aβ peptide (named H6A, H13A and H14A) [71-73] that point out to a slightly lower affinity than for the native peptide, H6A having a stronger affinity than the other two mutants. These results indicate that Aβ only needs two histidines for binding Cu(I), His13-His14 dyad being the major form.

I.C.2. Reactive Oxygen Species

a. ROS and oxidative stress

Reactive oxygen species (ROS) are radicals and molecules deriving from the incomplete reduction of dioxygen. They are produced in small quantity during the *in vivo* metabolism of oxygen, through four successive 1-electron reductions of O_2 leading to H_2O formation (Figure I.C-4). They are necessary to maintain the homeostasis in cells and play an important role in signaling [74] but are also reactive oxidants, able to damage biomolecules. In cells, endogenous enzymes are in charge of the antioxidant defense to prevent the ROS mediated damages.[47]

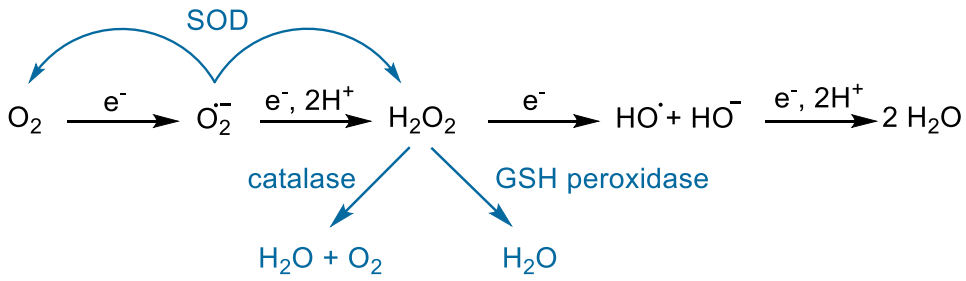

Figure I.C-4: Schematic view of the ROS production during oxygen reduction (black pathway) and the enzymes involved in ROS detoxification (blue pathways)

The superoxide ($O_2^{\bullet-}$) anion, the first ROS produced by the one-electron reduction of dioxygen, is capable of inactivating few enzymes,[47] but has a poor reactivity with most of the bio-inorganic substrates due to low rate constant (usually below 10^2 L mol^{-1} s^{-1}).[75-76] To remove a potential excess of $O_2^{\bullet-}$, endogenous enzymes called superoxide dismutases (SOD) are present in cells and can catalyze the superoxide dismutation (Figure I.C-5, reaction (1)) with a diffusion rate close to the limit (k around 10^9 L mol^{-1} s^{-1}).[76-77]

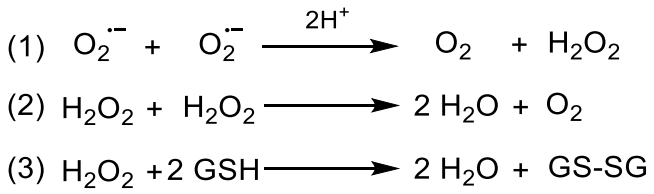

Figure I.C-5: (1) Dismutation of superoxide into dioxygen and hydrogen peroxide catalyzed in living systems by SOD. (2) Dismutation of hydrogen peroxide into dioxygen and water catalyzed in living systems by catalase. (3) Hydrogen peroxide reduction catalyzed by the glutathione peroxidase (GSH). GS-SH: Glutathione disulfide.

Hydrogen peroxide (H_2O_2) is the product of the one-electron reduction of superoxide. It can oxidize proteins with thiol groups and is deleterious in the presence of redox-active metal ions such as iron and copper as it can produce the hydroxyl radical during the Fenton reaction (Figure I.C-6, reaction (1)) or during the Haber-Weiss reaction with superoxide (Figure I.C-6, reaction (2)). H_2O_2 is regulated *in vivo* by two enzymes. The catalase catalyzes the dismutation of H_2O_2 into two molecules of water and one dioxygen (Figure I.C-5, reaction (2)) whereas the glutathione peroxidase (GSH) catalyzes its reduction in water (Figure I.C-5, reaction (3)).[78]

The hydroxyl radical ($HO^{\bullet}$) is the result of the third one-electron reduction of oxygen. It can also be produced in the presence of metal ions from H_2O_2 or H_2O_2 and $O_2^{\bullet -}$ by the Fenton reaction or the Haber-Weiss reaction respectively (Figure I.C-6). $HO^{\bullet}$ has a very short half-life (10^{-9} s) compared with $O_2^{\bullet -}$ (10^{-6} s) and is thus the more reactive and deleterious ROS,[74] being able to oxidize the biomolecules such as proteins, lipids, DNA[79] because of its very high redox potential (E°'=2.34 V [80]).

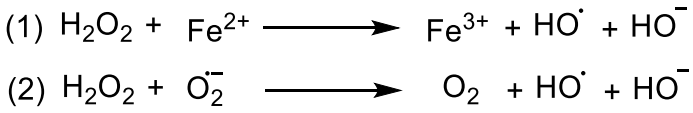

Figure I.C-6: (1) Fenton reaction (2) Haber-Weiss reaction catalyzed by iron ions.

To control the quantity of pro-oxidants (ROS) and prevent the damages on the biomolecules, the body has protecting mechanisms including enzymatic and chemical antioxidants. However, in some diseases such as AD [81], an imbalance may occur between pro-oxidants and antioxidants, due to a higher ROS production or a reduced activity of the enzymes responsible for the ROS degradation, leading to oxidative damages on biomolecules.[82]

b. Metal-catalyzed ROS production

Redox active metal ions such as copper and iron are involved in the ROS production *via* Fenton and Haber-Weiss reactions (Figure I.C-6). In the presence of a reducing agent, they can have a catalytic activity.[83] In AD, Cu and Fe can be coordinated to Aβ and the resulting complex could be directly involved in the ROS production. ROS production has been mostly studied with Cu-Aβ, as Fe-Aβ has a lower redox activity.[84] Iron is found in the amyloid plaques predominantly in a colloidal form (originating from ferritin), however histochemical studies indicate that it could also be bound to Aβ.[85] The coordination mode of Fe(II) with Aβ has been characterized [86] and Fe(III) does not form a stable complex with Aβ because it finally converts into $Fe(III)(HO)_3$ and precipitates. Thus, the physiological stable formation of Fe(III)-Aβ is unlikely. However, ROS production by Fe-Aβ still might be relevant as Fe(II)-Aβ is stable and the Fe(III) complex formed during ROS production might not have time to precipitate. As the involvement of iron bound to Aβ in ROS production is still unclear, we focus here only on Cu-Aβ.

In the case of copper, the pro-oxidant role of the Cu-Aβ system is not clearly established as the complex is more active in ROS production than several biological relevant Cu-peptides or Cu-proteins [87] but less efficient than loosely-bound copper.[84, 87-91] However, *in vitro* studies have shown that Cu-Aβ is able to catalyze the formation of H_2O_2 and $HO^\bullet$ in the presence of O_2 and a reducing agent such as ascorbate (Figure I.C-7).[84, 87-88, 92] Moreover, although it was generally proposed that H_2O_2 production by Cu-Aβ occurs *via* a two-electron process, a recent study has highlighted the formation of superoxide as an intermediate in the production of H_2O_2 by Cu-Aβ and O_2.[93]

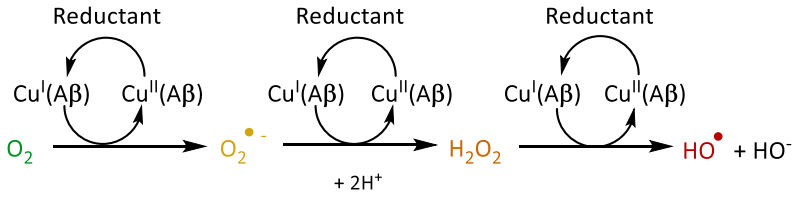

Figure I.C-7: Mechanism of ROS production from a reductant and dioxygen catalyzed by the Cu-Aβ complex. The ROS produced are the superoxide anion ($O_2^{\bullet-}$), hydrogen peroxide (H_2O_2) and the hydroxyl radical ($HO^\bullet$).

c. Coordination of copper with Aβ during redox cycling

Copper is redox-active and cycles between the +I and +II oxidative states when bound to Aβ. An electrochemistry study has shown that a preorganization mechanism was needed to allow the electron transfer for the oxidation of Cu(I) or the reduction of Cu(II) since the Cu(II) and Cu(I) coordination spheres are very different (Figure I.C-8, resting states).[94]

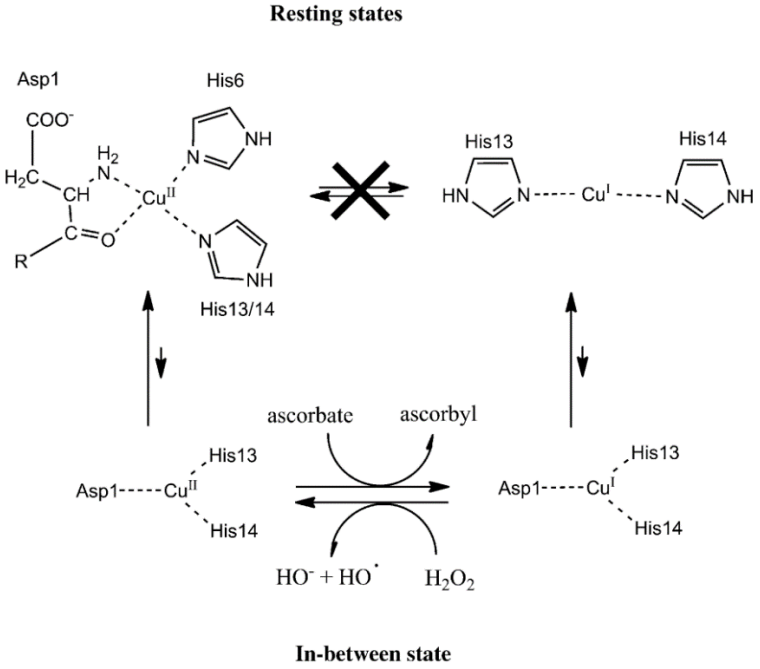

Figure I.C-8: Top: Resting states that are the most populated states of Cu(II)-Aβ (left) and Cu(I)-Aβ (right). The redox reaction between these states is sluggish due to a high reorganization energy. Bottom: putative mechanism of HO• production from H_2O_2 and ascorbate, through the efficient redox reaction of the in-between state. Picture from reference [95].

The energy required for the rearrangement between the Cu(I) and Cu(II) geometries (linear and square-planar respectively) being very high, the electron transfer would rather proceed *via* a low-populated redox-active state in which Cu(I) and Cu(II) binding modes are highly similar, thus inducing a low reorganization energy. This transient state, called "in-between" state, is in equilibrium with the resting states (Figure I.C-8, bottom section). It has been studied by calculations [96] and characterized with MS/MS by identifying the sites of oxidative damage on the peptide.[95] By comparing the non-specific oxidations detected on $A\beta_{28}$ after the radiation-induced ROS production with the copper-mediated oxidations of $A\beta_{28}$, Asp1, His 13 and His14 have been found to be the metal-specific targeted amino acid residues. Furthermore, kinetic studies of the copper-mediated $A\beta_{28}$ oxidation have shown that Asp1 would be the first amino acid residues damaged. Thus, in this study, the proposed ligands for both Cu(II) and Cu(I) coordination in the in-between state are Asp1, His 13 and His14. As they

have been found to be the main targets for HO•, they are supposed to be the amino acid residues the closest from copper during the metal-catalyzed ROS production.

I.C.3. Metal-catalyzed oxidation of Aβ

During the metal-catalyzed ROS production, the Aβ peptide undergoes oxidative damages. This is in line with the detection of oxidized Aβ in amyloid plaques *in vivo*.[97] Studies on single amino acid residue oxidations could allow a prediction on the residues targeted during the metal-catalyzed oxidation (MCO) of Aβ.[98-100] The physiological main targets for HO• are the sulfur-containing amino acids (methionine, cysteine), the basic amino acids (arginine, histidine, lysine) and the aromatic amino acids (phenylalanine, tyrosine, tryptophan).[101]

Table I.C-1 provides the main oxidation products of these amino acid residues. Oxidation of $A\beta_{28}$ by HO• produced by γ-radiolysis has shown that His and Phe residues are mainly targeted,[95] in line with the oxidations reported previously for free amino acid residues.

However, in the case of MCO of Aβ, the ROS are produced at the metal center. Thus, the oxidations are site-specific and can differ from the amino acid oxidations usually detected without metal.

Table I.C-1: Main oxidation products of the principal amino acid residues undergoing HO• attack.[101]

Amino acid residue	3-letter abbreviation	Products of oxidation by HO•
Cysteine	Cys	Cysteic acid Cystine
Methionine	Met	Methionine sulfoxide Methionine sulfone
Arginine	Arg	5-hydroxy-2-amino valeric acid
Histidine	His	2-oxohistidine
Lysine	Lys	3,4 or 5-hydroxylysine
Phenylalanine	Phe	2-hydroxyphenylalanine
Tryptophan	Trp	N'-Formylkynurenine Kynurenine
Tyrosine	Tyr	Dihydroxyphenylalanine (DOPA) Dityrosine

Several studies have reported the damages undergone by the Aβ peptide during the copper-mediated oxidation. The amino acid residues damaged are summarized in Figure I.C-9 and further described in the following paragraphs.

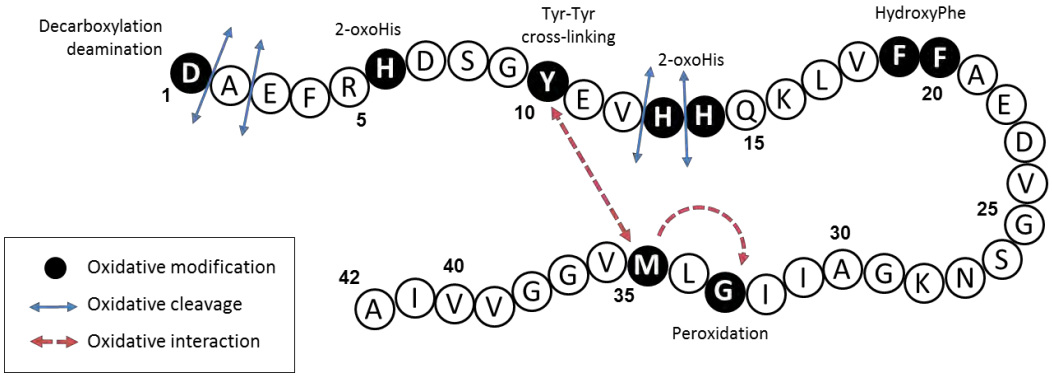

Figure I.C-9: Schematic view of the different oxidative modifications (black circle), cleavages (blue arrows) and interactions (red arrows) undergone by the $A\beta_{42}$ peptide during the copper-mediated oxidation (from reference [87]).

a. Histidines

The Aβ peptide contains 3 histidines located at the positions 6, 13 and 14. They are involved in both Cu(II) and Cu(I) coordination by their imidazole ring (see section I.C.1). Thus, they are targeted during MCO. Histidines have been found oxidized into 2-oxohistidines (Figure I.C-10) during MCO of Aβ bound to copper in the presence of ascorbate [88, 95, 102-103] or hydrogen peroxide.[104]

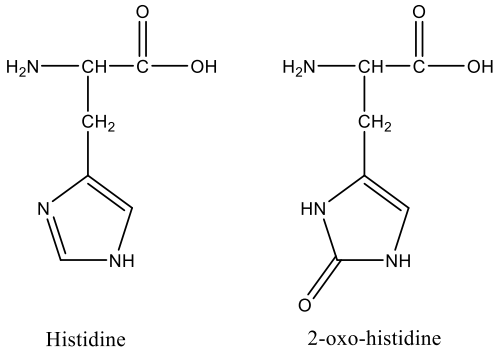

Figure I.C-10: Structural formula of histidine (left) and 2-oxo-histidine (right).

The mechanism of oxidation is shown in Figure I.C-11. His13 and His14 have been found to be more sensitive to oxidation, His6 being not detected on its oxidized form [95, 103-104] or affected after longer oxidation time.[102] This is in line with the predominant binding mode of Cu(I) to His13 and His14 (see section I.C.1.c).

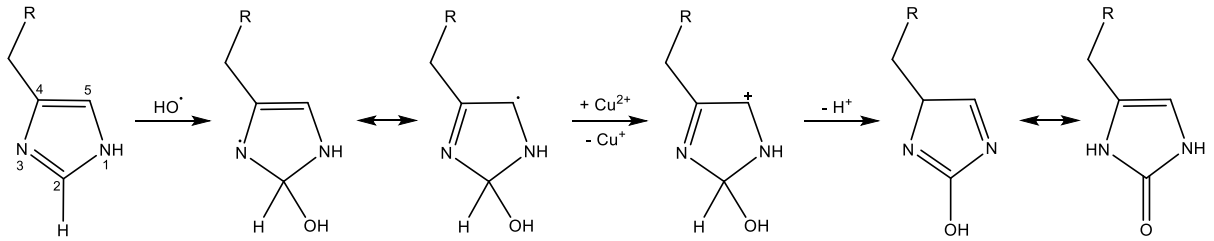

Figure I.C-11: 2-oxo-histidine formation from the oxidative attack of hydroxyl radical at the C-2 position of the imidazole ring of Histidine [105]

b. Aspartate

The Aβ peptide has 3 aspartates residues at positions 1, 7 and 23. In the literature, only Asp1 has been found to be oxidized. Actually, as Asp1 is involved in the coordination of Cu(II),[57-58] it is a preferential target for the hydroxyl radical produced at the metal center.

Different damages have been detected during MCO of Asp1 both in the presence of ascorbate [95, 106] and of hydrogen peroxide [104]. Figure I.C-12 shows an oxidative mechanism leading to the formation of either pyruvate (blue pathway), isocyanate (red pathway) or 2-hydroxyaspartate (green pathway) function through the formation of an alkoxyl radical.

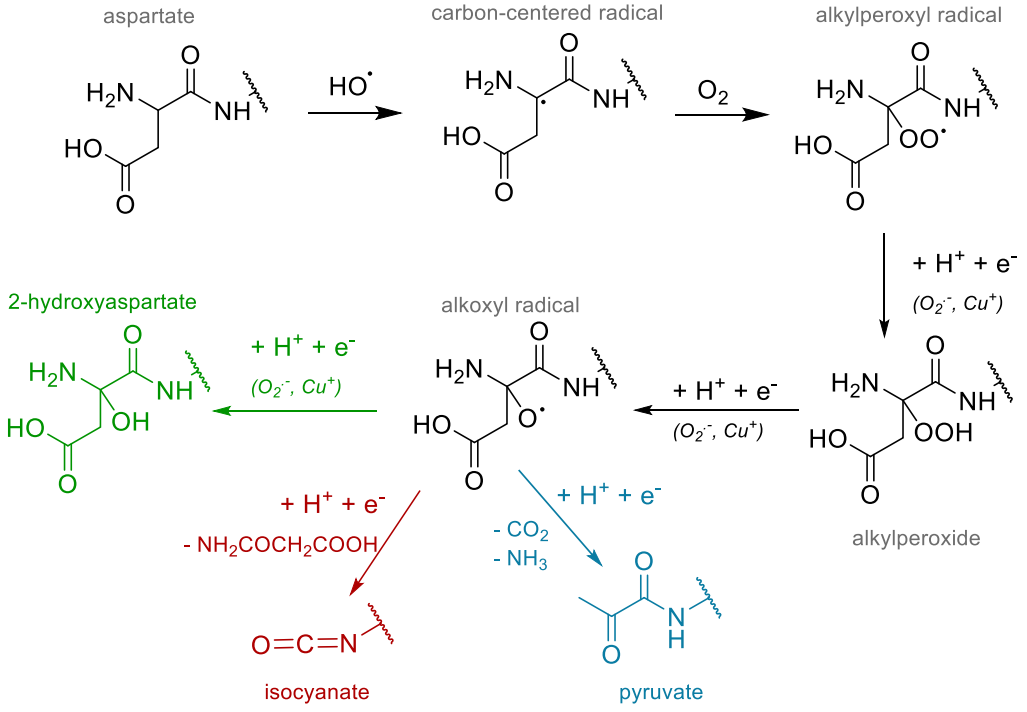

Figure I.C-12: Mechanism of aspartate oxidation with three different pathways starting from alkoxyl radical and leading to the formation of 2-hydroxyaspartate (green), isocyanate (red) and pyruvate (blue).

The oxidative decarboxylation and deamination of Asp1 leads to the formation of a pyruvate function (Figure I.C-12, blue pathway).[95, 104, 106] Asp1 is also subject to a backbone cleavage on the α-position of the peptide, leading to an isocyanate function (Figure I.C-12, red pathway).[95, 106] Another oxidation of Asp1 into 2-hydroxyaspartate corresponding to the formal addition of an oxygen atom has also been described (Figure I.C-12, green pathway).[95]

c. Tyrosine

Although the amino acid residues involved in copper coordination are more vulnerable to oxidation, non-coordinating amino acid residues can also be oxidized. It is the case for Tyr10 which is sensitive to oxidation and is responsible for the Aβ peptide cross-linking by dityrosine formation (Figure I.C-13).[98] This latter, induced by Cu(II), has been detected for Aβ in the presence of H_2O_2.[107] MCO of Tyr10 into dityrosine was found to have an impact on aggregation as Aβ cross-linking was correlated with the formation of covalent oligomers.[108-109]

Furthermore, a study has proposed that Tyr10 acts as a gate that promotes the electron transfer from Met35 to Cu(II) for its reduction in Cu(I).[110]

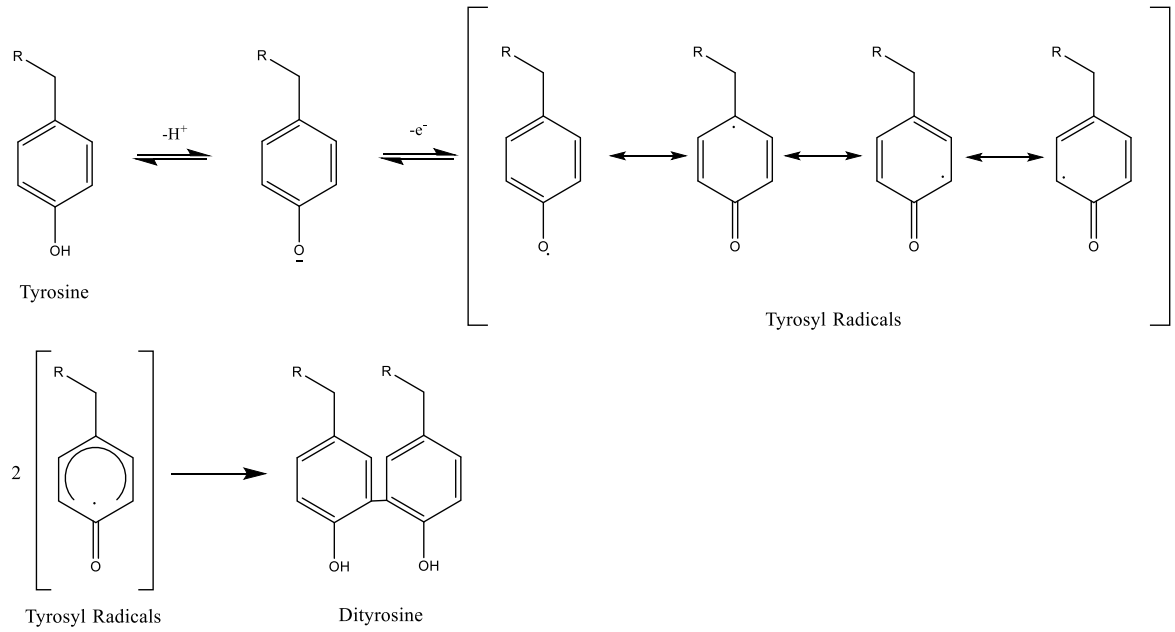

Figure I.C-13: Tyrosine cross-linking mechanism leading to the formation of dityrosine [111]

d. Phenylalanines

Three phenylalanines are present in the Aβ sequence at positions 4, 19 and 20. None of them are involved in the Cu(II) or Cu(I) coordination, nevertheless Phe19 and Phe20 have been found oxidized during MCO of Aβ in the presence of Cu(II) and ascorbate.[95] Phe19 and Phe20 has been detected with the formal addition of an oxygen atom, likely oxidized into hydroxyphenylalanine (Figure I.C-14).[98] This oxidation seems to occur after the oxidation of Asp1 which is involved in Cu binding.[95]

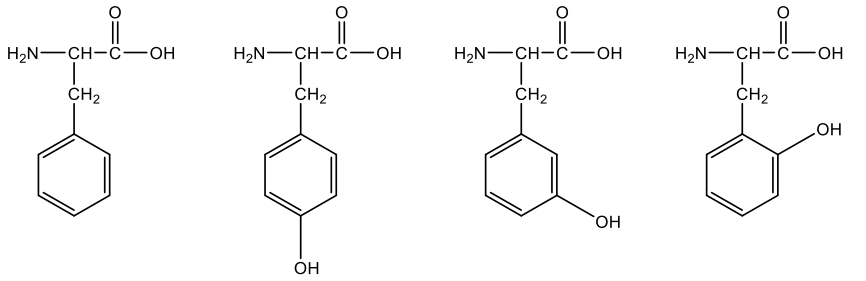

Figure I.C-14: Structural formula of phenylalanine and the three hydroxyphenylalanines.

e. Methionine

Methionine is an amino acid residue very sensitive to oxidation. *In vivo*, the enzyme methionine sulfoxide reductase is responsible for the reduction of the methionine sulfoxide (Figure I.C-15), a main oxidized form of the methionine.[112] Methionine can also be converted into sulfuranyl / hydroxysulfuranyl radical cation by a one-electron oxidation.[113]

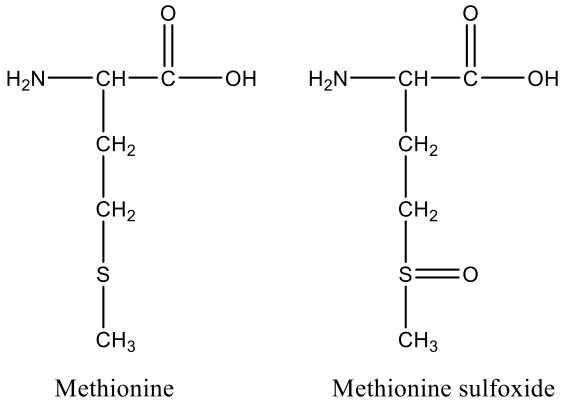

Figure I.C-15: Structural formula of methionine (left) and methionine sulfoxide (right).

Reviews have reported about oxidation of the methionine of the Aβ peptide located at position 35 and its role in toxicity and oxidative stress.[114-115] Although methionine is very sensitive to oxidation, its conversion into methionine sulfoxide occurs only after the oxidation of His13 and His14 during the *in vitro* MCO of Aβ in the presence of Cu(II)/ascorbate.[102] This highlights the site-specificity of the amino acid residue oxidation catalyzed by the bound copper.

Met35 has also been found to promote Tyr10 oxidation [116] and to interact with Gly33, inducing its peroxidation by promoting the formation of a carbon-centered radical, leading to a hydroperoxide.[90, 117]

f. Other cleavages

Other oxidative cleavages have been reported for Aβ bound to Cu(II) in the presence of H_2O_2 such as the cleavage of the peptide bond of Asp1/Ala2, Ala2/Glu3, Val12/His13 or His13/His14.[104]

References

[1] R. A. Stelzmann, H. Norman Schnitzlein and F. Reed Murtagh, *Clinical Anatomy* **1995**, *8*, 429-431.

[2] M. Goedert and M. G. Spillantini, *Science* **2006**, *314*, 777-781.

[3] M. Prince, A. Wimo, M. Guerchet, G. Ali, Y. Wu and M. Prina, *Alzheimer's Disease International, London* **2015**.

[4] B. Duthey, *Priority Medicines for Europe and the World. " A public Health Approach to Innovation"* **2004**, 1-74.

[5] *Alzheimer's & dementia: the journal of the Alzheimer's Association* **2015**, *11*, 332.

[6] M. P. Mattson, *Nature* **2004**, *430*, 631-639.

[7] L. O. Soto-Rojas, F. de la Cruz-López, M. A. O. Torres, A. Viramontes-Pintos, M. del Carmen Cárdenas-Aguayo, M. A. Meraz-Ríos, C. Salinas-Lara, B. Florán-Garduño and J. Luna-Muñoz, *Neuroinflammation and Alteration of the Blood-Brain Barrier in Alzheimers Disease*, in *Alzheimer's Disease - Challenges for the Future*, I. Zerr, InTech, **2015**.

[8] G. G. Glenner and C. W. Wong, *Biochemical and Biophysical Research Communications* **1984**, *120*, 885-890.

[9] M. Goedert, *Science* **2015**, *349*, 1255555.

[10] I. Grundke-Iqbal, K. Iqbal, Y. C. Tung, M. Quinlan, H. M. Wisniewski and L. I. Binder, *Proceedings of the National Academy of Sciences of the United States of America* **1986**, *83*, 4913-4917.

[11] L. Minati, T. Edginton, M. G. Bruzzone and G. Giaccone, *American journal of Alzheimer's disease and other dementias* **2009**, *24*, 95-121.

[12] S. C. Janicki and N. Schupf, *Current neurology and neuroscience reports* **2010**, *10*, 359-366.

[13] R. C. Barber, *Scientifica (Cairo)* **2012**, *2012*, 246210.

[14] F. K. Wiseman, T. Al-Janabi, J. Hardy, A. Karmiloff-Smith, D. Nizetic, V. L. Tybulewicz, E. M. Fisher and A. Strydom, *Nature Reviews Neuroscience* **2015**.

[15] J. Nasica-Labouze, P. H. Nguyen, F. Sterpone, O. Berthoumieu, N.-V. Buchete, S. Coté, A. De Simone, A. J. Doig, P. Faller and A. Garcia, *Chemical Reviews* **2015**, *115*, 3518-3563.

[16] G. McKhann, D. Drachman, M. Folstein, R. Katzman, D. Price and E. M. Stadlan, *Neurology* **1984**, *34*, 939-944.

[17] G. M. McKhann, D. S. Knopman, H. Chertkow, B. T. Hyman, C. R. Jack, C. H. Kawas, W. E. Klunk, W. J. Koroshetz, J. J. Manly and R. Mayeux, *Alzheimer's & Dementia* **2011**, *7*, 263-269.

[18] K. A. Johnson, N. C. Fox, R. A. Sperling and W. E. Klunk, *Cold Spring Harbor perspectives in medicine* **2012**, *2*, a006213.

[19] L. Mosconi, M. Brys, L. Glodzik-Sobanska, S. De Santi, H. Rusinek and M. J. De Leon, *Experimental gerontology* **2007**, *42*, 129-138.

[20] S. R. Choi, J. A. Schneider, D. A. Bennett, T. G. Beach, B. J. Bedell, S. P. Zehntner, M. Krautkramer, H. F. Kung, D. M. Skovronsky and F. Hefti, *Alzheimer Disease and Associated Disorders* **2012**, *26*, 8.

[21] A. Cortes-Blanco, C. Prieto-Yerro, R. Martinez-Lazaro, J. Zamora, A. Jiménez-Huete, M. Haberkamp, J. Pohly, H. Enzmann, J. Zinserling and V. Strassmann, *Alzheimer's & Dementia* **2014**, *10*, S395-S399.

[22] H. Hampel, L. S. Schneider, E. Giacobini, M. Kivipelto, S. Sindi, B. Dubois, K. Broich, R. Nisticò, P. S. Aisen and S. Lista, *Expert review of neurotherapeutics* **2015**, *15*, 83-105.

[23] R. Jakob-Roetne and H. Jacobsen, *Angewandte Chemie International Edition* **2009**, *48*, 3030-3059.

[24] N. N. Nalivaeva and A. J. Turner, *FEBS Letters* **2013**, *587*, 2046-2054.

[25] V. W. Chow, M. P. Mattson, P. C. Wong and M. Gleichmann, *Neuromolecular medicine* **2010**, *12*, 1-12.

[26] C. Haass, M. G. Schlossmacher, A. Y. Hung, C. Vigo-Pelfrey, A. Mellon, B. L. Ostaszewski, I. Lieberburg, E. H. Koo, D. Schenk, D. B. Teplow and D. J. Selkoe, *Nature* **1992**, *359*, 322-325.

[27] T. Saido and M. A. Leissring, *Cold Spring Harb Perspect Med* **2012**, *2*, a006379.

[28] D. Puzzo and O. Arancio, *J Alzheimers Dis* **2013**, *33 Suppl 1*, S111-120.

[29] M. Cruts, J. Theuns and C. Van Broeckhoven, *Hum Mutat* **2012**, *33*, 1340-1344.

[30] E. Karran, M. Mercken and B. De Strooper, *Nat Rev Drug Discov* **2011**, *10*, 698-712.

[31] D. M. Holtzman, J. C. Morris and A. M. Goate, *Science translational medicine* **2011**, *3*, 77sr71-77sr71.

[32] J. Hardy and D. Allsop, *Trends in pharmacological sciences* **1991**, *12*, 383-388.

[33] D. J. Selkoe, *Neuron* **1991**, *6*, 487-498.

[34] K. Beyreuther and C. L. Masters, *Brain Pathol* **1991**, *1*, 241-251.

[35] J. A. Hardy and G. A. Higgins, *Science* **1992**, *256*, 184.

[36] D. J. Selkoe and J. Hardy, *EMBO Molecular Medicine* **2016**, *8*, 595-608.

[37] C. Reitz, *International Journal of Alzheimer's Disease* **2012**, *2012*.

[38] K. Herrup, *Nature neuroscience* **2015**, 794-799.

[39] F. Ding, J. M. Borreguero, S. V. Buldyrey, H. E. Stanley and N. V. Dokholyan, *PROTEINS: Structure, Function, and Bioinformatics* **2003**, *53*, 220-228.

[40] E. Pham, L. Crews, K. Ubhi, L. Hansen, A. Adame, A. Cartier, D. Salmon, D. Galasko, S. Michael, J. N. Savas, J. R. Yates, C. Glabe and E. Masliah, *FEBS J* **2010**, *277*, 3051-3067.

[41] G. Forloni, V. Artuso, P. La Vitola and C. Balducci, *Mov Disord* **2016**.

[42] A. Deshpande, E. Mina, C. Glabe and J. Busciglio, *The Journal of neuroscience* **2006**, *26*, 6011-6018.

[43] C. G. Glabe, *Neurobiol Aging* **2006**, *27*, 570-575.

[44] M. A. Lovell, J. D. Robertson, W. J. Teesdale, J. L. Campbell and W. R. Markesbery, *Journal of the Neurological Sciences* **1998**, *158*, 47-52.

[45] A. Tiiman, P. Palumaa and V. Tõugu, *Neurochemistry International* **2013**, *62*, 367-378.

[46] P. Faller, C. Hureau and O. Berthoumieu, *Inorganic Chemistry* **2013**, *52*, 12193-12206.

[47] H. Bayir, *Critical care medicine* **2005**, *33*, S498-S501.

[48] P. Faller, C. Hureau and G. La Penna, *Accounts of chemical research* **2014**, *47*, 2252-2259.

[49] S. S. Leal, H. M. Botelho and C. M. Gomes, *Coordination Chemistry Reviews* **2012**, *256*, 2253-2270.

[50] R. Roychaudhuri, M. Yang, M. M. Hoshi and D. B. Teplow, *Journal of Biological Chemistry* **2009**, *284*, 4749-4753.

[51] A. A. Reinke and J. E. Gestwicki, *Chemical biology & drug design* **2011**, *77*, 399-411.

[52] M. Biancalana and S. Koide, *Biochimica et Biophysica Acta* **2010**, *1804*, 1405-1412.

[53] H. Kozlowski, M. Luczkowski, M. Remelli and D. Valensin, *Coordination Chemistry Reviews* **2012**, *256*, 2129-2141.

[54] C. Migliorini, E. Porciatti, M. Luczkowski and D. Valensin, *Coordination Chemistry Reviews* **2012**, *256*, 352-368.

[55] V. Tõugu and P. Palumaa, *Coordination Chemistry Reviews* **2012**, *256*, 2219-2224.

[56] B. Alies, A. Conte-Daban, S. p. Sayen, F. Collin, I. Kieffer, E. Guillon, P. Faller and C. Hureau, *Inorganic Chemistry* **2016**, *55*, 10499-10509.

[57] C. Hureau and P. Dorlet, *Coordination Chemistry Reviews* **2012**, *256*, 2175-2187.

[58] C. Hureau, *Coordination Chemistry Reviews* **2012**, *256*, 2164-2174.

[59] I. Zawisza, M. Rózga and W. Bal, *Coordination Chemistry Reviews* **2012**, *256*, 2297-2307.

[60] P. Dorlet, S. Gambarelli, P. Faller and C. Hureau, *Angewandte Chemie International Edition* **2009**, *48*, 9273-9276.
[61] C. Hureau, Y. Coppel, P. Dorlet, P. L. Solari, S. Sayen, E. Guillon, L. Sabater and P. Faller, *Angewandte Chemie International Edition* **2009**, *48*, 9522-9525.
[62] S. C. Drew, C. L. Masters and K. J. Barnham, *Journal of the American Chemical Society* **2009**, *131*, 8760-8761.
[63] S. C. Drew and K. J. Barnham, *Accounts of Chemical Research* **2011**, *44*, 1146-1155.
[64] S. C. Drew, C. J. Noble, C. L. Masters, G. R. Hanson and K. J. Barnham, *Journal of the American Chemical Society* **2009**, *131*, 1195-1207.
[65] B. Alies, H. Eury, C. Bijani, L. Rechignat, P. Faller and C. Hureau, *Inorganic Chemistry* **2011**, *50*, 11192-11201.
[66] C. Hureau, V. Balland, Y. Coppel, P. L. Solari, E. Fonda and P. Faller, *Journal of Biological Inorganic Chemistry* **2009**, *14*, 995-1000.
[67] J. Shearer and V. A. Szalai, *Journal of the American Chemical Society* **2008**, *130*, 17826-17835.
[68] R. A. Himes, G. Y. Park, A. N. Barry, N. J. Blackburn and K. D. Karlin, *Journal of the American Chemical Society* **2007**, *129*, 5352-5353.
[69] R. A. Himes, G. Y. Park, G. S. Siluvai, N. J. Blackburn and K. D. Karlin, *Angewandte Chemie International Edition* **2008**, *47*, 9084-9087.
[70] Y. Lu, M. Prudent, L. Qiao, M. A. Mendez and H. H. Girault, *Metallomics* **2010**, *2*.
[71] B. Alies, B. Badei, P. Faller and C. Hureau, *Chemistry – A European Journal* **2012**, *18*, 1161-1167.
[72] H. A. Feaga, R. C. Maduka, M. N. Foster and V. A. Szalai, *Inorganic Chemistry* **2011**, *50*, 1614-1618.
[73] T. R. Young, A. Kirchner, A. G. Wedd and Z. Xiao, *Metallomics* **2014**, *6*, 505-517.
[74] T. Devasagayam, J. Tilak, K. Boloor, K. S. Sane, S. S. Ghaskadbi and R. Lele, *Japi* **2004**, *52*, 4.
[75] M. Gardès-Albert and D. Jore, *Aspects physicochimiques des radicaux libres centrés sur l'oxygène*, pp. 6-23, in *Radicaux libres et stress oxydant : aspects biologiques et pathologiques*, J. Delattre, J.-L. Beaudeux and D. Bonnefont-Rousselot, Lavoisier, Paris, **2005**.
[76] B. H. Bielski, D. E. Cabelli, R. L. Arudi and A. B. Ross, *Journal of Physical and Chemical Reference Data* **1985**, *14*, 1041-1100.
[77] O. Iranzo, *Bioorganic chemistry* **2011**, *39*, 73-87.

[78] S. Signorella and C. Hureau, *Coordination Chemistry Reviews* **2012**, *256*, 1229-1245.
[79] L. M. Dorfman and G. E. Adams in *Reactivity of the hydroxyl radical in aqueous solutions*, *Vol.* DTIC Document, **1973**.
[80] P. Wardman, *Journal of Physical and Chemical Reference Data* **1989**, *18*, 1637-1755.
[81] W. R. Markesbery, *Free Radical Biology and Medicine* **1997**, *23*, 134-147.
[82] D. A. Butterfield, J. Drake, C. Pocernich and A. Castegna, *Trends in Molecular Medicine* **2001**, *7*, 548-554.
[83] B. Halliwell, *Journal of neurochemistry* **2006**, *97*, 1634-1658.
[84] M. Nakamura, N. Shishido, A. Nunomura, M. A. Smith, G. Perry, Y. Hayashi, K. Nakayama and T. Hayashi, *Biochemistry* **2007**, *46*, 12737-12743.
[85] M. A. Smith, P. L. Harris, L. M. Sayre and G. Perry, *Proceedings of the National Academy of Sciences* **1997**, *94*, 9866-9868.
[86] F. Bousejra-ElGarah, C. Bijani, Y. Coppel, P. Faller and C. Hureau, *Inorganic Chemistry* **2011**, *50*, 9024-9030.
[87] L. Guilloreau, S. Combalbert, A. Sournia-Saquet, H. Mazarguil and P. Faller, *Chembiochem* **2007**, *8*, 1317-1325.
[88] R. C. Nadal, S. E. J. Rigby and J. H. Viles, *Biochemistry* **2008**, *47*, 11653-11664.
[89] R. Baruch-Suchodolsky and B. Fischer, *Biochemistry* **2008**, *47*, 7796-7806.
[90] C. Hureau and P. Faller, *Biochimie* **2009**, *91*, 1212-1217.
[91] S. Chassaing, F. Collin, P. Dorlet, J. Gout, C. Hureau and P. Faller, *Current Topics in Medicinal Chemistry* **2012**, *12*, 2573-2595.
[92] S. I. Dikalov, M. P. Vitek and R. P. Mason, *Free Radical Biology and Medicine* **2004**, *36*, 340-347.
[93] K. Reybier, S. Ayala, B. Alies, J. V. Rodrigues, S. Bustos Rodriguez, G. La Penna, F. Collin, C. M. Gomes, C. Hureau and P. Faller, *Angewandte Chemie. International Ed. In English* **2016**, *55*, 1085-1089.
[94] V. Balland, C. Hureau and J.-M. Saveant, *Proceedings of the National Academy of Sciences of the United States of America* **2010**, *107*, 17113-17118.
[95] L.-E. Cassagnes, V. Hervé, F. Nepveu, C. Hureau, P. Faller and F. Collin, *Angewandte Chemie International Edition* **2013**, *52*, 11110-11113.
[96] G. La Penna, C. Hureau, O. Andreussi and P. Faller, *Journal of Physical Chemistry B* **2013**, *117*, 16455-16467.

[97] J. Näslund, A. Schierhorn, U. Hellman, L. Lannfelt, A. D. Roses, L. O. Tjernberg, J. Silberring, S. E. Gandy, B. Winblad and P. Greengard, *Proceedings of the National Academy of Sciences* **1994**, *91*, 8378-8382.
[98] E. R. Stadtman and R. L. Levine, *Amino Acids* **2003**, *25*, 207-218.
[99] E. Stadtman, *Annual Review of Biochemistry* **1993**, *62*, 797-821.
[100] E. R. Stadtman, *Methods in Enzymology* **1995**, *258*, 379-393.
[101] D. Bonnefont-Rousselot, J.-L. Beaudeux and J. Delattre, *Oxydation des acides aminés et des protéines*, pp. 147-167, in *Radicaux libres et stress oxydant : aspects biologiques et pathologiques*, J. Delattre, J.-L. Beaudeux and D. Bonnefont-Rousselot, Lavoisier, Paris, **2005**.
[102] C. Schöneich and T. D. Williams, *Chemical Research in Toxicology* **2002**, *15*, 717-722.
[103] K. Inoue, C. Garner, B. L. Ackermann, T. Oe and I. A. Blair, *Rapid Communications in Mass Spectrometry* **2006**, *20*, 911-918.
[104] T. Kowalik-Jankowska, M. Ruta, K. Wiśniewska, L. Łankiewicz and M. Dyba, *Journal of Inorganic Biochemistry* **2004**, *98*, 940-950.
[105] C. Schöneich, *Journal of Pharmaceutical and Biomedical Analysis* **2000**, *21*, 1093-1097.
[106] K. Inoue, A. Nakagawa, T. Hino and H. Oka, *Analytical Chemistry* **2009**, *81*, 1819-1825.
[107] C. S. Atwood, G. Perry, H. Zeng, Y. Kato, W. D. Jones, K.-Q. Ling, X. Huang, R. D. Moir, D. Wang, L. M. Sayre, M. A. Smith, S. G. Chen and A. I. Bush, *Biochemistry* **2004**, *43*, 560-568.
[108] A. P. Gunn, B. R. Roberts and A. I. Bush, *Rapid Generation of Dityrosine Cross-linked Aβ Oligomers via Cu-Redox Cycling*, pp. 3-10, in *Amyloid Proteins*, E. M. Sigurdsson, M. Calero and M. Gasset, Humana Press, Totowa, NJ, **2012**.
[109] Y. K. Al-Hilaly, T. L. Williams, M. Stewart-Parker, L. Ford, E. Skaria, M. Cole, W. G. Bucher, K. L. Morris, A. A. Sada and J. R. Thorpe, *Acta neuropathologica communications* **2013**, *1*.
[110] K. J. Barnham, F. Haeffner, G. D. Ciccotosto, C. C. Curtain, D. Tew, C. Mavros, K. Beyreuther, D. Carrington, C. L. Masters, R. A. Cherny, R. Cappai and A. I. Bush, *FASEB Journal* **2004**, *18*, 1427-1429.
[111] F. E. Ali, K. J. Barnham, C. J. Barrow and F. Separovic, *Journal of Inorganic Biochemistry* **2004**, *98*, 173-184.
[112] J. Moskovitz, *Austin J Pharmacol Ther* **2014**, *2*, 3.

[113] C. Schöneich, D. Pogocki, G. L. Hug and K. Bobrowski, *Journal of the American Chemical Society* **2003**, *125*, 13700-13713.
[114] C. Schöneich, *Biochimica et Biophysica Acta* **2005**, *1703*, 111-119.
[115] D. A. Butterfield and R. Sultana, *Journal of amino acids* **2011**, *2011*.
[116] F. E. Ali, F. Separovic, C. J. Barrow, R. A. Cherny, F. Fraser, A. I. Bush, C. L. Masters and K. J. Barnham, *Journal of Peptide Science* **2005**, *11*, 353-360.
[117] J. Kanski, S. Varadarajan, M. Aksenova and D. A. Butterfield, *Biochimica et Biophysica Acta, Molecular Basis of Disease* **2002**, *1586*, 190-198.

Chapter II

Chapter II: Methodologies

This chapter is a summary of the experimental conditions and techniques implemented for the studies presented throughout the manuscript. For each spectroscopic technique, the general principles are defined and the application of the technique to our study is described as well as the corresponding experimental conditions.

II.A. Preparation of the Aβ peptide

II.A.1. Solubilisation and monomerization

All the peptides are commercially available, in the form of powder (purchased from Genecust, Luxembourg, purity grade >95%). The shorter $A\beta_{16}$ and $A\beta_{28}$ peptides are weighed and solubilized in water, resulting in an acidic solution due to the presence of trifluoroacetate as counterion in the powder (pH 2). For the full-length peptide $A\beta_{40}$ which is subject to aggregation, the solution is prepared freshly. The powder is solubilized in NaOH 50 mM, resulting in a basic solution (pH 13) to remove preformed aggregates and slow down the aggregation, and further purified *via* Fast Protein Liquid Chromatography (FPLC) when used for aggregation studies (see Section II.A.4).

II.A.2. Dosage [1]

Usually, the Aβ peptide powder commercially available contains an unknown quantity of counterions (such as trifluoroacetate) and the dosage by weight is not precise. Thus, the dosage is performed by UV-Visible spectroscopy by using the absorption of Tyr10. The pH of each solution was taken into account as deprotonation of Tyr at high pH induces a change in the UV spectra obtained (Figure II.A-1).

For the UV-Visible dosage, the Tyr10 is considered as a free tyrosine amino acid residue. As the peptide can aggregate, a little light scattering can occur and has to be taken into account. Thus, to avoid an overestimation of the concentration, a correction is made by subtracting the background absorbance to the maximum of absorbance of Tyr.

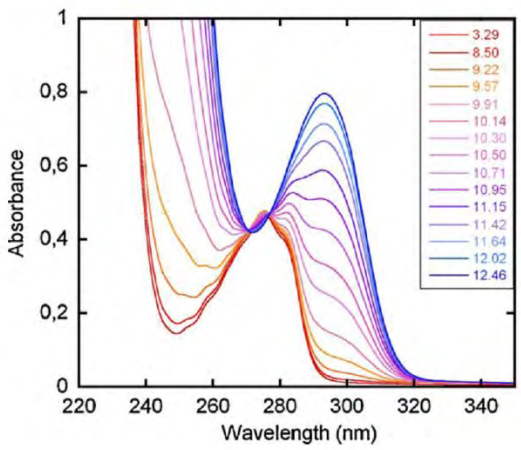

Figure II.A-1: pH titration of Tyr in $A\beta_{16}$ (0.3 mM). UV-vis absorption spectrum from tyrosine band (red) to tyrosinate band (blue). Picture from reference [1].

At low pH (until pH 8.5 according to Figure II.A-1), Tyr10 in the Aβ peptide has a maximum of absorbance at 276 nm and is corrected with the absorbance at 296 nm with an extinction coefficient of ε_{276}-ε_{296}=1410 $M^{-1}.cm^{-1}$.[1] At higher pH, the dosage has to be realized around pH 13, where only the deprotonated form of Tyr is present. Tyrosinate has a maximum of absorbance at 293 nm and is corrected by the absorbance at 360 nm with an extinction coefficient of ε_{293}-ε_{360}=2400 $M^{-1}.cm^{-1}$.[1]

For mutant or shorter peptides without Tyr (i.e. Y10F-Aβ or $A\beta_{1-7}$), the dosage was performed *via* phenylalanine absorption (ε_{258}-ε_{280}=195 $M^{-1}.cm^{-1}$ for one Phe).[2] More details about UV-visible spectroscopy are given in Section II.C.1.

II.A.3. Oxidation and purification of Aβ

The metal-catalyzed oxidation of Aβ is carried out at 60 µM of $A\beta_{28}$ or $A\beta_{40}$ with 50 µM of $CuSO_4$ and 0.5 mM of ascorbate in 50 mM of phosphate buffer at pH 7.4, under air atmosphere. The reaction occurs during 30 min under stirring and is completed when the ascorbate has fully reacted. Then, the solution is concentrated by centrifugation with Amicon Ultra 3 kDa membrane (Millipore), washed with Ethylenediaminetetraacetic acid (EDTA) (10 equivalents) to remove copper, then with water and finally with a NaOH (50 mM, pH ≈ 13) solution. The oxidized peptide solution is recovered and the concentration is determined by UV-visible absorption of Tyr10, considered as free tyrosine ((ε_{293}-ε_{360}) = 2400 $M^{-1}cm^{-1}$) in NaOH (50 mM, resulting pH ≈ 13). As the oxidized peptide solution has a background absorbance at 293 nm from an unknown origin, the curve is fitted to subtract the absorbance

due to the tailing (Figure II.A-2). The $A\beta_{28}$ peptide was used instead of $A\beta_{16}$ for technical reasons (membrane cut-off of 3 kDa).

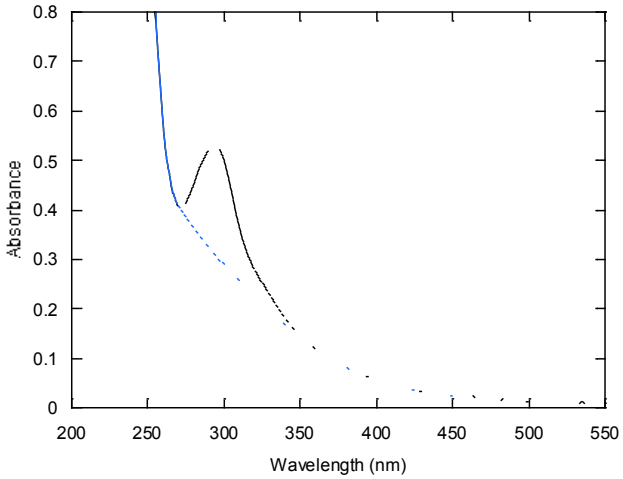

Figure II.A-2: UV-Vis spectrum of oxidized $A\beta_{28}$ (black curve) and fit (blue curve) to subtract the background absorbance from Tyr absorbance.

II.A.4. Preparation for aggregation

Aggregation studies are carried out with the full-length $A\beta_{40}$ peptide which is physiologically relevant and more prone to aggregation than the truncated $A\beta_{16}$ and $A\beta_{28}$ peptides. The full-length $A\beta_{40}$ has to be as much as possible in monomeric form at the beginning of the aggregation study. Thus, after their solubilisation in NaOH 50 mM (see Section II.A.1), the oxidized and non-oxidized $A\beta_{40}$ peptides are purified by FPLC to separate the monomeric from the oligomeric forms. The chromatography is carried out during 50 min with a Superdex 75 (10 x 300 mm) column in NaOH 15 mM as eluent. The collected fractions (500 µL) are then dosed by absorption of Tyr10 at high pH (see Section II.A.2) and used as it in the day.

The conditions for aggregation studies monitored by fluorescence will be further described in Section II.D.3.

II.B. Mass spectrometry

II.B.1. General principles

Mass spectrometry (MS) is an analytical technique which measures the mass of the molecules/atoms present in a sample. After ionization of the molecules in the gas phase, the ions are sorted on the basis of their mass-to-charge ratio (m/z), by subjecting them to an electric and/or magnetic field.

A mass spectrometer is composed of:

- An ion source which produces gas-phase ions from the molecules of the studied sample
- A mass analyzer whose goal is to sort the ions based on their m/z value ratio.
- A detector that provides an electric signal related to the number of detected ions.
- A data processing system (IT) to obtain a mass spectrum with the intensity given as a function of m/z.

All the results presented in this manuscript were obtained on mass spectrometers equipped with electrospray ionization (ESI) and ion trap.

II.B.2. Electrospray Ionization (ESI)

The electrospray ionization (ESI) is an atmospheric pressure ionization process developed by J.B. Fenn (Nobel Prize in Chemistry 2002) in 1984.[3] ESI is considered as a soft ionization technique as little fragmentations are obtained in the source. Its main advantage is to directly generate ions in gaseous phase from solution, under atmospheric pressure. This technique was first dedicated to proteins studies as it may produce multiple charged ions from large molecules owning several ionizable sites, thus improving the sensitivity and extending the mass range of the analyzer for the study of high molecular weight molecules such as proteins and peptides. Nowadays, ESI is also used for the study of smaller molecules. The principle of electrospray ionization is illustrated in Figure II.B-1.

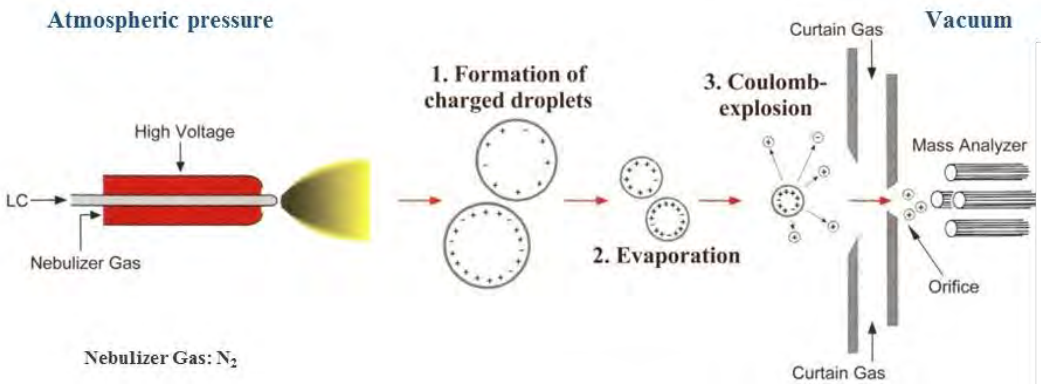

Figure II.B-1: Principle of electrospray ionization.

The liquid sample is infused at low flow rate (usually 1 to 100 $\mu L.min^{-1}$) through a capillary subjected to a high electric field, the latter being obtained by the application of a voltage difference (3.0 to 6.0 kV) between the capillary and a surrounding counter-electrode.[4] A constant flow of inert gas (nebulizer gas, usually N_2) move along the tube containing the capillary. At the end of the capillary, a spray is formed *via* the Tailor cone originated from the high voltage applied on the capillary. The sample is turned into charged micro-droplets in suspension. Those droplets are moving towards the counter-electrode and the solvent of the droplets evaporate, leading to smaller droplets. Afterwards, the charge density of the droplet becomes too high and the gas-phase ions are released during the Coulomb-explosion. The ions produced are then transported to the analyzer.

In ESI, the ions obtained can be cations or anions, generated by protonation or deprotonation of the molecules, respectively. As explained above, for molecules with several ionizable sites, the formation of multiple charged ions can occur, by addition/removal of several protons on the same molecule. Usually, the ions are either under the form $[M + nH]^{n+}$ in positive mode or $[M - nH]^{n-}$ in negative mode, where n is the number of protons. They are observed at the mass M+1 or M-1 for monocharged ions or more generally at the mass (M+n)/n or (M-n)/n for n-times charged ions. Thus, the technique is not suitable for molecules without protonation sites such as apolar compounds. Other types of ions can be detected such as sodium ($[M + Na]^+$) or potassium ($[M + K]^+$) adducts and in some cases, ammonium adduct $[M + NH_4]^+$. Furthermore, it is likely to detect dimers that are due to the bridging of two monomers by a proton (or Na^+/K^+). Those dimers are under the form $[M\cdots H\cdots M]^+$ or $[M\cdots H\cdots M]^-$ and observed at the mass 2M+1 or 2M-1 for monocharged ions.

II.B.3. Ion trap

a. Principle

In 1960, W. Paul (Nobel Prize in Physics 1989) and H. Steinwedel [5] described an ion trap which has been used for the mass spectrometry for the first time in 1984 by Stafford and his colleagues.[6] This analyzer selects ions in the ion flow arriving from the ion source and send them to the detector by deflecting them through an electric field. The ion trap consists of two hyperbolic electrodes called endcap electrodes and a hyperbolic ring electrode between them (Figure II.B-2).

Ions come through the entrance endcap electrode and are trapped in the ion trap center by an oscillating electric field that plays on the ion trajectory, allowing to isolate the ion into the trap or to eject it towards the detector. Actually, an appropriate variation of the electric field allows to specifically destabilized the ion trajectory in order to eject the ions one by one. This oscillating electric field originates from alternating voltages applied on the endcap electrodes (negative voltage) and on the ring electrode (positive voltage).

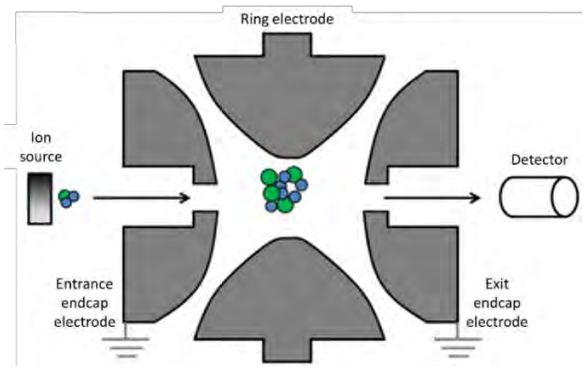

Figure II.B-2: Schematic representation of an ion trap.

The ion trap also allows to isolate specific ions, to fragment them and then to detect the fragment ions. This mode of operation is called tandem mass spectrometry (MS/MS or MS^2). Because fragment ions are trapped prior to be detected, another possibility is to isolate one of them and to fragment it: in this case, the mode of operation is MS/MS/MS or MS^3. This can be repeated several times (up to 10 on most of the commercially available spectrometers) and is called MS^n process (Figure II.B-3). However, for each additional fragmentation, a little part of the ions is lost in the trap and the ions detected are less intense and the technique is less sensitive.

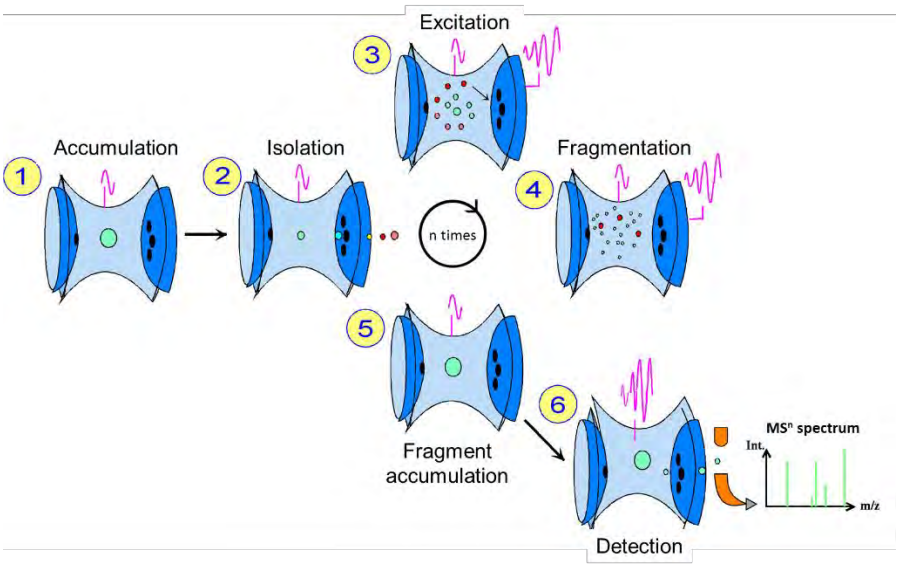

Figure II.B-3: Schematic view of the ion trap operation for successive fragmentation mode (MS^n).

After its accumulation and isolation in the ion trap, the ion is excited: a kinetic energy of the order of a few tens of eV is provided to make it resonate. With this energy, the ion collides with neutral atoms (helium) present in the trap and acquires an internal energy, resulting in bond breakage and leading to its fragmentation in smaller fragment ions. This type of fragmentation is known as Collision Induced Dissociation (CID).

b. Orbitrap [7]

The orbitrap, described in 2000 by Makarov [8] and marketed since 2005, is an ion trap analyzer composed of an inner spindle-shaped electrode and an outer barrel-shaped electrode, both subjected to a direct voltage. The ions are injected tangentially into the field, trapped in the orbitrap and they adopt an orbital motion around the spindle-shaped electrode. The specific geometry of the trap and the electrostatic attraction towards the inner electrode, compensated by the ions inertia, force the ions to cycle around the inner electrode in complex spiral patterns (Figure II.B-4, red arrow). The axial component of the resulting oscillations is independent of initial parameters of ions such as initial kinetic energy of injected ions. However, its frequency is proportional to $(m/z)^{-1/2}$. Thus, the axial oscillations of the ion are detected as an image current induced in the outer electrode and transformed into mass spectra using Fourier Transform. The orbitrap delivers low-ppm mass accuracy with high resolution (up to 150 000 for ions produced by laser ablation) and is thus employed to do High-Resolution Mass Spectrometry (HRMS).

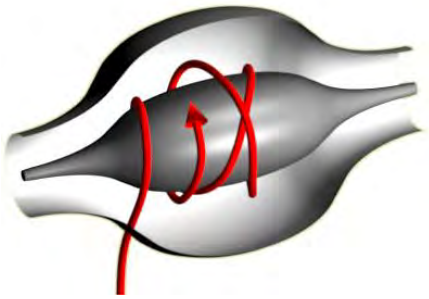

Figure II.B-4: Schematic view of the orbitrap. The red arrow shows the complex spiral trajectory of the ion around the inner electrode.

c. Tandem Mass Spectrometry (MS/MS) applied to proteomic analysis

The outbreak of electrospray ionization (ESI) has been a great advance for the study of biomolecules such as proteins by mass spectrometry. Furthermore, its combination with MS/MS allows to do proteomic analysis, consisting of the characterization of protein sequences. This technique is based on the controlled fragmentation of proteins/peptides leading to the

breakage of the peptide bonds of the protein. The protein/peptide fragmentation generates a series of ions of increasing mass, the mass difference between them being equal to the mass of the amino acid residues of the protein. Depending on the nature of the fragmentation, different ions can be formed and, whether the charge is carried by the N-terminal or by the C-terminal fragment, series of ions (a, b and/or c) and (x, y and/or z) are generated respectively (Figure II.B-5), according to the nomenclature of Biemann.[9]

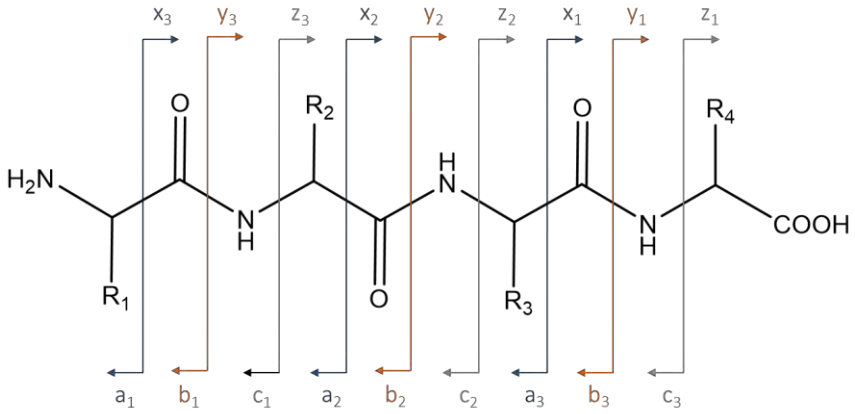

Figure II.B-5: Schematic view of the possible fragmentations undergone by a polypeptide chain.[9]

In the ion trap we used for our studies, the fragmentation occurs by CID leading to the peptide bond breakage and thus mainly to the formation of b and y ions (Figure II.B-5, orange arrows). By detecting and combining the series of ions, the sequence of the protein/peptide can be determined.

II.B.4. Analysis of Aβ by MS and MS/MS

a. MS/MS

Tandem Mass Spectrometry is a relevant tool for protein/peptide sequencing. It can also provide information and allow for identification of a modified amino acid residue in a polypeptide chain, since any modification will affect the masses of the corresponding b and y ions. Thus, the characterization of the oxidation sites of the Aβ peptide can be carried out by analyzing the oxidized peptide by MS/MS (usually coupled to liquid chromatography, LC-MS/MS), the b and y ions detected providing information about a mass shift on one amino acid residue of the sequence, related to its oxidation. However, CID fragmentation is usually less efficient as the mass of the molecule increases and the direct fragmentation of the whole $A\beta_{40}$ peptide (top-down fragmentation) did not provide reliable results with the spectrometer we

used. Thus, a proteolytic digestion was realized in order to cleave the Aβ peptide into smaller peptides, more easily fragmented (bottom-up fragmentation). Trypsin was chosen for digestion and cleaves peptides at the carboxyl side of the lysine or arginine residues, except when they are followed by a proline residue. The four tryptic peptides obtained from $A\beta_{40}$ digestion by trypsin are shown in Figure II.B-6, and their monoisotopic masses (m/z) used for their detection are listed in Table II.B-1

Table II.B-1 along with the ones of the $A\beta_{16}$, $A\beta_{28}$ and $A\beta_{40}$ peptides. A complete table listing the monoisotopic masses of the peptides studied as well as their oxidized counterparts is shown in Annex I.

Figure II.B-6: Sequence of the four tryptic peptides obtained after the $A\beta_{40}$ digestion by trypsin.

Table II.B-1: Monoisotopic apparent masses (m/z) of mono- and multi-protonated ions of $A\beta_{40}$, $A\beta_{28}$, $A\beta_{16}$ and the tryptic peptides ($A\beta_{1-5}$, $A\beta_{6-16}$, $A\beta_{17-28}$ and $A\beta_{29-40}$).

Name	Sequence	$[M+H]^+$	$[M+2H]^{2+}$	$[M+3H]^{3+}$	$[M+4H]^{4+}$	$[M+5H]^{5+}$
$A\beta_{40}$	DAEFRHDSGYEVHHQKLVFFAEDVGSNKGAIIGLMVGGVV	4328.1561	2164.5820	1443.3906	1082.7949	866.4375
$A\beta_{28}$	DAEFRHDSGYEVHHQKLVFFAEDVGSNK	3261.5353	1631.2716	1087.8503	816.1397	653.1133
$A\beta_{16}$	DAEFRHDSGYEVHHQK	1954.8796	977.9437	652.2984	489.4758	391.7822
$A\beta_{1-5}$	DAEFR	637.2945	319.1512	213.1034	160.0795	128.2652
$A\beta_{6-16}$	HDSGYEVHHQK	1336.6034	668.8056	446.2064	334.9067	268.1269
$A\beta_{17-28}$	LVFFAEDVGSNK	1325.6741	663.3410	442.5633	332.1744	265.9411
$A\beta_{29-40}$	GAIIGLMVGGVV	1085.6392	543.3235	362.5516	272.1657	217.9341

LC-MS and LC-MS/MS conditions

High Performance Liquid Chromatography / Mass Spectrometry (LC/MS) analysis was performed on an ion-trap mass spectrometer (LCQ DECA XP Max, ThermoFisher), equipped with an electrospray ionization source, coupled to an Ultimate 3000 LC System (Dionex, Voisins-le-Bretonneux, France). Samples (10 µL) at 60 µM of Aβ were injected onto the column (Acclaim 120 C18, 50 × 3 mm, 3 µm, ThermoScientific), at room temperature. The gradient elution was carried out with formic acid 0.1% (mobile phase A) and acetonitrile/water (80/20 v/v) formic acid 0.1% (mobile phase B) at a flow-rate of 0.5 $mL.min^{-1}$. The mobile phase gradient was programmed with the following time course: 5% mobile phase B at 0 min, held 3

minutes, linear increase to 55% B at 8 min, linear increase to 100% of B at 9 min, held 2 min, linear decrease to 5% B at 12 min and held 3 min. The mass spectrometer was used as a detector, working in the full scan positive mode between 150 and 2000 Da followed by data dependent scans of the two first most intense ions, with dynamic exclusion enabled. Isolation width was set at 1 Da and collision energy at 28% (units as given by the manufacturer), using wideband activation. The generated tandem MS data was searched using the SEQUEST algorithm against the human Aβ peptide sequence.

Conditions of tryptic digestion

The 100 µL solution of Aβ was filtered by using Amicon 3 kDa centrifugal device (Millipore) by centrifugation for 15 min at 13500 rpm, then washed and centrifuged twice with 200 µL sodium hydrogenocarbonate (100 mM, pH 8.0). The concentrated sample (approx. 50 µL) was recovered and transferred to an Eppendorf Protein LoBind 1.5 mL vial. Trypsin (0.05 µg/µL in formic acid 0.1%) was added to obtain a Aβ/trypsin ratio of 20/1 (w/w) and digestion was carried out at 37°C for 3h in a Thermomixer (Eppendorf), 10 s mixing at 750 rpm every minutes.

b. High-Resolution Mass Spectrometry (HRMS)

HRMS is a powerful tool to characterize molecules and biomolecules as it provides the exact mass of the ion related to them, thus allowing to differentiate two molecules of close masses. In our studies, HRMS was used: (i) to identify some of the oxidized amino acid residues of Aβ, (ii) to get the chromatographic traces of some specific ions of Aβ and associated peptides, thus allowing to perform relative quantification. HRMS was also used to check for digestion efficiency, systematically found close to 100 % (non-digested peptide not detected).

LC-HRMS conditions for the characterization of the oxidation sites of $A\beta_{40}$

The same operating conditions than for LC-MS (column and mobile phase gradient) were used to carry out high resolution mass spectrometry (LC/HRMS) experiments, by using a LTQ-Orbitrap XL mass spectrometer (ThermoFisher Scientific, Les Ulis, France) coupled to an Ultimate 3000 LC System (Dionex, Voisins-le-Bretonneux, France). The Orbitrap cell was operated in the full-scan mode at a resolution power of 60 000.

LC-HRMS conditions for the kinetics study of $A\beta_{40}$ oxidation

High Performance Liquid Chromatography / High Resolution Mass Spectrometry (LC/HRMS) analysis was performed on a LTQ-Orbitrap XL mass spectrometer (ThermoFisher Scientific, Les Ulis, France) coupled to an Ultimate 3000 LC System (Dionex, Voisins-le-Bretonneux, France). Sample (10 µL of Aβ tryptic digest) was injected onto the column (Phenomenex, Synergi Fusion RP-C18, 250 × 1 mm, 4 µm), at room temperature. Gradient elution was carried out with formic acid 0.1% (mobile phase A) and acetonitrile/water (80/20 v/v) formic acid 0.1% (mobile phase B) at a flow-rate of 50 $\mu L.min^{-1}$. The mobile phase gradient was programmed with the following time course: 12% mobile phase B at 0 min, held 3 minutes, linear increase to 100% B at 15 min, held 4 min, linear decrease to 12% B at 20 min and held 5 min. The mass spectrometer was used as a detector, the Orbitrap cell operating in the full-scan mode at a resolution power of 60 000.

II.C. UV-Visible spectroscopy

II.C.1. General principles

The UV-Visible spectroscopy (UV-Vis) is a technique applied to measure the light absorbance by a compound in the ultraviolet-visible spectral region. This region can be divided into three wavelength ranges: near UV (185-400 nm), visible (400-700 nm) and very-near infrared (700-1100 nm). Usually, the absorbance is not measured below 190 nm since dioxygen, water vapor and the quartz cuvettes used for the measurements absorb and thus disturb the measure.

The absorbance originates from the interaction of the photons of the light with the electrons of the bonds of the species present in the sample (such as molecules). Molecules with π-electrons or non-binding electrons (n-electrons) are susceptible to absorb in UV-Vis.

A spectrophotometer is composed of a light source (usually a combination of a deuterium lamp for the UV range (< 350 nm) and a tungsten filament for visible range (> 350 nm)), a dispersive system to select the wavelength, a space for the sample (usually in a cuvette) and a detector which converts the light detected into an electric signal. The selection of the wavelengths can be realized either (i) by a monochromator setup that isolates the different wavelengths of the light and introduce each monochromatic light into the sample or (ii) by a photodiode array (PDA) detector that detects the different wavelengths of the light passed through the sample after its dispersion by a spectrograph.

Figure II.C-1 is a schematic representation of an UV-Vis experiment. The UV-Vis light (or beam) with an initial intensity I_0 is created at the light source and goes through the sample. Upon light excitation, the energy given by the absorbed photon allows the transition of an electron from its ground state to an excited state. This energy has to correspond to the energy of permitted transitions (Figure II.C-1, green arrow in energy level diagram). Then, the light exiting from the sample with a transmitted intensity I_t is analyzed at the detector. An UV-Vis spectrum is obtained with absorption or transmission of the light (see definitions beyond) as a function of the wavelength.

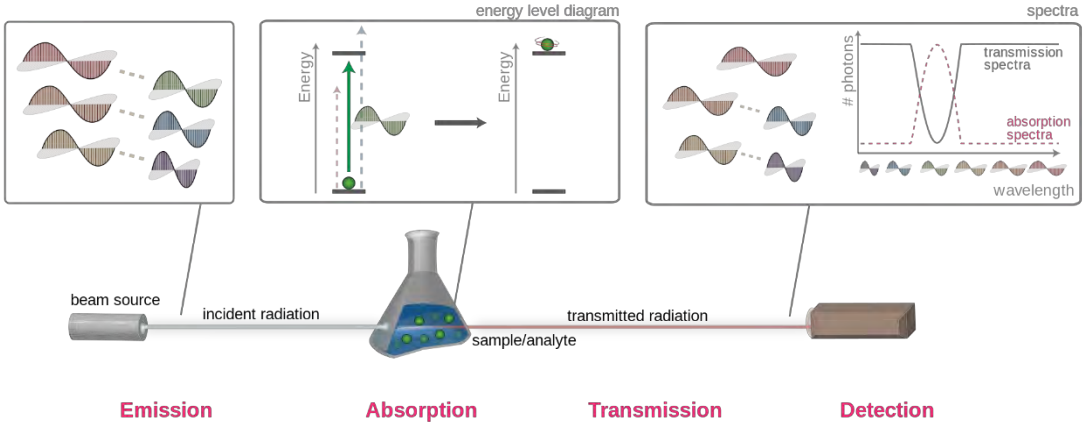

Figure II.C-1: A schematic view of an UV-Vis spectroscopy experiment.

As seen above, the detector converts the transmitted light into an electric signal. Two values can be extract from the data:

- the transmittance (T), defined as the transmitted intensity (I_t) over the initial intensity (I_0) ratio (Equation. II.C-1).

$$T = \frac{I_t}{I_0} \qquad \textbf{Equation. II.C-1}$$

- the absorbance (A), given by Equation. II.C-2.

$$A = -\log T \qquad \textbf{Equation. II.C-2}$$

UV-Vis can also be employed for quantitative analysis since the absorbance of the light can be directly related to the concentration of the compound in certain conditions defined by the Beer-Lambert law (Equation II.C-3).

$$A_\lambda = \varepsilon_\lambda . l . C \qquad \textbf{Equation II.C-3}$$

A_λ is the absorbance (no dimension), ε the molar extinction coefficient (in $L.mol^{-1}.cm^{-1}$), l the optical path length (in cm) and C is the concentration of the compound in solution (in $mol.L^{-1}$) for the wavelength λ where the measure is realized.

To be valid, the Beer-Lambert Law has to meet the following requirements [10]:

- A monochromatic light has to be used
- Low concentration of the compounds in the solution (A < 1, i.e. at least 10% of light is transmitted)
- Solution studied not fluorescent or heterogeneous
- No photochemical transformations of the compounds studied
- No interaction between the compounds studied and the solvent

The absorbance is an additive value. If for a given wavelength, two compounds 1 and 2 absorb, the total absorbance is equal to the sum of the absorbance of each compound, as given by Equation II.C-4.

$$\boldsymbol{A = A_1 + A_2 = l\,(\varepsilon_1.c_1 + \varepsilon_2.c_2)} \qquad \textbf{Equation II.C-4}$$

II.C.2. Ascorbate consumption

The Reactive Oxygen Species (ROS) produced by the Aβ/copper/ascorbate system can indirectly be monitored by ascorbate consumption. As discussed above (see Section I.C.2.b), ascorbate (Figure II.C-2a) gives an electron to reduce Cu(II)-Aβ and thus produce ROS. The decrease of ascorbate concentration can be monitored by UV-Visible spectroscopy as ascorbate has a maximal absorption in UV at 265 nm (Figure II.C-2b).

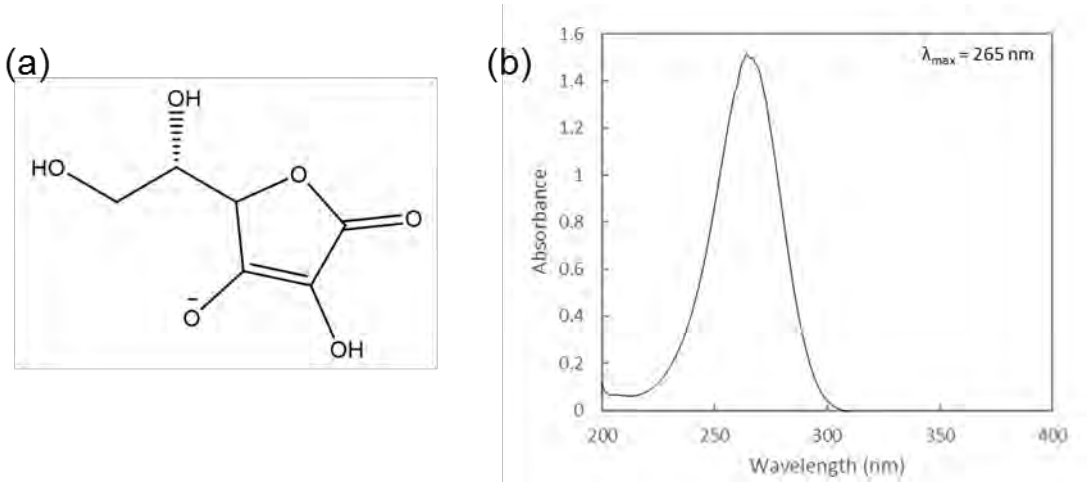

Figure II.C-2: (a) Structure of L-ascorbate anion and (b) UV-Visible spectrum of ascorbate (0.1 mM) in phosphate buffer (50 mM, pH 7.4) (right panel).

Ascorbate consumption conditions

Ascorbate consumption is monitored by UV-Visible spectroscopy at 265 nm in a 1 cm length cuvette containing a phosphate buffered solution (50 mM, pH 7.4) of Aβ (12 µM), $CuSO_4$ (10 µM) and ascorbate (100 µM). The ascorbate absorption is monitored every 10 s under shaking (800 rpm).

II.D. Fluorescence spectroscopy

II.D.1. General principles [10]

Fluorescence is an optical phenomenon that occurs usually on polyaromatic, plane or cyclic molecules named fluorophores. Upon a specific light excitation, they can re-emit light at a higher wavelength. The Jablonski diagram illustrates the fluorescence process (Figure II.D-1).

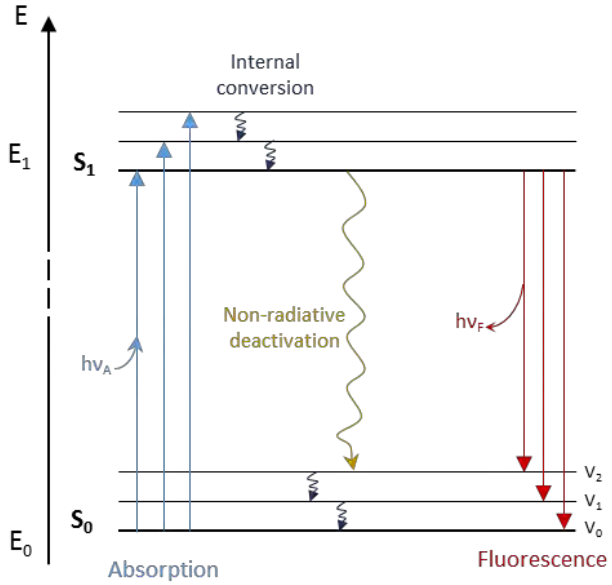

Figure II.D-1: Jablonski diagram.

When a molecule is submitted to a radiation ($h\nu_A$), a photon is absorbed and the electrons of the molecule move from the ground state S_0 to an excited state S_n ($n \geq 1$). For non-fluorescent molecules, the relaxation of the electron occurs *via* a non-radiative deactivation where the excitation energy is dissipated as heat. For fluorophores, the relaxation takes place *via* a radiative deactivation.

After the photon absorption, the molecule is in one of the vibrational states V_i of the excited state S_n. Upon intermolecular collisions, the electrons are relaxed to the V_0 level of S_n by a non-radiative internal conversion. A relaxation from the excited state S_n to S_{n-1} can also

occur by a non-radiative process. Thus, during the radiative deactivation, the emitted photon ($h\nu_F$) has usually a lower energy than the absorbed one ($h\nu_A$), resulting in a higher emitted wavelength. The difference between the positions of the band maxima of excitation and emission spectra is called Stokes shift (Figure II.D-2).

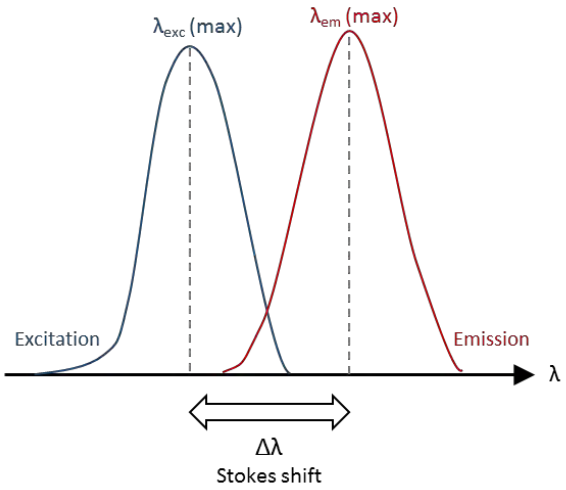

Figure II.D-2: Schematic spectrum of excitation (blue curve) and emission (red curve) of a fluorophore, highlighting the Stokes shift (difference between maximum wavelengths of emission and excitation).

A fluorophore is characterized by its excitation and emission wavelengths (Figure II.D-2) and by the quantum yield (Φ_f), the lifetime (τ) and the fluorescence intensity (I_f).

The quantum yield characterizes the efficiency of fluorescence compared with the other deactivation pathways for a given fluorophore. It is directly related to the ratio between the number of photons emitted and number of photons absorbed which is turned into the ratio of the fluorescence intensity (I_f) and the absorption intensity (I_a) (Equation II.D-1). The value of quantum yield is between 0 and 1, the best fluorophores having a quantum yield close to 1. Moreover, the quantum yield varies with the environment of the fluorophore such as concentration, pH and the nature of the solvent.

$$\boldsymbol{\Phi_f = \frac{number\ of\ photons\ emitted}{number\ of\ photons\ absorbed} = \frac{I_f}{I_a}} \qquad \textbf{Equation II.D-1}$$

The fluorescence lifetime (τ) corresponds to the time the fluorophore stays in the excited state before emitting a photon by radiative deactivation. The lifetime is dependent on the environment of the molecule. Usually, the lifetime of a fluorophore is in the nanosecond range.

The intensity of fluorescence emission of very weakly absorbing and diluted sample is directly related with its absorbance and thus with its concentration (Equation II.D-2).[10] This

relation allows to realized quantitative experiments, however it is important to establish the maximal concentration from which the fluorescence emission is not proportional to the concentration anymore.

$$I_f = 2.3\,\phi_f\,.\,I_0\,.\,A = 2.3\,\phi_f\,.\,I_0\,.\,\varepsilon\,.\,l\,.\,C \qquad \textbf{Equation II.D-2}$$

II.D.2. Fluorescence of 7-hydroxycoumarin-3-carboxylic acid

The hydroxyl radical scavenging was monitored with the fluorescence of the 7-hydroxycoumarin-3-carboxylic acid (7-OH-CCA, Figure II.D-3 right panel). This fluorescent probe is one of the oxidation products of the coumarin-3-carboxylic acid (CCA, Figure II.D-3 left panel) after reaction with the hydroxyl radical.[11]

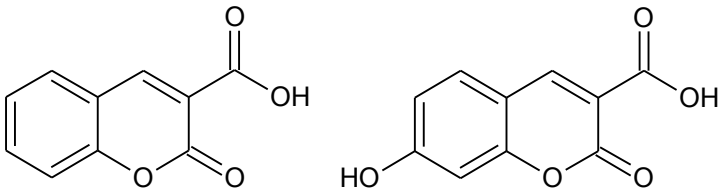

Figure II.D-3: Coumarin-3-carboxylic acid (left) and 7-hydroxycoumarin-3-carboxylic acid (right) structures.

7-OH-CCA is fluorescent at 450 nm upon excitation at 395 nm. The excitation and emission spectra of 7-OH-CCA are shown in Figure II.D-4.

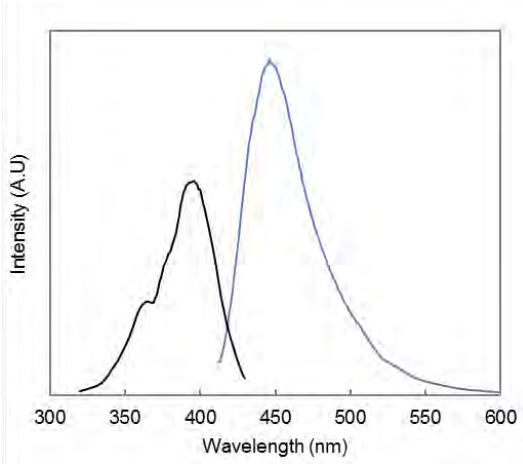

Figure II.D-4: Excitation spectrum (black curve, $\lambda_{emission}$ = 450 nm) and emission spectrum (blue curve, $\lambda_{excitation}$ = 395 nm) of the 7-hydroxycoumarin-3-carboxylic acid (50 µM) in phosphate buffer at pH 7.4.

In our experimental conditions, the fluorescence intensity is proportional to the number of 7-OH-CCA molecules formed, which in turn is proportional to the $HO^{\bullet}$ radicals trapped by CCA. Thus, monitoring 7-OH-CCA fluorescence gives information on the amount of $HO^{\bullet}$ radical exiting the Aβ/copper system, when ROS are produced in the presence of ascorbate.

The hydroxyl group of 7-OH-CCA has a pKa of 7.4 [11] and only the deprotonated form emits light at 450 nm. Thus, the pH has to be controlled very precisely during the experiments, especially since the experiments are performed at pH 7.4 in our studies.

7-OH-CCA Fluorescence conditions

The fluorescence of 7-OH-CCA is monitored at 450 nm upon excitation at 395 nm with a microplate reader, at 25°C. The microplate contains a phosphate buffered (50 mM, pH 7.4) solution of Aβ, with $CuSO_4$, and ascorbate or ascorbate and hydrogen peroxide (H_2O_2), depending on the studies.

II.D.3. Thioflavin T fluorescence

The Aβ peptide has the ability to aggregate into structured aggregates such as oligomers and fibrils (see Section I.B.4). The fibrils are known to be composed of β-sheet structures of the Aβ peptide.[12] To monitor the Aβ fibrillar formation, a fluorescent dye capable of interacting with β-sheet structures with a resulting enhanced fluorescence is commonly used: Thioflavin T (ThT).[13-14] ThT is a benzothiazole salt (Figure II.D-5a) used first as histological marker of amyloid fibrils and, due to its water solubility and its good affinity for fibrils (in the low µM range),[15] it was then used to monitor the aggregation process during *in vitro* experiments.

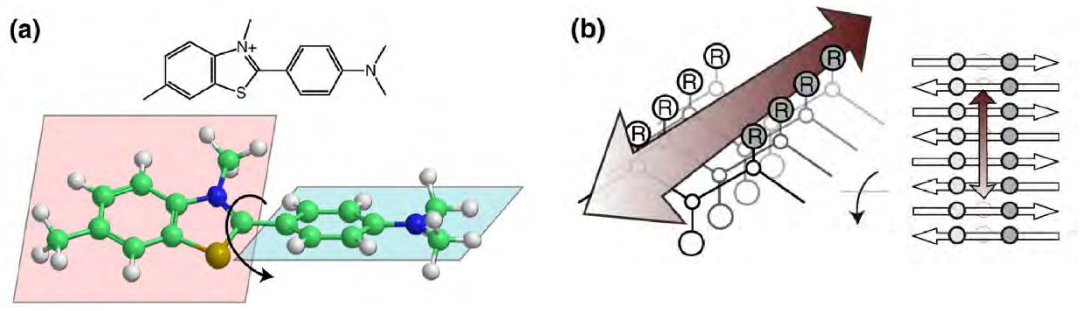

Figure II.D-5: (a) Structure of ThT (top) and representation of the rotation of the bond between the benzothiazole moiety (pink) and aniline moiety (blue) (bottom). (b) "Channel" model of ThT binding to fibril-like β-sheets. ThT is proposed to bind along surface side-chain grooves running parallel to the long axis of the β-sheet. Pictures from Reference [16]

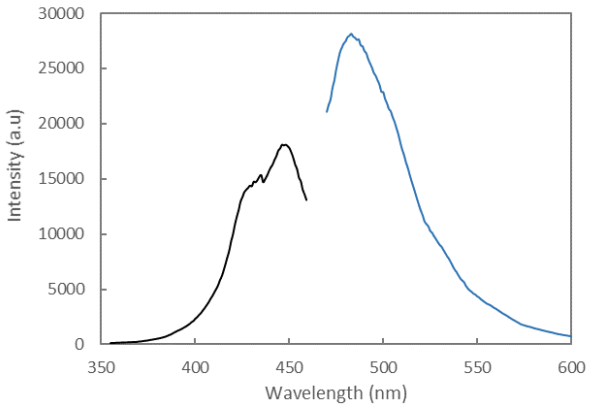

Figure II.D-6 : Excitation spectrum (black curve, $\lambda_{emission}$ = 480 nm) and emission spectrum (blue curve, $\lambda_{excitation}$ = 450 nm) of ThT in the presence of Aβ fibrils.

ThT dye fluoresces at 445 nm upon excitation at 385 nm. However, in the presence of β-sheet structures such as Aβ fibrils, ThT displays a bathochromic shift of both the excitation (450 nm) and emission (480 nm) maxima (Figure II.D-6), with a fluorescence yield enhanced (about one to three orders of magnitude).

The above described increment of the ThT fluorescence yield is related to its spatial arrangement. The carbon-carbon bond between the benzothiazole and the aniline moieties is free for rotation when ThT is not bound (Figure II.D-5a, bottom panel). This rotation quenches the excited states created upon photon excitation, resulting in a low fluorescence. However, the preclusion of the free rotation is supposed to arise upon binding to β-sheet structures such as fibrils. The rotational blockage of the bond between the two moieties preserves the excited states, leading to an enhanced fluorescence yield.[15-16]

Figure II.D-5b shows a proposed model of ThT binding to fibrils, named "Channel" model. In this model, ThT is proposed to bind to fibrils in channel-like motifs along the surface of the fibrils, in a parallel alignment to the long-axis of fibrils. As ThT interacts with fibrils made of the stacking of different amino acid sequences, the interaction seems to be independent of the amino acid chemical nature. Thus, the "Channel" model could be a good hypothesis for ThT binding to fibrils.

Aggregation conditions

For Aβ aggregation studies by fluorescence, the purified peptide (see Section II.A.4 for the preparation of the peptide) is incubated at 20 µM in a HEPES buffered solution (50 mM, pH 7.4) with ThT (10 µM) at 37°C during 200 h. The fluorescence is monitored at 480 nm upon excitation at 450 nm, every 5 min after 15 s of shaking at 200 rpm.

II.E. Proton Nuclear Magnetic Resonance

II.E.1. General principles

The nuclear magnetic resonance (NMR) is a spectroscopic technique widely used for the structural dynamics and chemical environment determination of molecules. This technique is based on the interaction between a nuclear spin and a magnetic field.

Every atomic nucleus is characterized by its spin, the total nuclear angular momentum quantum number. This is characterized by a quantum number I, which can be integer, half-integer or zero. Only nuclei with a non-zero quantum number can be studied by NMR since they can absorb and emit radiofrequencies. Nuclei with even mass (A) and charge (Z) (such as ^{12}C, ^{16}O) have a I = 0 and cannot be studied by NMR. Nuclei with an even mass A and an odd charge Z (such as ^{2}H, ^{14}N) have an integer value I while nuclei with an odd mass A (such as ^{1}H, ^{13}C,^{15}N) have a half-integral value I. ^{1}H nucleus is characterized by a nuclear spin of I = ½.

In the absence of a magnetic field, the spin moments of the nuclei are uniformly distributed and the total magnetic moment resulting is zero. However, when a magnetic field B_0 is applied, a Larmor precession occurs due to the interaction between the magnetic field and the magnetic moment of the nucleus. The ^{1}H nucleus can occupy 2 energy levels (2I+1) related to two spin alignments to $\overrightarrow{B_0}$: parallel (magnetic quantum number m = ½) or anti-parallel (m = -½) (Figure II.E-1). The level of lower energy is slightly more populated by nuclei than the other one, resulting in a non-zero magnetic moment vector sum called magnetization ($\overrightarrow{M}$) parallel to $\overrightarrow{B_0}$ (Figure II.E-2a).

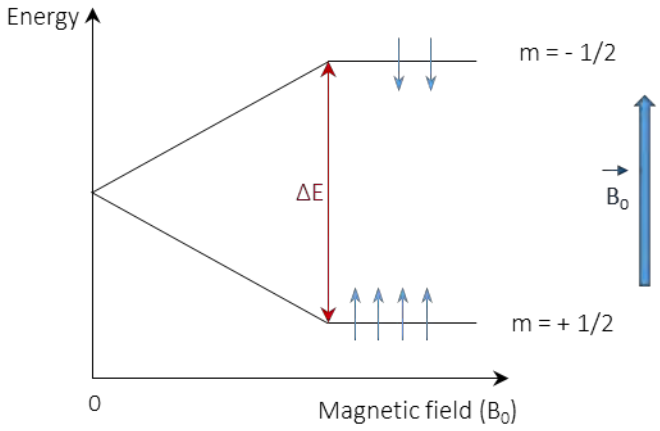

Figure II.E-1: Energy level of spin states for a nucleus with a spin I = ½ (such as ^{1}H) subjected to a magnetic field $\overrightarrow{B_0}$.

The difference of energy between the two spin states (ΔE) is directly related to the magnetic field strength, as shown by the Equation II.E-1.

$$\Delta E = h\nu = \frac{h}{2\pi} \cdot \gamma \cdot B_0 \qquad \textbf{Equation II.E-1}$$

where h is the Planck constant ($J.s^{-1}$), γ the gyromagnetic ratio ($rad \cdot s^{-1} \cdot T^{-1}$) and B_0 the magnetic field (T). Thus, the higher the magnetic field strength, the higher the energy difference between the two spin states and the higher the difference of population between these two states, leading to a more intense magnetic moment.

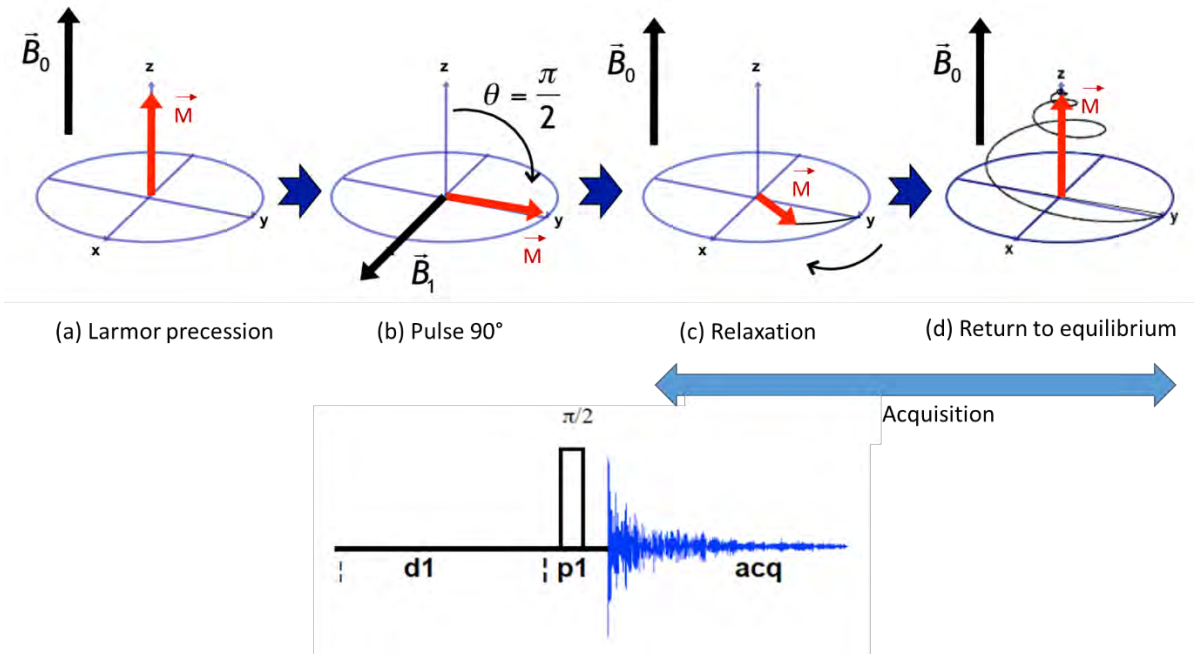

Figure II.E-2 Schematic view of the different phenomena during a ^{1}H NMR experiment.

In NMR spectroscopy, an radiofrequency $\overrightarrow{B_1}$ is applied on the sample, perpendicularly to $\overrightarrow{B_0}$. Its frequency is chosen to correspond to the one of Equation II.E-1 (called Larmor frequency). The radiofrequency is absorbed by the nucleus and the ratio of the population of the two spin states is changed, leading to a change of orientation of the magnetization $\overrightarrow{M}$ (Figure II.E-2b, red arrow). The duration of the radiofrequency application is related to the angle between the initial and final $\overrightarrow{M}$. Thus, $\overrightarrow{B_1}$ is applied as a pulse with a controlled duration (p1, in µs) to obtain a 90° angle.

The magnetization vector $\overrightarrow{M}$ precesses about the external magnetic field vector at the NMR frequency of the spins (Figure II.E-2c). This induces a current in the coil located in the

plane perpendicular to $\overrightarrow{B_0}$, creating an electrical signal oscillating at the NMR frequency named Free Induction Decay (FID). The magnetization does not precess infinitely in the transvers plane, it turns back to the equilibrium state (Figure II.E-2d) during the relaxation.

Two different types of relaxation are observed:

- the transverse relaxation characterized by time-constant T_2, corresponding to the decrease of the xy component of $\overrightarrow{M}$ to zero.
- the longitudinal relaxation characterized by time-constant T_1, corresponding to the increase of the z-axis component of $\overrightarrow{M}$ to its equilibrium value.

FID contains the vector sum of the NMR responses from all the excited spins and provides access to the T_1 and T_2 time-constants. The FID signal (intensity vs. time) is then transformed into a NMR spectrum (NMR absorption intensity vs. NMR frequency) by Fourier Transform (Figure II.E-3).

Figure II.E-3: Fourier transform of the Free Induction Decay (FID) into NMR spectrum.

The frequency of precession of each nucleus is dependent on the chemical environment such as electron environment and neighboring nuclei. A proton close to an electron-attracting group will have a higher frequency, and its proximity with other protons nuclei leads to spin-spin coupling. Thus, the frequency of each proton is informative on its chemical environment. The NMR spectrum obtained by Fourier Transform contains the intensity of NMR absorption as a function of the chemical shift δ (in ppm) calculated from Equation II.E-2.

$$\delta = \frac{\nu - \nu_{ref}}{\nu_{ref}} . 10^6 \qquad \textbf{Equation II.E-2}$$

Where ν is the proton frequency, ν_{ref} the frequency of the reference. For ^{1}H NMR experiments, the tetramethylsilane (TMS) is used as reference with its 12 protons that have the same chemical shift, far from the one of the protons usually studied.

II.E.2. Application to Aβ chemical structure study

a. Samples preparation

Aβ$_{28}$ peptide

A stock solution of Aβ$_{28}$ 2 mM was diluted with D_2O to reach a peptide concentration of 0.4 mM, and the pH was adjusted to 10.5 with NaOD 1 mM.

Aβ$_{28}$ox peptide

A stock solution of Aβ$_{28}$ox 2.7 mM (for preparation, see Section II.A.3) was diluted with D_2O to reach a peptide concentration of 0.4 mM, and the pH was adjusted to 10.5 with NaOD 1 mM. A volume of 600 µL is required to run the NMR experiment.

b. NMR conditions

The ^1H NMR experiments were recorded on a Bruker Avance 500 spectrometer equipped with a 5 mm triple resonance inverse Z-gradient probe (TBI ^1H, ^{31}P, BB). The presaturation of the water signal was achieved with a zqpr sequence (Bruker). ^1H NMR experiments are performed at 298K. The parameters for the acquisition are d1 = 30 and p1 = 6.6 µs.

II.F. Electron Paramagnetic Resonance

II.F.1. General principles

Electron Paramagnetic Resonance (EPR) is an absorption spectroscopy which has similarities with NMR. The electromagnetic waves interact with the magnetic moment associated with electrons and not with nuclei. Yevgeny Zavoisky and Brebis Bleaney have developed independently EPR at the same time in 1944. EPR is mainly employed for studying compounds with an impaired number of electrons such as radicals and paramagnetic metal complexes.

An electron is characterized by the spin quantum number S = ½, the magnetic moment µ and the two spin states m_s = - ½. and m_s = + ½. In the absence of a magnetic field, the electron

spin states are degenerated. However, when subjected to a magnetic field (B_0), the magnetic moment of the electron aligns itself parallel (m_s = - ½) or antiparralel (m_s = + ½) to B_0. It results in a removal of degeneracy, the spin states having thus two different energies, m_s = - ½ having the lower one (Figure II.F-1). Those energy levels are called Zeeman levels.

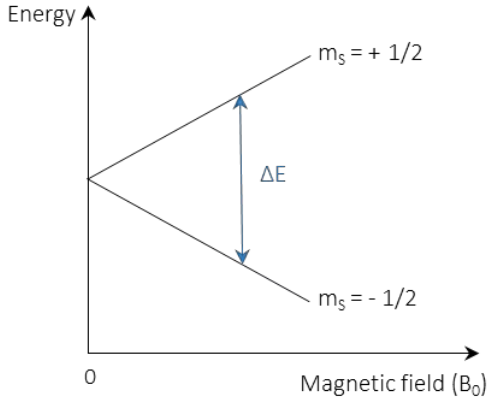

Figure II.F-1: Energy level of spin states for an electron subjected to a magnetic field $\overrightarrow{B_0}$.

The difference of energy between the two spin states (ΔE) is directly related to the magnetic field strength, as shown by the Equation II.F-1.

$$\Delta E = h\nu = g_e \cdot \mu_B \cdot B_0 \qquad \textbf{Equation II.F-1}$$

where h is the Planck's constant (6.626 x 10^{-34} J.s), ν the radiation frequency (in s^{-1}), g_e the Landé factor (2.00232 for a free electron), μ_B the Bohr magneton (9.2740 x 10^{-28} J.G $^{-1}$) and B_0 the external magnetic field (in G).

The application of an electromagnetic wave perpendicular to B_0 and with a frequency ν allows the transition between the two Zeeman levels, corresponding to an orientation change of the magnetic moment of the electron.

In EPR, an absorption spectrum is obtained by the detection of the residual electromagnetic field after it passed through the paramagnetic sample. The frequency is fixed and the magnetic field varies. When B_0 value of the applied magnetic field is directly related to the frequency of the electromagnetic wave (*via* Equation II.F-1), the wave is absorbed by the sample, leading to the transition between the Zeeman levels.

Figure II.F-2 shows a schematic view of an EPR equipment. A microwave source (usually a Gunn diode) provides the electromagnetic wave of fixed frequency ν, which goes through an attenuator, and is sent to the sample cavity by passing into the circulator. The sample cavity is surrounded by a magnet which generates the static magnetic field $\overrightarrow{B_0}$. The resulting

electromagnetic wave not absorbed by the sample is reflected back by the cavity and routed towards the detector diode.

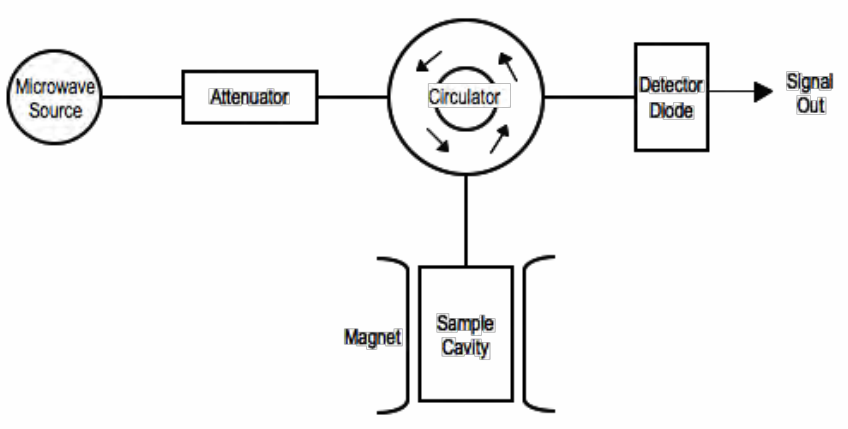

Figure II.F-2: Schematic representation of an EPR equipment.

The detection by the diode allows to obtain a spectrum with the absorption of the electromagnetic wave as a function of the magnetic field strength, generally reported in Gauss or milliTesla (Figure II.F-3, top). However, the EPR spectra are usually presented as the first derivative of the absorption as a function of the magnetic field strength (Figure II.F-3, bottom). From the spectrum, the Landé factor (g) can be calculated, specific for each system studied. In the case of a free electron, $g = g_e = 2.00232$.

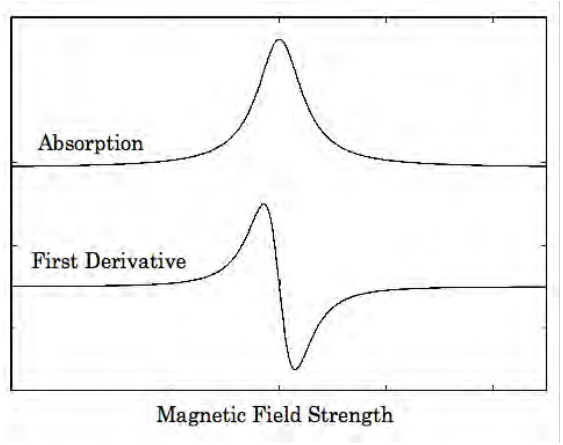

Figure II.F-3: Example of EPR spectrum. (Top) absorption and (bottom) first derivative as a function of the magnetic field strength.

For anisotropic systems such as metal ions complexes, the response of the molecule is different depending to its orientation with respect to the magnetic field. Thus, 3 transitions occur in x, y and z directions. 3 different Landé factors (g_x, g_y, g_z, described by the Equation II.F-2) characterize the system, resulting in 3 signals at respectively $B_{x,res}$, $B_{y,res}$ and $B_{z,res}$ values of magnetic field on the EPR spectrum.

$$g_{x/y/z} = \frac{h\nu}{\mu_B . B_{x/y/z\,res}}$$ **Equation II.F-2**

When the nucleus bearing the spin density has a nuclear spin I ≠ 0, a coupling of the electron magnetic moment occurs with the magnetic moment of the nucleus, called hyperfine coupling. The EPR spectrum is strongly impacted. The EPR spectrum will thus present a maximum of 2 I + 1 lines for each electronic transition, due to the electron / nuclear magnetic moment coupling. The hyperfine coupling constant of a nucleus (A) is directly related to the spectral line spacing $\mathcal{A}$ by the Equation II.F-3.

$$A = \frac{\mathcal{A} . g . \mu_B}{h\, c}$$ **Equation II.F-3**

$\mathcal{A}$ (in G) is the distance between two of the hyperfine lines, g the Landé factor, μ_B the Bohr magneton (9.2740 x 10^{-28} J.G $^{-1}$), h is the Planck's constant (6.626 x 10^{-34} J.s) and c the light speed (9.9979.10^{10} cm.s^{-1}). A is expressed in 10^{-4} cm^{-1}.

The electron magnetic moment can also interact with the nuclear magnetic moment of an another nucleus, resulting in a super-hyperfine coupling.

Thus, an EPR spectrum gives insights into the nature of the paramagnetic center and on its environment as well.

II.F.1. Application to Cu(II) coordination study

As Cu(II) ion is paramagnetic (d^9), EPR is a powerful technique for investigating binding modes of Cu(II) complexes. Cu(II)-peptide complexes have an axial symmetry, then 2 Landé factors $g_{//}$ (when the magnetic field is in the z axis direction, described by Equation II.F-4) and $g_{\perp}$ (when the magnetic field is in the xy plane, described by Equation II.F-5) characterize the system, resulting in two different signals centred at $B_{// res}$ and $B_{\perp res}$ values of magnetic field.

$$g_{//} = \frac{h\nu}{\mu_B . B_{// res}}$$ **Equation II.F-4**

$$g_{\perp} = \frac{h\nu}{\mu_B . B_{\perp res}}$$ **Equation II.F-5**

As Cu(II) has an electron spin of S = ½ and a nuclear spin of I = 3/2, the hyperfine coupling will result in four signals (2I+1) for each Zeeman transition. The signal related to $g_{//}$ is subdivided into 4 distinct signals, as shown in Figure II.F-4. The hyperfine coupling constant $A_{//}$ can be calculated from the spectrum, with the Equation II.F-6.

$$A_{//} = \frac{\mathcal{A}_{//}\, g_{//}\, \mu_B}{h\, c} \qquad \textbf{Equation II.F-6}$$

Where $\mathcal{A}_{//}$ (in G) is the distance between two of the hyperfine signals, $g_{//}$ the Landé factor, μ_B the Bohr magneton (9.2740 x 10^{-28} J.G $^{-1}$), h is the Planck's constant (6.626 x 10^{-34} J.s) and c the light speed (9.9979.10^{10} cm.s^{-1}). $A_{//}$ is expressed in 10^{-4} cm^{-1}.

The hyperfine interaction in the xy plane is generally much lower than the one in the z axis and is resulting in a broadening of the signal related to $g_{\perp}$ thus not resolved rather (see Figure II.F-4).[17]

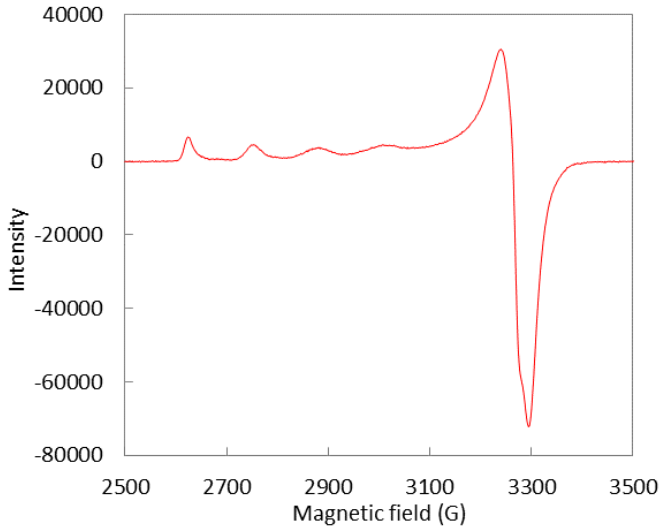

Figure II.F-4: EPR spectrum of Cu(II) in water.

The determination of the $A_{//}$, $g_{//}$ and $g_{\perp}$ values are essential to characterize the coordination mode of Cu(II)-Aβ. They give insights into the nature of the neighboring atoms in the equatorial plane (i.e. number of oxygens and nitrogens) according to Peisach and Blumberg empirical correlation.[18] Thus, these EPR parameters will be used for comparison between different Cu(II)-peptide complexes in our studies.

EPR conditions

EPR spectra were recorded on a Bruker Elexsys E500 spectrometer equipped with a continuous flow cryostat (Oxford). Analysis was performed with aqueous solution containing 10% of glycerol, ^{65}Cu (450 µM) and the Aβ peptide (500 µM). pH was adjusted with H_2SO_4 (1 M) and NaOH (1 M). Experimental parameters were set as follow: T = 120 K, ν = 9.5 GHz, microwave power = 20.5 mW, Amplitude modulation = 10.0 G, Modulation frequency = 100 kHz.

II.G. X-Ray Absorption Near Edge Structure (XANES)

II.G.1. X-Ray absorption: general principles [19]

X-rays are electromagnetic waves with wavelengths between 10^{-12} m and 10^{-8} m and an energy range of 0.1-100 keV, used in X-ray absorption spectroscopy (XAS) at synchrotron radiation facilities. This technique is based on the interaction between X-rays and matter. X-rays can be absorbed by an atom, resulting in an excitation of a core electron from its ground state to a high-energy electron unoccupied orbital or to the continuum. Figure II.G-1 shows the Bohr model which illustrates the phenomenon. When the electron is excited, a core hole is created, filled in approximately a femto-second after the relaxation of an electron from a high-energy electron orbital, with a release of energy, leading in some cases to fluorescence light emission. Depending on the X-ray energy, the excited electron can come from K-shell, L-shells or M-shells. The closer the electron from the nucleus, the higher the energy required to excite it.

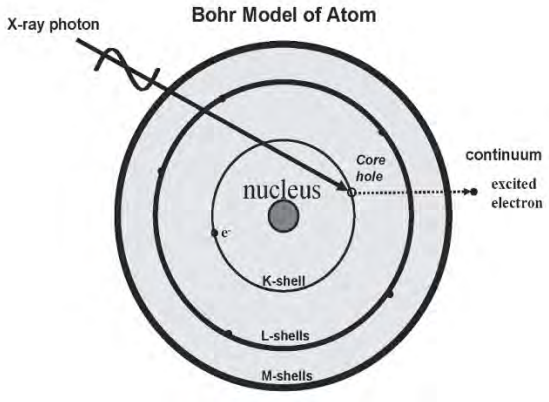

Figure II.G-1: Bohr model of an atom with the different electron shells.

XAS is based on the application of X-rays on a sample and the detection of either the absorption or the fluorescence generated during relaxation. The starting energy of X-rays is chosen in order to be lower than the absorption edge of the atom, and is increased during the experiment. XAS spectra are presented as the absorption/fluorescence as a function of the incident X-ray energy (in eV).

As an example, Figure II.G-2 shows a spectrum of the X-ray absorption of NiO as a function of the energy, as along with the X-ray Absorption Near Edge Structure (XANES) and the Extended X-ray Absorption Fine Structure (EXAFS) regions of the spectrum.

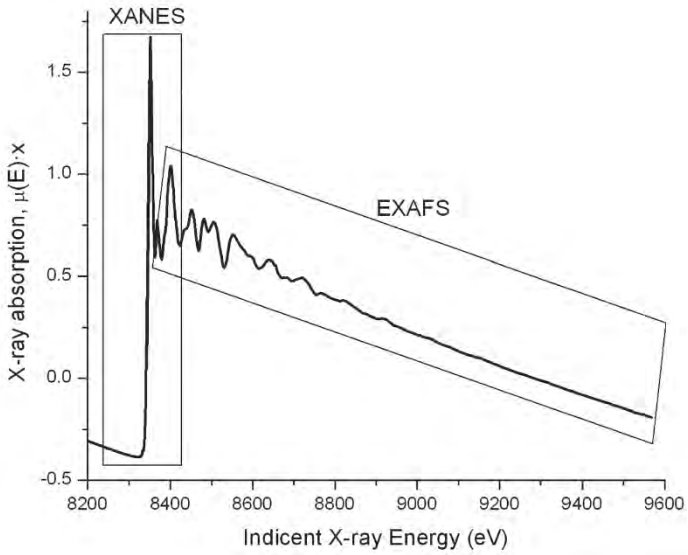

Figure II.G-2: NiO X-ray absorption spectrum highlighting the XANES and EXAFS regions.

XANES region is related to the excitation of a core electron towards an unoccupied orbital of higher energy of the atom, providing information on the valence state and the geometry of the studied species. For its part, EXAFS is related to the excitation of a core electron to the continuum and can be used to characterize the environment of the element studied in the sample. These techniques are widely used for the characterization of metal complex binding modes.

II.G.2. Application to Cu(I) and Zn(II) coordination

For our studies, XANES is realized in order to compare the fingerprints of the XANES signatures for different metal-peptide complexes. Cu(I)-peptide and Zn(II)-peptide are studied in Cu K-edge and Zn K-edge respectively. XANES is a method of choice for studying Cu(I)

and Zn(II) coordination to the Aβ peptide since few techniques are suitable for d^{10} ions coordination mode investigation.

a. Cu K-edge XANES conditions

The copper-containing Aβ solutions were injected into sample holders in between two Kapton windows (3M, cat. #1205; Minneapolis, MN) and immediately frozen in liquid nitrogen. All samples were maintained at 10-20 K throughout the data collection using a helium cryostat. Cu K-edge XANES spectra were recorded at the BM30B (FAME) French CRG beamline at the European Synchrotron Radiation Facility (ESRF, Grenoble, France). The storage ring was operating in uniform mode at 6 GeV with a 200 mA current. The beam energy was selected using an Si(220) N_2 cryo-cooled double-crystal monochromator with an experimental resolution of ~ 0.5 eV. The beam spot on the sample was approximately 200 × 100 μm² (H × V, FWHM). The spectra were collected in fluorescence mode by a 30-element Ge solid-state fluorescence detector (Canberra). The energy was calibrated with Cu metallic foils, such that the maximum of the first derivative was set at 8979 eV. Cu data were collected from 8830 to 8960 eV using 5 eV step and 2 s counting time, from 8960 to 9020 eV using 0.5 eV step and 3 s counting time, and from 9020 to 9300 eV with a k-step of 0.05 $Å^{-1}$ and a counting time increasing from 2 to 10 s.

For each sample, three spectra were averaged and resulting XANES spectra were background-corrected by a linear regression through the pre-edge region and a polynomial through the post-edge region and normalized to the edge jump. The beam was moved to a different position on the sample for each scan to avoid potential Cu photoreduction. All spectra were individually inspected prior to data averaging to ensure that beam damage was not occurring.

Cu(I) samples were prepared under a continuous flow of N_2 by direct addition (10 equiv.) of fresh made sodium dithionite ($Na_2S_2O_4$) stock solution (0.1 M) into the sample holder containing $CuSO_4$ (0.9 mM) and the peptide (1 mM) in the presence of 10% glycerol as cryoprotectant with the pH adjusted to 7.1. The sample was immediately frozen in liquid nitrogen. In such conditions, no significant pH drift due to the addition of $Na_2S_2O_4$ was detected.

b. Zn K-edge XANES conditions

The zinc-containing Aβ ($A\beta_{28}$, $A\beta_{28}$ox, H6A or H6A-H14A) solutions were injected into sample holders in between two Kapton windows (3M, cat. #1205; Minneapolis, MN) and immediately frozen in liquid nitrogen. All samples were maintained at 10-20 K throughout the data collection using a helium cryostat. Zn K-edge XANES spectra were recorded at the BM30B (FAME) French CRG beamline at the European Synchrotron Radiation Facility (ESRF, Grenoble, France). The storage ring was operating in uniform mode at 6 GeV with a 200 mA current. The beam energy was selected using a Si(220) N_2 cryo-cooled double-crystal monochromator with an experimental resolution of ~ 0.5 eV. The beam spot on the sample was approximately 200 × 100 μm² (H × V, FWHM). The spectra were collected in fluorescence mode by a 30-element Ge solid-state fluorescence detector (Canberra). The energy was calibrated with Zn metallic foils, such that the maximum of the first derivative was set at 9659 eV. Zn data were collected from 9510 to 9630 eV using 5 eV step and 3 s counting time, from 9630 to 9700 eV using 0.5 eV step and 3 s counting time, and from 9700 to 10000 eV with a k-step of 0.05 $Å^{-1}$ and 3s counting time.

For each sample, three spectra were averaged and resulting XANES spectra were background-corrected by a linear regression through the pre-edge region and a polynomial through the post-edge region and normalized to the edge jump. All spectra were individually inspected prior to data averaging to ensure that beam damage was not occurring.

Zn samples were prepared by adding the solution of $ZnSO_4$ (0.9 mM) and peptide (1 mM) in the presence of 10% glycerol as cryoprotectant (pH adjusted to 7.1) into the sample holder. The sample was immediately frozen in liquid nitrogen.

References

[1] P. Faller, C. Hureau, P. Dorlet, P. Hellwig, Y. Coppel, F. Collin and B. Alies, *Coordination Chemistry Reviews* **2012**, *256*, 2381-2396.

[2] B. Alies, G. LaPenna, S. Sayen, E. Guillon, C. Hureau and P. Faller, *Inorganic Chemistry* **2012**, *51*, 7897-7902.

[3] M. Yamashita and J. B. Fenn, *Journal of Physical Chemistry* **1984**, *88*, 4451-4459.

[4] E. De Hoffmann and V. Stroobant, *Spectrométrie de masse*, Dunod, Paris, **2005**.

[5] W. Paul and H. Steinwedel, *Apparatus for separating charged particles of different specific charges*, U.S. Patent, **1960**, 2939952.

[6] G. Stafford, P. Kelley, J. Syka, W. Reynolds and J. Todd, *International Journal of Mass Spectrometry and Ion Processes* **1984**, *60*, 85-98.

[7] M. Scigelova and A. Makarov, *Proteomics* **2006**, *6*, 16-21.

[8] A. Makarov, *Analytical Chemistry* **2000**, *72*, 1156-1162.

[9] K. Biemann, *Methods in Enzymology* **1990**, *193*, 455-479.

[10] F. Rouessac and A. Rouessac, *Analyse Chimique: Méthodes et techniques instrumentales modernes*, Dunod, **2009**.

[11] Y. Manevich, K. D. Held and J. E. Biaglow, *Radiation Research* **1997**, *148*, 580-591.

[12] F. Ding, J. M. Borreguero, S. V. Buldyrey, H. E. Stanley and N. V. Dokholyan, *PROTEINS: Structure, Function, and Bioinformatics* **2003**, *53*, 220-228.

[13] A. A. Reinke and J. E. Gestwicki, *Chemical biology & drug design* **2011**, *77*, 399-411.

[14] H. LeVine, *Methods in Enzymology* **1999**, *309*, 274-284.

[15] S. Noël, S. Cadet, E. Gras and C. Hureau, *Chemical Society Reviews* **2013**, *42*, 7747-7762.

[16] M. Biancalana and S. Koide, *Biochimica et Biophysica Acta* **2010**, *1804*, 1405-1412.

[17] G. Blondin and Y.-M. Frapart, *L'Actualité chimique* **1996**, *198*, 112-124.

[18] J. Peisach and W. Blumberg, *Archives of Biochemistry and Biophysics* **1974**, *165*, 691-708.

[19] S. Kelly, D. Hesterberg and B. Ravel, *Analysis of soils and minerals using X-ray absorption spectroscopy*, pp. 387-463, in *Methods of soil analysis Part 5 - Mineralogical Methods*, A. L. U. L. R. Drees, **2008**.

Chapter III

Chapter III: Oxidation of the Aβ peptide

This chapter focuses on the oxidation of the Aβ peptide by the Cu/ascorbate/O_2 system and the characterization of its oxidation sites. First, the oxidation of $A\beta_{40}$ is investigated by using Liquid Chromatography coupled to Tandem Mass Spectrometry (LC-MS/MS) and to High Resolution Mass Spectrometry (LC-HRMS), in order to characterize the oxidative damages on Aβ and to identify the oxidized amino acid residues. The study is complemented by proton Nuclear Magnetic Resonance (^{1}H NMR) analysis of the oxidized and non-oxidized Aβ peptide. The kinetics of the amino acid residues oxidation of $A\beta_{40}$ is finally monitored by LC-HRMS. All these studies may provide information on the chemical modifications undergone by the amino acid residues of Aβ during oxidation, and will be further useful for studying the consequence of Aβ oxidation regarding Reactive Oxygen Species (ROS) production and aggregation, two events implicated in Alzheimer's Disease.

III.A. Characterization of the oxidation sites

During the ROS production catalyzed by the Cu-Aβ complex, the Aβ peptide is targeted by ROS. The amino acid residues damaged by ROS undergo chemical modifications, leading to a change of their mass. Thus, the characterization of Aβ oxidation can be investigated by MS.

After Metal Catalyzed Oxidation (MCO) of Aβ by the copper/ascorbate/O_2 system, purification and tryptic digestion, the sample is analyzed by LC-HRMS in order to measure the exact mass of every tryptic peptides and thus deduce the nature of the chemical modification undergone. Then, LC-MS/MS analysis of the sample is carried out in order to sequence the peptide and identify the amino acid residues targeted by ROS. The combination of HRMS and MS/MS is a great source of information for the investigation of the oxidation sites on the Aβ peptide.

III.A.1. Experimental section

Copper(II)-catalyzed oxidation of the $A\beta_{40}$ peptide was carried out by mixing $A\beta_{40}$, Cu(II) and ascorbate in phosphate buffer (50 mM, pH 7.4) to reach final concentrations of respectively 60, 50 and 500 µM (sub-stoichiometry of copper to avoid free Cu(II) in solution) in a reaction mixture volume of 100 µL. Incubation was done at room temperature for at least 15 min. Trypsin digestion was then realized in order to obtain the four tryptic peptides described above (see Section II.B.3). LC-HRMS and LC-MS/MS conditions are detailed in Section II.B.4.

III.A.2. Results

a. Detection of the oxidized tryptic peptides by LC-HRMS

The digested oxidized $A\beta_{40}$ was analyzed by LC-HRMS and the specific modifications due to amino acid residues oxidation were searched. As a reminder, the most common products obtained upon ROS oxidation of Aβ result from: (i) formal addition of one oxygen atom (mass shift of +16 Da), (ii) formal addition of molecular oxygen (+32 Da), (iii) carbonylation (+14 Da), (iv) decarboxylation/deamination of Asp1 (-45 Da), (v) oxidative cleavage of Asp1 (-89 Da), (vi) dityrosine cross-linking (formally -1 Da) (see Section I.C.3 for more information).

From the total ion current (TIC) chromatogram obtained, chromatograms were traced from the theoretical monoisotopic masses of each tryptic peptide of $A\beta_{40}$ and for their oxidized counterparts. Mass spectra were extracted at the retention time where the maximal intensity of the chromatographic peak is detected, showing the experimental monoisotopic masses. Thus, the theoretical and experimental monoisotopic masses were compared to evaluate the accuracy of the detection. All the masses were measured with a mass accuracy of 5 ppm.

For the tryptic $A\beta_{1\text{-}5}$ peptide that contains the N-terminal part of the peptide, four different ions are found (Figure III.A-1). First, the ion at m/z 637.2925 corresponds to the mono-protonated non-oxidized $A\beta_{1\text{-}5}$. Ions at m/z 592.2715 and 548.2444, related to mass shifts of -45 Da and -89 Da, are specific mass modifications assigned respectively to the decarboxylation and deamination of Asp1 ($DAEFR_{dd}$) and to the oxidative cleavage of Asp1 ($DAEFR_{ox}$).

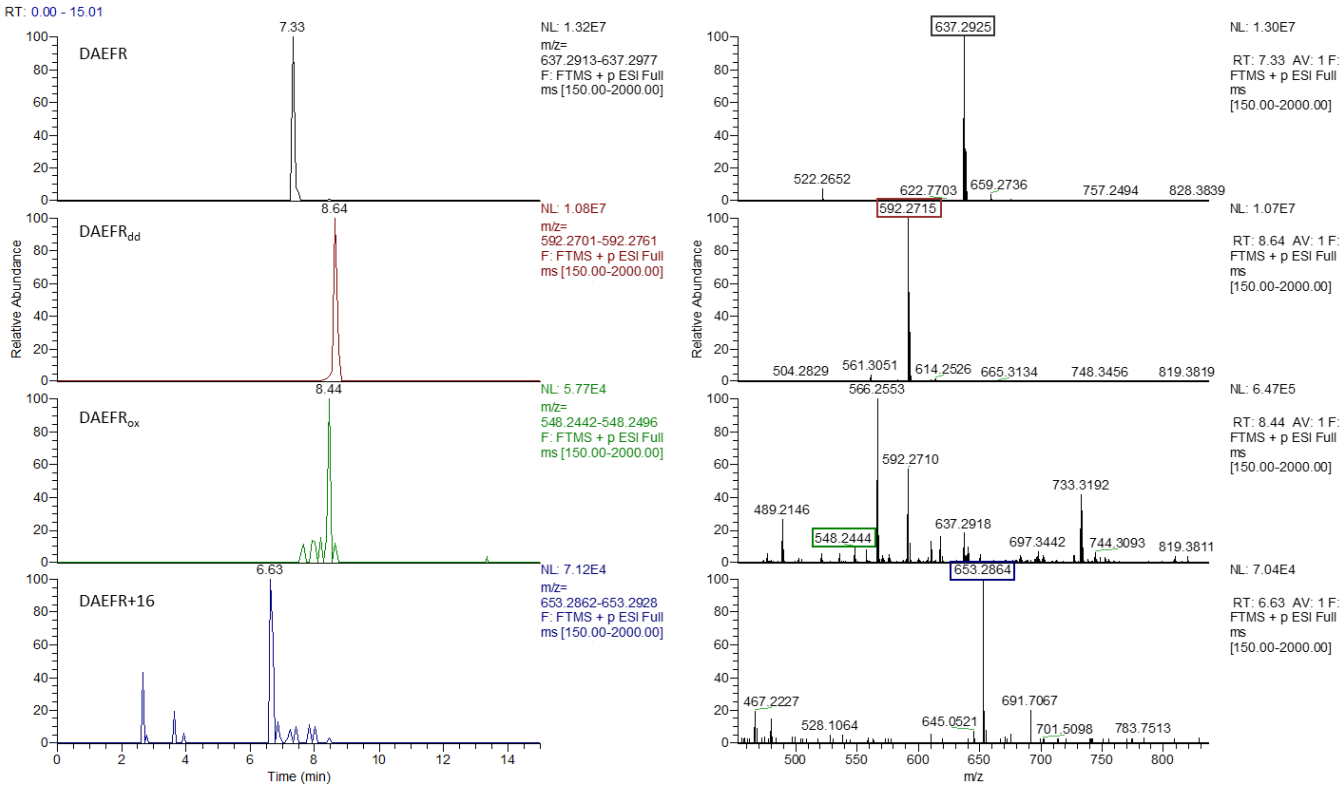

	$[M+H]^+_{th}$	$[M+H]^+_{exp}$	Δm (ppm)
DAEFR	637.2945	637.2925	-3.1
DAEFR$_{dd}$	592.2731	592.2715	-2.7
DAEFR$_{ox}$	548.2469	548.2444	-4.6
DAEFR+16	653.2895	653.2864	-4.7

Figure III.A-1: (Top, left panel) Trace chromatograms of DAEFR and its oxidation products DAEFR$_{dd}$, DAEFR$_{ox}$ and DAEFR+16 obtained by LC-HRMS for Aβ$_{40}$ submitted to MCO for 15 min. (Top, right panel) Mass spectra extracted from the corresponding trace chromatograms at the retention time of maximal intensity of the peak. (Bottom) Theoretical (th) and experimental (exp) monoisotopic masses of native and oxidized Aβ$_{1-5}$ tryptic peptides and mass difference between experimental and theoretical masses. NL: normalized intensity, RT: retention time (min).

The mono-protonated ion at m/z 653.2864 corresponding to a mass increment of 16 Da (named DAEFR+16) refers to the formal addition of an oxygen atom on one amino acid residue, probably on Phe4 which is the residue the most prone to oxidation (for amino acid residues subject to oxidation, see Section I.C.3). DAEFR$_{dd}$ seems to be the main oxidized peptide detected as its chromatographic peak is much intense (intensity around 10^7) compared with the ones of DAEFR$_{ox}$ and DAEFR+16 (intensity around 10^4) (Figure III.A-1, left panel).

Figure III.A-2 shows the mass spectra obtained for the Aβ$_{6-16}$ tryptic peptide and its two oxidized homologs. The doubly protonated ion at m/z 668.8032 is the major ion of Aβ$_{6-16}$ detected in the sample. Two other doubly protonated ions are detected at m/z 676.7997 and 684.7979, corresponding to the Aβ$_{6-16}$ peptide with the formal addition of one and two oxygen atoms, respectively (+ 16 Da and +32 Da).

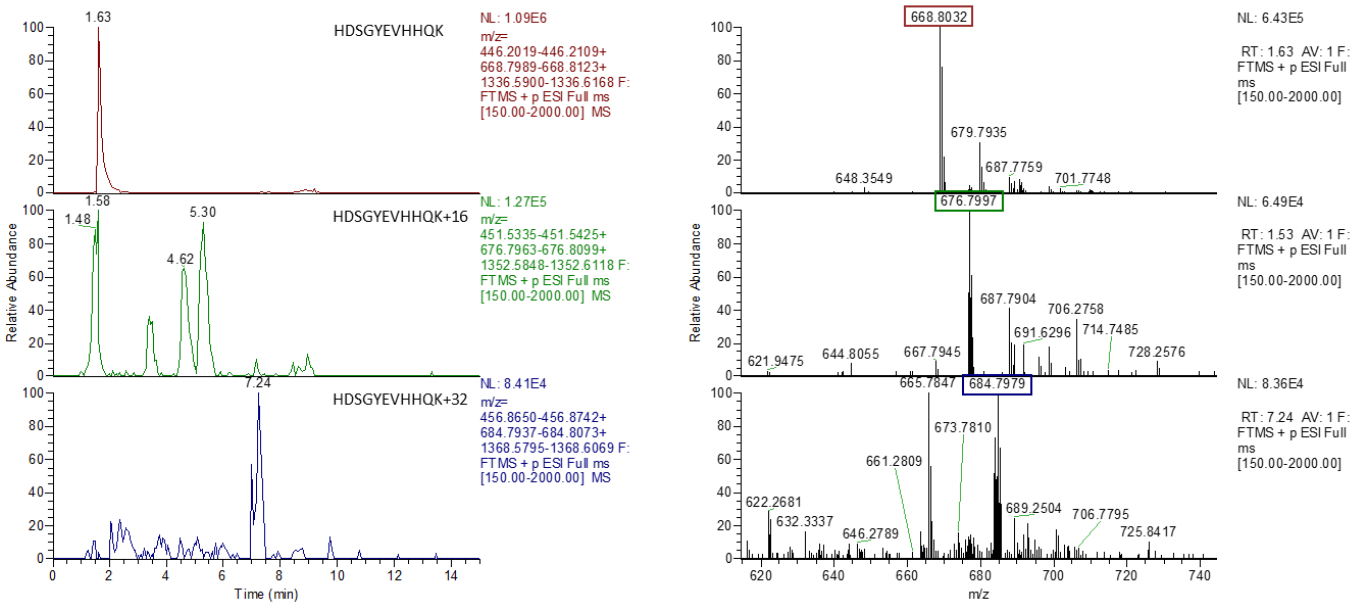

	$[M+2H]^{2+}_{th}$	$[M+2H]^{2+}_{exp}$	Δm (ppm)
HDSGYEVHHQK	668.8056	668.8032	-3.6
HDSGYEVHHQK+16	676.8031	676.7997	-5.0
HDSGYEVHHQK+32	684.8005	684.7979	-3.8

Figure III.A-2: (Top, left panel) Trace chromatograms of HDSGYEVHHQK and its oxidation products HDSGYEVHHQK+16 and HDSGYEVHHQK+32 obtained by LC-HRMS for $Aβ_{40}$ submitted to MCO for 15 min. (Top, right panel) Mass spectra extracted from the corresponding trace chromatograms at the retention time of maximal intensity of the peak. (Bottom) Theoretical (th) and experimental (exp) monoisotopic masses of native and oxidized $Aβ_{6-16}$ tryptic peptides and mass difference between experimental and theoretical masses. NL: normalized intensity, RT: retention time (min).

The exact nature of the oxidized amino acid residues cannot be determined here, even if, among the residues of the tryptic $Aβ_{6-16}$ peptide, histidine and tyrosine residues are the most sensitive to oxidation by $HO^{\bullet}$.[1] Several peaks are detected on the chromatogram trace of HDGYEVHHQK+16, probably due to the presence of different oxidized species with a mass shift of +16 Da. For HDGYEVHHQK+32, only one peak is detected with a low intensity.

Only one oxidation has been detected for the tryptic $Aβ_{17-28}$ peptide (Figure III.A-3), with a mass shift of +16 Da, corresponding to the formal addition of an oxygen atom. The most intense ions detected are the doubly protonated ions at m/z 663.3383 and 671.3361, corresponding to the non-oxidized and oxidized $Aβ_{17-28}$. No second oxidation was detected, as it was the case for the tryptic $Aβ_{6-16}$ peptide.

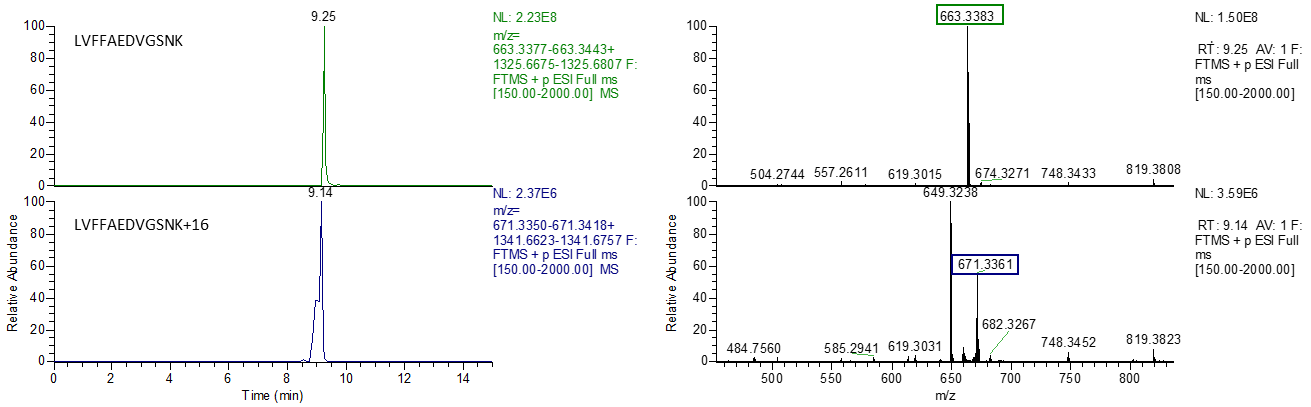

	$[M+2H]^{2+}_{th}$	$[M+2H]^{2+}_{exp}$	Δm (ppm)
LVFFAEDVGSNK	663.3410	663.3383	-4.1
LVFFAEDVGSNK+16	671.3384	671.3361	-3.4

Figure III.A-3: (Top, left panel) Trace chromatograms of LVFFAEDVGSNK and its oxidation product LVFFAEDVGSNK+16 obtained by LC-HRMS for Aβ$_{40}$ submitted to MCO for 15 min. (Top, right panel) Mass spectra extracted from the corresponding trace chromatograms at the retention time of maximal intensity of the peak. (Bottom) Theoretical (th) and experimental (exp) monoisotopic masses of native and oxidized Aβ$_{17-28}$ tryptic peptides and mass difference between experimental and theoretical masses. NL: normalized intensity, RT: retention time (min).

Finally, analysis of Aβ$_{29-40}$ (Figure I.A-4) revealed one most intense ion at m/z of 1085.6384 (unoxidized peptide), along with a second one at m/z 1101.6321, corresponding to a mass shift of +16 Da. As Aβ$_{29-40}$ has one methionine residue in its sequence, which is a very sensitive amino acid residue (see Section I.C.3.e), we can assume that it is oxidized into methionine sulfoxide during MCO of Aβ.

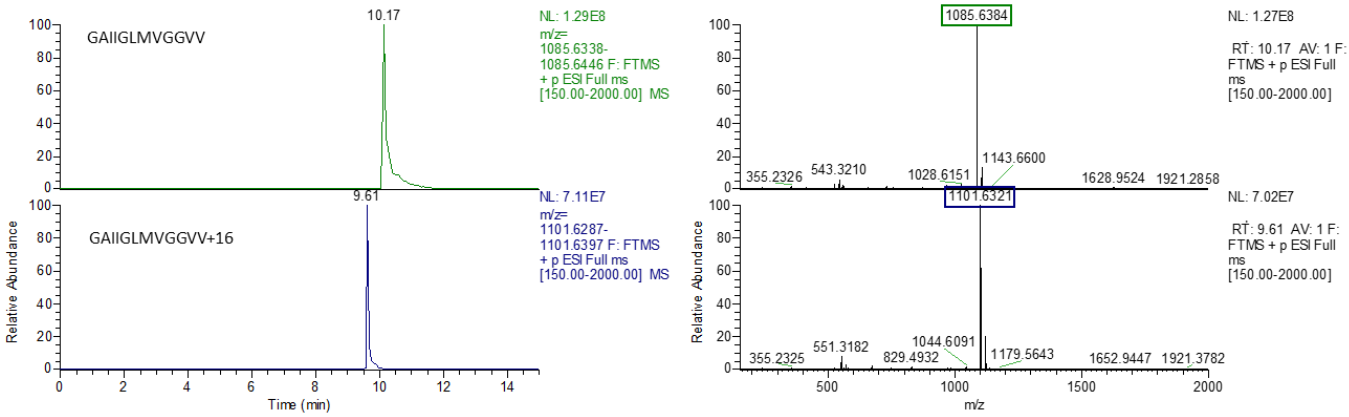

	$[M+H]^{+}_{th}$	$[M+H]^{+}_{exp}$	Δm (ppm)
GAIIGLMVGGVV	1085.6392	1085.6384	-0.7
GAIIGLMVGGVV+16	1101.6342	1101.6321	-1.9

Figure III.A-4: : (Top, left panel) Trace chromatograms of GAIIGLMVGGVV and its oxidation product GAIIGLMVGGVV+16 obtained by LC-HRMS for Aβ$_{40}$ submitted to MCO for 15 min. (Top, right panel) Mass spectra extracted from the corresponding trace chromatograms at the retention time of maximal intensity of the peak.(Bottom) Theoretical (th) and experimental (exp) monoisotopic masses of native and oxidized Aβ$_{29-40}$ tryptic peptides and mass difference between experimental and theoretical masses. NL: normalized intensity, RT: retention time (min).

Table III.A-1 summarizes the detected non-oxidized and oxidized tryptic peptides along with the monoisotopic masses of their corresponding protonated ions. Specific mass shifts of -45 Da and -89 Da have been found on the N-terminal tryptic peptide $A\beta_{1-5}$, corresponding respectively to the decarboxylation-deamination and to the oxidative cleavage of Asp1.[2-3] Usually, aromatic amino acid residues are more prone to oxidation than aliphatic ones,[4] in particular because of their high electron density which favors the hydroxyl radicals attack. Thus, the results obtained highlight the particular sensitivity of Asp1 during Aβ oxidation. The two oxidative damages detected on Asp1 strongly affect the chemical structure of the N-terminal part of the peptide (see Section I.C.3.b for chemical structures). Such a modification would probably have a significant impact on the behavior of the oxidized Aβ peptide regarding copper coordination, ROS production and aggregation.

Common oxidations (mass increase of 16 Da) were also detected on every tryptic peptide. As oxidation leading to the formal addition of an oxygen atom can occur on several amino acid residues, we cannot conclude on the nature of the damaged amino acid residue of each tryptic peptide, even if some of the amino acid residues are more sensitive than the other ones. The same tryptic peptides were thus sequenced by LC-MS/MS in order to identify the oxidized amino acid residues.

Table III.A-1: Theoretical monoisotopic masses (m/z) of mono- and doubly-protonated ions of the tryptic peptides of non-oxidized and oxidized $A\beta_{40}$ detected. +16 and +32 account for the formal addition of one and two oxygen atoms during oxidation.

Position	Peptide	$[M+H]^+$	$[M+2H]^{2+}$
1-5	DAEFR	637.2945	319.1512
1-5	DAEFR+16	653.2895	327.1486
1-5	$DAEFR_{dd}$*	592.2731	296.6405
1-5	$DAEFR_{ox}$**	548.2469	274.6273
6-16	HDSGYEVHHQK	1336.6034	668.8056
6-16	HDSGYEVHHQK+16	1352.5983	676.8031
6-16	HDSGYEVHHQK+32	1368.5932	684.8005
17-28	LVFFAEDVGSNK	1325.6741	663.3410
17-28	LVFFAEDVGSNK+16	1341.6690	671.3384
29-40	GAIIGLMVGGVV	1085.6392	543.3235
29-40	GAIIGLMVGGVV+16	1101.6342	551.3210

* $DAEFR_{dd}$: oxidative decarboxylation and deamination of Asp1
** $DAEFR_{ox}$: oxidative cleavage of Asp1

b. Characterization of the oxidation sites by LC-MS/MS

After oxidation, purification and digestion, the $A\beta_{40}$ peptide was analyzed by LC-MS/MS in order to determine the site of oxidation on each tryptic peptide. As explained in

Section II.B.3.c, by using Collision Induced Dissociation (CID), the peptide is cleaved at the peptide bond, leading to the formation of b and y ions, whose differences in mass are equal to the mass of the residues.[5] These ions are detected and their masses compared to the theoretical masses obtained from the peptide sequence. The oxidized residues are identified when the b or y ions values are increased by +16, as compared to the non-oxidized peptide.

The N-terminal tryptic $A\beta_{1-5}$ peptide was first analyzed by LC-MS/MS but the spectra obtained were not informative. This small peptide is usually fragmented as a mono-protonated ion, leading to a poor quality of the MS/MS spectrum. In addition, the terminal arginine residue (an amino acid residue which has the highest pKa value of the side-chain function) tends to preclude the proton mobility during fragmentation, resulting in the absence of b ions.[6]

Figure III.A-5 shows two MS/MS spectra of the doubly protonated ion of the oxidized $A\beta_{6-16}$ (+ 16 Da). For the first one (top), the oxidation is detected on His13, oxidized in 2-oxohistidine while for the second one (bottom), His14 is detected oxidized in 2-oxohistidine.[7] For both MS/MS spectra, the peptide sequence is well covered by both the b and y ions, allowing a reliable characterization of the oxidation of His13 and His14.

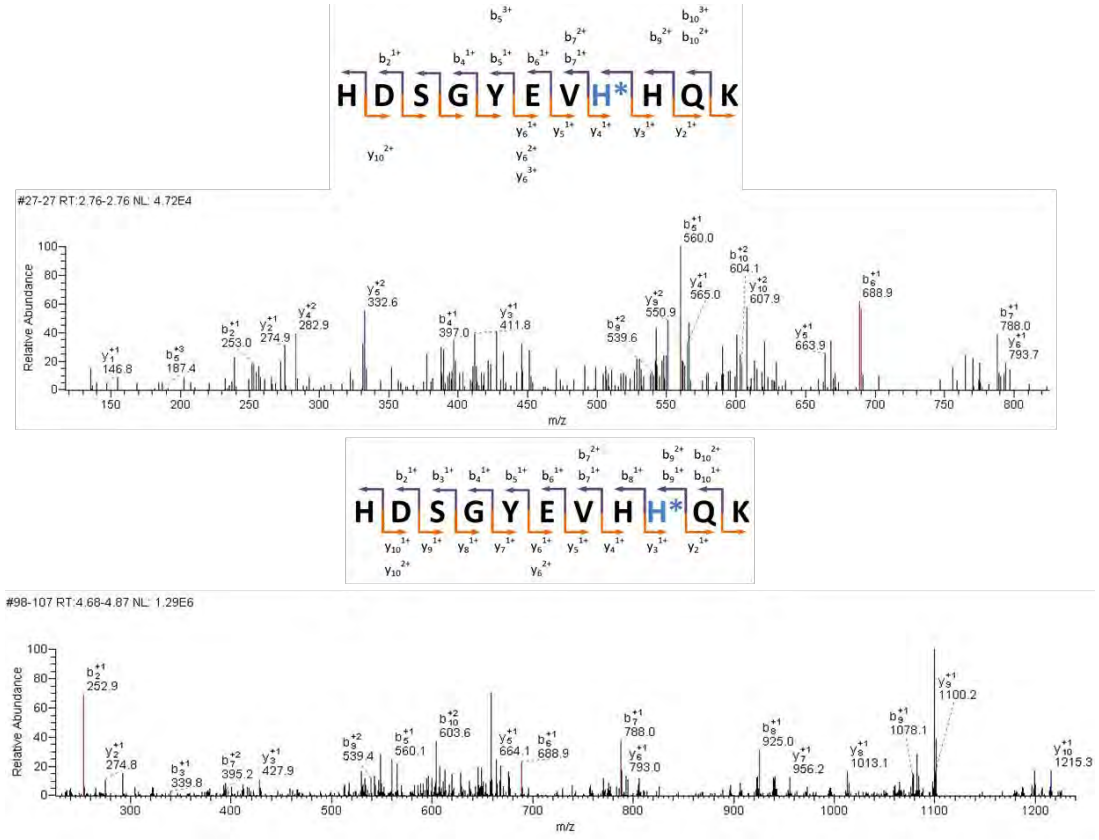

Figure III.A-5: Fragmentation spectra of doubly protonated ion (m/z 676.9) of the tryptic $A\beta_{6-16}$ peptide allowing for identification of His13 (top) or His14 (bottom) oxidation. b and y ions series (charge 1+, 2+ and 3+) detected are summarized in the peptide sequence. * indicates an increase of mass of +16 Da on the colored amino acid residue.

No other MS/MS spectrum was obtained, assuming that only those two amino acid residues are oxidized in the 6-16 moiety of $A\beta_{40}$.With these results, we can reasonably assume that the mass shift of +32 Da previously detected in HRMS is related to the oxidation of both His13 and His14 into 2-oxohistidine on the same peptide. However, this hypothesis cannot be confirmed here as no $A\beta_{6-16}$ ion with an increase of mass of 32 Da was fragmented and detected in MS/MS. This could be due to the fact that only a few part of the $A\beta_{40}$ peptide undergoes this double oxidation, resulting in a too low concentration to allow fragmentation.

Two different oxidations were also found on the $A\beta_{17-28}$ tryptic peptide, as shown in the two MS/MS spectra of the doubly protonated ion corresponding to $A\beta_{17-28}$ with a mass shift of +16 Da in Figure III.A-6. The two oxidations are located respectively on Phe19 and Phe20. The +16 Da mass shift on phenylalanine is related to the formation of hydrophenylalanine (see Section I.C.3.d for chemical structure).[8] Although two amino acid residues are targeted by ROS, no double oxidation of $A\beta_{17-28}$ was detected in LC-HRMS or in LC-MS/MS, as it was the case for $A\beta_{6-16}$. The oxidations of Phe19 and Phe20 may occur on the same peptide, but this double oxidation is likely to occur in minority on the Aβ peptide and is thus not detected in MS.

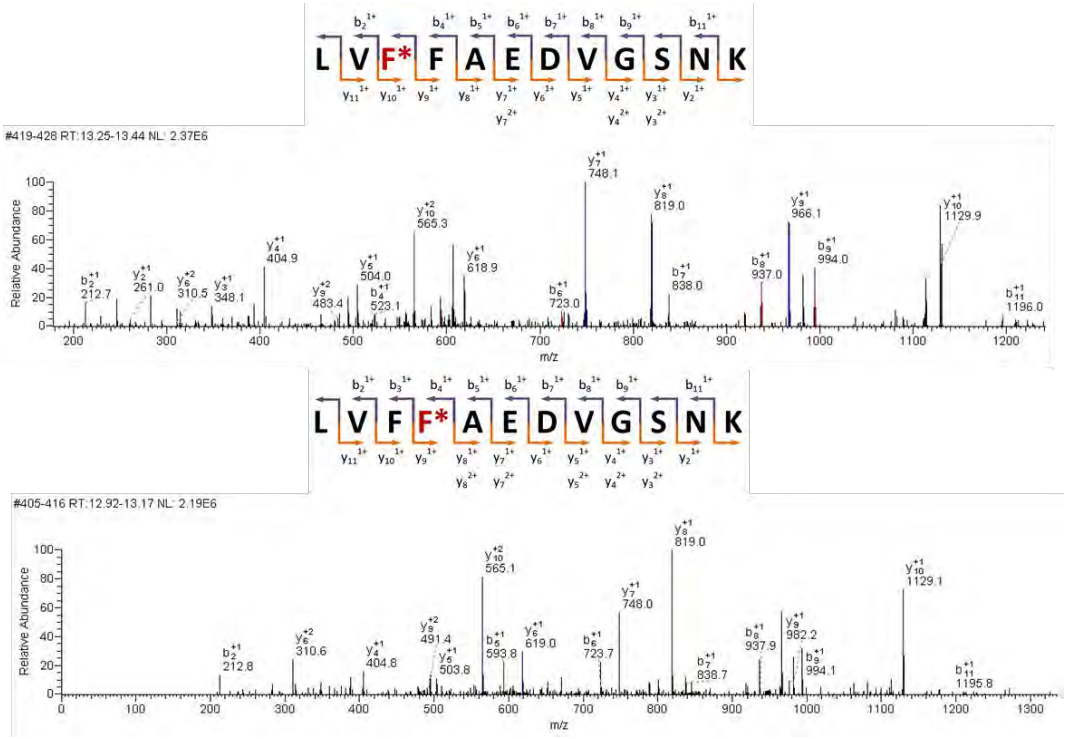

Figure III.A-6: Fragmentation spectra of doubly protonated ion (m/z 671.4) of tryptic $A\beta_{17-28}$ with oxidation on Phe19 (top) or Phe20 (bottom). b and y ions series (charge 1+ and 2+) detected are summarized in the peptide sequence. * indicates an increase of mass of +16 Da on the colored amino acid residue.

The $A\beta_{29-40}$ tryptic peptide was finally sequenced and, as assumed above, the oxidation detected with a mass shift of +16 Da is located on Met35, as shown by Figure III.A-7. This was expected and previously described [9-12] as methionine residue is very sensitive to oxidation and can be damaged by both the hydrogen peroxide [13-14] and the hydroxyl radical [1, 14] which are produced during metal-catalyzed ROS production.[15-16]

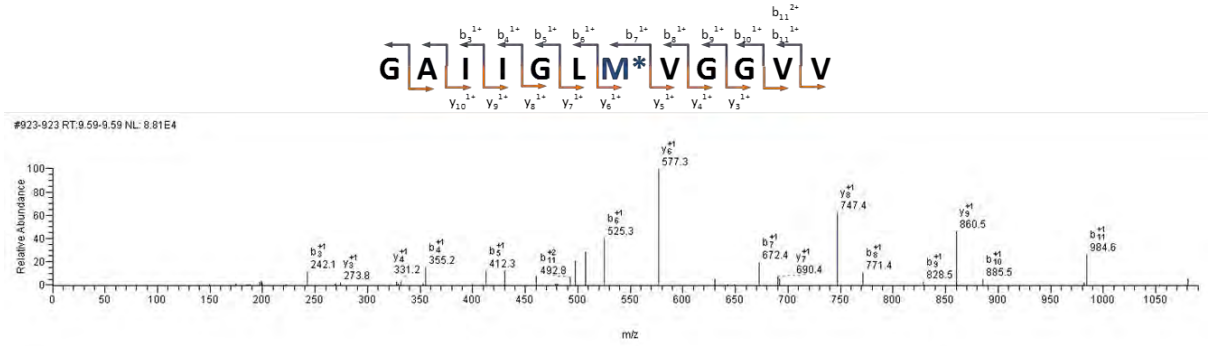

Figure III.A-7: Fragmentation spectra of doubly protonated ion (m/z 551.3) of tryptic $A\beta_{29-40}$ with oxidation on Met35. b and y ions series (charge 1+ and 2+) detected are summarized in the peptide sequence. * indicates an increase of mass of +16 Da on the colored amino acid residue.

The results obtained on $A\beta_{40}$ corroborate the study previously realized in the team with the truncated $A\beta_{28}$ peptide.[17] Similar oxidative damages and targeted residues were detected: oxidative cleavage and decarboxylation-deamination of Asp1,[2-3] His13 and His14 oxidized into 2-oxohistidine [7] and Phe19 and 20 detected as hydroxyphenylalanine.[8] Furthermore, Met35 was also found oxidized into methionine sulfoxide, in good agreement with what is widely described in the literature.[18-19] Figure III.A-8 summarizes the oxidations detected on $A\beta_{40}$ in the present study along with the chemical structures of the oxidized amino acid residues.

Among the identified oxidized residues, three of them (Asp1, His13 and His14) are proposed to be involved in the coordination of copper in the "in-between" state of Cu-Aβ,[17] i.e. in the redox competent state responsible for ROS production (see Section I.C.2.c). They are thus in close vicinity of copper and are preferential targets for the ROS attack. Their oxidation during MCO of Aβ was expected. This is not the case for Phe or Met residues, whose oxidation could appear as side damages resulting from an escaping of the ROS away from the catalytic center. At this point, we cannot conclude on the identity of the amino acid residues targeted first by $HO^{\bullet}$ because the level of oxidation for each targeted residue identified above is not known. The following part tends to answer this question.

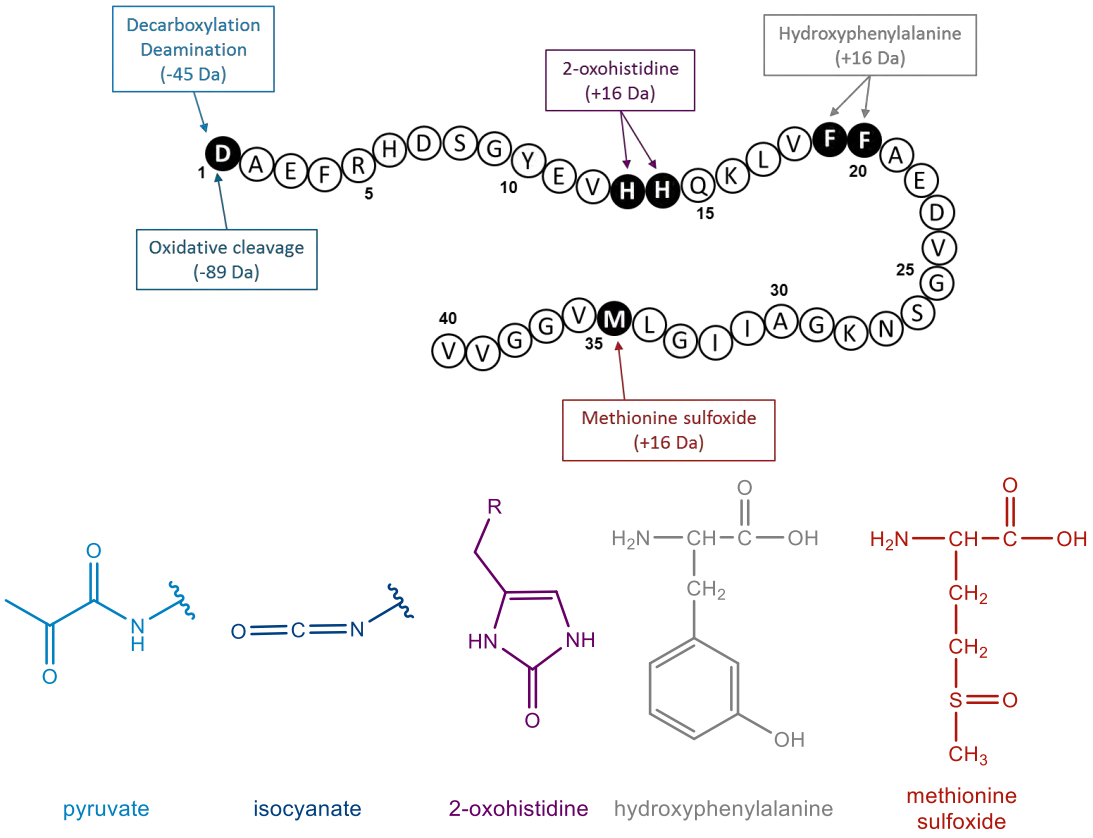

Figure III.A-8: (Top) Peptide sequence of Aβ$_{40}$ with the oxidized amino acid residues (black circle) detected along with the nature of oxidation and the change of mass and (bottom) chemical structure of the oxidized amino acid residues. The 3-hydroxyphenylalanine is shown as an example of phenylalanine oxidation product, but the 2- and 4-hydroxyphenylalanines can also be formed (see Section I.C.3.d).

III.B. Kinetics of Aβ$_{40}$ oxidation

The characterization of the amino acid residues of Aβ targeted by ROS and the nature of the oxidations, as investigated above, is carried out at the end of the reaction. In order to understand in what order the oxidative attack of ROS happens during MCO and what are the preferential targets of the ROS attack (among those identified above), the kinetics of the Aβ$_{40}$ peptide oxidation was monitored by LC-HRMS. Among the several amino acid residues oxidized, some of them could be preferentially targeted by ROS. Thus, the reaction started by mixing Aβ, copper and ascorbate, was stopped every minutes and the resulting reaction mixture was then analyzed by LC-HRMS.

A semi-quantitative approach was used to study the level of each oxidized residue as a function of the reaction time.

III.B.1. Experimental section

Copper(II)-catalyzed oxidation of the $A\beta_{40}$ peptide was carried out by mixing $A\beta_{40}$, Cu(II) and ascorbate in phosphate buffer (50 mM, pH 7.4) to reach final concentrations of 60, 50 and 500 µM, respectively (substoichiometry of copper to avoid free Cu(II) in solution) for a reaction mixture volume of 2 mL. Incubation was done at room temperature for a controlled reaction time. A volume of 100 µL of the reaction mixture was taken out every minutes between 0 and 14 min and the reaction was stopped by adding 400 µL of HCl 14.8 mM (final pH 2). At pH 2, copper is not bound to Aβ anymore and ascorbate is fully protonated into ascorbic acid (pKa 4.2 [20]), thus the ROS production is stopped. The 400 µL solution of Aβ was filtered by using Amicon 3 kDa centrifugal device (Millipore) by centrifugation for 15 min at 13500 rpm. The final volume is around 100 µL (volume before dilution in HCl). Trypsin digestion was then carried out and the four tryptic peptides described before were obtained (see Section II.B.3 for more details).

III.B.2. Results

The trace chromatograms were obtained for every oxidized tryptic peptide of $A\beta_{40}$, by using two monoisotopic ions corresponding to two charge states of the peptide. The mass accuracy was systematically set below 10 ppm. The m/z ratio used for the detection are listed in Table III.A-1. Figure III.B-1 shows the area ratio between the oxidized peptide and the equivalent non-oxidized peptide (control at t=0) as a function of reaction time. Such a calculated ratio gives a general tendency of the evolution of the oxidized species throughout the completion of the reaction. It cannot be considered as an accurate quantification because each peptide has a different propensity to get ionized in the ESI source and cannot be formally compared to another one.

Decarboxylation-deamination of Asp1 ($DAEFR_{dd}$) seems to be the major oxidative reaction since the level of $DAEFR_{dd}$ strongly increases with the reaction time. $DAEFR_{ox}$ (oxidative cleavage of Asp1) also increases with time, but to a much lesser extent (Figure III.B-1a). The level of $DAEFR_{dd}$ is increasing with time and seem to stop after 8 min. For $DAEFR_{ox}$, the tendency is less clear, but the formation rate of $DAEFR_{ox}$ seems also to slow down after 8 min.

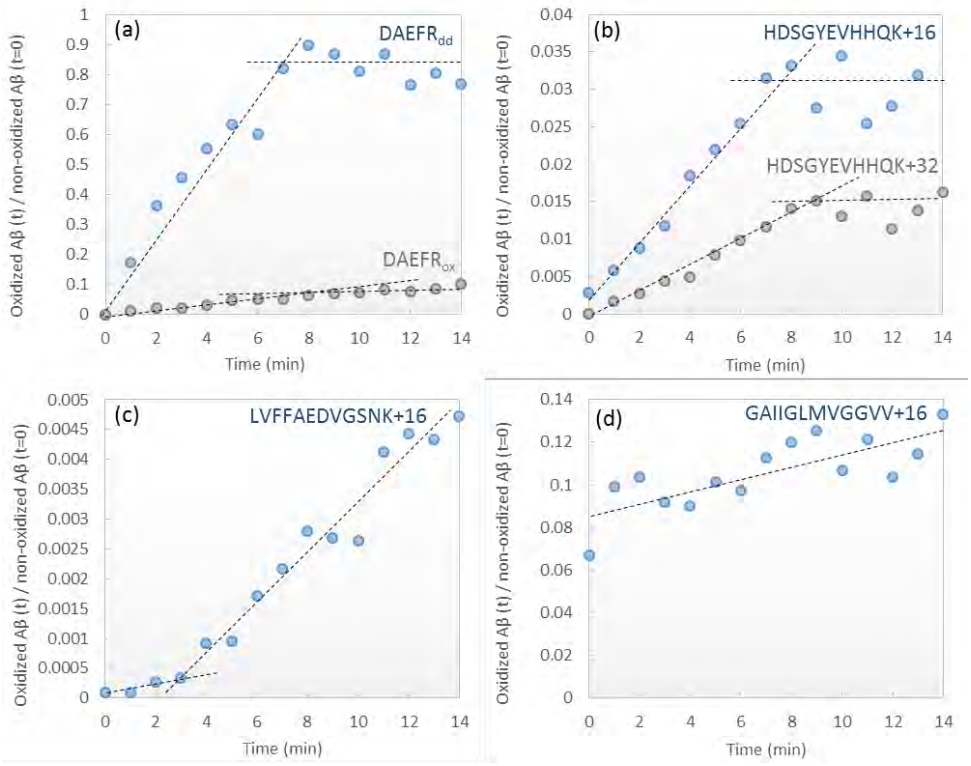

Figure III.B-1: Oxidation of the Aβ$_{40}$ tryptic peptides as a function of the time. Area ratio between the oxidized and the equivalent non-oxidized (control, t=0) tryptic peptide of Aβ$_{40}$ as a function of the reaction time. (a) Decarboxylation and deamination of Asp1 (DAEFR$_{dd}$) and oxidative cleavage of Asp1 (DAEFR$_{ox}$); (b) oxidation of His13/His14 (HDSGYEVHHQK+16 and +32); (c) oxidation of Phe19/20 (LVFFAEDVGSNK+16); (d) oxidation of Met35 (GAIIGLMVGGVV+16). Mass tolerance set at 10 ppm. m/z ratios used for detection are specified in Table III.A-1.

The same tendency is observed for the formation of the two oxidized species of Aβ$_{6-16}$ (Figure III.B-1b) HDSGYEVHHQK+16 and HDSGYEVHHQK+32, increasing during the first 8 min and then reaching a plateau.

As shown above, LVFFAEDVGSNK+16 can be assigned to the oxidation of either Phe19 or Phe20 (Figure III.B-1c). The tryptic peptide with the oxidation on both Phe was not detected (i.e. LVFFAEDVGSNK+32). Phe oxidation seems to be slower than Asp1 or His oxidation, in particular at the beginning of the reaction where a lag phase is observed. The curve starts to increase after 2 min of reaction and does not seem to reach a plateau around 8 min.

For several reasons, the evolution of Met35 oxidation as a function of the reaction time does not provide interesting information. First, methionine is very sensitive to oxidation and peptide/protein handling commonly participate to its oxidation. This is probably the reason why Met35 is already oxidized before MCO of Aβ has started (Figure III.B-1d). Second, methionine sulfoxide formed by the ROS attack can be reduced in non-oxidized methionine by ascorbate.[21] As ascorbate is present in quite high concentration in the reaction mixture, this phenomenon would be responsible for an underestimation of the level of methionine sulfoxide generated

during MCO. However, a slight increase of the gradient is observed during the reaction, thus Met35 seems to be oxidized during the course of the reaction.

To summarize, Asp1, His13 and His14 seem to be the first targets of ROS attack. Similar tendencies were obtained with the truncated $A\beta_{28}$ peptide, resulting in a proposition of Cu-Aβ binding mode in the "in-between" state.[17] As Asp1, His13 and His14 are the first targets for $HO^{\bullet}$ during the ROS production, and because they are involved in Cu(II) or/and Cu(I) coordination in the resting states, [22-27] they were proposed to participate in Cu binding in this transient state. The results obtained with $A\beta_{40}$ are consistent with this hypothesis. With this in mind, the stop of Asp and His oxidations after 8 min could be interpreted as a change of coordination during MCO. Indeed, if Asp1, His13 and His14 are involved in copper coordination during the ROS production, they are first targeted and are quickly oxidized. Thus, as they are damaged, they may not be good ligand under their oxidized form, leading to a change of coordination.

Phe oxidation starts after a 2-min lag phase and reach a much lower level of oxidation. As Asp1, His13 and His14 residues are targeted first by $HO^{\bullet}$, the oxidation of phenylalanine residues is likely to be a side damage of the ROS production by the system, and would start when the amino acid residues targeted first by $HO^{\bullet}$ are sufficiently oxidized to let escape the ROS. This is in line with the lag phase at the beginning of the reaction, indicating that Phe residues are not directly targeted by $HO^{\bullet}$, although they are very sensitive to $HO^{\bullet}$ oxidation.[1] The same applies for Met35 which is not coordinated to copper.

III.C. NMR study of Aβox

The above results were obtained by MS based techniques. In order to corroborate them, we wanted to analyze $A\beta_{ox}$ by using a different technique. The chemical modification undergone by the amino acid residues of Aβ after MCO were analyzed by ^1H NMR. We have chosen to use the truncated $A\beta_{28}$ instead of $A\beta_{40}$, as the complete attribution of the ^1H NMR is available.[28] As the only damage observed on the 29-40 moiety of $A\beta_{40}$ was attributed to Met35 oxidation and is well-described,[9-12] we keep the essential information by working on $A\beta_{28}$ instead of $A\beta_{40}$.

III.C.1. Experimental section

The methodology and conditions used for these experiments are detailed in Section II.E.2.

III.C.2. Results

^{1}H NMR of $A\beta_{28}$ leads to a spectrum with numerous peaks. In order to be able to observe the impact of oxidation on the targeted amino acid residues (Asp1, His13, His14, Phe19 and Phe20), the present study was carried out at pH 10.5, where H_α of Asp1 and the aromatic protons of both His and Phe residues are well separated from other protons and thus easily detectable.

A complete NMR study of $A\beta_{28}$ was previously realized in the team,[28] leading to the attribution of all the protons of $A\beta_{28}$ (see Annex II for ^{1}H chemical shifts table and $A\beta_{28}$ sequence along with the atom identifiers of each amino acid residue). Although the study was carried out at pH 7.4, it was useful to help us to attribute the protons of the amino acid residues of interest.

Figure III.C-1 shows the ^{1}H NMR spectra obtained for $A\beta_{28}$ (black line) and $A\beta_{28}$ox (blue line) in the four shift ranges of interest: 0.5-2.0, 2.0-3.3, 3.5-4.7 and 6.7-7.9 ppm. Oxidation strongly affects the ^{1}H NMR signal, as the peaks of $A\beta_{28}$ox are very broad compared with the one of $A\beta_{28}$. Thus, only a qualitative comparison is made between $A\beta_{28}$ and $A\beta_{28}$ox. The amino acid residues of the C-terminal moiety are not affected by oxidation: Asp23, Val24, Gly25, Ser26 Asn27 and possibly Ala21 and Lys28. For the latter two, their proton signals have similar chemical shifts than Ala2 and Lys16 (around 1.4 ppm). The two doublets of Ala2 and Ala21 form a triplet-like signal and the two doublets of triplets of Lys16 and Lys28 are hidden under the Ala signals. After oxidation, a doublet corresponding to H_β protons of an Ala residue in observed, hiding a part of another signal, probably a doublet of triplets of the H_γ protons of a Lys residue. Thus, as the amino acid residues close to Ala21 and Lys28 are not affected by oxidation, it is likely that Ala2 and Lys16 are affected by oxidation and Ala21 and that Lys28 are not.

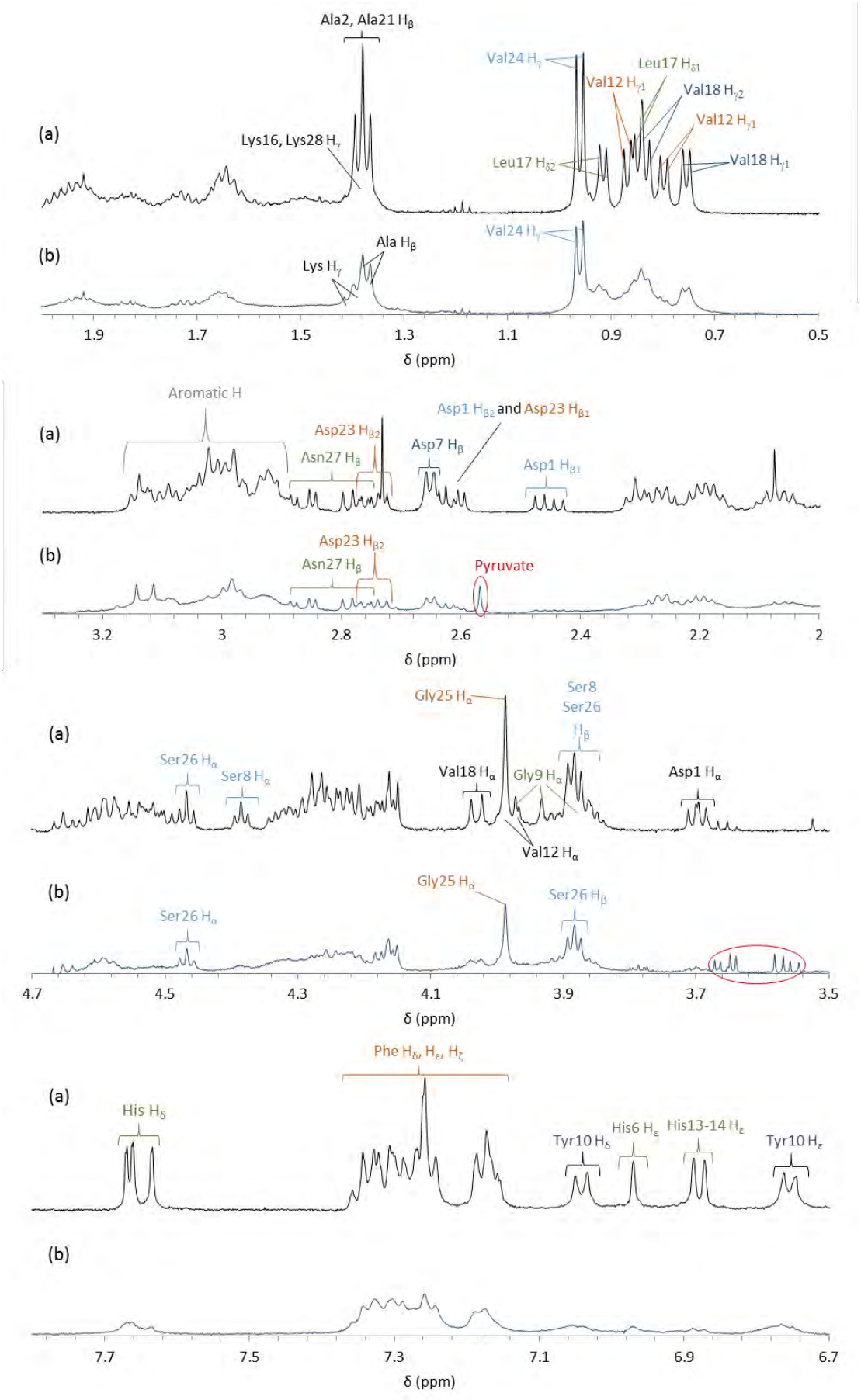

Figure III.C-1: ^{1}H NMR spectra of Aβ$_{28}$ (a) and Aβ$_{28}$ox (b) at pH 10.5.

Unlike the C-terminal moiety of Aβox (from Ala21 to Lys28) which is not disturbed by oxidation, the majority of the amino acid residues of the N-terminal moiety are strongly affected. For example, the apolar aliphatic amino acid residues such as Val and Leu residues have broaden protons signals (around 0.7-0.9 ppm) although they are weakly sensitive to oxidation.[1] Thus, the oxidation of some amino acid residues of the N-terminal moiety of $A\beta_{28}$ seems to affect the proton signals of the neighboring amino acid residues. As Val and Leu residues (except Val24 which is not affected by oxidation) are close to His13, His14, Phe19 or Phe20, which are found oxidized in MS experiments (see Section III.A), this could explain their broad NMR signals.

However, some signals seem to be wider than the ones of Val and Leu residues. In particular, the signals of H_α and H_β protons of Asp1 (at 3.68 and 2.45 ppm) are almost erased. Moreover, a signal is observed at 2.6 ppm only in $A\beta_{28}$ox (Figure III.C-1b, red oval). This is likely to be the signal of the three equivalent protons of the methyl group in the pyruvate function formed by the decarboxylation-deamination of Asp1 (see Section I.C.3.b). Thus, the results are in line with the oxidation of Asp1 by decarboxylation-deamination detected in MS (see Section III.A).

Signals assigned to H_δ and H_ε of His6, His13 and His14 are observed at chemical shifts around 7.6 and 6.9 ppm respectively. H_α and H_β peaks of His are not noticeable since they have chemical shifts around 3 and 4.5 ppm, as numerous other protons of the peptide (Figure III.C-1) and are thus difficult to isolate. ^{1}H NMR peaks of His are also strongly affected by oxidation. The same tendency is observed for the other aromatic residues (Phe and Tyr residues).

Another signal is present only in the $A\beta_{28}$ox spectrum around 3.6 ppm, with a signature corresponding to two diastereotopic protons. These protons are probably related to an oxidation product of Aβ, but the origin is unknown as its chemical shift does not correspond to an oxidized amino acid residue listed above (see Section I.C.3) or detected previously in MS (see Section III.A).

III.C.3. Summary

The interpretation of ^{1}H NMR spectrum of $A\beta_{28}$ox was made difficult by the strong broadening of the peaks obtained. The origin of this broadening could tentatively be explained by the fact that (i) different oxidized species are generated during MCO of Aβ, thus leading to different chemical shifts for a given proton, (ii) the numerous chemical modifications undergone by the peptide may also change the environment of the protons owned by the amino

acid residues not oxidized that are close to the oxidized one and (iii) the high level of concentration needed to perform NMR experiments requires for Aβox to be highly reconcentrated (from 60 µM to 400 µM), which might result in a modification of the sample (e.g. oligomerization for instance).

However, the presence of signals not affected have highlighted that the C-terminal moiety of the $A\beta_{28}$ peptide (between Ala21 and Lys28) is not affected by oxidation. This is in line with identification of Asp1, His13, His14, Phe19 and Phe20 as the only oxidized amino acid residues detected in MS.

In the 1-20 part of $A\beta_{28}$, the NMR spectrum of $A\beta_{28}$ox does not provide information on the oxidized amino acid residues as the majority of the signals are broad. Thus, the identification of Asp1, His13 and His14 as the main oxidized amino acid residues in MS cannot be confirmed by NMR. However, the presence of a peak in $A\beta_{28}$ox spectrum attributed to the methyl group of the pyruvate confirms the oxidation of Asp1 by decarboxylation and deamination.

III.D. Conclusion

In the present study, LC-HRMS, LC-MS/MS and ^{1}H NMR have been used to investigate the oxidation of the Aβ peptide during the ROS production. Both techniques have highlighted the chemical changes undergone by the peptide due to the ROS oxidative attack.

MS experiments enabled to determine the oxidized amino acid residues of the Aβ sequence and to characterize the nature of the oxidation undergone by each amino acid residue. Asp1 is found oxidized either by decarboxylation-deamination or by oxidative cleavage, leading to the formation of a pyruvate or an isocyanate function respectively. His13 and 14 are found oxidized into 2-oxohistdines, Phe19 and Phe20 into hydroxyphenylalanine and Met35 into methionine sulfoxide. Furthermore, through a kinetic study of the amino acid residues oxidation, Asp1, His13 and His14 have been found to be the main targets of ROS, while Phe19, Phe20 and Met35 are secondarily targeted. The results are in line with the previous study realized on the truncated $A\beta_{28}$ [17] and complete it by showing that (i) as expected, Met35 is also oxidized during the MCO of $A\beta_{40}$ but as a secondary target and (ii) that $A\beta_{28}$ is an appropriate model for oxidation studies as the same main oxidations are detected for both the truncated and the full-length peptides.

Although the ^{1}H NMR spectrum of $A\beta_{28}$ox is not easily exploitable since the proton signals are broaden, the presence of signals not disturbed by oxidation has shown that no oxidation occurs in the 21 to 28 part of the $A\beta_{28}$. Moreover, the decarboxylation and

deamination undergone by Asp1, leading to the formation of a N-terminal pyruvate function, is confirmed by the presence of a signal attributed to the protons of the pyruvate methyl group.

Kinetic study of the amino acid residues oxidation has also shown that besides being the main targets, Asp1, His13 and His14 are strongly oxidized during the first minutes of the MCO and then are not targeted anymore. This phenomenon was also observed in the previous study [17] and has led to the proposition that these three amino acid residues would be the main ligands for Cu(II) and Cu(I) in the "in-between" state (see Section I.C.2.c) during the ROS production. As they are targeted by the ROS, the chemical modifications they undergo may impact their aptitude to be a good ligand for copper. Hence, a change of coordination may occur and would explain the reason why they are not oxidized anymore after a few minutes of MCO.

As addressed above (see Section I.C.1) Asp1, His13 and His14 are also involved in Cu(II) or/and Cu(I) coordination in the resting states. Thus, the MCO of Aβ may have consequences on the copper coordination both in the resting and "in-between" states.

References

[1] L. M. Dorfman and G. E. Adams in *Reactivity of the hydroxyl radical in aqueous solutions*, *Vol.* DTIC Document, **1973**.

[2] T. Kowalik-Jankowska, M. Ruta, K. Wiśniewska, L. Łankiewicz and M. Dyba, *Journal of Inorganic Biochemistry* **2004**, *98*, 940-950.

[3] K. Inoue, A. Nakagawa, T. Hino and H. Oka, *Analytical Chemistry* **2009**, *81*, 1819-1825.

[4] E. Stadtman, *Annual Review of Biochemistry* **1993**, *62*, 797-821.

[5] K. Biemann, *Methods in Enzymology* **1990**, *193*, 455-479.

[6] A. R. Dongre, J. L. Jones, Á. Somogyi and V. H. Wysocki, *Journal of the American Chemical Society* **1996**, *118*, 8365-8374.

[7] S. A. Lewisch and R. L. Levine, *Analytical Biochemistry* **1995**, *231*, 440-446.

[8] E. R. Stadtman and R. L. Levine, *Amino Acids* **2003**, *25*, 207-218.

[9] M. Palmblad, A. Westlind-Danielsson and J. Bergquist, *The Journal of biological chemistry* **2002**, *277*, 19506-19510.

[10] F. Misiti, M. E. Clementi and B. Giardina, *Neurochemistry International* **2010**, *56*, 597-602.

[11] M. Friedemann, E. Helk, A. Tiiman, K. Zovo, P. Palumaa and V. Tõugu, *Biochemistry and Biophysics Reports* **2015**, *3*, 94-99.

[12] M. Gu and J. H. Viles, *Biochimica et Biophysica Acta, Proteins and Proteomics* **2016**.

[13] Y. Shechter, Y. Burstein and A. Patchornik, *Biochemistry* **1975**, *14*, 4497-4503.

[14] W. Vogt, *Free Radical Biology and Medicine* **1995**, *18*, 93-105.

[15] S. I. Dikalov, M. P. Vitek and R. P. Mason, *Free Radical Biology and Medicine* **2004**, *36*, 340-347.

[16] C. Hureau and P. Faller, *Biochimie* **2009**, *91*, 1212-1217.

[17] L.-E. Cassagnes, V. Hervé, F. Nepveu, C. Hureau, P. Faller and F. Collin, *Angewandte Chemie International Edition* **2013**, *52*, 11110-11113.

[18] C. Schöneich, *Biochimica et Biophysica Acta* **2005**, *1703*, 111-119.

[19] D. A. Butterfield and R. Sultana, *Journal of amino acids* **2011**, *2011*.

[20] M. A. Ross, *Journal of Chromatography B: Biomedical Sciences and Applications* **1994**, *657*, 197-200.

[21] C. Schöneich, *Archives of Biochemistry and Biophysics* **2002**, *397*, 370-376.

[22] C. Hureau and P. Dorlet, *Coordination Chemistry Reviews* **2012**, *256*, 2175-2187.

[23] C. Hureau, *Coordination Chemistry Reviews* **2012**, *256*, 2164-2174.

[24] C. Migliorini, E. Porciatti, M. Luczkowski and D. Valensin, *Coordination Chemistry Reviews* **2012**, *256*, 352-368.

[25] I. Zawisza, M. Rózga and W. Bal, *Coordination Chemistry Reviews* **2012**, *256*, 2297-2307.

[26] C. Hureau, V. Balland, Y. Coppel, P. L. Solari, E. Fonda and P. Faller, *Journal of Biological Inorganic Chemistry* **2009**, *14*, 995-1000.

[27] J. Shearer and V. A. Szalai, *Journal of the American Chemical Society* **2008**, *130*, 17826-17835.

[28] H. Eury in *Etude de l'intéraction de la thioflavine T et de complexes de ru (ii) avec le peptide amyloïde bêta dans le cadre de la maladie d'alzheimer*, *Vol.* **2013**.

Chapter IV

Chapter IV: Consequences of Aβ oxidation

This chapter focuses on the consequences of the Aβ peptide oxidation regarding metal coordination, as well as Reactive Oxygen Species (ROS) production and peptide aggregation, two key events of Alzheimer's Disease (AD).[1] The coordination of Cu(II), Cu(I) and Zn(II) coordination to the oxidized Aβ peptide (Aβox) has been investigated by Electron Paramagnetic Resonance (EPR) and X-ray absorption (XANES). The ROS production during metal-catalyzed oxidation (MCO) of Aβ has been studied at different steps of Aβ oxidation. Finally, the impact of Aβ oxidation on fibrils formation has been studied by Thioflavin T (ThT) fluorescence and Transmission Electron Microscopy (TEM).

IV.A. Cu coordination and ROS production with Aβox

This section focuses on the impact of Aβ oxidation on Cu(I) and Cu(II) binding modes and on the ROS production. It is composed of an article published in the journal *Metallomics* in 2016 [2] along with a summary of the article, written in French (requirement of the doctoral school). The supporting information related to the article are situated at the end of the chapter.

IV.A.1. Article

Metallomics

PAPER

View Article Online
View Journal

Cite this: DOI: 10.1039/c6mt00150e

Metal-catalyzed oxidation of Aβ and the resulting reorganization of Cu binding sites promote ROS production†

Clémence Cheignon,*[abc] Peter Faller,‡[ab] Denis Testemale,[de] Christelle Hureau[ab] and Fabrice Collin*[abc]

Received 5th July 2016,
Accepted 24th August 2016

DOI: 10.1039/c6mt00150e

www.rsc.org/metallomics

In the context of Alzheimer's disease (AD), the production of HO• by copper–amyloid beta (Aβ) in the presence of ascorbate is known to be deleterious for the Aβ peptide itself and also for the surrounding molecules, thus establishing a direct link between AD and oxidative stress. The metal-catalyzed oxidation (MCO) of Aβ primarily targets the residues involved in copper coordination during HO• production. In the present work, we demonstrate that the oxidative damage undergone by Aβ during MCO lead to a change in copper coordination, with enhanced catalytic properties that increases the rates of ascorbate consumption and HO• production, and the amount of HO• released by the system. This phenomenon is observed after the peptide has been sufficiently oxidized.

Introduction

In 2012, 36 million people suffered from Alzheimer's disease (AD), the widespread neurodegenerative disease. A hallmark of this disease is the presence of senile plaques in the brain,[1] mainly composed of the amyloid-β peptide (Aβ)[2] in an aggregated form. The peptide is also found in a soluble form in healthy brains.[3] A high concentration of metals, such as copper, zinc and iron, are also found in the plaques.[4–6] Cu and Zn are bound directly to the Aβ peptide. Among them, copper is redox-active and can catalyze the production of Reactive Oxygen Species (ROS) when bound to Aβ.[7–9] In the presence of dioxygen and a reductant such as ascorbate, the Cu–Aβ system can produce the superoxide anion ($O_2^{\bullet -}$), hydrogen peroxide (H_2O_2) and the hydroxyl radical (HO•) *in vitro*.[8,10,11] The latter is the most reactive and can cause oxidative damage to the surrounding biomolecules, such as lipids, nucleic acids and proteins (with the rate constant usually ranging from 10^9 to 10^{10} L mol^{-1} s^{-1} [12]), including Aβ itself, which is found to be oxidized in amyloid plaques *in vivo*.[13] The link between AD and oxidative stress is also supported by DNA oxidation, proteins and lipid peroxidation, as evidenced in the brain of AD patients.[14,15]

The coordination mode of copper with Aβ is of interest for a better understanding of the metal-catalyzed ROS production. At physiological pH, two coordination modes with a square-planar geometry were identified for the Cu(II)–Aβ complex, called components I and II (Fig. 1a),[16,17] involving in particular Asp1 and the His residues His6, 13 and 14. The two forms are in pH-dependent equilibrium with a pK_a value of 7.8.[18] In addition, dynamic exchange between ligands on a given binding position is also observed.[19] Cu(I) is linked to Aβ in a linear fashion by two of the three His residues present in the Aβ sequence, in a fast dynamic exchange between ligands.[19,20] The major form involves His13 and His14 (Fig. 1b).

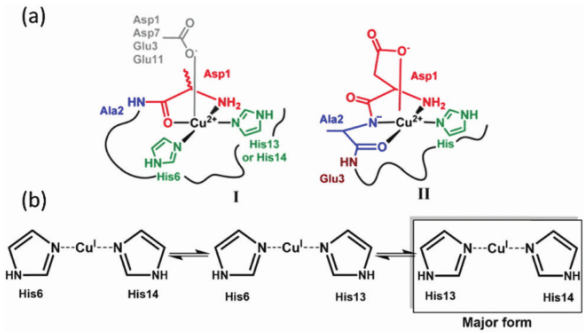

Fig. 1 (a) Cu(II) coordination and (b) Cu(I) coordination to the Aβ peptide.[16,20]

[a] LCC (Laboratoire de Chimie de Coordination), CNRS UPR 8241, 205 route de Narbonne, 31062 Toulouse Cedex 09, France. E-mail: clemence.cheignon@lcc-toulouse.fr, fabrice.collin@univ-tlse3.fr; Tel: +33 (0)5 61 33 31 56
[b] Université de Toulouse, UPS, INPT, 31077 Toulouse, France
[c] UMR 152 Pharma Dev, Université de Toulouse, IRD, UPS, France
[d] University of Grenoble Alpes, Institut NEEL, F-38000 Grenoble, France
[e] CNRS, Institut NEEL, F-38000 Grenoble, France

† Electronic supplementary information (ESI) available: Monoisotopic masses of the peptide, mass spectrometric data, fluorescence curves, linear combination fitting, UV-vis data, HPLC-UV data, and EPR data. See DOI: 10.1039/c6mt00150e

‡ Current address: Institut de Chimie (UMR 7177), 4 rue B. Pascal, F-67000 Strasbourg, France.

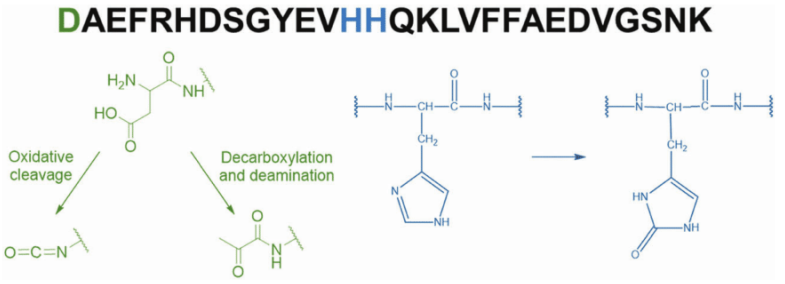

Fig. 2 Amino acid sequence of the $A\beta_{28}$ peptide (top) along with the main targeted amino acid residues (in color) and the chemical structure of the oxidation products (bottom). Asp1 oxidation leads to the formation of either an isocyanate or a pyruvate function[21,25] (green) and His13 and His14 oxidation reactions lead to the formation of 2-oxohistidines[21,23,24] (blue).

To catalyze the ROS production, copper has to cycle between its two redox states. As the coordination of Cu(I) and Cu(II) with Aβ is very different, the direct electron transfer between those two states (called the resting states) is too slow, due to the high requirement of rearrangement energy. The electron transfer rather proceeds *via* a low-populated redox-competent state, called the "in-between" state, for which Cu(I) and Cu(II) coordination with Aβ is close enough to allow minimal energy for reorganization.[21,22]

The metal-catalyzed oxidation (MCO) of Aβ by the Cu–Aβ/ascorbate/O_2 system has been previously studied.[21,23,24] Because ROS are produced at the metal center, the Aβ peptide residues are the preferential targets for an $HO^{\bullet}$ attack. In line with their involvement in copper coordination in the "in-between" state of Cu–Aβ,[21] Asp1, His13 and His14 are the major oxidized residues (Fig. 2). Asp1 oxidation was proposed to lead to the formation of either an isocyanate or a pyruvate function *via* oxidative cleavage or decarboxylation and deamination, respectively,[21,25] while His13 and 14 are found to be oxidized into 2-oxohistidines.[21,23,24] The oxidation of Asp1 was found to be three times higher than the oxidation of histidine, with decarboxylation/deamination as a preferential mechanism (5 times higher than the oxidative cleavage).

Thus, the oxidation of the major ligands leading to the oxidized Aβ peptide (Aβox as named below), could have an impact on the coordination sites of copper with Aβ. The impact could be different for the two oxidation degrees of both the resting and "in-between" states of Cu–Aβ. These structural changes might result in a modification of the catalytic properties of the complex.

Thus, in the present study, we report first on the consequence of the oxidation of the Aβ peptide on the coordination of Cu(I) and Cu(II) resting states by X-ray absorption near edge spectroscopy (XANES) and electron paramagnetic resonance (EPR). Then we analyze the impact of Aβ oxidation on the Cu-induced ROS production by mass spectrometry, UV-visible and fluorescence spectroscopies.

Experimental

Chemicals

The Cu(II) used was from $CuSO_4{\cdot}5(H_2O)$ and purchased from Sigma. A stock solution of Cu(II) (10 mM) was prepared in ultrapure water. Phosphate buffer was bought from Sigma-Aldrich and dissolved in ultrapure water to reach a 100 mM concentration and pH 7.4. HEPES buffer was bought from Sigma and dissolved in ultrapure water to reach a 0.5 M concentration and pH 7.1. Ascorbate solutions were freshly prepared a few minutes prior to each experiment by dissolving sodium L-ascorbate (Sigma) in ultrapure water. Hydrogen peroxide (H_2O_2) solutions were freshly prepared from a 30 wt% H_2O solution purchased from Sigma-Aldrich. A stock solution of coumarin-3-carboxylic acid (CCA) 1 mM (from Sigma) was prepared in phosphate buffer (0.1 M, pH 7.4) at room temperature. Ethylene diamine tetraacetic acid (EDTA) was purchased from Sigma-Aldrich and dissolved in ultrapure water to reach a concentration of 40 mM. Sodium dithionite was bought from Sigma-Aldrich and dissolved in ultrapure water a few minutes prior to each experiment.

Peptides

All the synthetic peptides were bought from GeneCust (Dudelange, Luxembourg), with a purity grade of >95%. Stock solutions of $A\beta_{28}$ (sequence DAEFRHDSGYEVHHQKLVFFAEDVGSNK), $AcA\beta_{28}$ (sequence Ac-DAEFRHDSGYEVHHQKLVFFAEDVGSNK), $A\beta_7$ (sequence DAEFRHD), $A\beta_{16}$ (sequence DAEFRHDSGYEVHHQK), $AcA\beta_{16}$ (Ac-DAEFRHDSGYEVHHQK) and D7H–$A\beta_{16}$ (sequence DAEFRHHSGYEVHHQK) peptides were prepared by dissolving the powder in ultrapure water (resulting pH ≈ 2). The peptide concentration was then determined by UV-visible absorption of Tyr10 considered as free tyrosine (at pH 2, $(\varepsilon_{276} - \varepsilon_{296})$ = 1410 M^{-1} cm^{-1}). For $A\beta_7$, the absorption of Phe ($(\varepsilon_{258} - \varepsilon_{280})$ = 190 M^{-1} cm^{-1}) was used.

Oxidation of the Aβ peptide

The $A\beta_{28}$ peptide (60 μM) was oxidized in a phosphate buffered solution (50 mM, pH 7.4) containing Cu(II) (50 μM) and ascorbate (0.5 mM) for 30 min. Then, the solution was concentrated with a Amicon Ultra 3 kDa membrane (Millipore), washed with EDTA (10 equiv.) to remove copper, then with water and finally with NaOH (50 mM, pH ≈ 13). The oxidized peptide solution was recovered and the concentration of the oxidized Aβ peptide was then determined through the UV-visible absorption of Tyr10, considered as free tyrosine ($(\varepsilon_{293} - \varepsilon_{360})$ = 2400 M^{-1} cm^{-1}) in NaOH (50 mM, resulting pH ≈ 13).

As the oxidized peptide solution has a background absorbance at 293 nm, the curve is fitted to subtract the absorbance due to the tailing (see Fig. S1, ESI†) from the Tyr absorption. The $A\beta_{28}$ peptide was used for technical reasons (membrane cut-off of 3 kDa).

HO• production monitoring

Fluorescence experiments were performed on a multi-plate reader FLUOstar Optima 96-well plate reader system (BMG Labtech) at 25 °C. Two automatic injectors were used to add ascorbate and hydrogen peroxide solutions into the wells during experiments. Coumarin-3-carboxylic acid (CCA) was used as a probe to detect HO•, as it reacts with CCA to form 7-hydroxycoumarin-3-carboxylic acid (7-OH-CCA), which is fluorescent at 452 nm upon excitation at 395 nm. The intensity of the fluorescence signal is proportional to the number of 7-OH-CCA molecules formed, which in turn is proportional to the HO• radicals released.[26] A fixed volume of 2 μL of ascorbate (2 mM) and 2 μL of hydrogen peroxide (5 mM) were added every 15 min for 2 hours to 200 μL of phosphate buffered (pH 7.4, 50 mM) solutions containing CCA (0.5 mM) and Cu(II) (20 μM) with or without the Aβ peptide ($A\beta_{16}$, $A\beta_{7}$, $AcA\beta_{16}$, D7H–$A\beta_{16}$, $A\beta_{28}$, $AcA\beta_{28}$, or $A\beta_{40}$) (25 μM). The fluorescence was monitored every 30 s.

Ascorbate consumption experiments

UV-Vis spectra were recorded on an Agilent 8453 UV-visible spectrophotometer at 25 °C. The intensity of the ascorbate (Asc) absorption band at λ = 265 nm (ε = 14 500 M^{-1} cm^{-1}) was monitored as a function of time, in 50 mM phosphate buffer, pH 7.4 containing 10 μM of Cu(II), 12 μM of peptide and 100 μM of Asc.

EPR measurements

EPR spectra were recorded on a Bruker Elexsys E500 spectrometer equipped with a continuous flow cryostat (Oxford). Analysis was performed using an aqueous solution containing 10% of glycerol, ^{65}Cu (450 μM) and peptide (500 μM). The pH was adjusted to 12.5 with NaOH (1 M). Experimental parameters were set as follows: T = 120 K, ν = 9.5 GHz, microwave power = 20.5 mW, amplitude modulation = 10.0 G, and modulation frequency = 100 kHz.

Mass spectrometry

High Performance Liquid Chromatography/High Resolution Mass Spectrometry (HPLC/HRMS) analysis was performed on a LTQ-Orbitrap XL mass spectrometer (Thermo Fisher Scientific, Les Ulis, France), equipped with an electrospray ionization source, and coupled to an Ultimate 3000 LC System (Dionex, Voisins-le-Bretonneux, France). The sample (10 μL) was injected onto the column (Phenomenex, Synergi Fusion RP-C18, 250 × 1 mm, 4 μm) at room temperature. Gradient elution was carried out with formic acid 0.1% (mobile phase A) and acetonitrile/water (80/20 v/v) formic acid 0.1% (mobile phase B) at a flow-rate of 50 μL min^{-1}. The mobile phase gradient was programmed with the following time course: 12% mobile phase B at 0 min, held for 3 minutes, linear increase to 100% B at 15 min, held for 4 min, and linear decrease to 12% B at 20 min and held for 5 min. The mass spectrometer was used as a detector, working in the full scan positive mode between 50 and 2000 Da. The Orbitrap cell was operated in the full-scan mode at a resolution power of 60 000. HPLC/HRMS was also used to check for digestion efficiency, systematically found close to 100% (non-digested peptides were not detected).

Proteolytic digestion

The solution of Aβ was filtered using an Amicon 3 kDa centrifugal device (Millipore) by centrifugation for 15 min at 13 500 rpm, then washed and centrifuged twice with 200 μL sodium hydrogenocarbonate (100 mM, pH 8). The concentrated sample (approx. 50 μL) was recovered and transferred to an Eppendorf ProteinLoBind 1.5 mL vial. Trypsin (0.05 ng μL^{-1} in formic acid 0.1%) was added to obtain an Aβ/trypsin ratio of 20/1 (w/w) and digestion was carried out at 37 °C for 3 h in a Thermomixer (Eppendorf), with 10 s mixing at 750 rpm every min.

Cu K-edge X-ray absorption measurements

The copper-containing Aβ ($A\beta_{28}$, $A\beta_{28}$ox or $A\beta_{7}$) solutions were injected into sample holders in between two Kapton windows (3 M, cat. #1205; Minneapolis, MN) and immediately frozen in liquid nitrogen. All samples were maintained at 10–20 K throughout data collection using a helium cryostat. Cu K-edge XANES (X-ray absorption near edge structure) spectra were recorded at the BM30B (FAME) French CRG beamline at the European Synchrotron Radiation Facility (ESRF, Grenoble, France).[27] The storage ring was operated in a uniform mode at 6 GeV with a 200 mA current. The beam energy was selected using an Si(220) N_2 cryo-cooled double-crystal monochromator with an experimental resolution of ~0.5 eV.[28] The beam spot on the sample was approximately 200 × 100 μm^2 ($H \times V$, FWHM). The spectra were collected in a fluorescence mode using a 30-element Ge solid-state fluorescence detector (Canberra). The energy was calibrated with Cu metallic foils, such that the maximum energy of the first derivative was set at 8979 eV. Cu data were collected from 8830 to 8960 eV using 5 eV step and 2 s counting time, from 8960 to 9020 eV using 0.5 eV step and 3 s counting time, and from 9020 to 9300 eV with a k-step of 0.05 $Å^{-1}$ and the counting time increasing from 2 to 10 s.

For each sample, three spectra were averaged and the resulting XANES spectra were background-corrected by linear regression through the pre-edge region and a polynomial through the post-edge region and normalized to the edge jump. The beam was moved to a different position on the sample for each scan to avoid potential Cu photoreduction. All spectra were individually inspected prior to data averaging to ensure that beam damage was not occurring.

Cu(I) samples were prepared under a continuous flow of N_2 by direct addition (10 equiv.) of fresh made sodium dithionite ($Na_2S_2O_4$) stock solution (0.1 M) into the sample holder containing $CuSO_4$ (0.9 mM) and the peptide (1 mM) in the presence of 10% glycerol as a cryoprotectant with the pH adjusted to 7.1. The sample was immediately frozen in liquid nitrogen. Under such conditions, no significant pH drift due to the addition of $Na_2S_2O_4$ was measured.

View Article Online
Paper Metallomics

Results

Introductory remarks

This study focused on two peptides, $A\beta_{16}$ and $A\beta_{28}$, as valuable counterparts of the full-length peptides. These two short peptides are: (i) valuable models for studying copper coordination and ROS production since copper binds to the N-terminal part of Aβ (16 first residues)[29–32] and (ii) easier to handle than the full-length peptide ($A\beta_{40/42}$), which is more prone to aggregation.

In the first three parts of the paper, where oxidized Aβ (Aβox) is under focus, the $A\beta_{28}$ peptide was used as well as the truncated $A\beta_7$ peptide and the acetylated $A\beta_{28}$ peptide ($AcA\beta_{28}$). $A\beta_7$ only bears one histidine residue, and is thus a valuable model to mimic His13 and His14 oxidation reactions. $AcA\beta_{28}$ has a blocked N-terminal moiety and is an appropriate model to mimic Asp1 oxidation, as its N-terminal amine is not involved anymore in Cu(II) coordination.

In the last part describing the evolution of $HO^\bullet$ release during Aβ oxidation, the $A\beta_{16}$ peptide is used for comparison with the truncated $A\beta_7$ peptide, the acetylated $A\beta_{16}$ ($AcA\beta_{16}$) and the mutated D7H–$A\beta_{16}$. The latter is a familial AD mutation resulting in a peptide with 1 His more than $A\beta_{16}$, thus its study is both of mechanistic and biological interest.

Aβox refers to a mixture of biologically oxidized species (see Fig. S2, ESI†). Complete elucidation of the nature as well as the proportion of various oxidized species might be of interest. However, for the present study, knowing the main oxidation reactions that have been previously reported[21] is sufficient.

Coordination of copper to Aβox

As previously shown,[21,23,24] the $HO^\bullet$ radicals produced by the Cu/Aβ/ascorbate/O_2 system are deleterious for the Aβ peptide itself. Because they are generated at the metal center, several residues of Aβ involved in Cu(I) and Cu(II) coordination (namely Asp1, His13 and His14) are oxidized, leading to Aβox. The oxidation of Aβ leads to the formation of a mixture of peptides with different oxidation sites. The experimental conditions for peptide oxidation have been previously studied.[33] In the present study, the $A\beta_{28}$ peptide was oxidized in the presence of 0.8 equiv. of copper and 8 equiv. of ascorbate, in order to ensure that 80% of the peptide is oxidized (at least one amino acid residue is oxidized) (Fig. S3, ESI†). At the end of the reaction, the oxidized peptide (Aβox) was purified using membrane filtration to completely remove any remaining copper bound to the peptide (see the Experimental section), then quantified by UV-Vis and Cu was added again to Aβox or $A\beta_{28}$ for the spectroscopic studies of Cu(I) and Cu(II) coordination.

Cu(I) coordination to Aβox. X-ray absorption near edge spectroscopy (XANES) is a very sensitive tool to probe the Cu(I) environment. It has been successfully applied to the spectroscopy of silent metal ions bound to flexible peptides. The XANES spectra of the three Cu(I) samples were collected: Cu(I) coordinated to the non-oxidized Aβ peptide, to the oxidized Aβ peptide (Aβox) and to the truncated $A\beta_7$ peptide (Fig. 3). $A\beta_7$, bearing only the His at position 6, was chosen as a model for Cu(I)-binding to the oxidized peptide since His13 and His14 are the primary targets of oxidation and thus supposed to lose their efficiency in Cu coordination.

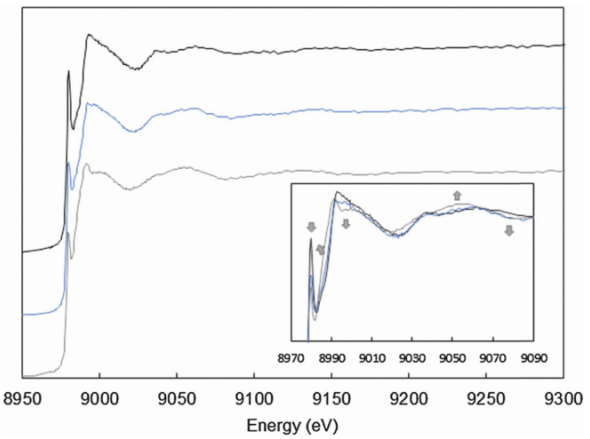

Fig. 3 Cu XANES K-edge X-ray absorption spectra of $A\beta_{28}$–Cu(I) (black curve), Aβox–Cu(I) (blue curve) and $A\beta_7$–Cu(I) (grey curve). The conditions were as follows: 0.9 mM Cu(II), 1 mM peptide, and 10 mM dithionite in a HEPES buffer (0.1 M, pH 7.1) solution. Arrows indicate the evolution of the Aβox–Cu(I) signature compared with the $A\beta_{28}$–Cu(I) signature. Inset: zoom of the 8970–9090 eV range.

Single His mutants were not studied since it is anticipated that the oxidation of one of the three His does not affect the coordination much. Indeed, Cu(I) coordination requires only two His residues, as proved by NMR studies[20,34] or by affinities of single His–Ala mutation of the Aβ peptide.[34–36] In Fig. 3, the pre-edge feature at 8982 eV, assigned to the 1s → 4p electric dipole allowed transition, is visible. Its intensity is characteristic of a Cu(I) species coordinated to 2 ligands in a linear fashion in Aβ–Cu(I),[37] as previously reported.[20,32,38,39] The intensity is lower for $A\beta_7$, indicating an increment of the number of ligands,[37] likely one His of the peptide and 2 or 3 ligands from the solvent. In the case of the Cu(I)–Aβox species, this pre-edge signature tends to be closer to that obtained for Cu(I)–$A\beta_7$. At a higher energy, in particular around 8985, 8995, 9050 and 9075 eV (arrows in the inset of Fig. 3), the XANES spectrum of $A\beta_{28}$ox shows features that are intermediate between the ones of Cu(I)–$A\beta_{28}$ and the ones of Cu(I)–$A\beta_7$ (Fig. 3). A linear combination fitting of the XANES provides the relative contribution of the two possible coordination modes: 40% of Cu(I) is coordinated as in Cu(I)–$A\beta_7$ (Fig. S4, ESI†), and the other part of Cu(I) is coordinated to the peptide as in Cu(I)–Aβ, with 2 His. This is consistent with the oxidative damage undergone by both His13 and His14 residues during Aβ oxidation[21] that would disrupt the normal coordination of copper in Aβ–Cu(I), known to involve the same residues.[20]

Cu(II) coordination to Aβox. The potential change in the coordination of Cu(II) to Aβox was studied by Electron Paramagnetic Resonance (EPR). The comparison of the signature of Cu(II)–Aβox and Cu(II)–$A\beta_{28}$ at pH 7.4 shows a coordination change of a part of the Cu, however interpretation is not conclusive (Fig. S5, ESI†). Hence to probe the Cu(II) environment inside Aβox and the integrity of the N-terminal amine, we also performed EPR studies at a higher pH. At pH 12.5, the EPR spectrum of Cu(II)–Aβox is indeed different to the one of Cu(II)–$A\beta_{28}$ and somehow reminiscent to the one of Cu(II)–$AcA\beta_{28}$[35,36,40] (Fig. 4), where $AcA\beta_{28}$ is the N-terminal

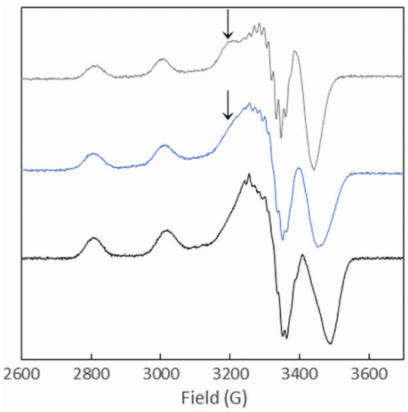

Fig. 4 EPR spectra of Cu(II)–Aβox (blue curve), Cu(II)–$A\beta_{28}$ (black curve) and Cu(II)–$AcA\beta_{28}$ (grey curve) at pH 12.5. Aqueous solution with 10% of glycerol containing ^{65}Cu (450 μM) and peptide (500 μM). T = 120 K, ν = 9.5 GHz, microwave power = 20.5 mW, amplitude modulation = 10.0 G, and modulation frequency = 100 kHz.

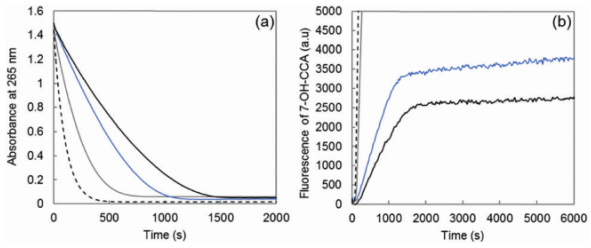

Fig. 5 (a) Ascorbate consumption by Cu–$A\beta_{28}$ (black curve), Cu–Aβox (blue curve), Cu–$A\beta_7$ (grey curve) and free Cu (dashed curve) measured using UV spectrophotometry (λ = 265 nm) as a function of the reaction time; phosphate buffered solution (50 mM, pH 7.4), Cu(II) 10 μM, peptide 12 μM and ascorbate 100 μM. (b) Fluorescence as a function of the time of 7-OH-CCA resulting from the oxidation of CCA obtained for Cu–$A\beta_{28}$ (black curve), Cu–Aβox (blue curve), Cu–$A\beta_7$ (grey curve) and free Cu (dashed curve); phosphate buffered solution (50 mM, pH 7.4), Cu(II) 50 μM, peptide 60 μM (oxidized or non-oxidized), ascorbate 500 μM and CCA 500 μM.

acetylated counterpart of $A\beta_{28}$. The fingerprint is actually an intermediate between those of Cu(II)–$A\beta_{28}$ and Cu(II)–$AcA\beta_{28}$. It was fitted through a linear combination (Fig. S6, ESI†) with 40% of Cu(II)–$AcA\beta_{28}$ and 60% of Cu(II)–$A\beta_{28}$. This shows that for 40% of the Aβox species in solution, the terminal $-NH_2$ is no longer involved in Cu(II) coordination in line with the Asp1 oxidative damage of the peptide previously described.[21,24,25] Probing the impact of His oxidation by EPR is hazardous since at pH 7.4 only a modification in the repartition between components I and II are expected, while at pH 12.5 the His residues are not involved anymore in Cu(II)–$A\beta_{28}$.[30]

In brief, our data are in line with the interpretation that Cu(II)–Aβox complexes include a significant proportion of binding sites similar to those of Cu(II)–$AcA\beta_{28}$ due to Asp1 oxidation, while His oxidation reactions induce the formation of Cu(I)–$A\beta_7$ like species.

HO• production by Cu–Aβox

The metal-catalyzed oxidation of Aβ leads to a change in both Cu(II) and Cu(I) coordination sites that would impact Cu(I) and Cu(II) affinities both in the resting and "in-between" states. Regarding Cu(I) binding, it has been previously shown that a single His–Ala mutation does not change the affinity significantly[34–36] while a double His–Ala mutation induces a decrease of about two orders of magnitude.[35] For Cu(II), the prevention of N-terminal amine binding also leads to a decrease of about two orders of magnitude[35,40,41] while two His–Ala mutations have only a slight impact.[35] Hence the oxidation of the Aβ peptide induces a general decrease in the Cu(I) or Cu(II) affinity although it is not possible to quantify it for the "in-between" state. As a consequence, the oxidation of the Aβ peptide and the resulting modification of the Cu sites could (i) increase the rate of ROS production as a direct impact and (ii) result in a contribution of free Cu in the global ROS production as an indirect effect due to the decrease of Cu affinity for Aβox.

In the present work, the production of HO• was studied by both ascorbate oxidation, monitored by UV-visible spectroscopy, and the fluorescence of 7-OH-CCA, an oxidation product of CCA resulting from HO• scavenging. The 7-OH-CCA fluorescence is proportional to the HO• quantity trapped by CCA.[33] The production of HO• was compared between Cu–$A\beta_{28}$, Cu–Aβox and Cu–$A\beta_7$ (Fig. 5).

The rate of both ascorbate oxidation and 7-OH-CCA formation is much higher for free copper than for Cu–Aβ, in line with the literature.[8,42–45] Then, the rate of ascorbate consumption has the following order: $A\beta_7$ > Aβox > $A\beta_{28}$ (Fig. 5a). A similar trend is obtained for the rate (gradient of the curve) of HO• production (Fig. 5b). In particular, Cu bound to the oxidized peptide reacts to consume ascorbate and produce HO• faster than Cu linked to the non-oxidized peptide. The catalytic behavior of copper bound to Aβox is between Cu–$A\beta_{28}$ and Cu–$A\beta_7$, in line with the binding mode of Cu(I) to Aβox which includes peptide with two oxidation reactions on the His residues and with the lower affinity of Aβox for copper. Thus, the binding mode of copper to Aβ is affected by Aβ oxidation, which in turn increases its catalytic activity for the production of ROS. As shown above by XANES and EPR experiments, the coordination of copper in the resting states is modified upon Aβ oxidation. The higher catalytic activity of Cu–Aβox and the resulting faster HO• production show that the coordination of Cu(I) and Cu(II) within the "in-between" state (the only redox-competent species) is also modified.

The quantity of ROS released by the Cu–peptide system (corresponding to the HO• available for the oxidative damage of exogenous molecules) has also been evaluated. It is given by the fluorescence value at the plateau. The total amount of HO• trapped by CCA follows the trend: $A\beta_7 \gg$ Aβox > $A\beta_{28}$ (Fig. 5b, plateau of the curve), in line with a partial decrease of the Aβox ability to trap HO•.

Effect of H_2O_2 on Aβ oxidation and ascorbate consumption

In the above studies, Aβ oxidation was induced by the ROS produced by the Cu–Aβ/ascorbate system, in the presence of molecular oxygen. The hydroxyl radical (HO•) produced by the Fenton-like reaction catalyzed by copper (Scheme 1) is the most reactive one and thus supposed to be mainly responsible for the

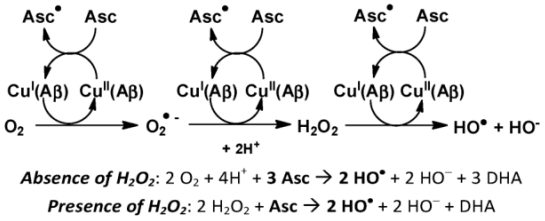

Scheme 1 Metal-catalyzed Reactive Oxygen Species (ROS) production in the presence of the amyloid-β peptide (Aβ); Asc = ascorbate, DHA = dehydroascorbate.

oxidation of the Aβ residues. The other two ROS produced by the system, hydrogen peroxide and the superoxide anion, may react in some cases with a specific target, for instance with methionine residues in peptides and proteins, to form methionine sulfoxide. However, they are much less reactive than the hydroxyl radical. We were interested in comparing the behavior of the system, in terms of Aβ oxidation and ascorbate consumption, in the presence or absence of hydrogen peroxide, in order to evaluate the catalytic properties of the system and identify the targeted residues under these experimental conditions. As hydroxyl radicals are the sole species produced in the presence of H_2O_2, such a comparison should also provide information on the reactivity of O_2 and $O_2^{\bullet -}$ with Aβ during MCO.

The MCO of Aβ was compared after 1, 2 or 3 successive additions of ascorbate or ascorbate and H_2O_2. The presence of H_2O_2 in solution leads to a 3 times higher oxidation of Aβ compared to the absence of H_2O_2 (Fig. 6a). This is in line with the expectation that Aβ oxidation is mainly due to HO•, based on the known mechanism of ROS production by Cu–Aβ for which the production of HO• is 3 times higher in the presence of H_2O_2 compared to the absence of H_2O_2 (Scheme 1). Indeed, in the absence of H_2O_2, 3 electrons (and hence 1.5 ascorbate) are needed to form one HO•. In the presence of H_2O_2 only one electron is needed to produce one HO•. There is no remaining non-oxidized Aβ peptide after 3 successive additions of ascorbate and H_2O_2, meaning that at least one amino acid residue of Aβ is

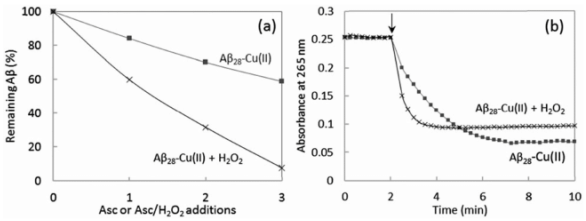

Fig. 6 (a) Remaining non-oxidized $Aβ_{28}$ after successive additions of ascorbate (4 nmol, final conc. 20 μM) or ascorbate/H_2O_2 (4/10 nmol, final conc. 20/50 μM). $Aβ_{28}$ 25 μM and Cu^{2+} 20 μM, phosphate buffered pH 7.4 (50 mM). Ordinate: ratio between the peak area of non-oxidized $Aβ_{28}$ and the reference peak area of non-ox $Aβ_{28}$ (no addition of ascorbate nor H_2O_2). HPLC/HRMS, *m/z* 1087.8503, 816.1397, 653.1133 ($[M + nH]^{n+}$, n = 3, 4, 5), 5 ppm accuracy. (b) Ascorbate consumption measured at 265 nm as a function of the reaction time; $Aβ_{28}$ 25 μM, Cu^{2+} 20 μM, phosphate buffered pH 7.4 (50 mM), ascorbate 20 μM, with or without H_2O_2 50 μM.

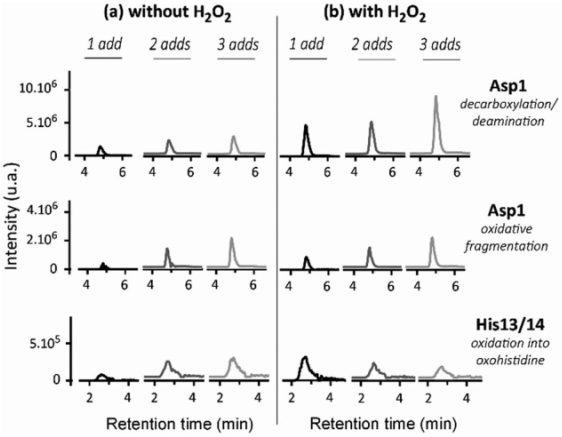

Fig. 7 Oxidation of Aβ in the absence or presence of H_2O_2. Trace chromatograms obtained by HPLC/HRMS of the Aβ oxidized tryptic peptides $DAEFR_{dd}$ (decarboxylation and deamination of Asp1), $DAEFR_{ox}$ (oxidative fragmentation of Asp1), and HDSGYEVHHQK + 16 after 1 (black curve), 2 (dark grey curve) or 3 (light grey curve) additions of ascorbate (4 nmol, final conc. 20 μM; left panel) or ascorbate/H_2O_2 (4/10 nmol, final conc. 20/50 μM; right panel). $Aβ_{28}$ 25 μM and Cu(II) 20 μM, phosphate buffered pH 7.4 (50 mM). Mass tolerance set at 5 ppm; *m/z* ratios used for the detection are specified in Table S1 (ESI†). The corresponding raw chromatograms are given in Fig. S7–S9 (ESI†). The oxidized residues were identified by HR-MS (Asp1 oxidation, see Table S2, ESI†) and by MS/MS (His13 and His14 oxidation reactions, see Fig. S10 and S11, ESI†).

oxidized. At the same time, the ascorbate consumption rate is also higher in the presence of hydrogen peroxide (Fig. 6b). The first electron transfer from Cu(I) to O_2 is the rate limiting step of ROS production by Cu–Aβ;[46] adding H_2O_2 eliminates this step and thus increases the ascorbate consumption rate.

The oxidative damage on Aβ has been characterized using HPLC/HRMS after MCO in the presence or absence of H_2O_2 (Fig. 7). As expected, the oxidative damage undergone by Aβ is the same in the presence or absence of H_2O_2. This tends to indicate that the hydroxyl radical is mainly responsible for them. Asp1, His13 and His14 are the three major targets of HO• attack during metal-catalyzed oxidation. Their generation is dependent on the amount of ascorbate and H_2O_2 added in the solution: the higher the number of additions of ascorbate or ascorbate/H_2O_2, the higher the level of Aβ oxidation. Moreover, the presence of H_2O_2 exacerbates the effect (Fig. 7b) as the chromatographic peaks reach a higher level than in the absence of H_2O_2 (Fig. 7a) for a given [Asc]. This is in line with the higher degradation of Aβ in the presence of H_2O_2 (Fig. 7a). Thus, the presence of H_2O_2 (1) leads to the same oxidative damage of Aβ and (2) achieves a higher degradation state of Aβ per oxidized ascorbate. In other words, it is possible to achieve the same Aβ degradation state with 3 times less successive additions of ascorbate in the presence of H_2O_2, because the system is more efficient in producing HO• radicals.

Evolution of HO• release by Cu–Aβ upon oxidation

The above studies done with Aβox have been carried out after 80% of the peptide is oxidized. We also aim to understand how the oxidation of the peptide impacts the HO• release for different

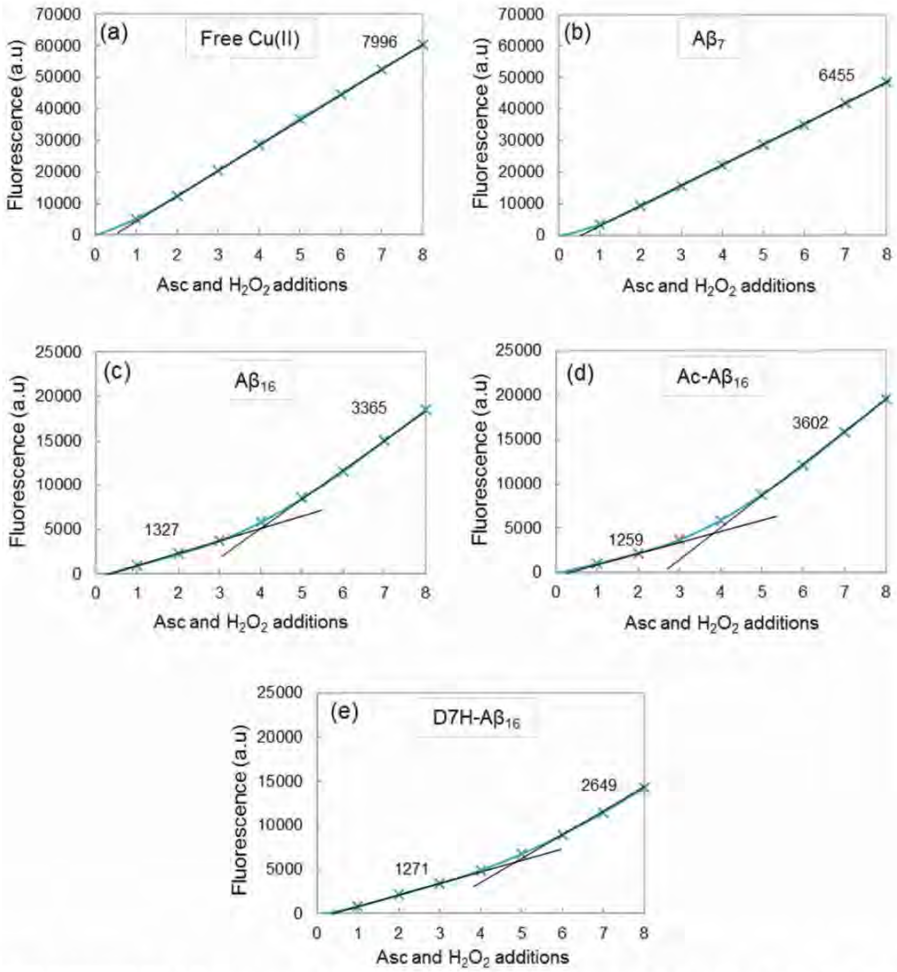

Fig. 8 Cu–Aβ induced HO• trapped by CCA. Fluorescence intensity at the plateau of phosphate buffered solution (50 mM) containing Cu (20 μM), peptide (25 μM), and CCA (0.5 mM) as a function of the number of ascorbate and H_2O_2 additions. A total of 8 additions of 2 μL ascorbate (2 mM) and 2 μL hydrogen peroxide (5 mM) are realized, *i.e.* 4 and 10 nmol for each addition respectively (initial concentrations reaching 20 and 50 μM for the first addition, respectively). Gradients of the linear parts of the curves are indicated in black. The gradient and determination coefficients of fits for each curve are given in the ESI,† Table S3.

oxidation states of the peptide. The native $A\beta_{16}$ peptide as well as the truncated or mutated peptides $A\beta_7$, $AcA\beta_{16}$ and $D7H\text{–}A\beta_{16}$ were studied and compared (see the Introductory remarks for more details on the peptides).

In order to study the HO• release by Cu–Aβ at increasing degrees of peptide oxidation, successive fixed amounts of ascorbate and hydrogen peroxide were added to the solution containing the Cu–Aβ complex. Based on the observation that with or without H_2O_2 the same damage occurs (Fig. 7), we used the system with H_2O_2 due to practical reasons (to avoid excessive dilution and HO• trapping at a very high ascorbate concentration[33]). The fluorescence intensity was measured at the end of the reaction (at the plateau) and thus provided information on the total amount of HO• trapped by CCA for each addition of ascorbate and H_2O_2 (fluorescence curves are given in the ESI,† Fig. S12).

Fig. 8 shows the fluorescence at the plateau as a function of the number of ascorbate and H_2O_2 additions for free Cu (Fig. 8a) and for Cu coordinated to the peptides (Fig. 8b–e). The highest fluorescence was obtained with free copper (Fig. 8a) because the maximum HO• radicals are trapped by CCA (no peptide in solution). A similar result is obtained when copper is coordinated to $A\beta_7$ (Fig. 8b), with a slightly lower gradient of the curve. This indicates that with $A\beta_7$, only a small quantity of HO• is trapped by the peptide and therefore only a small fraction of Cu is bound to $A\beta_7$ under these conditions (*i.e.* very diluted compared to spectroscopic studies). Copper, when coordinated to $A\beta_{16}$, $AcA\beta_{16}$ or $D7H\text{–}A\beta_{16}$, exhibits a strongly different behavior regarding the total amount of the HO• trapped by CCA (Fig. 8c–e). The total fluorescence after each addition of ascorbate and H_2O_2 is much lower than that of free copper, resulting in much lower gradients. As the HO• are produced at the metal center and because the peptide is coordinated to Cu, Aβ is the first target for the radical attack. This results in a strong decrease in the HO• radicals directly trapped by CCA.

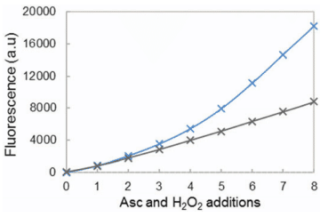

Fig. 9 Fluorescence intensity at the plateau of phosphate buffered solution (50 mM) containing 20 μM of Cu, 25 μM (blue curve) or 50 μM (grey curve) of the $A\beta_{16}$ peptide, and CCA (0.5 mM) as a function of the number of ascorbate and H_2O_2 additions. A total of 8 additions of 2 μL ascorbate (2 mM) and 2 μL hydrogen peroxide (5 mM) are realized, *i.e.* 4 and 10 nmol for each addition respectively (initial concentrations reaching 20 and 50 μM for the first addition, respectively). Gradients of the linear parts of the curves are indicated in black. The gradient and determination coefficients of fits for each curve are given in the ESI,† Table S3.

In addition, the curves exhibit two different linear parts, the first one with a low gradient is obtained for the 3–4 first additions of ascorbate and H_2O_2, and the second one with a higher gradient is obtained after several additions of ascorbate and H_2O_2. The modification of the N-terminal part of the peptide does not appear to affect the $HO^\bullet$ release, as the gradients are similar for Cu–$A\beta_{16}$ and Cu–Ac$A\beta_{16}$ (Fig. 8c and d). A comparable gradient is also obtained for Cu–(D7H–$A\beta_{16}$) (Fig. 8e), for the first part of the curve. A similar behavior is observed with the longer $A\beta_{28}$ and $A\beta_{40}$ peptides (ESI,† Fig. S13).

The higher gradients observed in the second part of the fluorescence curves (Fig. 8c–e) can be linked to a change in copper coordination due to peptide oxidation by $HO^\bullet$. The increase in the slopes is observed after 3 additions of ascorbate and H_2O_2 for Aβ (Fig. 8c), *i.e.* after the peptide has been mostly oxidized at least once (Fig. 6a). The break of the curve for D7H–$A\beta_{16}$ (Fig. 8e) occurs after 4 additions of ascorbate and H_2O_2 instead of 3 additions for $A\beta_{16}$ (Fig. 8c). D7H–$A\beta_{16}$ has one more His residue than $A\beta_{16}$ and thus one additional target for $HO^\bullet$ and one supplementary position for copper coordination. Supplementary addition of ascorbate and H_2O_2 is thus needed so that the peptide is sufficiently oxidized and the quantity of $HO^\bullet$ scavenged by CCA increases.

This is in line with data shown in Fig. 9, where fluorescence was compared at different Aβ/Cu ratios: 12/10 (blue curve) and 20/10 (grey curve). The break of the curve is no longer observed at the highest ratio 20/10, indicating that throughout the 8 successive additions of ascorbate and hydrogen peroxide, the total amount of $HO^\bullet$ trapped by CCA remains constant. The Aβ peptide is still oxidized and it would lose its efficiency in coordinating copper. However, the resulting loosely bound copper would be further coordinated by the part of the non-oxidized Aβ peptide that remains in solution.

By comparison of the fluorescence gradients after 3 additions of ascorbate and hydrogen peroxide (Fig. 8c, first and second gradients), it appears that the Aβ peptide is oxidized to the point of being two to three times less efficient in $HO^\bullet$ scavenging but still two times more efficient than the $A\beta_7$ peptide (Fig. 8b). This is in line with a Cu center mainly bound to the Aβox peptide but not to the $A\beta_7$ peptide.

Concluding remarks

As shown above, the metal catalyzed oxidation of the Aβ peptide leads to a change in copper coordination for both the Cu(I) and Cu(II) resting states as probed, respectively, by XANES and EPR and it is anticipated that this is also true for the catalytic species involved in ROS production, the "in-between" state. Indeed, it was previously described that the production of $HO^\bullet$ radicals by the Aβ-copper system proceeds *via* an "in-between" state involving Asp1, His13 and His14 in the coordination sphere of copper.[21] A similar oxidative protein and its consequences on the Cu binding site and on the enzyme activity have been recently reported for the Cu, Zn SOD, in the presence of H_2O_2[47] and in the presence of Cu/asc/O_2 as a model system.[48]

Such coordination modifications impact the rate of $HO^\bullet$ production *via* two additive mechanisms: (i) a direct one due to a different binding site in the "in-between" state that has faster kinetics and (ii) an indirect one, relying on a decrease in Cu binding affinities for Aβox. This latter mechanism leads to a significant amount of free Cu under diluted conditions that would contribute to enhanced ROS production. In addition, the oxidation of the Aβ peptide induces a less efficient scavenging of the $HO^\bullet$ that could be due to a different Cu coordination site as discussed above or/and to a lower number of potential targets on the peptide. It was indeed previously shown that the oxidation of the Aβ residues stops after a certain reaction time, showing that $HO^\bullet$ is no longer trapped by Aβ.[21]

In a more biological environment, Aβ oxidation by the Cu–Aβ complex triggers a positive feedback loop that leads to a more deleterious oxidative stress due to both an enhanced ROS production rate and a decreased $HO^\bullet$ scavenging ability.

Acknowledgements

The authors acknowledge L. Debrauwer and E. Jamin for providing the Orbitrap mass spectrometer (MetaToul-AXIOM, INRA, UMR1331 Toxalim, Toulouse, France) and the ESRF for provision of synchrotron radiation on the FAME beamline (Proposal 30-02-1099). L. Rechignat is acknowledged for EPR experiments and M. Jones is acknowledged for the preparation of oxidized peptide and the UV-Vis spectra. This work was supported by the French National Agency of Research (ANR-13-BSV5-0016). C. H. thanks the ERC aLzINK – Contract no. 638712 for their financial support.

Notes and references

1 D. J. Selkoe, *Science*, 2002, **298**, 789.
2 G. G. Glenner and C. W. Wong, *Biochem. Biophys. Res. Commun.*, 1984, **120**, 885.
3 C. Haass, M. G. Schlossmacher, A. Y. Hung, C. Vigo-Pelfrey, A. Mellon, B. L. Ostaszewski, I. Lieberburg, E. H. Koo, D. Schenk, D. B. Teplow and D. J. Selkoe, *Nature*, 1992, **359**, 322.
4 M. A. Lovell, J. D. Robertson, W. J. Teesdale, J. L. Campbell and W. R. Markesbery, *J. Neurol. Sci.*, 1998, **158**, 47.

5 L. M. Miller, Q. Wang, T. P. Telivala, R. J. Smith, A. Lanzirotti and J. Miklossy, *J. Struct. Biol.*, 2006, **155**, 30.
6 A. C. Leskovjan, A. Lanzirotti and L. M. Miller, *NeuroImage*, 2009, **47**, 1215.
7 X. Huang, C. S. Atwood, M. A. Hartshorn, G. Multhaup, L. E. Goldstein, R. C. Scarpa, M. P. Cuajungco, D. N. Gray, J. Lim and R. D. Moir, *Biochemistry*, 1999, **38**, 7609.
8 C. Hureau and P. Faller, *Biochimie*, 2009, **91**, 1212.
9 C. Opazo, X. Huang, R. A. Cherny, R. D. Moir, A. E. Roher, A. R. White, R. Cappai, C. L. Masters, R. E. Tanzi, N. C. Inestrosa and A. I. Bush, *J. Biol. Chem.*, 2002, **277**, 40302.
10 D. G. Smith, R. Cappai and K. J. Barnham, *Biochim. Biophys. Acta, Biomembr.*, 2007, **1768**, 1976.
11 K. Reybier, S. Ayala, B. Alies, J. V. Rodrigues, S. Bustos Rodriguez, G. La Penna, F. Collin, C. M. Gomes, C. Hureau and P. Faller, *Angew. Chem., Int. Ed.*, 2016, **55**, 1085.
12 R. A. Farhataziz and A. Ross, *Hydroxyl radical and perhydroxyl radical and their radical ions*, NSRDS-NBS, 1977, vol. 59.
13 J. Näslund, A. Schierhorn, U. Hellman, L. Lannfelt, A. D. Roses, L. O. Tjernberg, J. Silberring, S. E. Gandy, B. Winblad and P. Greengard, *Proc. Natl. Acad. Sci. U. S. A.*, 1994, **91**, 8378.
14 K. J. Barnham, C. L. Masters and A. I. Bush, *Nat. Rev. Drug Discovery*, 2004, **3**, 205.
15 L. M. Sayre, G. Perry and M. A. Smith, *Chem. Res. Toxicol.*, 2008, **21**, 172.
16 C. Hureau, *Coord. Chem. Rev.*, 2012, **256**, 2164.
17 C. Migliorini, E. Porciatti, M. Luczkowski and D. Valensin, *Coord. Chem. Rev.*, 2012, **256**, 352.
18 C. Hureau and P. Dorlet, *Coord. Chem. Rev.*, 2012, **256**, 2175.
19 C. Hureau, Y. Coppel, P. Dorlet, P. L. Solari, S. Sayen, E. Guillon, L. Sabater and P. Faller, *Angew. Chem., Int. Ed.*, 2009, **48**, 9522.
20 C. Hureau, V. Balland, Y. Coppel, P. L. Solari, E. Fonda and P. Faller, *JBIC, J. Biol. Inorg. Chem.*, 2009, **14**, 995.
21 L.-E. Cassagnes, V. Hervé, F. Nepveu, C. Hureau, P. Faller and F. Collin, *Angew. Chem., Int. Ed.*, 2013, **52**, 11110.
22 V. Balland, C. Hureau and J.-M. Saveant, *Proc. Natl. Acad. Sci. U. S. A.*, 2010, **107**, 17113.
23 K. Inoue, C. Garner, B. L. Ackermann, T. Oe and I. A. Blair, *Rapid Commun. Mass Spectrom.*, 2006, **20**, 911.
24 T. Kowalik-Jankowska, M. Ruta, K. Wiśniewska, L. Łankiewicz and M. Dyba, *J. Inorg. Biochem.*, 2004, **98**, 940.
25 K. Inoue, A. Nakagawa, T. Hino and H. Oka, *Anal. Chem.*, 2009, **81**, 1819.
26 Y. Manevich, K. D. Held and J. E. Biaglow, *Radiat. Res.*, 1997, **148**, 580.
27 O. Proux, X. Biquard, E. Lahera, J. J. Menthonnex, A. Prat, O. Ulrich, Y. Soldo, P. Trevisson, G. Kapoujyan, G. Perroux, P. Taunier, D. Grand, P. Jeantet, M. Deleglise, J. P. Roux and J. L. Hazemann, *Phys. Scr., T*, 2005, **115**, 970.
28 O. Proux, V. Nassif, A. Prat, O. Ulrich, E. Lahera, X. Biquard, J. J. Menthonnex and J. L. Hazemann, *J. Synchrotron Radiat.*, 2006, **13**, 59.
29 V. Minicozzi, F. Stellato, M. Comai, M. D. Serra, C. Potrich, W. Meyer-Klaucke and S. Morante, *J. Biol. Chem.*, 2008, **283**, 10784.
30 C. Hureau, *Coord. Chem. Rev.*, 2012, **256**, 2164.
31 C. D. Syme, R. C. Nadal, S. E. J. Rigby and J. H. Viles, *J. Biol. Chem.*, 2004, **279**, 18169.
32 J. Shearer and V. A. Szalai, *J. Am. Chem. Soc.*, 2008, **130**, 17826.
33 C. Cheignon, F. Collin, P. Faller and C. Hureau, *Dalton Trans.*, 2016, **45**, 12627.
34 B. Alies, B. Badei, P. Faller and C. Hureau, *Chem. – Eur. J.*, 2012, **18**, 1161.
35 T. R. Young, A. Kirchner, A. G. Wedd and Z. Xiao, *Metallomics*, 2014, **6**, 505.
36 H. A. Feaga, R. C. Maduka, M. N. Foster and V. A. Szalai, *Inorg. Chem.*, 2011, **50**, 1614.
37 L. S. Kau, D. J. Spira-Solomon, J. E. Penner-Hahn, K. O. Hodgson and E. I. Solomon, *J. Am. Chem. Soc.*, 1987, **109**, 6433.
38 R. A. Himes, G. Y. Park, G. S. Siluvai, N. J. Blackburn and K. D. Karlin, *Angew. Chem., Int. Ed.*, 2008, **47**, 9084.
39 R. A. Himes, G. Y. Park, A. N. Barry, N. J. Blackburn and K. D. Karlin, *J. Am. Chem. Soc.*, 2007, **129**, 5352.
40 B. Alies, C. Bijani, S. Sayen, E. Guillon, P. Faller and C. Hureau, *Inorg. Chem.*, 2012, **51**, 12988.
41 L. Hong, T. M. Carducci, W. D. Bush, C. G. Dudzik, G. L. Millhauser and J. D. Simon, *J. Phys. Chem. B*, 2010, **114**, 11261.
42 M. Nakamura, N. Shishido, A. Nunomura, M. A. Smith, G. Perry, Y. Hayashi, K. Nakayama and T. Hayashi, *Biochemistry*, 2007, **46**, 12737.
43 R. C. Nadal, S. E. J. Rigby and J. H. Viles, *Biochemistry*, 2008, **47**, 11653.
44 S. Noël, F. Perez, J. T. Pedersen, B. Alies, S. Ladeira, S. Sayen, E. Guillon, E. Gras and C. Hureau, *J. Inorg. Biochem.*, 2012, **117**, 322.
45 B. Alies, I. Sasaki, O. Proux, S. Sayen, E. Guillon, P. Faller and C. Hureau, *Chem. Commun.*, 2013, **49**, 1214.
46 P. Strizhak, *Theor. Exp. Chem.*, 1994, **30**, 239.
47 R. H. Gottfredsen, U. G. Larsen, J. J. Enghild and S. V. Petersen, *Redox Biol.*, 2013, **1**, 24.
48 H. Uehara, S. Luo, B. Aryal, R. L. Levine and V. A. Rao, *Free Radical Biol. Med.*, 2016, **94**, 161.

IV.A.2. French summary

Cet article, publié dans la revue *Metallomics* en 2016,[2] porte sur les conséquences de l'oxydation du peptide Aβ sur la production des espèces réactives de l'oxygène (ROS) et la coordination avec les ions Cu(I) et Cu(II). En présence d'oxygène et d'un agent réducteur comme l'ascorbate, le complexe cuivre-peptide a la capacité de produire des ROS en cyclant entre les états redox Cu(I) et Cu(II). Dans le chapitre précédent, nous avons montré que le peptide Aβ est une cible privilégiée pour les radicaux hydroxyles ainsi générés et nous avons identifié les acides aminés Asp1, His13 et His14 comme cibles préférentielles du radical hydroxyle. Ils sont tous trois connus pour être impliqués dans la sphère de coordination de Cu(II) et /ou Cu(I) (voir Section I.C.1), comme le montre la Figure IV.A-1.

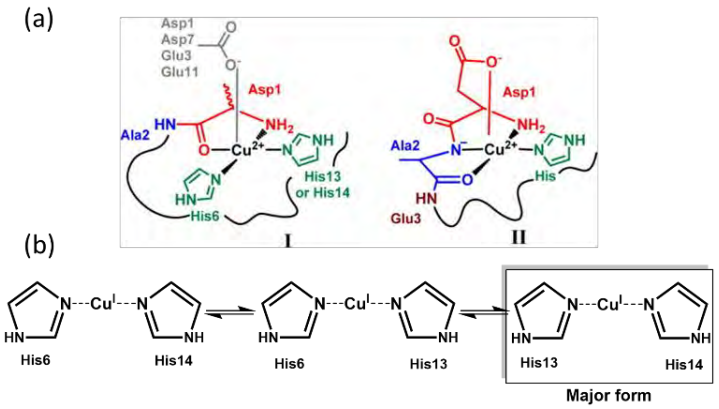

Figure IV.A-1: Modes de coordination du peptide Aβ avec les ions Cu(II) (panel a) et Cu(I) (panel b) à pH physiologique.[2]

Dans cette étude, le peptide $A\beta_{28}$ a été oxydé en présence de Cu et d'ascorbate, menant à un mélange nommé Aβox, contenant 20 % de Aβ non-oxydé et 80 % de diverses espèces oxydées, dont les principales oxydations sont ciblées sur l'Asp1, les His13 et His14. Le mode de coordination de Aβox avec Cu(I) et Cu(II) a été étudié par comparaison avec deux peptides Aβ commerciaux modifiés dont le comportement vis-à-vis de la coordination du cuivre doit permettre de mimer les oxydations sur les acides aminés de Aβox. Le peptide tronqué $A\beta_7$ ne contient qu'un seul résidu His, il est utilisé pour mimer la double oxydation sur les His13 et His14. Le peptide possédant une amine N-terminale acétylée (peptide nommé AcAβ) est quant à lui utilisé pour mimer l'oxydation sur Asp1, car l'ajout du groupement acétyle empêche la coordination du cuivre à l'amine terminale.

Le mode de coordination de Cu(I) avec Aβox a été étudié par absorption des rayons X (XANES) en comparant la signature XANES du complexe Cu(I)-Aβox avec celles de Cu(I) lié au peptide non-oxydé Aβ ou lié au peptide tronqué $A\beta_7$. Il a été trouvé que la signature de Cu(I)-Aβox est intermédiaire entre celles de Cu(I)-Aβ et de Cu(I)-$A\beta_7$. Une combinaison linéaire des signatures XANES a montré qu'environ 40 % de Cu(I) était coordiné à Aβox de la même manière que Cu(I)-$A\beta_7$, ce qui signifierait qu'environ 40 % des espèces oxydées ont subi des dommages sur deux résidus histidine.

La coordination de Aβox avec Cu(II) a été étudiée par résonance paramagnétique électronique (RPE) en comparant la signature RPE du complexe Cu(II)-Aβox avec celles des complexes Cu(II)-Aβ et Cu(II)-AcAβ. De la même manière que pour Cu(I), il a été déduit grâce à une combinaison linéaire des spectres RPE qu'environ 40 % de Cu(II) est coordiné à Aβox de la même manière qu'AcAβ (pas de coordination de l'amine terminale). On peut en déduire qu'environ 40 % des espèces oxydées dans l'échantillon de Aβox ont subi des dommages oxydatifs sur l'Asp1. Par ailleurs, nous avons montré que les deux modes de coordination de Cu(I) et de Cu(II) sont fortement impactés par l'oxydation du peptide Aβ, avec comme conséquence directe un probable changement quant à la production de ROS.

La production de ROS par le complexe Cu-Aβox a été étudiée en suivant (1) la consommation d'ascorbate en fonction du temps par spectroscopie UV-Visible, et (2) la production de l'acide 7-hydroxycoumarine-3-carboxylique (7-OH-CCA), un produit fluorescent issu de la réaction de l'acide coumarine-3-carboxylique (CCA) avec le radical hydroxyle, par spectroscopie de fluorescence. Le suivi cinétique de la fluorescence du 7-OH-CCA lors de la production de ROS donne une indication sur la vitesse et la quantité de $HO^{\bullet}$ piégés par le CCA, et donc sur la quantité de $HO^{\bullet}$ s'échappant du complexe Cu-Aβ et pouvant ainsi oxyder les molécules environnantes. Comme une partie des radicaux réagit avec Aβ, la cible la plus proche du site de production de $HO^{\bullet}$, on ne peut pas directement lier l'intensité de fluorescence à la quantité de $HO^{\bullet}$ générés par le système Cu-Aβ/ascorbate/O_2.

La comparaison des courbes de la consommation d'ascorbate par les complexes Cu-Aβ et Cu-Aβox a montré que le cuivre lié au peptide oxydé produit des ROS plus rapidement que celui lié au peptide non-oxydé. Le cuivre lié au peptide oxydé présente donc une activité catalytique plus importante qu'avec le peptide non-oxydé.

Le suivi cinétique de la captation de HO• par CCA a également montré que le complexe Cu-Aβox laisse échapper plus de radicaux que Cu-Aβ. En première approche, ce résultat peut être expliqué par le fait que le peptide est oxydé et qu'il y a donc moins de cibles potentielles sur Aβox pour les radicaux hydroxyles. Cela est en accord avec l'arrêt de l'oxydation de Asp1 et de His13 et His14 observé au cours de l'oxydation catalysée par le cuivre (voir Section III.B.2). Il faut cependant prendre également en compte le changement de coordination de Aβox avec le cuivre.

Les études précédentes ont été réalisées avec Aβox, elles donnent donc des informations sur l'impact de l'oxydation de Aβ à la fin de la réaction. Afin de comprendre comment l'oxydation de Aβ impacte la libération de radicaux hydroxyles dans le milieu, la quantité de HO• captés par le CCA (formant le 7-HO-CCA) a été étudiée à différentes étapes d'oxydation du peptide Aβ. Pour ce faire, ascorbate et peroxyde d'hydrogène ont été ajoutés en faible quantité 8 fois à une solution contenant le complexe Cu-peptide, en suivant pour chaque ajout la cinétique de formation du 7-HO-CCA.

Pour cette étude, plusieurs peptides modifiés ont été utilisés : les peptides AcAβ et $Aβ_7$, déjà utilisés dans les études précédentes et également le peptide mutant D7H qui a un résidu histidine supplémentaire dans sa séquence peptidique. La quantité de HO• produits par Cu-$Aβ_7$ et piégés par le CCA reste constante quel que soit le nombre d'ajouts de réactifs (ascorbate et peroxyde d'hydrogène) et se rapproche de celle du cuivre libre. Pour Cu-Aβ, la quantité de HO• piégés est presque 5 fois plus faible que pour Cu-$Aβ_7$, mais elle augmente brusquement au 4ème ajout de réactifs. Un résultat similaire est observé pour Cu-AcAβ, et le même phénomène est visible pour Cu-D7H au bout du 5ème ajout de réactifs.

Ce phénomène peut être lié à un changement de coordination du cuivre lorsque le peptide est suffisamment oxydé. Cette hypothèse est corroborée par l'augmentation de HO• piégés qui a lieu pour un ajout supplémentaire de réactifs avec D7H : ayant un résidu histidine en plus dans sa séquence, il a donc un ligand supplémentaire pour le cuivre et une cible de plus à oxyder. En doublant la concentration de Aβ par rapport à celle du cuivre, on n'observe plus d'augmentation de la quantité de HO• piégés au cours des 8 ajouts d'ascorbate et de H_2O_2. Dans ces conditions, seule la moitié du peptide est coordinée au cuivre. Durant l'oxydation, lorsque le peptide est suffisamment oxydé pour induire un changement du mode de coordination, il est

probable que le cuivre lié au peptide oxydé soit chélaté par un autre peptide non-oxydé présent dans le milieu, et garde donc le même comportement que Cu-Aβ quant à la production de ROS. Cela tend à montrer que l'affinité du cuivre pour le peptide oxydé est moindre que pour le peptide non-oxydé.

En replaçant cette étude dans un contexte plus biologique, l'oxydation du peptide Aβ en présence de cuivre et d'ascorbate induit un processus qui conduirait *in fine* à un stress oxydant plus délétère pour les molécules environnantes, en particulier à cause d'une augmentation de la vitesse de production des ROS et d'une quantité plus importante de radicaux HO• libérés par le système (Figure IV.A-2).

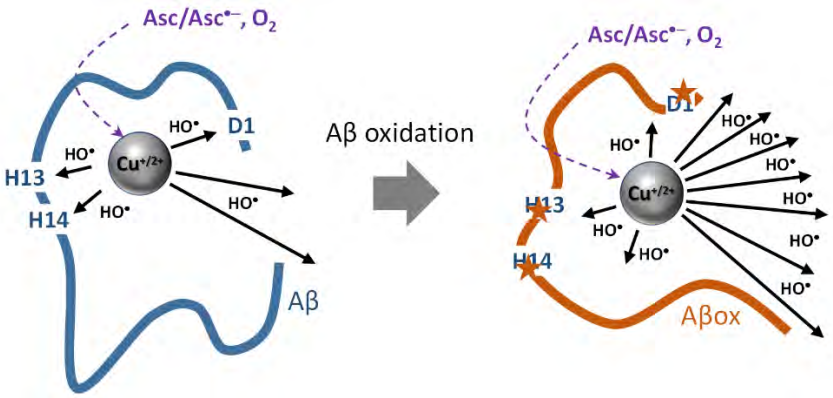

Figure IV.A-2: Vue schématique de l'attaque oxydative du radical hydroxyle sur le peptide Aβ lors de la production d'espèces réactives de l'oxygène.[2]

IV.B. Zn coordination with Aβox

Zn ions are found in the amyloid plaques extracted from AD brains [3] and they can form complexes with the Aβ peptide. According to the proposed models (see Section I.C.1.a), Zn(II) would be bound by imidazole rings of His6 and either His13 or His14 residues in equilibrium, the carboxylate group of Glu11 and the carboxylate group of either Asp1, Glu3 or Asp7, with a preference for Asp1.[4] Asp1, His13 and His14 being found oxidized during MCO of Aβ, the binding mode of Zn(II) might be impacted by Aβ oxidation, as previously observed for Cu(II) and Cu(I) (Section IV.A). In the present study, the impact of Aβ oxidation on Zn(II) coordination is investigated by XANES. Several mutated peptides are employed to mimic the oxidation of each amino acid residue. As Zn(II) has a d^{10} electronic configuration, it is "silent" is most of the classical spectroscopic techniques such as UV-Vis and EPR. Hence, XANES belongs to the few techniques suitable for Zn(II) coordination mode investigation.

IV.B.1. Experimental section

Stock solutions of $A\beta_{28}$ (sequence DAEFRHDSGYEVHHQKLVFFAEDVGSNK), D1N (sequence NAEFRHDSGYEVHHQK), H13A (sequence DAEFRHDSGYEVAHQK), H6A-H13A (sequence DAEFRADSGYEVAHQK) and H6A-H14A (sequence DAEFRADSG-YEVHAQK) were prepared and titrated (see Section II.A for more details). The preparation, purification and dosage of $A\beta_{28}$ox is detailed in Section II.A.3. $ZnSO_4.H_2O$ was purchased from Strem Chemicals. A Zn(II) stock solution (10 mM) was prepared in ultrapure water. HEPES buffer was bought from Sigma and dissolved in ultrapure water to reach a 0.5 M concentration and a pH 5.2 adjusted with NaOH (10 M) to obtain a final pH of 7.1. The methodology and the conditions of the Zn XANES experiments are detailed in Section II.G.2.b.

IV.B.2. Results

The main oxidized amino acid residues of $A\beta_{28}$ox (Asp1, His 13 and His14, see Chapter III) are involved in the coordination of Zn(II). Thus, in order to investigate the impact of Aβ oxidation on Zn(II) coordination, mutated peptides are used to mimic Aβox. The D1N mutated $A\beta_{16}$ peptide does not have any N-terminal carboxylate group and is employed to mimic the oxidation of Asp1. H13A mutated $A\beta_{16}$ peptide bears only two His on its sequence and is used to mimic the oxidation of one His residue. In addition, H6A-H13A and H6A-H14A mutated

$A\beta_{16}$ peptides are used to mimic the oxidation of two His residues. In the above study (Section IV.A), $A\beta_7$ (sequence DAEFRHD) was used to mimic the double His oxidation, but as Zn(II) also binds Glu11, its use would simulate a double His oxidation along with an unavailability of Glu11 for binding.

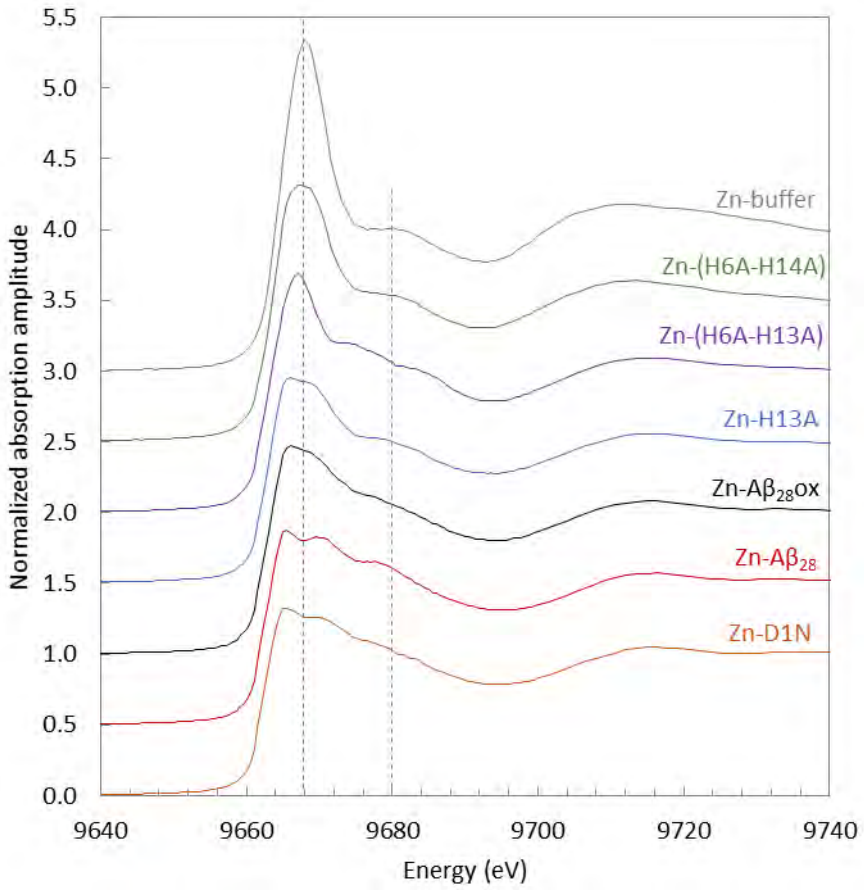

Figure IV.B-1: Zn XANES K-edge X-ray absorption spectra of $A\beta_{28}$-Zn(II) (red curve), $AcA\beta_{16}$-Zn(II) (orange curve), $A\beta_{28}$ox-Zn(II) (black curve), H13A-Zn(II) (blue curve), (H6A-H13A)-Zn(II) (purple curve), (H6A-H14A)-Zn(II) (green curve) and Zn(II) in buffer (grey curve). The conditions were as follow: 0.9 mM Zn(II), 1 mM peptide in a HEPES buffer (0.1 M, pH 7.1) solution.

Figure IV.B-1 shows the Zn K-edge XANES spectra of Zn-$A\beta_{28}$ (red curve), Zn-$A\beta_{28}$ox (black curve), Zn-D1N (orange curve), Zn-H13A (blue curve), Zn-(H6A-H14A) (green curve) and Zn in buffer (grey curve). The XANES signatures of several Zn-peptide complexes are very different around 9670 eV, i.e. in the white line region which is very sensitive to the site geometry. In particular, the XANES signatures of Zn-$A\beta_{28}$ox and Zn-$A\beta_{28}$ are different between 9660 and 9680 eV, meaning that Aβ oxidation has an impact on Zn coordination, as expected.

First, the XANES signature of Zn-D1N is very close to that of Zn-Aβ, suggesting that a modification of the N-terminal part of Aβ does not induce a strong change in Zn coordination. Oxidation of Asp1 thus would not contribute that much to the Zn-Aβox signature, even if its carboxylate group, involved in Zn coordination, is strongly affected during Aβ oxidation. This

could be explained by the dynamic exchange existing between the carboxylate groups of Asp1, Glu3 and Asp7 regarding Zn coordination.[4]

The behavior of Zn-Aβ$_{28}$ox seems to be close to that of Zn-H13A, Zn-(H6A-H13A) and Zn-(H6A-H14A), since XANES signatures exhibit some similarities. A broaden peak is observed at 9665-9670 eV for Zn-Aβox and could result from the growth of a peak at 9668 eV, whose shape evolves to become well-defined, from Zn-H13A to Zn-(H6AH14A) and to Zn-buffer. A similar evolution is observed for another growing and broaden peak detected at 9680 eV, which clearly appears in Zn-buffer spectrum. These elements would suggest that Zn affinity for Aβ would decrease upon Aβ oxidation, because the residues involved in zinc coordination are mainly targeted during MCO. In particular, the oxidation of one or two histidine residues would be responsible for this. This is in line with the affinity values of Zn for His mutants, lower than for Aβ.[4]

Unfortunately, as the signatures in the white line region are broad, define precisely the several binding modes of Zn with oxidized species is precluded. For the same reason, it was not possible to obtain reliable linear combination fitting of the Zn-Aβox signature, as we found that different conclusions can be made according to the result of the fitting (see Annex III for examples of linear combination fittings).

It has been previously shown that the intensity of the Zn XANES white line was related to the number of ligands in the Zn(II) complex.[5] In the case of D1N, Aβ$_{28}$ and H13A peptides, the white line intensity is 1.3 (or 1.4 for H13A), related to a four-coordination of the metal center. The same results were previously obtained for the other two His mutants (H6A and H14A).[4] Zn in buffer related white line intensity (around 2.3) allows to deduce that 6 ligands are coordinated to loosely bound Zn. In the case of H6A-H13 and H6A-H14A, both intensities being equal to 1.7, it is likely that Zn is bound by 5 ligands, probably including carboxylate groups instead of His residues. Zn-Aβ$_{28}$ox related white line intensity being equal to 1.4, the number of ligands is the same than for Aβ$_{28}$ or H13A.

In summary, the XANES signature of Zn-Aβ$_{28}$ox shows that the Zn binding mode is affected when Aβ is oxidized, mainly because of the oxidation of His residue(s). However, the modification is not drastic as the number of ligands does not change. The oxidation of Asp1 would not have a substantial impact on Zn binding mode, in line with the existing dynamic exchange between Asp1, Glu3 and Asp7 in Zn coordination.

In the amyloid cascade hypothesis, the coordination of Zn ion to Aβ is proposed to modulate the aggregation process (see Section I.B.3) and hence to impact the morphology of the formed aggregates.[6-7] Thus, besides the fact that the chemical modifications undergone by Aβ during ROS attack could directly impact its ability to aggregate, the change of Zn binding mode due to Aβ oxidation could also have an effect on the aggregation process in the presence of Zn.

IV.C. Aggregation of Aβox

Aggregation of the Aβ peptide is one of the main events of AD, leading to the formation of amyloid plaques.[8] As addressed above (see Section I.B.4), Aβ is an unfolded peptide which is prone to aggregation and can form β-sheet rich structures.[9] In the previous chapter, the oxidized amino acid residues have been identified after MCO of the full-length $A\beta_{40}$ peptide. Asp1, His13 and His14 are the main amino acid residues targeted by ROS, but some minor oxidations may also occur on Phe19, Phe20 and Met35. As $A\beta_{40}$ undergoes chemical modifications during MCO, its propensity to aggregate into β-sheet rich structures might be affected. In the present study, the aggregation capability of both $A\beta_{40}$ and $A\beta_{40}$ox is studied and compared. Aggregation into β-sheet structures is monitored by Thioflavin-T (ThT) fluorescence as a function of time,[10-11] and the presence (or absence) of fibrillar species at the end of the fluorescence experiment is investigated by Transmission Electron Microscopy (TEM).[12] This part presents the preliminary results we obtained on $A\beta_{40}$ and $A\beta_{40}$ox aggregation without metals.

IV.C.1. Experimental section

The preparation of $A\beta_{40}$ and $A\beta_{40}$ox solutions is detailed in Section II.A. The solutions of $A\beta_{40}$ and $A\beta_{40}$ox (20 µM) were incubated during 200 h at 37°C and the fibril formation was monitored by ThT fluorescence (the fluorescence conditions are presented in Section II.D.3). The fluorescence curves obtained are an average of the fluorescence curves of 3 replicates. Then, the solutions were collected and prepared for TEM using the conventional negative staining procedure. 20 µL of solution was adsorbed on Formvar-carbon-coated grids for 2 min, blotted, and negatively stained with uranyl acetate (1%) for 1 min. Grids were examined with a TEM (Jeol JEM-1400, JEOL Inc, Peabody, MA, USA) at 80 kV. Images were acquired using a digital camera (Gatan Orius, Gatan Inc, Pleasanton, CA, USA) at ×25 000 magnification. As

Phosphate buffer reacts with uranyl acetate, HEPES buffer was preferred and employed for TEM experiments, and thus for ThT fluorescence experiments, as well.

IV.C.2. Results

a. Aggregation of Aβ and Aβox

ThT is a fluorescent dye whose fluorescence yield is enhanced when it interacts with β-sheet rich structures such as Aβ fibrils (see Section II.D.3 for more details).[13-14] In addition, it displays a bathochromic shift of both excitation and emission maximum wavelengths.[15] Thus, ThT fluorescence monitoring is well-suited for kinetic study of Aβ aggregation into fibrils. Both $A\beta_{40}ox$ and $A\beta_{40}$ solutions incubated at 37°C in the presence of ThT were monitored by fluorescence. Figure IV.C-1 shows the ThT fluorescence as a function of the reaction time for $A\beta_{40}$ (grey curve) and $A\beta_{40}ox$ (blue curve). For $A\beta_{40}$, fluorescence starts to increase after around 90 hours, meaning that the peptide aggregates and forms β-sheet structures (fibrils). The fluorescence half time is observed at t ½ = 134 hours. For $A\beta_{40}ox$, fluorescence remains at the background level all along the 200 hours of the reaction time. This absence of fluorescence increase suggests that oxidation has a strong impact on the aggregation capability of Aβ because $A\beta_{40}ox$ does not form any β-sheet structures.

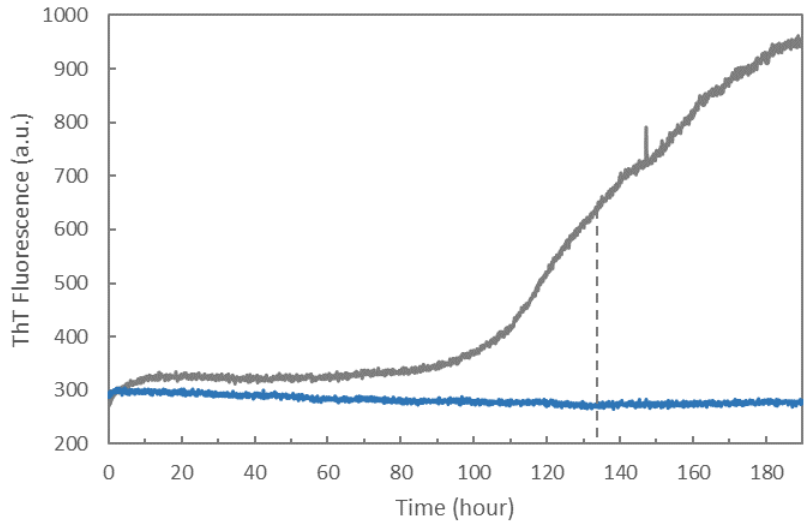

Figure IV.C-1: β-sheet formation during $A\beta_{40}$ (grey curve) and $A\beta_{40}ox$ (blue curve) aggregation. ThT fluorescence as a function of the time of HEPES (50 mM, pH 7.4) buffered solution containing $A\beta_{40}$ or $A\beta_{40}ox$ (20 µM) and ThT (10 µM) incubated at 37 °C.

b. Morphology of Aβ aggregates

At the end of the ThT fluorescence experiment (at 200 hours), the solutions of $A\beta_{40}$ and $A\beta_{40}ox$ were analyzed by TEM. With this technique, the sample does not undergo a strong treatment prior to analysis (see Section IV.C.1) and we can reasonably suppose that its integrity is maintained. In addition, TEM rapidly gives an overview of the sample state. An example of the pictures obtained for both samples is shown in Figure IV.C-2.

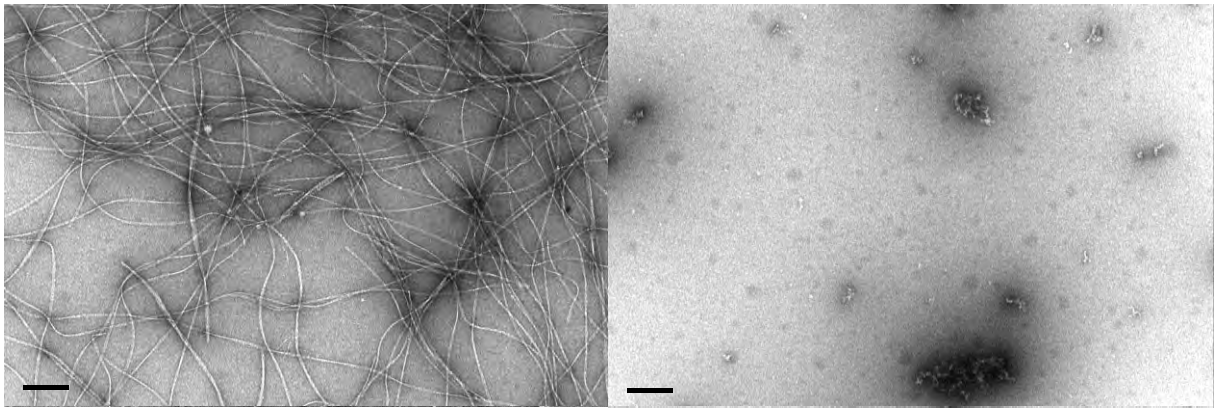

Figure IV.C-2: TEM pictures of $A\beta_{40}$ (left) and $A\beta_{40}ox$ (right) after 200 h of aggregation at 37°C.

The incubated $A\beta_{40}$ solution contains numerous fibers (Figure IV.C-2, left picture) while $A\beta_{40}ox$ solution (Figure IV.C-2, right picture) does not contain any fibrillar aggregates. However, aggregates are observed, corresponding to more amorphous species. This result is in line with what we obtained with ThT fluorescence.

Aβox thus appears as being not able to form fibrillar species which is an interesting result. In the model proposed to describe Aβ arrangement during fibril formation (Figure IV.C-3), the two histidine residues His13 and His14 are included in the β-sheet formation. Their oxidation during MCO of Aβ could be responsible for a further inhibition of the fibrillization process. The polarity change because of the insertion of one oxygen atom (conversion of histidine into 2-oxohistidine, see Section I.C.3.a for chemical structures) could be one explanation.

The change of the overall charge of the peptide could also be the origin of the modification of aggregation process.[16-17] The oxidation of the protonated Asp1 residue can lead to the formation of the neutral pyruvate function.[18-20] Thus, although Asp1 is not located

on the peptide moiety responsible for aggregation, its alteration could disturb the aggregation process.

The aggregation study of mutated peptides (such as H13A-$A\beta_{40}$, H14A-$A\beta_{40}$ to mimic His oxidation or the N-terminal acetylated AcAβ to mimic Asp1 oxidation) could be interesting to determine if the Asp1 or the His oxidation is the origin of the Aβ fibrillization inhibition.

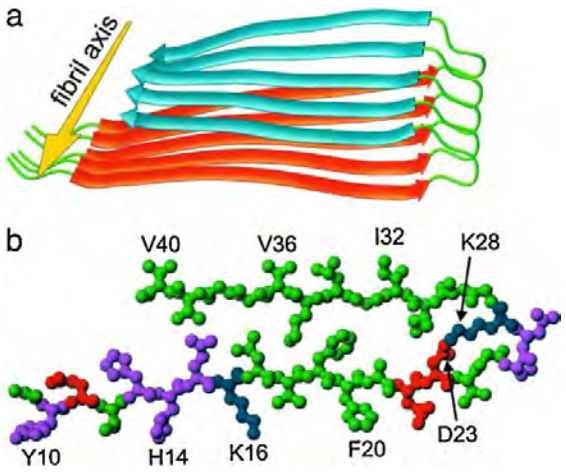

Figure IV.C-3: Structural model for $A\beta_{40}$ fibrils, obtained from solid state NMR constraints. (a) Representation of a single molecular layer constituted by a double-layered structure, with a parallel β-sheets formed by residues 12–24 (orange) and 30–40 (blue). The arrow shows the direction of the long axis of the fibril. (b) $A\beta_{40}$ viewed down the long axis of the fibril. Green colors correspond to hydrophobic sidechains, magenta to polar, blue to positive and red to negative ones. Picture from Ref [21].

IV.C.3. Outlook

The preliminary results obtained by both fluorescence and TEM are very promising as they highlight a strong modification in the aggregation process of Aβ subjected to MCO. Similar results were previously obtained after catalytic photo-oxygenation of Aβ.[22] However, as aggregation is a very sensitive process, the results have to be taken with caution. A series of controls should be carried out in order to ensure that the different aggregation behavior of Aβox effectively comes from the oxidative damages undergone by Aβ and not from the multistep purification procedure (described in Section II.A) of Aβox. The purification procedure undergone by the oxidized peptide will be carried out on the non-oxidized $A\beta_{40}$ as well to ensure that it does aggregate after the procedure. Moreover, aggregation experiments will be realized with a mixture of oxidized and non-oxidized peptides at different ratios and compared with the samples containing the same quantity of non-oxidized peptide than in the mixture. The comparison of the fluorescence curves might be informative on the possible effect of $A\beta_{40}$ox

on $A\beta_{40}$ aggregation process. The set of new experiments is being carried out at the laboratory and should complete the presently described results.

IV.D. Conclusion

In the present studies, the impact of MCO of Aβ has been investigated on metal ions coordination, ROS production and aggregation.

Zn(II), Cu(I) and Cu(II) binding modes with Aβox have been probed by XANES for the former two and by EPR for the latter. Aβ oxidation leads to a change in the coordination of the three metal ions. In addition, Cu(I) XANES and Cu(II) EPR results allowed to get relative quantification of the oxidative damages: around 40 % of Asp1 would be damaged and not available anymore for binding while around 40 % of the oxidized species would have two oxidized His.

ROS production catalyzed by Cu-Aβox was also investigated. Cu-Aβox has a higher catalytic activity and released more $HO^{\bullet}$ than Cu-Aβ. The change in ROS production occurred at a specific step of Aβ oxidation, when the peptide is sufficiently oxidized to induce a change in Cu coordination.

Both aggregation monitoring by ThT fluorescence and sample imaging by TEM highlight a strong modification of the Aβ aggregation process, leading to amorphous-like aggregates instead of fibrillar aggregates. These preliminary results have to be validated by further controls and future experiments could be carried out with mutated peptides in order to determine if one specific amino acid residue oxidation in particular affects the aggregation process. Zn and Cu binding modes with Aβ were also strongly affected by Aβ oxidation. As Zn and Cu ions can modulate the aggregation process by binding Aβ,[6-7] the impact of Aβ oxidation on the aggregation in the presence of Cu or Zn would also be studied.

The oxidation of the Aβ peptide occurring during ROS production induces strong modifications in ROS production and aggregation, two key events of AD. It seems to favor the amorphous-like aggregates such as oligomeric species which are proposed to be more toxic than fibers.[23-24] It also leads to an enhanced catalytic activity for ROS production. Thus, Aβ oxidation appears to be a detrimental event for AD, for both aggregation and ROS production processes.

References

[1] *Alzheimer's & dementia: the journal of the Alzheimer's Association* **2015**, *11*, 332.

[2] C. Cheignon, P. Faller, D. Testemale, C. Hureau and F. Collin, *Metallomics* **2016**, *8*, 1081-1089.

[3] M. A. Lovell, J. D. Robertson, W. J. Teesdale, J. L. Campbell and W. R. Markesbery, *Journal of the Neurological Sciences* **1998**, *158*, 47-52.

[4] B. Alies, A. Conte-Daban, S. p. Sayen, F. Collin, I. Kieffer, E. Guillon, P. Faller and C. Hureau, *Inorganic Chemistry* **2016**, *55*, 10499-10509.

[5] L. Giachini, G. Veronesi, F. Francia, G. Venturoli and F. Boscherini, *Journal of synchrotron radiation* **2010**, *17*, 41-52.

[6] P. Faller, C. Hureau and O. Berthoumieu, *Inorganic Chemistry* **2013**, *52*, 12193-12206.

[7] A. Tiiman, P. Palumaa and V. Tõugu, *Neurochemistry International* **2013**, *62*, 367-378.

[8] D. M. Holtzman, J. C. Morris and A. M. Goate, *Science translational medicine* **2011**, *3*, 77sr71-77sr71.

[9] F. Ding, J. M. Borreguero, S. V. Buldyrey, H. E. Stanley and N. V. Dokholyan, *PROTEINS: Structure, Function, and Bioinformatics* **2003**, *53*, 220-228.

[10] H. LeVine, *Methods in Enzymology* **1999**, *309*, 274-284.

[11] A. A. Reinke and J. E. Gestwicki, *Chemical biology & drug design* **2011**, *77*, 399-411.

[12] M. R. Nilsson, *Methods* **2004**, *34*, 151-160.

[13] S. Noël, S. Cadet, E. Gras and C. Hureau, *Chemical Society Reviews* **2013**, *42*, 7747-7762.

[14] A. I. Sulatskaya, I. M. Kuznetsova and K. K. Turoverov, *Journal of Physical Chemistry B* **2012**, *116*, 2538-2544.

[15] M. Biancalana and S. Koide, *Biochimica et Biophysica Acta* **2010**, *1804*, 1405-1412.

[16] B. Alies, G. LaPenna, S. Sayen, E. Guillon, C. Hureau and P. Faller, *Inorganic Chemistry* **2012**, *51*, 7897-7902.

[17] M. Lopez De La Paz, K. Goldie, J. Zurdo, E. Lacroix, C. M. Dobson, A. Hoenger and L. Serrano, *Proceedings of the National Academy of Sciences of the United States of America* **2002**, *99*, 16052-16057.

[18] T. Kowalik-Jankowska, M. Ruta, K. Wiśniewska, L. Łankiewicz and M. Dyba, *Journal of Inorganic Biochemistry* **2004**, *98*, 940-950.

[19] K. Inoue, A. Nakagawa, T. Hino and H. Oka, *Analytical Chemistry* **2009**, *81*, 1819-1825.

[20] L.-E. Cassagnes, V. Hervé, F. Nepveu, C. Hureau, P. Faller and F. Collin, *Angewandte Chemie International Edition* **2013**, *52*, 11110-11113.

[21] D. Valensin, C. Gabbiani and L. Messori, *Coordination Chemistry Reviews* **2012**, *256*, 2357-2366.

[22] A. Taniguchi, D. Sasaki, A. Shiohara, T. Iwatsubo, T. Tomita, Y. Sohma and M. Kanai, *Angewandte Chemie International Edition* **2013**, *52*, 1-5.

[23] G. Forloni, V. Artuso, P. La Vitola and C. Balducci, *Mov Disord* **2016**.

[24] A. Deshpande, E. Mina, C. Glabe and J. Busciglio, *The Journal of neuroscience* **2006**, *26*, 6011-6018.

Supporting information

Metal-catalyzed oxidation of Aβ and the resulting reorganization of the Cu binding sites promote ROS production

Clémence Cheignon*, Peter Faller, Denis Testemale, Christelle Hureau and Fabrice Collin*

Supporting Information

Experimental

Titration of $A\beta_{28}$, $AcA\beta_{28}$ and $A\beta_{40}$

All the synthetic peptides were bought from GeneCust (Dudelange, Luxembourg), with purity grade > 95%. Stock solutions of the $A\beta_{28}$ (sequence DAEFRHDSGYEVHHQKLVFFAEDVGSNK) and Ac-$A\beta_{28}$ (sequence AcDAEFRHDSGYEVHHQKLVFFAEDVGSNK), peptides were prepared by dissolving the powder in milliQ water (resulting pH ≈ 2). Peptide concentration was then determined by UV-visible absorption of Tyr10 considered as free tyrosine (at pH 2, $(\varepsilon_{276}-\varepsilon_{296}) = 1410\ M^{-1}\ cm^{-1}$). Stock solution of $A\beta_{40}$ peptide (sequence DAEFRHDSGYEVHHQKLVFFAEDVGSNKGAIIGLMVGGVV) was prepared by dissolving the powder in NaOH (50 mM) and purifying the solution in FPLC. The peptide concentration was then determined by UV-visible absorption of Tyr10, considered as free tyrosine ($(\varepsilon_{293}-\varepsilon_{360}) = 2400\ M^{-1}cm^{-1}$) in NaOH (50 mM, resulting pH ≈ 13).

Proteolytic digestion

The solution of Aβ was filtered using Amicon 3 kDa centrifugal device (Millipore) by centrifugation for 15 min at 13500 rpm, then washed and centrifuged twice with 200 µL sodium hydrogenocarbonate (100 mM, pH 8). The concentrated sample (approx. 50 µL) was recovered and transferred to an Eppendorf ProteinLoBind 1.5 mL vial. Trypsin (0.05 ng/µL in formic acid 0.1%) was added to obtain a Aβ/trypsin ratio of 20/1 (w/w) and digestion was carried out at 37°C for 3h in a Thermomixer (Eppendorf), 10 s mixing at 750 rpm every min.

Mass spectrometry

High Performance Liquid Chromatography / Mass Spectrometry (HPLC/MS) analysis was performed on an ion-trap mass spectrometer (LCQ DECA XP Max, ThermoFisher), equipped with an electrospray ionization source, coupled to a SpectraSystem HPLC system. Sample (10 µL of Aβ tryptic digest) was injected onto the column (Phenomenex, Synergi Fusion RP-C18, 250 × 1 mm, 4 µm), at room temperature. Gradient elution was carried out with formic acid 0.1% (mobile phase A) and acetonitrile/water (80/20 v/v) formic acid 0.1% (mobile phase B) at a flow-rate of 50 $\mu L.min^{-1}$. The mobile phase gradient was programmed with the following time course: 12% mobile phase B at 0 min, held 3 minutes, linear increase to 100% B at 15 min, held 4 min, linear decrease to 12% B at 20 min and held 5 min. The mass spectrometer was used as a detector, working in the full scan positive mode between 50 and 2000 Da followed by data dependent scans of the two first most intense ions, with dynamic exclusion enabled. Isolation width was set at 1 Da and collision energy at 28% (units as given by the manufacturer), using wideband activation. The generated tandem MS data was searched using the SEQUEST algorithm against the human Aβ peptide sequence. Dynamic modifications were specified according to the expected mass shift due to the Aβ peptide oxidation (Supporting Information, Table s1). The same operating conditions (column and mobile phase gradient) were used to carry out high resolution mass spectrometry (HPLC/HRMS) experiments, by using a LTQ-Orbitrap XL mass spectrometer (ThermoFisher Scientific, Les Ulis, France) coupled to an Ultimate 3000 LC System (Dionex, Voisins-le-Bretonneux, France). The Orbitrap cell was operated in the full-scan mode at a resolution power of 60 000. HPLC/HRMS was also used to check for digestion efficiency, systematically found close to100 % (non-digested peptide not detected).

HPLC

High Performance Liquid Chromatography analysis was performed on an Agilent 1200 series device (Agilent technologies) equipped with a DAD detector. Sample (10 µL) was injected onto the column (Acclaim 120 C18, 50 × 3 mm, 3 µm, ThermoScientific), at room temperature. The gradient elution was carried out with formic acid 0.1% (mobile phase A) and acetonitrile/water (80/20 v/v) formic acid 0.1% (mobile phase B) at a flow-rate of 0.5 $mL.min^{-1}$. The mobile phase gradient was programmed with the following time course: 5% mobile phase B at 0 min, held 3 minutes, linear increase to 55% B at 8 min, linear increase to 100% of B at 9 min, held 2 min, linear decrease to 5% B at 12 min and held 3 min. Aβ28 was detected with the absorption of Tyr10 at 276 nm.

Tables

Table S1: **Monoisotopic masses used for high resolution mass spectrometry**. Monoisotopic apparent masses (m/z in Th) of mono-, di- and triply-protonated ions of the tryptic peptides of oxidized $A\beta_{16}$; +16 accounts for the formal addition of one oxygen atom during oxidation (conversion of Histidine into oxohistidine).

Position	Peptide	$[M+H]^+$	$[M+2H]^{2+}$	$[M+3H]^{3+}$
1-5	$DAEFR_{dd}$*	592.2731	296.6405	198.0963
	$DAEFR_{ox}$**	548.2469	274.6274	183.4208
6-16	HDSGYEVHHQK+16	1352.5983	676.8031	451.5380

* $DAEFR_{dd}$: oxidative decarboxylation and deamination of Asp1

** $DAEFR_{ox}$: oxidative cleavage of Asp1

Table S2: **Identification of the oxidized residues of Aβ, when oxidized in the presence of H_2O_2**. Calculated (calc) and experimental (exp, obtained by HPLC/HRMS) monoisotopic masses of $DAEFR_{dd}$ and $DAEFR_{ox}$ and mass difference (in ppm) between experimental and calculated masses. Aβ peptide oxidized in the presence of H_2O_2 and digested by trypsin. Same experimental conditions as the ones of Figures S5 and S6.

Identification of Asp1 oxidation was performed by high-resolution mass spectrometry on monoisotopic masses of the tryptic peptides because MS/MS spectra were not enough informative: (1) too small peptides are usually fragmented as monoprotonated ions, leading to poor quality MS/MS spectra and (2) the terminal arginine residue of DAEFR blocks the proton mobility during MS/MS experiment, resulting in the absence of b ions (important for Asp1 mass shift determination). For the identification of His oxidation, see the MS/MS spectra in Figure S8 and S9.

Peptide	MH^+_{calc}	MH^+_{exp}	Δm (ppm)
$DAEFR_{dd}$	592.2731	592.2714	-2.9
$DAEFR_{ox}$	548.2469	548.2451	-3.3

Table S3: **Linear fitting of HO• production curves**. Gradient and determination coefficients of fits for each curve of Figures 7 and 8, for the two linear parts.

	First linear part			Second linear part		
	Gradient	Number of points	R^2	Gradient	Number of points	R^2
Free Cu(II)	7956	8	0.9998			
Cu-$A\beta_7$	6455	8	0.9997			
Cu-$A\beta_{16}$	1327	4	0.9972	3365	4	0.9991
Cu-$AcA\beta_{16}$	1259	4	0.9945	3602	4	0.9995
Cu-D7H- $A\beta_{16}$	1271	5	0.9954	2648	3	0.9996
Cu-$A\beta_{28}$	842	5	0.9926	2352	3	0.9984
Cu-$AcA\beta_{28}$	827	4	0.9938	3344	3	0.9992
Cu-$A\beta_{40}$	1275	5	0.9920	3103	4	0.9979
Cu-$A\beta_{16}$ 20/50	1153	8	0.9987			

Figures

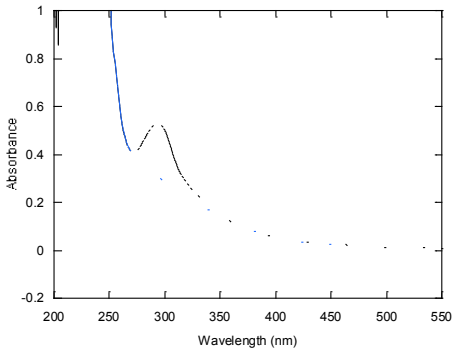

Figure S1: **Quantification of the oxidized Aβ peptide**. UV spectrum of oxidized $A\beta_{28}$ (black curve) and cubic spline interpolation (blue curve) to subtract the background absorbance of unknown origin from Tyr absorption.

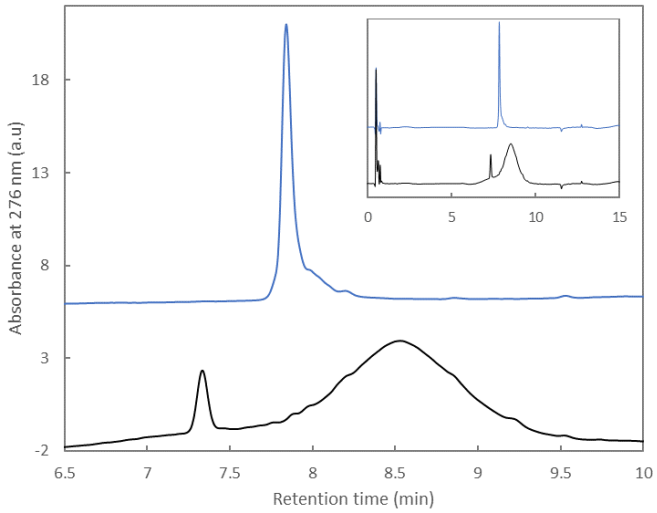

Figure S2: Trace chromatogram of Aβ28 (60 µM) after 30 min in the presence of Cu (50µM) (blue curve) or Cu (50 µM) and ascorbate (0.5 mM) (black curve) in phosphate buffer pH 7.4 (50 mM). $Aβ_{28}$ is detected by UV-Visible spectroscopy with the absorption of the Tyr10 at the wavelength of maximal absorption at acidic pH (276 nm).

The trace chromatogram of the oxidized $Aβ_{28}$ (Figure S2, black curve) shows the presence of several species unlike non-oxidized $Aβ_{28}$ (Figure S2, blue curve). Indeed, the single peak in $Aβ_{28}$ chromatogram indicates that only one species is present in the sample while several peaks including a broad one are observed in the oxidized $Aβ_{28}$ sample, indicating that several oxidized species are present in the mixture.

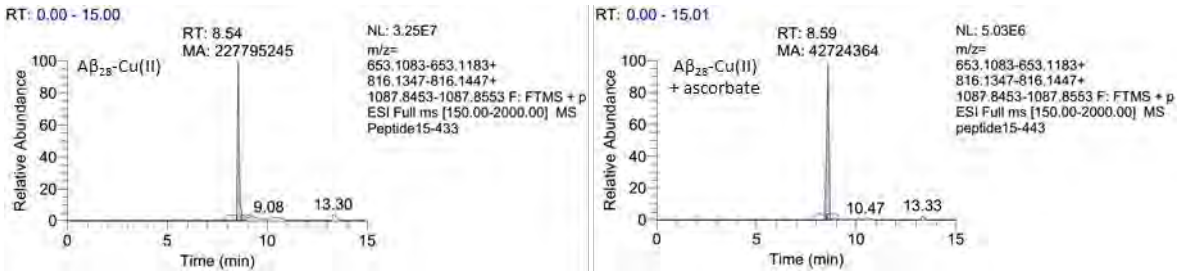

Figure S3: **Remaining $Aβ_{28}$ peptide.** Trace chromatograms of $Aβ_{28}$ (60 µM) after 30 min in the presence of Cu (50µM) (left panel) or Cu (50 µM) and ascorbate (0.5 mM) (right panel) in phosphate buffer pH 7.4 (50 mM). Aβ28 is detected with the $[M+3H]^{3+}$, $[M+4H]^{4+}$ and $[M+5H]^{5+}$ m/z ratio ions: 1087.8503, 816.1397 and 653.1133. Mass tolerance set at 5 ppm. Ratio between the chromatogram area of $Aβ_{28}$-Cu(II) with ascorbate to chromatogram area of $Aβ_{28}$-Cu(II) without ascorbate is around 0.2, meaning that around 80% of $Aβ_{28}$ is oxidized (at least one amino acid residue is oxidized).

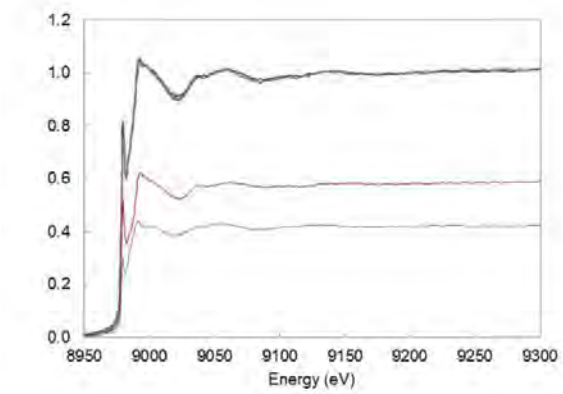

Quantitative results of linear combination fitting

Linear combination fitting carried out with the software Athena

R-factor = 0.0017131
Chi-square = 0.02825
Reduced chi-square = 0.0001733

standard	weight
HEPES-Cu(I)	0.000 (± 0.036)
$A\beta_{28}$-Cu(I)	**0.580** (± 0.028)
$A\beta_{7}$-Cu(I)	**0.420** (± 0.075)
sum	1.000

Figure S4: **Linear Combination Fitting of $A\beta_{28}$-Cu(I) and $A\beta_{7}$-Cu(I) to reproduce Aβox-Cu(I) spectrum**. The fitting allows deducing that around 40% of Cu(I) is bound the same way than $A\beta_{7}$ (bearing only one His), and that no Cu(I) is released in buffer (0% of Cu(I)-HEPES contribution). Quantitative results of linear combination fitting (Right panel) and the resulting XANES spectra with 42% Cu(I)-$A\beta_{7}$ and 58% Cu(I)-$A\beta_{28}$ XANES signatures (blue curve) compared to Cu(I)-Aβox XANES spectrum (grey curve). Cu(I)-$A\beta_{7}$ (green curve) and Cu(I)-$A\beta_{28}$ (red curve) XANES signatures, weighted according to the result found in the linear combination fitting, are also shown (Left panel).

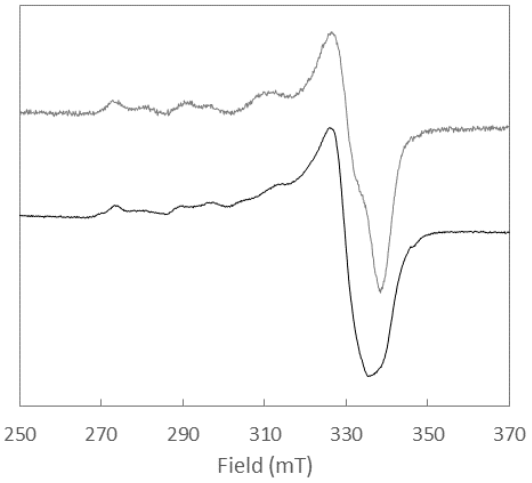

Figure S5: EPR spectra of Cu(II)-Aβox (black line) and Cu(II)-$A\beta_{28}$ (grey line) at pH 7.4. Aqueous solution with 10% of glycerol containing ^{65}Cu (450 µM) and peptide (500 µM). T = 120 K, v = 9.5 GHz, microwave power = 20.5 mW, Amplitude modulation = 10.0 G, Modulation frequency = 100 kHz.

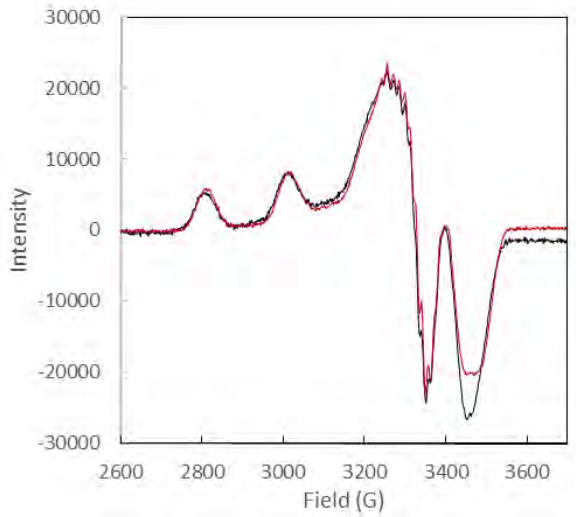

Figure S6: Linear combination fitting of 60% Cu(II)-Aβ$_{28}$ and 40% Cu(II)-AcAβ$_{28}$ (red line) compared to Cu(II)-Aβox signature (black line).

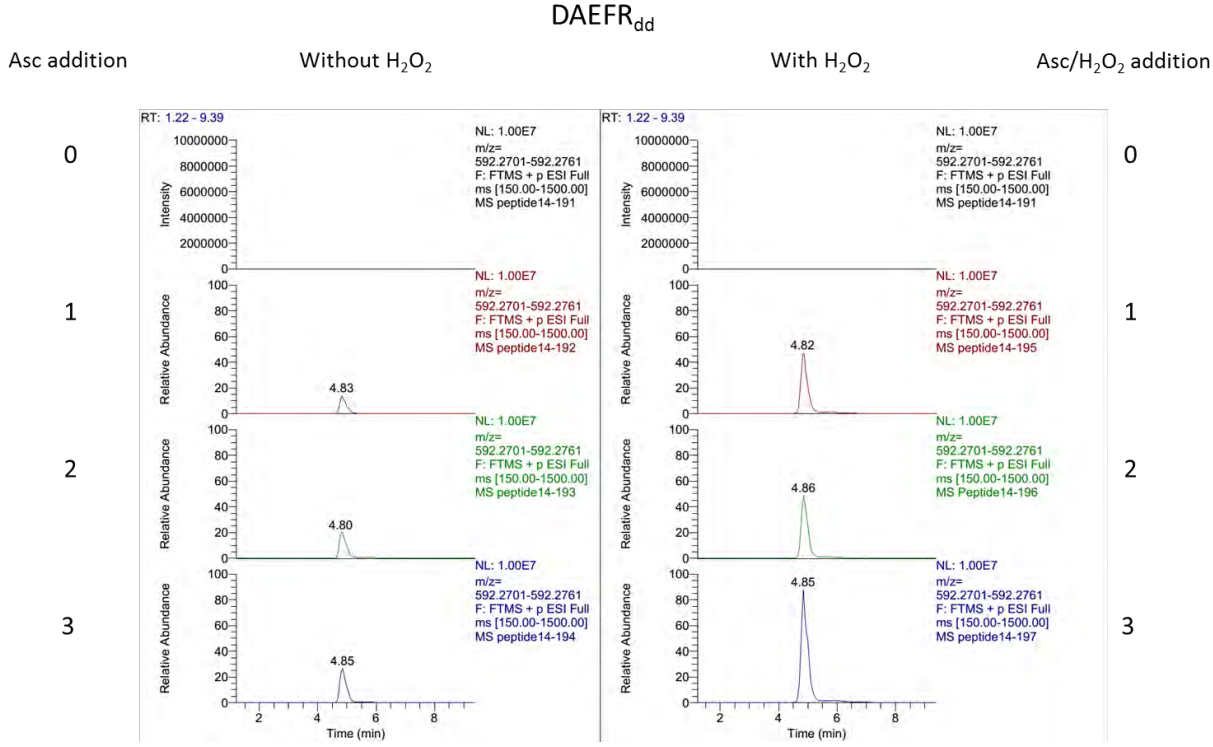

Figure S7: **Oxidation of Asp1 (DAEFR$_{dd}$) in the presence or absence of H_2O_2.** Trace chromatograms of the Aβ oxidized tryptic peptide DAEFR$_{dd}$ (decarboxylation and deamination of Asp1), after successive additions of ascorbate (4 nmol, final conc. 20 µM; left panel) or ascorbate/H_2O_2 (4/10 nmol, final conc. 20/50 µM; right panel). Aβ$_{28}$ 25 µM and Cu(II) 20 µM, phosphate buffered pH 7.4 (50 mM). Mass tolerance set at 5 ppm; m/z ratios used for detection are specified in Table S1.

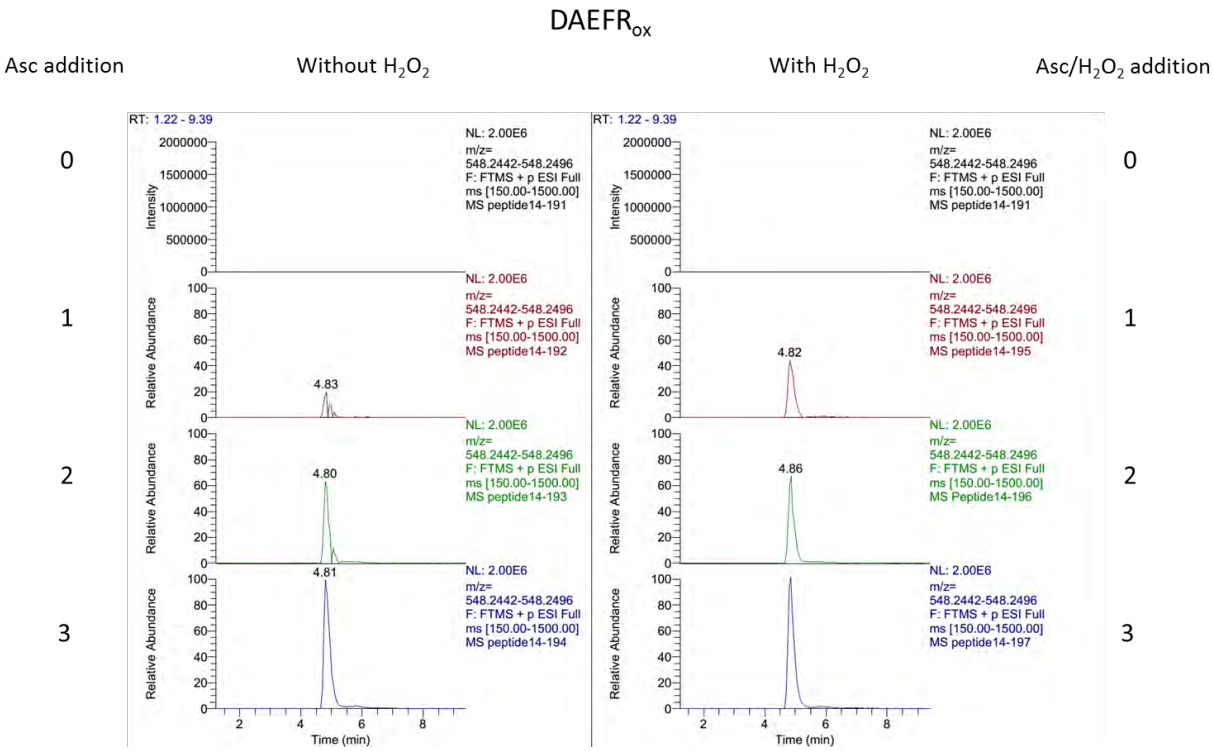

Figure S8: **Oxidation of Asp1 (DAEFR$_{ox}$) in the presence or absence of H_2O_2**Trace chromatograms of the oxidized Aβ tryptic peptide DAEFR$_{ox}$ (oxidative cleavage of Asp1), after successive additions of ascorbate (4 nmol, final conc. 20 µM; left panel) or ascorbate/H_2O_2 (4/10 nmol, final conc. 20/50 µM; right panel). Aβ_{28} 25 µM and Cu(II) 20 µM, phosphate buffered pH 7.4 (50 mM). Mass tolerance set at 5 ppm; m/z ratios used for detection are specified in Table S1.

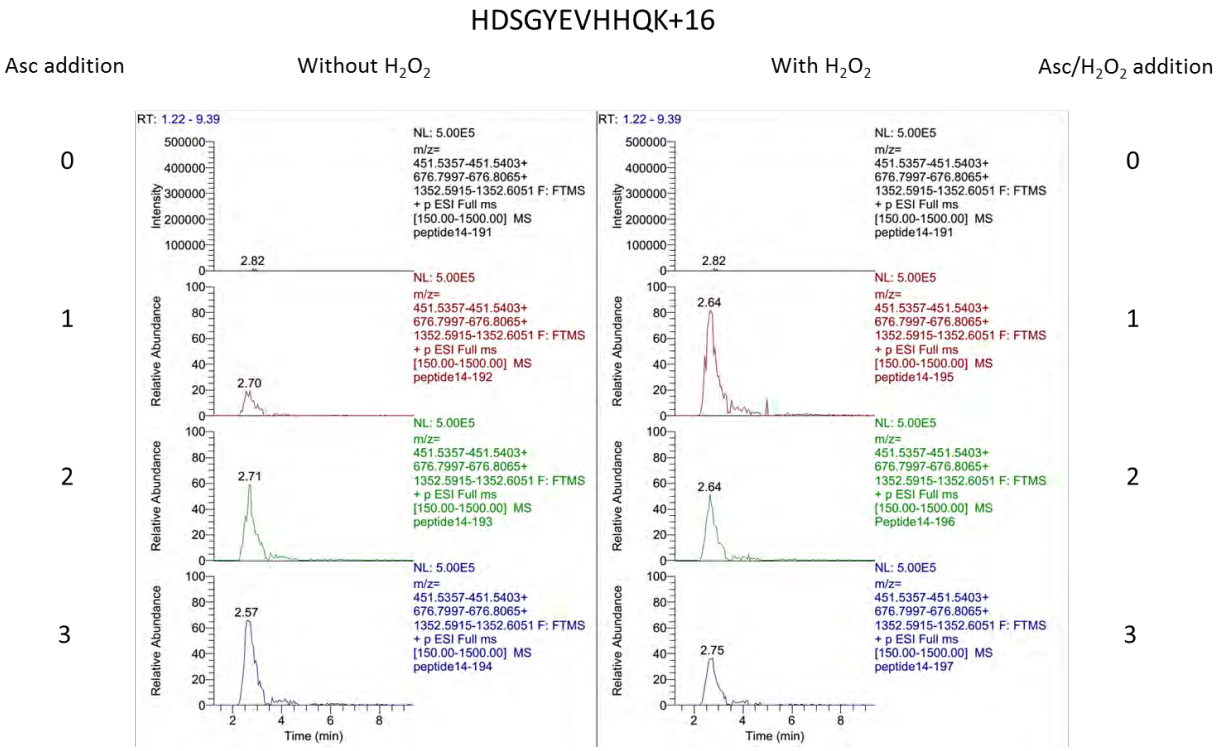

Figure S9: **Oxidation of His (HDSGYEVHHQK+16) in the presence or absence of H_2O_2.**Trace chromatograms of the oxidized Aβ tryptic peptide HDSGYEVHHQK+16 (formal addition of an oxygen atom), after successive additions of ascorbate (4 nmol, final conc. 20 µM; left panel) or ascorbate/H_2O_2 (4/10 nmol, final conc. 20/50 µM; right panel). $A\beta_{28}$ 25 µM and Cu(II) 20 µM, phosphate buffered pH 7.4 (50 mM). Mass tolerance set at 5 ppm; m/z ratios used for detection are specified in Table S1.

DTA for scans: 105-108
Precursor ion: 677.43
Mass type: mono
Mod's: (DAEFRHSGYVQKLFNM* +16.00000) (DAEFRHSGYVQKLFNM# +32.00000) (DAEFRHSGYVQKLFNM@ -45.00000) (DAEFRHSGYVQKLFNM^

Ion series for charge: +1

AA	A ions	B ions	B* ions	Bo ions	C ions	Y ions	Y* ions	Yo ions	Z ions
H		138.07							
D		253.09				1215.54			
S		340.13				1100.52			
G		397.15				1013.49			
Y		560.21				956.46			
E		689.25				793.40			
V		788.32				664.36			
H*		941.38				565.29			
H		1078.44				412.23			
Q		1206.50				275.17			
K						147.11			

DTA for scans: 105-108
Precursor ion: 677.43
Mass type: mono
Mod's: (DAEFRHSGYVQKLFNM* +16.00000) (DAEFRHSGYVQKLFNM# +32.00000) (DAEFRHSGYVQKLFNM@ -45.00000) (DAEFRHSGYVQKLFNM^

Ion series for charge: +2

AA	A ions	B ions	B* ions	Bo ions	C ions	Y ions	Y* ions	Yo ions	Z ions
H		69.54							
D		127.05				608.28			
S		170.57				550.76			
G		199.08				507.25			
Y		280.61				478.74			
E		345.13				397.20			
V		394.66				332.68			
H*		471.19				283.15			
H		539.72				206.62			
Q		603.75				138.09			
K						74.06			

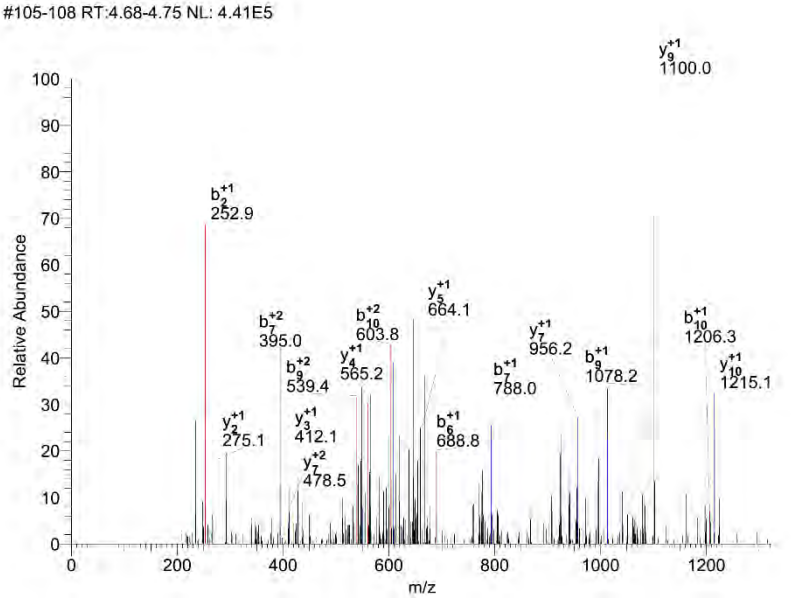

Figure S10: **MCO of Aβ in the presence of H_2O_2, identification of oxidized His13**. Series of b and y ions (charge 1+ and 2+) used for the identification of the oxidation of His13, and corresponding MS/MS spectrum of the doubly protonated ion of HDSGYEVHHQK+16. Same experimental conditions as the ones of Figure S8.

DTA for scan: 131
Precursor ion: 677.06
Mass type: mono
Mod's: (DAEFRHSGYVQKLFNM* +16.00000) (DAEFRHSGYVQKLFNM# +32.00000) (DAEFRHSGYVQKLFNM@ -45.00000) (DAEFRHSGYVQKLFNM^

Ion series for charge: +1

AA	A ions	B ions	B* ions	Bo ions	C ions	Y ions	Y* ions	Yo ions	Z ions
H		138.07							
D		253.09				1215.54			
S		340.13				1100.52			
G		397.15				1013.49			
Y		560.21				956.46			
E		689.25				793.40			
V		788.32				664.36			
H		925.38				565.29			
H*		1078.44				428.23			
Q		1206.50				275.17			
K						147.11			

DTA for scan: 131
Precursor ion: 677.06
Mass type: mono
Mod's: (DAEFRHSGYVQKLFNM* +16.00000) (DAEFRHSGYVQKLFNM# +32.00000) (DAEFRHSGYVQKLFNM@ -45.00000) (DAEFRHSGYVQKLFNM^

Ion series for charge: +2

AA	A ions	B ions	B* ions	Bo ions	C ions	Y ions	Y* ions	Yo ions	Z ions
H		69.54							
D		127.05				608.28			
S		170.57				550.76			
G		199.08				507.25			
Y		280.61				478.74			
E		345.13				397.20			
V		394.66				332.68			
H		463.19				283.15			
H*		539.72				214.62			
Q		603.75				138.09			
K						74.06			

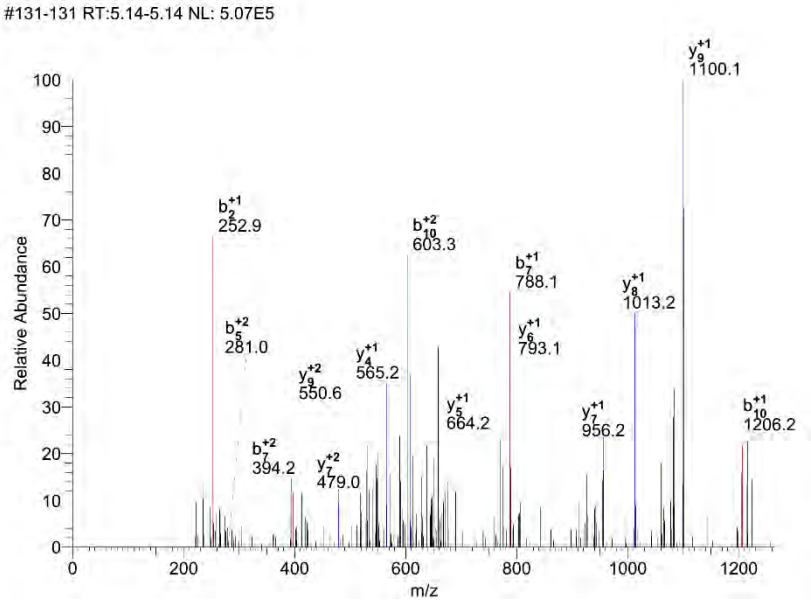

Figure S11: **MCO of Aβ in the presence of H_2O_2, identification of oxidized His14**. Series of b and y ions (charge 1+ and 2+) used for the identification of the oxidation of His14, and corresponding MS/MS spectrum of the doubly protonated ion of HDSGYEVHHQK+16. Same experimental conditions as the ones of Figure S8.

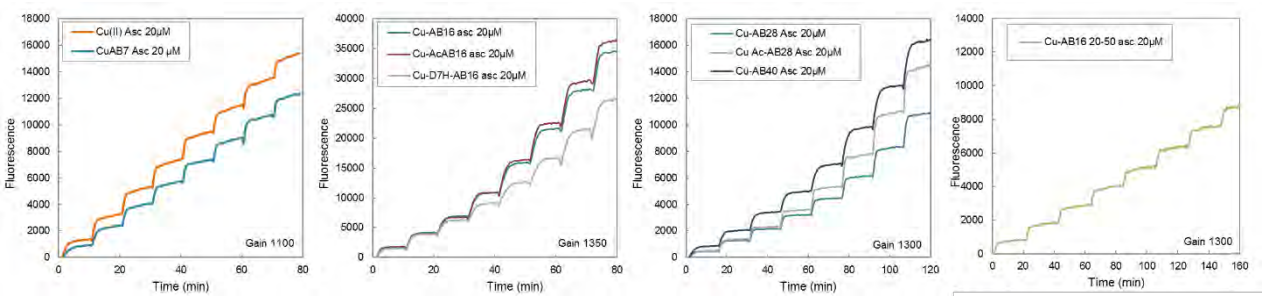

Figure S12: Fluorescence curves of phosphate buffered solutions (50 mM) containing Cu (20 µM), Aβ peptide (25 µM, except the green curve: 50 µM), CCA (0,5 mM) with additions of ascorbate (20 µM) and hydrogen peroxide (50 µM) realized every 15 min during 2 hours.

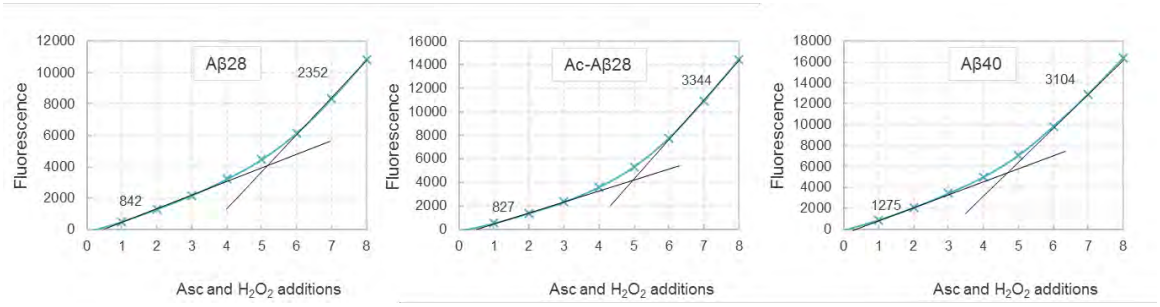

Figure S13: Fluorescence at the plateau of phosphate buffered solution (50 mM) containing Cu (20 µM), Aβ peptide (25 µM), CCA (0,5 mM) as a function of the number of ascorbate and H_2O_2 additions. A total of 8 additions of 2 µL ascorbate (2 mM) and 2 µL hydrogen peroxide (5 mM) are realized, i.e. respectively 4 and 10 nmol for each addition (initial concentrations reaching 20 and 50 µM for the first addition, respectively).

Chapter V

Chapter V: Characterization of a redox competent Cu binding mode in the « in-between » State

The chapter focuses on the study of copper mediated $HO^{\bullet}$ production in the presence of modified Aβ peptides, for the characterization of the Cu coordination sphere of the redox competent species responsible for ROS production. The chapter is composed of a manuscript that will be submitted soon, along with a summary of the article, written in French (requirement of the doctoral school). The supporting information related to the article is situated at the end of the chapter (Section V.C).

V.A. Article

Identification of key structural features of the elusive Cu-Aβ complex involved in oxidative stress in Alzheimer's Disease

Clémence Cheignon [a,b,c], Megan Jones [a,b], Elena Atrián-Blasco [a,b], Isabelle Kieffer [d,e], Peter Faller [a,b,†], Fabrice Collin [a,b,c,*] and Christelle Hureau [a,b,*]

a. LCC (Laboratoire de Chimie de Coordination), CNRS UPR 8241, 205 route de Narbonne, 31062 Toulouse Cedex 09 (France).

b. Université de Toulouse ; UPS, INPT, 31077 Toulouse (France).

c. UMR 152 Pharma Dev, Université de Toulouse, IRD, UPS, France.

d. Observatoire des Sciences de l'Univers de Grenoble (OSUG), CNRS UMS 832, 414 Rue de la Piscine, 38400 Saint Martin d'Hères, France

e. BM30B/FAME, ESRF, The European Synchrotron, 71 Avenue des Martyrs, 38000 Grenoble, France

KEYWORDS ROS / amyloid peptide / mechanism / copper / spectroscopy

ABSTRACT: Oxidative stress is linked to the etiology of Alzheimer's disease (AD), the most common cause of dementia in the elderly. Redox active metal ions such as copper catalyze the production of Reactive Oxygen Species (ROS) when bound to the amyloid-β (Aβ) peptide encountered in AD. This reaction proceeds through a low-populated Cu-Aβ state, noted "in-between state (IBS)". However, the structural nature of this redox competent Cu-Aβ complex responsible for ROS production remains to be elucidated. Here, we report the use of complementary methods (X-ray absorption spectroscopy, EPR, NMR, fluorescence, UV-Vis) to characterize Cu binding to a wide series of modified peptides and to evaluate the ROS production by the resulting Cu-peptides complexes. The amino acid residues involved in the IBS Cu-Aβ species were identified. In addition, a possible mechanism by which the ROS are produced is also proposed. These two main fallouts are expected to impact the current vision of oxidative stress in AD but also in any other diseases involving amyloidogenic peptides with weakly structured copper binding sites.

Introduction

An important feature in Alzheimer Disease (AD) is the presence of oxidative damages on neuronal lipids and proteins, which clearly links oxidative stress to AD.[1-6] Oxidative stress can have different origins, but the overproduction of Reactive Oxygen Species (ROS) is considered as a major contribution. Loosely bound metal ions like copper and iron are very efficient catalysts for the production of ROS.[7] Metal ions are involved in AD and other neurodegenerative pathologies.[8-14] In AD, high concentrations of metal ions have been found in amyloid plaques, a hallmark of AD, where they are bound to the amyloid-β peptide (Aβ).[15,16] In particular, copper ions bound to Aβ are redox-competent and able to catalytically cycle between Cu(I) and Cu(II), in the presence of a reductant (e.g. ascorbate), to generate ROS such as $HO^{\bullet}$, $O_2^{\bullet-}$ or H_2O_2.[17-20] Thus, the coordination mode of Aβ with copper ions plays a crucial role since ROS production is metal-catalyzed.

Cu(I) and Cu(II) coordination spheres are quite different. Near physiological pH, two Cu(II)-Aβ binding modes (called components I and II) coexist, both with a distorted square-planar geometry (Figure 1a)[21-23] while Cu(I) is bound in a linear fashion by two of the three His residues present in the Aβ sequence, in a dynamic exchange (Figure 1b).[24,25] An electrochemistry study has previously shown that the redox process between Cu(I)-Aβ /Cu(II)-Aβ is governed by a so-called "POET" (Pre-Organization Electron Transfer) mechanism.[26] This electron transfer proceeds through a small fraction of the peptide in equilibrium with the resting states (RS) of Aβ-Cu(I) and Aβ-Cu(II), whose

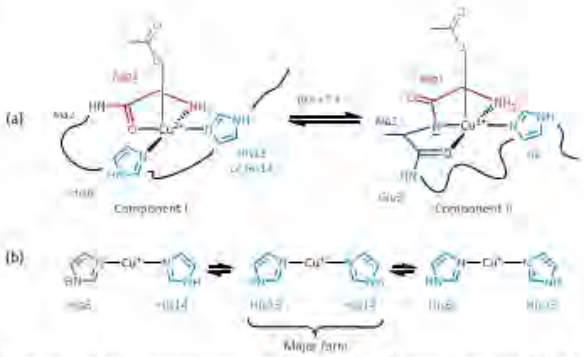

Figure 1. Cu(II) coordination (a) and Cu(I) coordination (b) to the Aβ peptide in the resting states.[21,24,25]

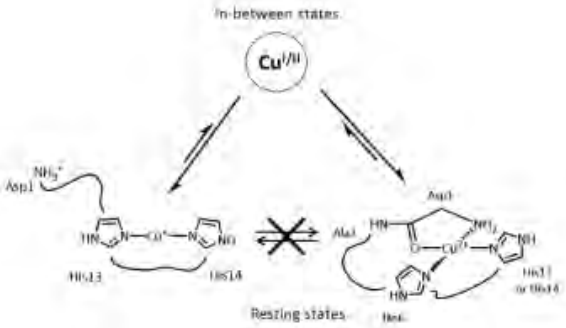

Figure 2. Schematic view of the equilibrium between the resting and In-between states of Cu-Aβ complex during ROS production.

coordination mode is described above (Figure 1). In this weakly populated state, called "in-between state" (IBS), the Aβ peptide surrounds the Cu center in such a way as to speed up the electron transfer (Figure 2).

Accordingly, in the IBS, the reorganization energy is minimal,[26] and thus it is anticipated that neither ligand exchange nor strong geometric modification occurs between the Cu(I) and Cu(II) states. Note that such IBS is reachable due to the very flexible nature of peptide.[22,27] Because this state is low-populated, the structure of the Cu site cannot be directly determined using classical spectroscopic methods. As this state should be engaged in the ROS production, some structural features can be obtained from the oxidative damages undergone by the peptide itself.[28] According to this mass spectrometry study,[28] Asp1, His13 and His14 are involved in the coordination sphere of copper as they are the main amino acid residues specifically targeted by HO• during the ROS production. In addition, only few computational studies aimed at elucidating the Cu environment in the redox competent state of Cu-Aβ.[29-32] Thus, the IBS is little described although it is responsible for the metal-catalyzed ROS production, contributing to oxidative stress in AD.

In the present study, we propose a single binding mode for both Cu(I)-Aβ and Cu(II)-Aβ in the IBS. This proposed

Table 1. Peptide sequence of the mutated, modified and truncated Aβ peptides used for the study along with their binding mode with Cu(II) and Cu(I) at pH 7.4 and pKa of the transition between the two Cu(II) components present at pH 7.4.

Type of modification	Name	Sequence	Cu(II) binding mode(s) present at pH 7.4[a]	pKa[b]	Cu(I) binding mode
-	$A\beta_{16}$	DAEFRHDSGYEVHHQK	(I) ^{H2N}D^{CO}AEFR^{Nim}HDSGYEV^{Nim}[HH]QK	7.8 [33]	2 N_{im} [24,25]
Mutation of carboxylate group	E3Q	DAQFRHDSGYEVHHQK	(II) ^{H2N}D^{N-}A^{CO}EFR^{Nim}[H]DSGYEV[HH]QK	7.8 [34]	-
	D7N	DAEFRHNSGYEVHHQK		7.9 [33]	
	E11Q	DAEFRHDSGYQVHHQK		7.5 [33]	
Murine mutation	Y10F	DAEFRHDSGFEVHHQK		7.5 [35]	
	R5G	DAEFGHDSGYEVHHQK			
	$mA\beta_{16}$	DAEFGHDSGFEVRHQK	(II^m) ^{H2N}D^{CO}AEFG$^{N-,Nim}$HDSGYEVHHQK	6.2 [35]	
N-terminal deletion	$A\beta_{3-16}$	EFRHDSGYEVHHQK	(I) ^{H2N}E^{N-}FR^{Nim}H^{CO}DSGYEVHHQK (III) ^{H2N}E^{N-}FR^{Nim}H^{N-}DSGYEV[HH]QK	7.5 [36]	-
N-terminal modification	$A\beta_{pE3-16}$	(pE)FRHDSGYEVHHQK**	(II') DAEFRHDSGYEV^{Nim}H$^{N-,Nim}$HQK, X (III') DAEFRHDSGYEV^{N-}H$^{N-,Nim}$HQK, X	7.7 [36]	
	$AcA\beta_{16}$	AcDAEFRHDSGYEVHHQK**	(II') N_{im}, N-, X, Y (III') N_{im}, 2N-, X	7.5 [33,37]	2 N_{im}
N-terminal mutation	D1E	EAEFRHDSGYEVHHQK	(I) ^{H2N}E^{CO}AEFR^{Nim}HDSGYEV^{Nim}[HH]QK (II) ^{H2N}E^{N-}A^{CO}EFR^{Nim}[H]DSGYEV[HH]QK	6.0	2 N_{im}
	D1N	NAEFRHDSGYEVHHQK	*(I) & (II) Similar as $A\beta_{16}$*	6.0 [33]	
His mutation	H6R	DAEFRRDSGYEVHHQK	(I) ^{H2N}D^{CO}AEFRRDSGYEV^{Nim}H^{Nim}HQK	7.2 [33]	-
	H6A	DAEFRADSGYEVHHQK	*(II) Similar as $A\beta_{16}$*	7.3 [33]	2 N_{im}
	H13A H14A	DAEFRHDSGYEVAHQK DAEFRHDSGYEVHAQK	*(I) & (II) Similar as $A\beta_{16}$*	7.5 [33]	
	H13R	DAEFRHDSGYEVRHQK	*(I) & (II) Similar as $A\beta_{16}$*	7.2 [35]	-
Suppl. His	D7H	DAEFRHHSGYEVHHQK	*(I) & (II) Similar as $A\beta_{16}$*	7.3	2 N_{im}
C-terminal truncation	$A\beta_7$	DAEFRHD	*Similar as $A\beta_{16}$ (component II)*	6.0 [c]	≠ 2 N_{im} [38]
Double His mutation	H6A-H13A	DAEFRADSGYEVAHQK			≠ 2 N_{im}
	H6A-H14A	DAEFRADSGYEVHAQK			-

Colored data have been obtained in the present study by EPR (blue) and XANES (green) experiments (spectra are given in Figures S1 to S4 of the supporting information).

[a] The square brackets depict the dynamic exchange existing between histidine residues; N_{im} = nitrogen atom from imidazole ring; CO, N• = carbonyl and amidyl nitrogen of the peptide bond; H_2N = N-terminal amine.

[b] pKa of transition between the two Cu(II) components present at pH 7.4.

[c] Minimal pH where component II is majority.

** AcD refers to the N-terminally acetylated aspartate*

*** pE refers to pyroglutamate.*

2

coordination model was deduced from studies on the impact of Aβ peptide sequence modifications towards Cu-induced ROS production, in the presence of ascorbate and dioxygen. We use fluorescence and UV-Visible spectroscopies to monitor the HO• trapping and ascorbate consumption respectively, as well as X-ray Absorption Near Edge Spectroscopy (XANES), Electron Paramagnetic Resonance (EPR) and Nuclear Magnetic Resonance (NMR) to describe the RS of the Cu-complexes.

Results

The present study deals with the identification of key structural features of the IBS. To reach such an objective, a series of modified peptides has been used. Hence, we have first determined the Cu(I) and Cu(II) coordination to those peptides in the RS, when not available in the literature and gathered all the data in Table 1. This will be detailed in the first paragraph of the result part while the other two focus on the characterizations of the IBS.

Coordination of Cu(I) and Cu(II) to modified Aβ peptides in the RS

The C-terminally truncated $A\beta_{16}$ peptide was used instead of the full-length $A\beta_{40}$ peptide because the first 16 amino acid residues encompass the metal ion binding sites,[21,25,39,40] thus representing a valuable model of metal coordination to the full-length peptide.

In order to determine the amino acid residues of Aβ involved in copper coordination during the ROS production, a series of mutated and N-terminally protected and truncated Aβ peptides were studied. A complete list of these peptides, along with their sequences and residues involved in Cu(I) and Cu(II) coordination in the RS, is given in Table 1. One part of the data was collected from the literature, while the other one was obtained by XANES and EPR experiments, respectively (spectra are given in Supporting Information, Figures S1 to S4).

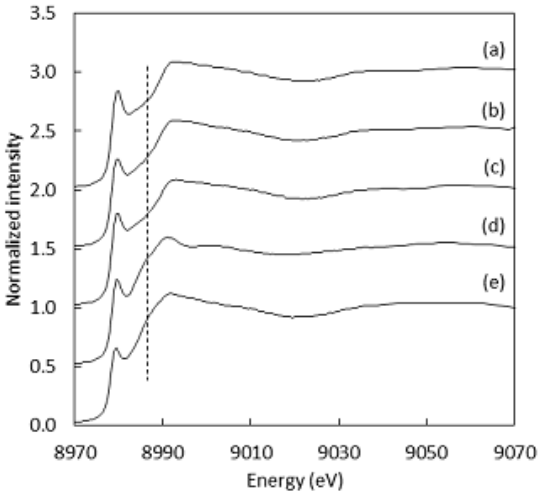

Figure 3. Cu XANES K-edge X-ray absorption spectra of (a) Cu(I)-Aβ16, (b) Cu(I)-D7H, (c) Cu(I)-H6A, (d) Cu(I)-(H6A-H13A) and (e) Cu(I) in buffer at pH 7.1.

Regarding Cu(I), the linear coordination by two His residues found with $A\beta_{16}$ was also detected with peptides containing at least two His residues, as illustrated by the XANES study of Cu(I)-$AcA\beta_{16}$, Cu(I)-D1N and Cu(I)-D1E, Cu(I)-H6A, Cu(I)-H13A, Cu(I)-H14A and Cu(I)-D7H, (Figures S1 and S2), showing the characteristic intensity of the 1s→4p feature (around 0.7-0.8).[24,25,41] As an example, XANES signatures of Cu(I)-$A\beta_{16}$, Cu(I)-D7H and Cu(I)-H6A are shown in Figure 3. Peptides containing only one His show a different XANES signature than Cu(I)-$A\beta_{16}$ and Cu(I) in buffer, as illustrated by Cu(I)-(H6A-H13A) (dotted line in Figure 3d) and Cu(I)-$A\beta_7$ (Figure S3). This underlines the importance of having two His for the native Cu(I) binding. When only one His is present, the signature is compatible with an increase of the ligands number on Cu(I),[41] and cannot be reproduced by a linear combination of signatures of Cu(I)-Aβ and Cu(I) in buffer only.

To gain more insights into Cu(I) binding to the 1-His containing peptides, NMR experiments were performed for H6A-H14A, H6A-H13A and $A\beta_7$ peptides (Figure 4 for an illustration with H6A-H14A peptide, and Figures S5 and S6 for the other peptides) according to reported protocols for the parent $A\beta_{16}$.[24,42,43] For comparison, ^{1}H NMR spectra of $A\beta_{16}$ in the absence and the presence of 1 equivalent of Cu(I) is reminded in Figure 4. With the latter peptide, Cu(I) is bound by two of the three His residues in dynamic exchange.[24,25] The Cu(I) binding to the peptide modifies the electron density of the protons in its vicinity resulting in a chemical shift.[24] For instance, the H_δ and H_ε protons of His13, present at about 7.75 and 6.93 ppm, are strongly shifted indicating that His13 residue is involved in Cu(I) binding.

In the case of H6A-H14A (Figure 4) and H6A-H13A (Figure S5), H_α, $H_{\beta1}$ and $H_{\beta2}$ of Asp1 are impacted by Cu(I) addition (4.00, 2.70 and 2.57 ppm) indicating that Asp1 is bound to Cu(I) by both the N- terminal amine and the carboxylate side chain (for $A\beta_7$, see supporting information, Figure S6). This is different to what is observed for the Asp1 protons of $A\beta_{16}$ (4.00, 2.70 and 2.57 ppm), which are not impacted by Cu(I) addition. This is in line with a change of Cu(I) coordination with the 1-His peptides.

H_ε, H_ζ and H_δ protons (around 7.2 ppm) peaks of Phe4 shift and broaden upon addition of Cu(I). However, the same is observed with $A\beta_{16}$ (Figure 4). This effect is probably linked to the spatial reorganization of the peptide due to Cu(I) binding to Aβ. Based on NMR and XANES data, we propose that the Cu(I) sphere in 1-His containing peptides involves the N-terminal amine, the side chain of one His residue and Asp1 carboxylate group.

Regarding Cu(II), several data were extracted from the literature (Table 1). In particular, Cu(II) coordination to Aβ was previously studied and was found to involve NH_2 of Asp1, C=O from the Asp1-Ala2 peptide bond, and N atoms from the imidazole ring of His6 and His13/14 in equilibrium for the main component present at physiological pH (component I). The minor species at physiological pH (component II) is characterized by a Cu(II) center bound by the NH_2 from Asp1, N^- from the Asp1-Ala2 peptide bond, C=O from the Ala2-Glu3 peptide bond and one N atom from the imidazole ring of His6/13/14 in

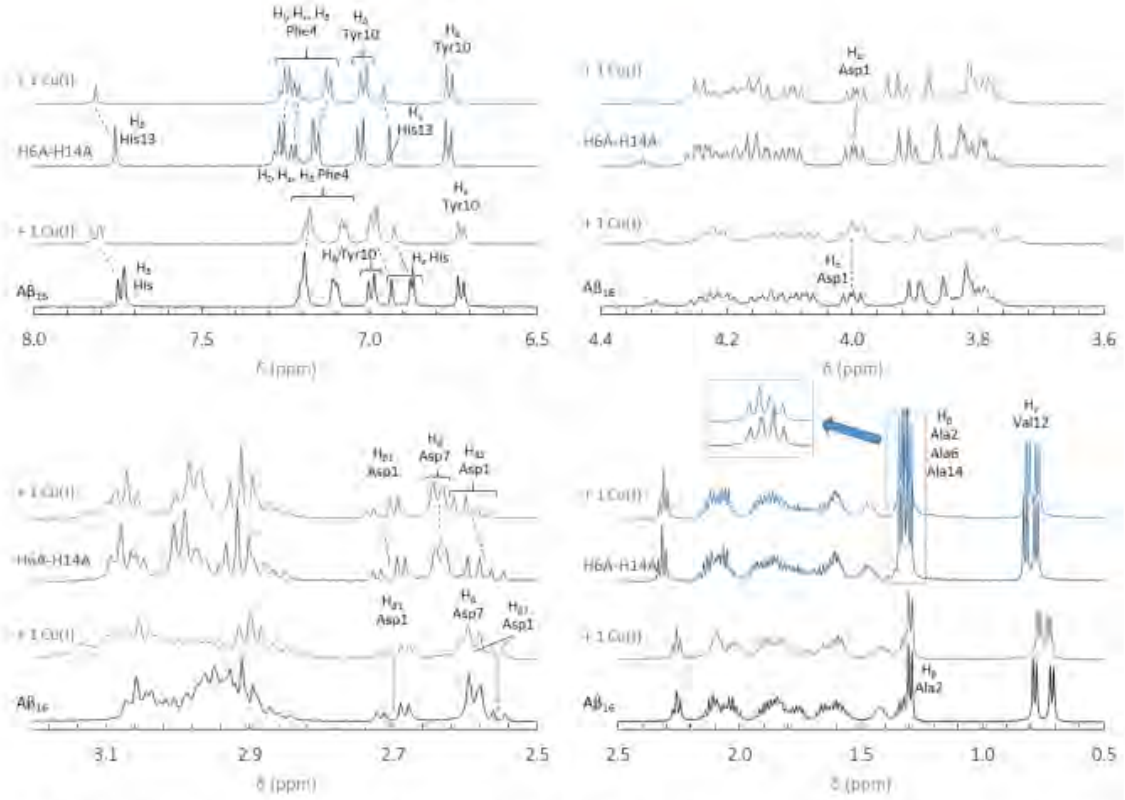

Figure 4. ^{1}H NMR spectra of $A\beta_{16}$ (black curve) with 1 equivalent of Cu(I) (grey curve) and ^{1}H NMR spectra of H6A-H14A (dark blue curve) with 1 equivalent of Cu(I) (light blue curve) at pH 7.3. The chemical shifts of protons observed with the addition of Cu(I) are indicated with dotted lines. All chemical shifts were referenced at 0.00 ppm relative to internal TSP.

equilibrium. The pH of interconversion between components I and II (noted pKa value) equals 7.8 (Table 1).[33] Several modifications were found to have significant impacts on the pKa values but not on the coordination mode: E3Q, D7N, E11Q, Y10F, D1N, H6R, H6A, H13A, H13R and H14A.[33-35] In contrast, N-terminal truncation or blockage ($A\beta_{3\text{-}16}$, $A\beta_{p3\text{-}16}$ and $AcA\beta_{16}$) strongly affects the coordination sphere.[33,36,37] Finally, although Arg5 is not directly involved in the coordination sphere, the R5G mutation, one of the three amino acid changes from the murine peptide (R5G, Y10F and H13R) was previously found to affect the Cu(II) binding modes, and to decrease the pKa value by 1.5 pH unit.[35] To complement the data collected from the literature, EPR experiments were carried out to gain insights into Cu(II) coordination to D1E, D7H, $A\beta_7$, H6A-H13A and H6A-H14A (the complete set of EPR spectra as a function of pH and the corresponding EPR parameters are given in Supplementary Information, Figure S4 and Table S1, respectively). As a matter of illustration, the EPR signatures of Cu(II)-$A\beta_{16}$, Cu(II)-D7H, Cu(II)-D1E and Cu(II)-(H6A-H13A) at pH 7.5 are shown in Figure 5.

The removal of one His on the sequence (H6A, H6R, H13A, etc.) had only a slight impact on both the pKa(I/II) value and the Cu(II) coordination.[33,35] Similarly, the addition of one His (D7H) does not modify either the Cu(II) binding modes or the pKa(I/II). D1E mutation leads to a strong decrease in the pKa(I/II) value while keeping similar copper coordination modes than $A\beta_{16}$ (Figure S4) as previously shown for the D1N mutation.[33] Finally, the double removal of His ($A\beta_7$ truncation, H6A-H13A or H6A-H14A double mutation) has a strong impact on Cu(II) speciation with component II largely predominant above pH 7.0 (Figure 5d and Figure S4).

Thus, Cu(I) binding mode is mainly affected when only one His residue is present on the peptide. With respect to Cu(II), N-terminal modifications, R5G mutation and double His mutation strongly modify its main coordination spheres at physiological pH. Furthermore, His modifications have only an impact on the components' pKa value. These changes are observed for Cu-Aβ peptides in the RS, but could also have an impact on the coordination mode of both Cu(I) and Cu(II) in the IBS (the redox competent one), and consequently modulate the ROS production by the corresponding peptides.

In this part, we have determined the main Cu(I) and Cu(II) coordination of the native $A\beta_{16}$ and several modified counterparts in the RS. Next part aims at investigating the coordination mode of Cu in the IBS.

4

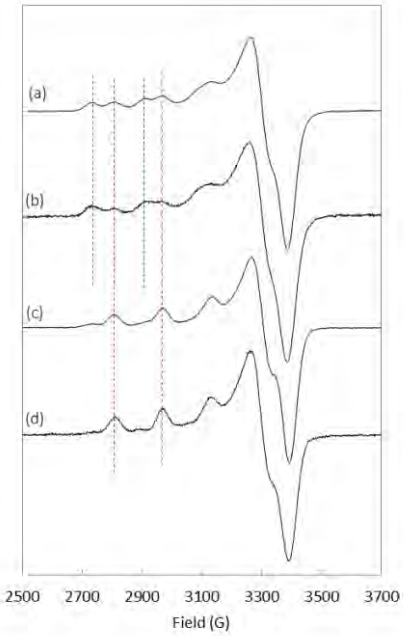

Figure 5. EPR spectra of ^{65}Cu(II) coordinated to (a) Aβ$_{16}$, (b) D7H, (c) D1E or (d) H6A-H13A at pH 7.5. Blue and red dashed lines indicate the signatures related to component I and component II, respectively. Aqueous solution of ^{65}Cu(II) (0.45 mM), peptide (0.5 mM) with 10 % of glycerol.

Probing the His and N-terminal amine involvement in the IBS.

In order to identify the amino acid residues involved in the copper coordination in the IBS, we studied the ROS production catalyzed by Cu-Aβ in the presence of ascorbate, with the different peptides listed in Table 1. The HO• production was followed by the fluorescence of 7-hydroxycoumarin-3-carboxylic acid (7-OH-CCA), an oxidation product resulting from HO• trapping by coumarin-3-carboxylic acid (CCA). The 7-OH-CCA fluorescence is proportional to the quantity of HO• trapped by CCA and thus to the amount of HO• released by the Cu-Aβ system.[44,45]

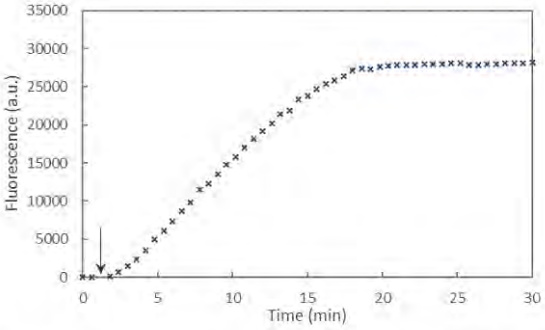

Figure 6. Fluorescence as a function of the time of 7-OH-CCA resulting from CCA oxidation by HO• produced by Cu-Aβ$_{16}$ in the presence of ascorbate. The arrow shows the beginning of the reaction, started with the addition of ascorbate (0.5 mM) in a phosphate buffered solution (pH 7.4, 50 mM) containing Aβ$_{16}$ (60 µM), Cu(II) (50 µM) and CCA (0.5 mM).

The fluorescence curve obtained with Cu-Aβ$_{16}$ in the presence of ascorbate is shown in Figure 6. Fluorescence starts to increase when ascorbate is added in solution, then grows quite linearly with time, and finally reaches a plateau that corresponds to the complete consumption of ascorbate (approximately 20 minutes). From this curve, two values were measured: the gradient of the initial slope of the linear part and the total fluorescence at the plateau. These two values are linked to the amount of HO• released by the Cu-Aβ system. From the fluorescence curves (Supplementary Information, Figure S7), the gradient of 7-OH-

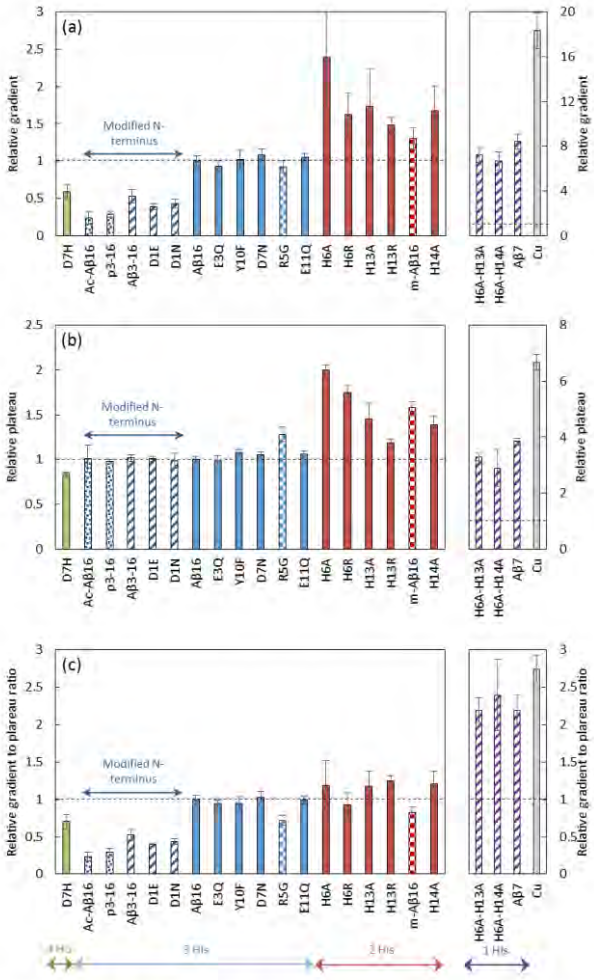

Figure 7. HO• scavenging by CCA. Initial gradient (a), plateau of fluorescence (b) and gradient to plateau ratio (c) of 7-OHCCA fluorescence resulting from oxidation of CCA 500 µM in the presence of native or modified Aβ$_{16}$ peptide 60 µM, Cu(II) 50 µM and ascorbate 500 µM; phosphate-buffered (50 mM) solutions at pH 7.4. Copper in buffer (grey bar) or in the presence of a peptide with 4 His (green bar), 3 His (blue bar), 2 His (red bar), 1 His (purple bar), or 3 His and a modified N-terminus (dark blue bar), coordinated predominantly in component I (plain bar), component II (striped bar) or other components (II' and III' (spotted bar), IIm (checkered bar), See Table 1 for details). Fluorescence curves are given in ESI (Figure S7). Gradient and fluorescence at the plateau are given as relative values (n=9 ± standard deviation) calculated as ratio with those obtained with Cu-Aβ$_{16}$.

5

CCA formation (Figure 7a) and the total fluorescence at the plateau (Figure 7b) were measured, for each peptide listed in Table 1, and expressed as relative values as compared with those obtained for the $A\beta_{16}$ peptide. Peptides are sorted by number of His on Aβ sequence: 4 His (green bar), 3 His (blue bars), 2 His (red bars) and 1 His (purple bars).

Gradient and fluorescence at the plateau values inform on the rate of 7-OH-CCA formation and on the quantity of 7-OH-CCA formed, respectively. In order to deduce the rate of HO• production, we used the ratio of gradient over plateau of the 7-OH-CCA formation. As such, the inherent capacities of the various peptides to scavenge HO• responsible for the different plateau intensities were taken into account and corrected for (Figure 7c, and Supporting Information for more details). His residues have such an ability as illustrated by High-Resolution Mass Spectrometry (LC-HRMS) experiments showing that ratio of N-terminal oxidation vs. the other oxidations decreases when increasing the number of His in the peptide sequence (see Supporting Information, Figure S8, Tables S2 and S3).

Analysis of the data such obtained lead to several conclusions: (i) the mutations leading to the predominance of component II for Cu(II) binding mode in the RS (stripped bars) compared to component (I) (plain bars) would not have a systematic impact on the HO• production rate (Figure 7c). Some of these mutants induce a lower production rate (D1E, D1N, R5G and $mA\beta_{16}$) while the other ones generate HO• much faster (H6A-H13A, H6A-H14A and $A\beta_7$). Thus, it is likely that the predominance of component I or II is not a key event in the HO• production.

(ii) The number of His on Aβ sequence impacts the HO• production rate: the less the His residues in the Aβ sequence, the faster the hydroxyl radical production. While a clear difference appears between 1-His containing and 2- to 4-His containing peptides, slighter changes are observed between 2-, 3- and 4-His containing peptides. Decreasing the number of His residues impacts the Cu(I) (and to a lesser extent the Cu(II)) affinities.[42,46-48] Hence the contribution of loosely bound Cu in the whole process was studied: the clear difference here observed is not due to the contribution of a larger amount of Cu bound to the buffer [38] or to the second site of Aβ [49] with the former peptide (compared to the latter ones) (See Figure S9 and details in the Supporting Information). Thus, His mutation appears as a key event in the intrinsic HO• production rate, and the transition from 2 His to 1 His residue on the Aβ sequence strongly impacts the reaction.

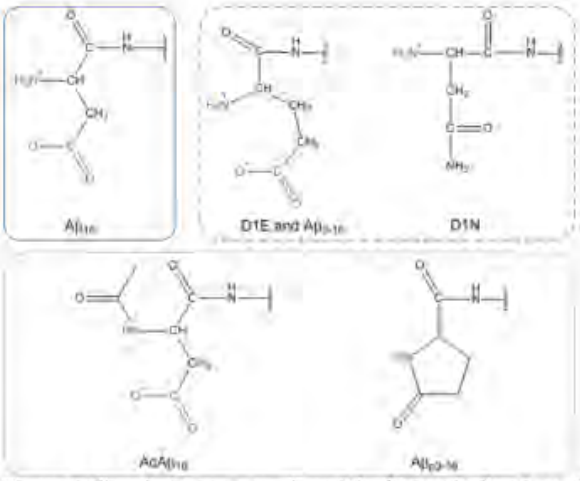

Figure 8. Chemical representation of the N-terminal moiety of the $A\beta_{16}$ (plain frame), D1E, $A\beta_{3-16}$, D1N, (dashed frame), $AcA\beta_{16}$ and $A\beta_{p3-16}$ (dotted frame). The N-terminal amine and carboxylate group are colored in blue and green respectively.

The mutation of 2 His residues impacts the coordination in both Cu(I) and Cu(II) RS: it leads to the main presence of Cu(II) complex in component II (Table 1) and to a modification of the Cu(I) sphere (See above, Figure S3). As having Cu(II) in component I or II seem not to influence the HO• production rate (see (i)), the different nature of the Cu(I) RS with 1-His peptide is likely at the origin of such an increase of the HO• production rate.

(iii) The modification of the N-terminal moiety of Aβ (dark blue bars) strongly slows the HO• production rate down. Several modifications were studied and can be sorted into two sub-classes: (1) modification of the side-chain of the first residue (D1E, D1N, $A\beta_{3-16}$) and (2) blockage of the N-terminal amine ($AcA\beta_{16}$ and $A\beta_{p3-16}$). The chemical structure of their N-terminal moiety is shown in Figure 8.

For the first sub-class, the carboxylate group present on Asp is either removed (D1N) or still present on a one-carbon longer side chain (D1E, $A\beta_{3-16}$) and the N-terminal amine is still available for binding. For the second sub-class, the N-terminal amine is not available for Cu(II) binding and the carboxylate group is available only with $AcA\beta_{16}$. As all the modifications (side chain modification of the N-terminal moiety or N-terminal amine blockage) result in a strong slowing down of HO• production, it can be assumed that both terminal NH_2 and the carboxylate group from the Asp side chain have a link with the IBS. However, the N-terminal amine unavailability ($AcA\beta_{16}$ and $A\beta_{p3-16}$) has a stronger effect than changes on the side chain (D1E, $A\beta_{3-16}$ and D1N).

Probing the implication of the Asp1 carboxylate group in the IBS.

The unavailability of the N-terminal amine is a key event for ROS production, as peptides with a blocked amine have the lowest HO• production rate. Hence, the N-terminal amine likely binds Cu in the IBS. Modification of the side chain (carboxylate group) of the first residue of Aβ has also a strong effect on the HO• production rate (Figure 7c, dark blue striped bars), although to a lesser extent. It is worth noting that in contrast to Cu(II), Cu(I) is not bound by the N-terminal amine in the RS. Indeed, while the Cu(II) Lewis acidity induces the deprotonation of the amine, Cu(I) is unable to do so, and the amine remains protonated at physiological pH. Hence to enter the coordination sphere of Cu in the IBS starting from Cu(I), the N-terminal amine has to be concomitantly deprotonated. With this in mind, two hypotheses may be proposed to connect the carboxylate group of the N-terminal side chain with the IBS, either by a direct or an indirect way.

First, the carboxylate group of Asp1 could directly bind Cu in the IBS. This is in line with the fact that: (i) the carboxylate group of Asp1 is one of the Cu(II) ligands at apical position in the RS, in equilibrium with the one of Asp7 and Glu residues.[49-51] (ii) the HO• production rate of D1N and D1E is lower, because D1N does no longer contain a

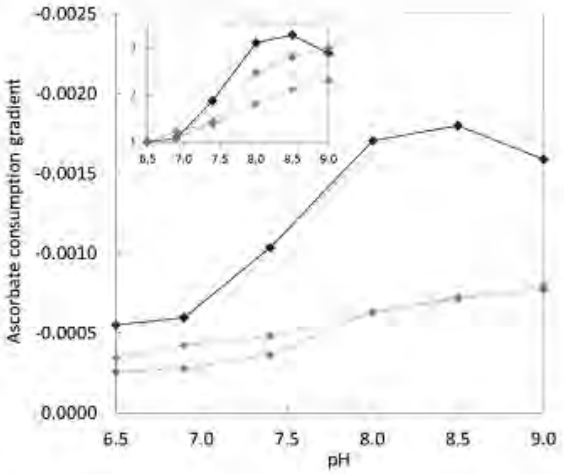

Figure 9. Gradient of ascorbate consumption by Cu-peptide as a function of a time. $A\beta_{16}$ (black curve), D1E (blue curve) or D1N (green curve) (20 µM), Cu (10 µM) and ascorbate (100 µM) in HEPES buffered solution (pH 6.5, 7.0, or 7.4) or POPSO buffered solution (pH 8.0, 8.5 or 9.0). Inset: relative gradient calculated by divided the gradient value at the given pH by the gradient at pH 6.5 for each peptide, as a function of the pH. Ascorbate consumption followed by UV-Visible spectroscopy at λ_{max} = 265 nm. The UV-Vis curves are shown in Figure S10.

carboxylate group and D1E forms a (NH_2, COO^-) 7 atoms metallacycle less stable than the (NH_2, COO^-) 6 atoms metallacycle formed with Asp (in $A\beta_{16}$).

Second, the carboxylate group of Asp1 is not a ligand of copper in the IBS, but would rather assist the protona tion/deprotonation process of the N-terminal amine (pKa = 7.8 in the presence of Cu(I), see Supporting Information, Figure S11) associated with the Cu-Aβ redox cycling. In this case, one expects that the effect of carboxylate would decrease progressively with increasing pH due to the intrinsic deprotonation of the N-terminal amine.

In order to discriminate between these two possibilities (i.e. COO^- (Asp) directly bound to Cu or in H-interaction with the N-terminal amine), the ascorbate consumption rate was followed as a function of pH for Cu-$A\beta_{16}$, Cu-D1E and Cu-D1N. The ascorbate consumption was monitored by UV spectroscopy at the wavelength of maximal ascorbate absorption (265 nm). This technique was chosen instead of the 7-OH-CCA fluorescence monitoring used in the above study as the 7-OH-CCA fluorescence is very sensitive to pH,[44] and as previously described the ascorbate consumption rate mirrors the ROS production rate by Cu-Aβ.[43,44,47,52-55]

Figure 9 shows the gradient of the initial slopes of ascorbate consumption as a function of the pH for each Cu-peptide system. Regardless of the peptide under focus, increasing the pH from 6.5 to 9.0 induces a two to three-fold increase of the ascorbate consumption rate in line with the requirement to deprotonate the N-terminal amine (inset in Figure 9). This indicates that the presence of Asp1 carboxylate in Cu-$A\beta_{16}$ does not help the deprotonation process. In addition, Cu-$A\beta_{16}$ ascorbate consumption rate is much higher than the one of the others two complexes at any measured pH (black curve) including when the N-terminal amine is deprotonated (Figure 9). These results are strongly in favor of a direct coordination of the COO^- (Asp1) side chain in the IBS.

Discussion

Model of IBS.

Based on the electrochemical data,[26] which showed that the reorganization energy between the two redox states in the IBS is minimal (λ = 0.3 eV), we postulate that the coordinating groups of both Cu(I) and Cu(II) are the same. As a consequence, the redox state of the Cu ions will not be specified in the next paragraphs.

The global rate of ROS production mainly depends (i) on the population of the IBS, which is correlated to the coordination sphere closeness between the RS and the IBS and (ii) on the intrinsic reactivity of the IBS. Both points have been taken into account to identify the Cu ligands in the IBS. In the model such deduced and shown in Figure 10, the Cu ion is bound by three ligands of the Aβ peptide, namely the N-terminal amine, the carboxylate group of Asp1 and the imidazole ring of one His residue (mainly His13 or His14, based on reference [28]) and by a substrate (O_2, $O_2^{\bullet-}$, H_2O_2 or ascorbate).

Involvement of the N-terminal amine

The N-terminal amine is proposed to be the main anchor of the Cu center in the IBS. This is deduced from three main observations. First, Cu(Ac-$A\beta_{16}$) and Cu($A\beta_{p3-16}$) complexes display a much lower $HO^\bullet$ production rate compared to Cu($A\beta_{16}$) species. Second, the pH dependent study of ascorbate consumption by Cu($A\beta_{16}$) species shows that the higher the pH, the faster the ascorbate consumption indicating that the deprotonation of the N-terminal amine (and consequent binding to the Cu center) favors the reaction. Last, it has been previously reported that a strong oxidative attack of Asp1 occurs during ROS production.[28,56,57]

Involvement of the side-chain of Asp1

The carboxylate side chain of Asp1 is also involved in Cu binding in the IBS, thus making a 6-membered metallacycle with the N-terminal amine. This is proposed based on the lower ROS production rate of Cu(D1E), Cu(D1N) and Cu($A\beta_{3-16}$) complexes compared to Cu($A\beta_{16}$) species, as probed by $HO^\bullet$ and ascorbate consumption. The possibility of having an indirect interaction of the COO^- group with the terminal NH_3^+ amine was disfavored by the pH-dependent

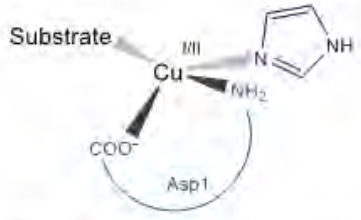

Figure 10. Schematic view of a proposed redox competent binding mode of Aβ-Cu(I/II) in the IBS during ROS production in the presence of substrate (O_2, $O_2^{\bullet-}$, H_2O_2 or ascorbate). Light grey and dark grey bonds correspond to backwards and forwards pointing bonds, respectively.

study of ascorbate consumption with Cu(D1E), Cu(D1N) and Cu($A\beta_{16}$) complexes.

Involvement of the side-chain of one His

Using the $HO^{\bullet}$ production study, we have shown that the rate strongly increases when only one His is present in the sequence. This indicates either that the RS and the IBS have a very similar Cu environment or that the nature of the IBS is changed. The former hypothesis is comforted by the binding mode of Cu(I) ($A\beta_7$, H6A-H14A, H6A-H14A) complexes deduced from NMR study in which Cu(I) is bound by the N-terminal amine, the Asp1 carboxylate side-chain and one His imidazole whereas two His residues bind the Cu(I) in the Cu($A\beta_{16}$). Having only one His forces the coordination of the N-terminal amine and of the side-chain of Asp1 in the Cu(I) RS. The observed increase of the ROS production rate perfectly matches with the involvement of the N-terminal amine and COO^- (Asp1) proposed above.

The IBS model deduced here varies from our former proposition,[28] by the number of His involved (one here against the two His13 and His14 previously) and by the identification of the Asp1 bidentate binding, via the N-terminal amine and the carboxylate side chain. Indeed, the involvement of the His13-His14 couple was inferred from the oxidative damages they underwent during ROS production. Such damages are also in line with the interchangeability of those two His in the IBS. Regarding Asp1, we have in the present work managed to better elucidate its binding mode while in our former study only the amino acid residue was identified.

ROS production mechanism: a working hypothesis

Based on the present results and on literature data,[18,26,28-32,58-61] a proposed mechanism of electron transfer involving the Cu(II) and Cu(I) complexes in the RS, the redox competent Cu(I/II) species in the IBS (Figure 10), and the substrate either ascorbate or O_2 are shown in Figure 11.

On the reductive pathway (left in Figure 11), we propose that ascorbate coordinates the Cu(II) ion, resulting in a coordination with 4 ligands in a D_{2d} geometry. This geometry is a typical intermediate geometry between D_{4h}, characteristic of the Cu(II) ion and Td, characteristic of the Cu(I) ion. Then, reduction of the metal center occurs. During the last step, the oxidized ascorbate is released and the Cu(I) IBS is formed.

On the oxidative pathway (right in Figure 11), three substrates can be involved: O_2, $O_2^{\bullet-}$ and H_2O_2. It has been suggested that the reduction of O_2 to $O_2^{\bullet-}$ is the rate determining step. [62] Thus, the case of O_2 is illustrated in Figure 11 but similar reactions could be proposed for $O_2^{\bullet-}$ and H_2O_2 as well. η^1 end-on binding of O_2 to the Cu(I) in the IBS is proposed leading to a D_{2d} of the resulting species. Then oxidation of the metal center occurs concomitantly with formation of a η^1 end-on superoxo species. The release of $O_2^{\bullet-}$ leads to the initial Cu(II) IBS species.

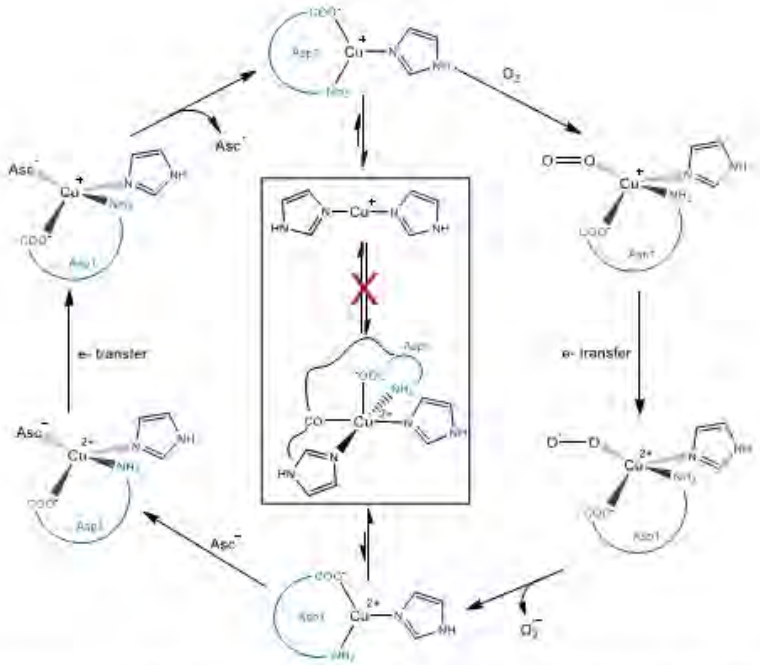

Figure 11. Schematic representation of the proposed mechanism of electron transfer between Cu(II)-Aβ and ascorbate (Asc^-) and between Cu(I)-Aβ and O_2 leading to the formation of $O_2^{\bullet-}$. Cu binding modes in the RS (rectangle) and Cu binding modes of the species in the IBS during the production of $O_2^{\bullet-}$. Light grey and dark grey bonds correspond to backwards and forwards pointing bonds respectively. $Asc^{\bullet}$ represents ascorbyl radical.

8

As pointed out, the proposed mechanism is a working hypothesis. Indeed, there are still many important questions to be investigated regarding the detailed ROS production mechanism. In particular, the reduction of the Cu(II) centre by ascorbate by an inner-sphere mechanism has been favored here,[59,63] but the outer sphere mechanism cannot be excluded. The peptide oxidation has been proposed to occur via the release of the oxidative agents (in particular $HO^{\bullet}$) based on the detection of $O_2^{\bullet-}$, H_2O_2 and $HO^{\bullet}$ and on the absence of any evidence of Cu-oxo species,[64] but a participation of metal-centred oxidation cannot be fully ruled out. Also, a η^1 end-on binding of oxygenated substrate has been preferred based on a minimal reorganization of the Cu coordination sphere, but a η^2 side-on binding mode may be possible as well. These issues have been recently addressed by computational methods but no clear-cut result has been obtained. [29-32]

In the course of experiments, it appears that the initial rate of ROS production might be more relevant than the total amount of ROS generated with regard to the IBS. This is well illustrated by the comparison between $A\beta_{16}$ and Ac-$A\beta_{16}$, both Cu complexes releasing the same amount of ROS but with a very different rate in link with involvement of the N-terminal amine in the IBS.

Furthermore, the positive feedback loop of the ROS production observed previously,[38] i.e. the increase of ROS production by Cu-Aβ once the peptide is itself oxidized, might be linked to the nature of the IBS found here. Indeed, His oxidation will lead to a RS closer to the IBS contributing to an increase in the ROS production rate. But this will be counter-balanced by Asp1 oxidation that will in contrast induce another type of IBS, resulting in a slower rate.

Conclusion

In the present paper, we have investigated the effects of Aβ sequence modifications towards the copper-induced $HO^{\bullet}$ production. Two modifications strongly impact the rate of the reaction: (i) the N-terminal modification of Asp1, either the terminal amine blockage or/and the carboxylate function deletion and (ii) the removal of 2 His residues from the peptide sequence. The influence of these modifications on ROS production rate are indicative of the Cu binding mode in the IBS, responsible for ROS production. An electron transfer mechanism has been proposed, involving the RS and IBS of Cu-Aβ with ascorbate and O_2 substrates.

Thus, we provide for the first time a coordination model of the Cu-Aβ complex in the elusive state responsible for oxidative stress in AD. This model based on spectroscopic studies is in line with proposition from computational studies.[29,30,32] Recently, it has been shown that Cu-Aβ aggregates keep a ROS production ability.[65,66] However, the production is slower compared to the one of monomeric Cu-Aβ species.[52] This is fully in line with the present results: access to the redox competent state may indeed be hampered by the formation of the aggregates and the subsequent burying of the Cu sites in a too rigid environment.

The mechanism of ROS production by the Aβ peptide might be well generalized to other flexible peptides accommodating different coordination spheres in Cu(I) and Cu(II) redox states. This includes α-synuclein involved in Parkinson's disease,[52,67-69] and biologically relevant Aβ peptides including Familial AD mutants.[22,70] In particular, for familial mutants of AD or other peptides, our results show that one cannot predict the impact of a mutation on the ROS production rate by using the RS coordination, because the IBS is structurally different. Hence, in order to anticipate whether a mutation can impact ROS production, the structure of the IBS has first to be known.

Experimental Section

Chemicals

Cu(II) used was from $CuSO_4.5(H_2O)$ and purchased from Sigma. Stock solution of Cu(II) 2mM was prepared in ultrapure water and kept at -20°C. Phosphate buffer was bought from Sigma-Aldrich and dissolved in ultrapure water to reach a 0.1 M concentration and a pH 7.4. HEPES buffer was bought from Sigma and dissolved in ultrapure water to reach solutions at pH 6.5, 7.0 and 7.4 (0.5 M). POPSO buffer was bought from Sigma and dissolved in ultrapure water to reach solutions at pH 8.0 and 8.5 (0.5 M). Ammonium bicarbonate was purchased from Fluka. A stock solution (0.1 M, pH 8.0) was prepared in ultrapure water. Ascorbate solutions were freshly prepared few minutes prior to each experimental set by dissolving sodium L-ascorbate (Fluka) in ultrapure water. A stock solution of coumarin-3-carboxylic acid (CCA) 1 mM (from Sigma) was prepared in phosphate buffer (0.1 M, pH 7.4) at room temperature.

Peptides

All the peptide (see Table 1 for the sequences) were bought from GeneCust (Dudelange, Luxembourg), with purity grade > 95%. Stock solutions of peptide were prepared by dissolving the powder in ultrapure water (resistivity 18.2 MΩ) (resulting pH 2). The peptide concentration was then determined at pH 2 by UV-visible absorption of Tyr10 considered as free tyrosine (Δε (276nm-296nm) = 1410 M^{-1} cm^{-1}) for a tyrosine-containing peptide, by UV-visible absorption of Phe4 (Δε (258nm-280nm) = 195 M^{-1} cm^{-1}) for $A\beta_7$ and by UV-visible absorption of Phe4 and Phe10 (Δε (258nm-280nm) = 390 M^{-1} cm^{-1}) for Y10F and m-$A\beta_{16}$. Stock solution of $A\beta_{40}$ peptide was prepared by dissolving the powder in NaOH (50mM) and passing the solution through FPLC to obtain the monomeric fraction. The peptide concentration was then determined in NaOH (50mM) by UV-visible absorption of Tyr10, considered as free tyrosine (Δε (293nm-360nm) = 2400 M^{-1} cm^{-1}). All pH values are given with a ± 0.2 pH unit error.

$HO^{\bullet}$ scavenging monitoring

Coumarin-3-carboxylic acid (CCA) was used as a probe to detect $HO^{\bullet}$, as it reacts with CCA to form the 7-hydroxycoumarin-3-carboxylic acid (7-OH-CCA), which is fluorescent at 452 nm upon excitation at 395 nm. The

intensity of the fluorescence signal is proportional to the number of 7-OH-CCA molecules formed, which in turn is proportional to the HO• radicals released.[45] As HO• can react with the HEPES buffer, phosphate buffer is preferred in this particular test. Fluorescence experiments were performed on a multimode microplate reader system CLARIOstar (BMG Labtech). An automatic injector was used to add ascorbate (500µM) into the wells containing phosphate-buffered (50 mM, pH7.4) solutions with Aβ peptide or mutant (60 µM), Cu^{2+} (50 µM) and CCA (0.5 mM). The fluorescence was measured every 36 s during 1 hour, and the ascorbate was injected at 72 s, starting the reaction.

Ascorbate consumption experiments

UV-Vis spectra were recorded on an Agilent 8453 UV-Visible spectrophotometer at 25°C. Intensity of the ascorbate (Asc) absorption band at λ_{max} = 265 nm (ε = 14 500 $M^{-1}.cm^{-1}$) was monitored as a function of the time in HEPES buffered solution (pH 6.5, 7.0, or 7.4) or POPSO buffered solution (pH 8.0 or 8.5) containing $A\beta_{16}$, D1E-$A\beta_{16}$, D1N-$A\beta_{16}$, Ac-$A\beta_{16}$, $A\beta_{3\text{-}16}$ or $A\beta_{p3\text{-}16}$ (20 µM), Cu (10 µM) and ascorbate (100 µM). The absorbance was measured every 10 s during 40 min and the gradient was calculated with the first 6 measures (1 min) of the experiment after the addition of Cu^{2+} to start the reaction. Each experiment was performed 3 times in order to ensure the reliability of the measure.

^{1}H NMR spectroscopy

Studies were performed or D_2O. However, for clarity and consistency, we decided to use the notation pH even when the measurements were made in D_2O. The pD was measured using a classical glass electrode according to pD = pH* + 0.4, and the apparent pH value was adjusted according equation pH = (pD − 0.32)/1.044,[71] or equivalentlyaccording to pH = 0.929pH* + 0.41,[72] to be in ionization conditions equivalent to those in H_2O.

Stock solutions of H6A-H14A and $A\beta_{16}$ were prepared by dissolving the powder in D_2O and titrated as described above. Cu(I) addition to H6A-H14A and $A\beta_{16}$ was carried out as follow: 1 equivalent of Cu(II) was added to a 0.5 mM solution of peptide in 0.2 M phosphate buffer in D_2O. The buffer pH was adjusted to 7.3 using NaOD and D_2SO_4. 2 equivalents per Cu ion of 0.1 M freshly prepared dithionite solution in D_2O were added under Ar atmosphere to the Cu(II)-Aβ solution in a NMR sealed tube.

The ^{1}H NMR experiments were recorded on a Bruker Avance 500 spectrometer equipped with a 5 mm triple resonance inverse Z-gradient probe (TBI 1H, 31P, BB). The presaturation of the water signal was achieved with a zqpr sequence (Bruker). ^{1}H NMR experiments are performed at 298K.

ASSOCIATED CONTENT

Supporting Information

Fluorescence data, UV-vis curves, XANES and EPR data, EPR parameters table, ^{1}H NMR data

This material is available free of charge via the Internet at http://pubs.acs.org

AUTHOR INFORMATION

Corresponding Authors

* fabrice.collin@univ-tlse3.fr; christelle.hureau@lcc-toulouse.fr

Present Address

† Institut de Chimie (UMR 7177), 4 rue B. Pascal, F-67000 Strasbourg, France.

Author Contributions

All authors have given approval to the final version of the manuscript.

Funding Sources

This work was supported by the French agency for research ANR (grant ANR-13-BSV5-0016) and by the ERC aLzINK – StG-638712.

Notes

Any additional relevant notes should be placed here.

ACKNOWLEDGMENTS

The authors acknowledge the European Synchrotron Radiation Facility for the provision of the beamtime and the BM30B (FAME) beamline staff for their support; Prof. E. Guillon, S. Sayen and A. Conte-Daban for their help in the recording of the XANES data; L. Debrauwer and E. Jamin for providing the Orbitrap mass spectrometer (MetaToul-AXIOM (INRA, UMR1331 Toxalim, Toulouse, France), MetaboHUB-ANR-11-INBS-0010); C. Bijani and L. Rechignat for ^{1}H NMR and EPR data recording respectively.

ABBREVIATIONS

AD, Alzheimer's Disease; Aβ, Amyloid-β peptide; CCA, Coumarin-3-carboxylic acid; EPR, Electron Paramagnetic Resonance; IBS, In-Between State; NMR, Nuclear Magnetic Resonance; ROS, Reactive Oxygen Species; RS, Resting State; XANES, X-Ray Absorption Near-Edge Structure; 7-OH-CCA, 7-hydroxycoumarin-3-carboxylic acid.

REFERENCES

(1) Butterfield, D. A.; Lauderback, C. M. *Free Radic Biol Med* **2002**, *32*, 1050.
(2) Butterfield, D. A.; Reed, T.; Newman, S. F.; Sultana, R. *Free Radic Biol Med* **2007**, *43*, 658.
(3) Markesbery, W. R. *Free Radic Biol Med* **1997**, *23*, 134.
(4) Yatin, S. M.; Varadarajan, S.; Link, C. D.; Butterfield, D. A. *Neurobiol. Aging* **1999**, *20*, 325.
(5) Zhao, Y.; Zhao, B. *Oxidative medicine and cellular longevity* **2013**, *2013*.
(6) Tönnies, E.; Trushina, E. *J. Alzheimer's Dis.* **2017**, 1.
(7) Kalinowski, D. S.; Stefani, C.; Toyokuni, S.; Ganz, T.; Anderson, G. J.; Subramaniam, N. V.; Trinder, D.; Olynyk, J. K.; Chua, A.; Jansson, P. J. *Biochim. Biophys. Acta, Mol Cell Res* **2016**, *1863*, 727.
(8) Ayton, S.; Lei, P.; Bush, A. I. *Free Radical Biol. Med.* **2013**, *62*, 76.
(9) Kozlowski, H.; Luczkowski, M.; Remelli, M.; Valensin, D. *Coord. Chem. Rev.* **2012**, *256*, 2129.
(10) Eskici, G.; Axelsen, P. H. *Biochemistry* **2012**, *51*, 6289.
(11) Li, K.; Reichmann, H. *J. Neural Transm.* **2016**, *123*, 389.
(12) Ayton, S.; Lei, P.; Bush, A. I. *Neurotherapeutics* **2015**, *12*, 109.
(13) Jellinger, K. A. *Int. Rev. Neurobiol.* **2013**, *110*, 1.
(14) Jomova, K.; Vondrakova, D.; Lawson, M.; Valko, M. *Mol. Cell. Biochem.* **2010**, *345*, 91.

(15) Lovell, M. A.; Robertson, J. D.; Teesdale, W. J.; Campbell, J. L.; Markesbery, W. R. *J Neurol Sci* **1998**, *158*, 47.
(16) Miller, L. M.; Wang, Q.; Telivala, T. P.; Smith, R. J.; Lanzirotti, A.; Miklossy, J. *J Struct Biol* **2006**, *155*, 30.
(17) Hureau, C.; Faller, P. *Biochimie* **2009**, *91*, 1212.
(18) Reybier, K.; Ayala, S.; Alies, B.; Rodrigues, J. V.; Bustos Rodriguez, S.; La Penna, G.; Collin, F.; Gomes, C. M.; Hureau, C.; Faller, P. *Angew. Chem. Int. Ed. Engl.* **2016**, *55*, 1085.
(19) Chassaing, S.; Collin, F.; Dorlet, P.; Gout, J.; Hureau, C.; Faller, P. *Curr. Top. Med. Chem.* **2012**, *12*, 2573.
(20) Smith, D. G.; Cappai, R.; Barnham, K. J. *Biochim. Biophys. Acta, Biomembr.* **2007**, *1768*, 1976.
(21) Hureau, C. *Coord. Chem. Rev.* **2012**, *256*, 2164.
(22) Hureau, C.; Dorlet, P. *Coord. Chem. Rev.* **2012**, *256*, 2175.
(23) Drew, S. C.; Barnham, K. J. *Acc. Chem. Res.* **2011**, *44*, 1146.
(24) Hureau, C.; Balland, V.; Coppel, Y.; Solari, P. L.; Fonda, E.; Faller, P. *J. Biol. Inorg. Chem.* **2009**, *14*, 995.
(25) Shearer, J.; Szalai, V. A. *J. Am. Chem. Soc.* **2008**, *130*, 17826.
(26) Balland, V.; Hureau, C.; Saveant, J.-M. *Proc. Natl. Acad. Sci. U. S. A.* **2010**, *107*, 17113.
(27) Faller, P.; Hureau, C.; La Penna, G. *Acc. Chem. Res.* **2014**, *47*, 2252.
(28) Cassagnes, L.-E.; Hervé, V.; Nepveu, F.; Hureau, C.; Faller, P.; Collin, F. *Angew. Chem. Int. Ed.* **2013**, *52*, 11110.
(29) La Penna, G.; Hureau, C.; Andreussi, O.; Faller, P. *J. Phys. Chem. B* **2013**, *117*, 16455.
(30) Mirats, A.; Alí-Torres, J.; Rodríguez-Santiago, L.; Sodupe, M.; La Penna, G. *Phys. Chem. Chem. Phys.* **2015**, *17*, 27270.
(31) Furlan, S.; Hureau, C.; Faller, P.; La Penna, G. *J. Phys. Chem. B* **2012**, *116*, 11899.
(32) Prosdocimi, T.; De Gioia, L.; Zampella, G.; Bertini, L. *J. Biol. Inorg. Chem.* **2016**, *21*, 197.
(33) Alies, B.; Eury, H.; Bijani, C.; Rechignat, L.; Faller, P.; Hureau, C. *Inorg. Chem.* **2011**, *50*, 11192.
(34) Karr, J. W.; Szalai, V. A. *J. Am. Chem. Soc.* **2007**, *129*, 3796.
(35) Eury, H.; Bijani, C.; Faller, P.; Hureau, C. *Angew. Chem. Int. Ed.* **2011**, *50*, 901.
(36) Alies, B.; Bijani, C.; Sayen, S.; Guillon, E.; Faller, P.; Hureau, C. *Inorg. Chem.* **2012**, *51*, 12988.
(37) Kowalik-Jankowska, T.; Ruta, M.; Wiśniewska, K.; Łankiewicz, L. *J. Inorg. Biochem.* **2003**, *95*, 270.
(38) Cheignon, C.; Faller, P.; Testemale, D.; Hureau, C.; Collin, F. *Metallomics* **2016**, *8*, 1081.
(39) Minicozzi, V.; Stellato, F.; Comai, M.; Serra, M. D.; Potrich, C.; Meyer-Klaucke, W.; Morante, S. *J. Biol. Chem.* **2008**, *283*, 10784.
(40) Syme, C. D.; Nadal, R. C.; Rigby, S. E. J.; Viles, J. H. *J. Biol. Chem.* **2004**, *279*, 18169.
(41) Kau, L. S.; Spira-Solomon, D. J.; Penner-Hahn, J. E.; Hodgson, K. O.; Solomon, E. I. *J. Am. Chem. Soc.* **1987**, *109*, 6433.
(42) Alies, B.; Badei, B.; Faller, P.; Hureau, C. *Chem. Eur. J.* **2012**, *18*, 1161.
(43) Alies, B.; Sasaki, I.; Proux, O.; Sayen, S.; Guillon, E.; Faller, P.; Hureau, C. *Chem. Commun.* **2013**, *49*, 1214.
(44) Cheignon, C.; Collin, F.; Faller, P.; Hureau, C. *Dalton Trans.* **2016**, *45*, 12627.
(45) Manevich, Y.; Held, K. D.; Biaglow, J. E. *Radiat. Res.* **1997**, *148*, 580.
(46) Alies, B.; Renaglia, E.; Rózga, M.; Bal, W.; Faller, P.; Hureau, C. *Anal. Chem.* **2013**, *85*, 1501.
(47) Young, T. R.; Kirchner, A.; Wedd, A. G.; Xiao, Z. *Metallomics* **2014**, *6*, 505.
(48) Conte-Daban, A.; Borghesani, V.; Sayen, S.; Guillon, E.; Journaux, Y.; Gontard, G.; Lisnard, L.; Hureau, C. *Anal. Chem.* **2017**, Accepted.
(49) Hureau, C.; Coppel, Y.; Dorlet, P.; Solari, P. L.; Sayen, S.; Guillon, E.; Sabater, L.; Faller, P. *Angew. Chem. Int. Ed.* **2009**, *48*, 9522.
(50) Dorlet, P.; Gambarelli, S.; Faller, P.; Hureau, C. *Angew. Chem. Int. Ed.* **2009**, *48*, 9273.
(51) Drew, S. C.; Masters, C. L.; Barnham, K. J. *J. Am. Chem. Soc.* **2009**, *131*, 8760.
(52) Pedersen, J. T.; Chen, S. W.; Borg, C. B.; Ness, S.; Bahl, J. M.; Heegard, N. H.; Dobson, C. M.; Hemmingsen, L.; Cremades, N.; Teilum, K. *J. Am. Chem. Soc.* **2016**.
(53) Atrián-Blasco, E.; Cerrada, E.; Conte-Daban, A.; Testemale, D.; Faller, P.; Laguna, M.; Hureau, C. *Metallomics* **2015**, *7*, 1229.
(54) Noël, S.; Perez, F.; Pedersen, J. T.; Alies, B.; Ladeira, S.; Sayen, S.; Guillon, E.; Gras, E.; Hureau, C. *J. Inorg. Biochem.* **2012**, *117*, 322.
(55) Jiang, D.; Li, X.; Liu, L.; Yagnik, G. B.; Zhou, F. *J. Phys. Chem. B* **2010**, *114*, 4896.
(56) Inoue, K.; Nakagawa, A.; Hino, T.; Oka, H. *Anal. Chem.* **2009**, *81*, 1819.
(57) Kowalik-Jankowska, T.; Ruta, M.; Wiśniewska, K.; Łankiewicz, L.; Dyba, M. *J. Inorg. Biochem.* **2004**, *98*, 940.
(58) Hewitt, N.; Rauk, A. *J. Phys. Chem. B* **2009**, *113*, 1202.
(59) Giacovazzi, R.; Ciofini, I.; Rao, L.; Amatore, C.; Adamo, C. *Phys. Chem. Chem. Phys.* **2014**, *16*, 10169.
(60) Que, L.; Tolman, W. B. *Nature* **2008**, *455*, 333.
(61) Solomon, E. I.; Heppner, D. E.; Johnston, E. M.; Ginsbach, J. W.; Cirera, J.; Qayyum, M.; Kieber-Emmons, M. T.; Kjaergaard, C. H.; Hadt, R. G.; Tian, L. *Chem. Rev.* **2014**, *114*, 3659.
(62) Strizhak, P. *Theor. Exp. Chem.* **1994**, *30*, 239.
(63) Burg, A.; Meyerstein, D. *Adv. Inorg. Chem.* **2012**, *64*, 219.
(64) Engelmann, X.; Monte-Pérez, I.; Ray, K. *Angew. Chem. Int. Ed.* **2016**.
(65) Parthasarathy, S.; Yoo, B.; McElheny, D.; Tay, W.; Ishii, Y. *J. Biol. Chem.* **2014**, *289*, 9998.
(66) Mayes, J.; Tinker-Mill, C.; Kolosov, O.; Zhang, H.; Tabner, B. J.; Allsop, D. *J. Biol. Chem.* **2014**, *289*, 12052.
(67) Valensin, D.; Dell'Acqua, S.; Kozlowski, H.; Casella, L. *J. Inorg. Biochem.* **2016**.
(68) Rodríguez, E. E.; Arcos-López, T.; Trujano-Ortiz, L. G.; Fernández, C. O.; González, F. J.; Vela, A.; Quintanar, L. *J. Biol. Inorg. Chem.* **2016**, *21*, 691.
(69) Miotto, M. C.; Rodriguez, E. E.; Valiente-Gabioud, A. A.; Torres-Monserrat, V.; Binolfi, A.; Quintanar, L.; Zweckstetter, M.; Griesinger, C.; Fernandez, C. O. *Inorg. Chem.* **2014**, *53*, 4350.
(70) Holtzman, D. M.; Morris, J. C.; Goate, A. M. *Sci. Transl. Med.* **2011**, *3*, 77sr1.
(71) Delgado, R.; Da Silva, J. F.; Amorim, M.; Cabral, M.; Chaves, S.; Costa, J. *Anal. Chim. Acta* **1991**, *245*, 271.
(72) Krężel, A.; Bal, W. *J. Inorg. Biochem.* **2004**, *98*, 161.

V.B. French summary

Lors de la production d'espèces réactives de l'oxygène (ROS) par le complexe Cu-Aβ, un état de coordination redox compétent et transitoire, appelé état « in-between » (IB) permet le transfert électronique menant à la production des ROS (décrit dans la Section I.C.2.c). Les géométries des modes de coordination des ions Cu(I) et Cu(II) avec le peptide Aβ étant très éloignées dans les états au repos, le passage par l'état IB est nécessaire pour que le cuivre cycle entre ses états d'oxydation +1 et +2 (Figure V.B-1). Cet état IB est caractérisé par des modes de coordination des ions Cu(I) et Cu(II) supposés plus proches voire similaires, permettant le transfert électronique avec une énergie de réarrangement entre les deux modes de coordination bien plus faible que dans le cas des états au repos. Cet état fugace étant très peu peuplé (de l'ordre de 0.1 % [1]), la caractérisation directe de son mode de coordination par les techniques spectroscopiques traditionnelles [2] n'est pas possible.

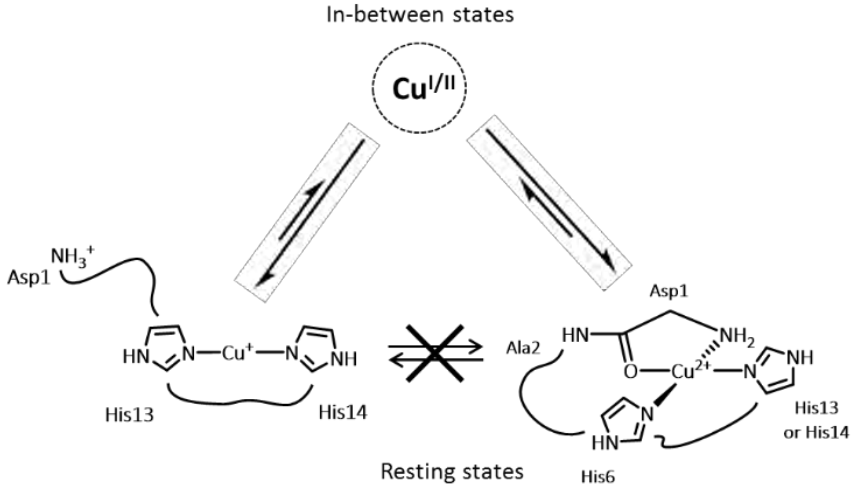

Figure V.B-1: Vue schématique de l'équilibre entre les états "resting" (au repos) et "in-between" du complexe Cu-Aβ pendant la production de ROS.

La détection des principales oxydations encourues par le peptide Aβ durant la production de ROS par spectrométrie de masse (MS) a mené à la proposition de 3 principaux ligands du cuivre dans l'état IB.[3] L'aspartate situé en première position, et les histidines situées en position 13 et 14, qui sont impliqués dans la coordination de Cu(I) ou/et de Cu(II) au repos (voir Section I.C.1), sont les principaux acides aminés retrouvés oxydés après la production de ROS. Il est donc proposé que ces 3 acides aminés sont également les ligands du cuivre dans l'état IB qui est responsable de la production de ROS. La Figure V.B-2 schématise les réarrangements entre les états au repos, appelés états « resting » et les états IB, ainsi que les

transferts électroniques entre Cu(II)-Aβ et l'ascorbate et entre Cu(I)-Aβ et le peroxyde d'hydrogène.

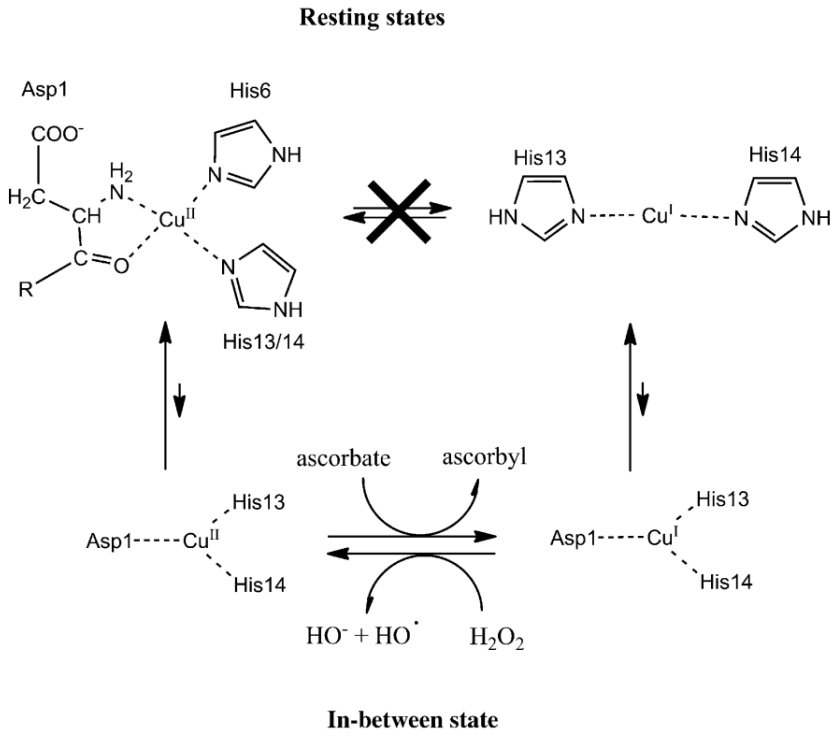

Figure V.B-2: Représentation schématique des modes de coordination de Cu(II)-Aβ et Cu(I)-Aβ au repos (resting states) et la proposition de mode de coordination de Cu(I/II)-Aβ dans l'état « in-between ». [3]

Comme le cuivre a un mode de coordination avec le peptide Aβ impliquant des acides aminés spécifiques, la mutation de ces derniers entraîne un changement du mode de coordination. Les modes de coordination de Cu(I) et Cu(II) dans les états au repos ont été étudiés avec de nombreux mutants de Aβ. Pour Cu(II), la non-disponibilité de l'amine terminale de l'Asp1 (*via* l'utilisation d'un peptide avec une acétylation de l'amine N-terminale) entraîne un profond changement de coordination.[4-5] Pour Cu(I), la présence d'une seule histidine dans la séquence (*via* la mutation de deux histidines par des alanines) a également un impact sur le mode de coordination.[6] De la même manière, la mutation d'un acide aminé impliqué dans la sphère de coordination du cuivre dans l'état IB devrait induire une variation dans la production des ROS, puisque c'est cet état qui est responsable du transfert électronique.

La production de ROS par le cuivre avec les différents peptides modifiés a été suivie par la fluorescence de l'acide 7-hydroxycoumarine-3-carboxylique (7-OH-CCA), produit par le piégeage des radicaux hydroxyles (HO•) par l'acide coumarine-3-carboxylique (CCA). Le

blocage de l'amine terminale ainsi que la mutation de l'Asp1 menant à un changement de la chaîne latérale contenant le groupe carboxylate de l'Asp1 ont fortement diminué la vitesse de production de HO•. Il a donc été déduit qu'à la fois l'amine terminale et l'oxygène du groupe carboxylate de l'Asp1 sont engagés dans la coordination du cuivre dans l'état IB. Il a également été montré que le nombre d'histidines présents dans la séquence peptidique a un impact sur la vitesse de production des radicaux hydroxyles. Moins il y a d'histidines, plus les HO• sont produits rapidement. De plus, cet effet est accru lorsque la séquence peptidique ne contient qu'une seule histidine.

Le mode de coordination du Cu(I) avec les peptides ne possédant qu'une histidine, a été étudié par RMN du proton. Il a été montré que Cu(I) est coordiné par l'amine N-terminale de l'Asp1, le cycle imidazole de l'His et un groupe carboxylate. Toutes ces informations ont permis la proposition d'un mode de coordination unique des ions Cu(I) et Cu(II) avec le peptide Aβ dans l'état « in-between », responsable de la formation de ROS. L'ion métallique serait lié à l'amine N-terminale et au groupe carboxylate de l'Asp1, ainsi qu'à une histidine (voir Figure V.B-3). La séquence de Aβ comprenant 3 histidines, celles-ci sont supposées être en échange dynamique, comme cela est le cas dans les états au repos.

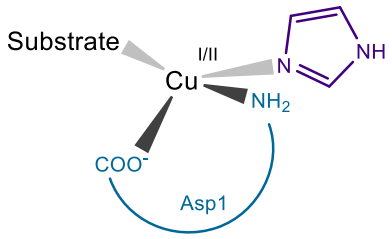

Figure V.B-3: Représentation schématique du mode de coordination proposé de Cu(I/II)-Aβ dans l'état « in-between » lors de la production de ROS en présence d'un substrat.

La modification de la chaine latérale de l'aspartate 1 et l'indisponibilité de l'amine N-terminale du peptide ont tous les deux menés à une forte diminution de la vitesse de production de HO•. De plus, une étude de la consommation d'ascorbate à plusieurs pH par les différents peptides modifiés en N-terminal a confirmé que les deux groupements de l'Asp1 sont bien impliqués dans la coordination du cuivre dans l'état transitoire qui conduit à la formation des ROS.

La forte augmentation de la vitesse de production des radicaux hydroxyles par le cuivre lié à un peptide n'ayant qu'une histidine (tel que $A\beta_7$) pouvait avoir deux origines : (i) la

modification du mode de coordination du cuivre dans l'état « in-between », ce qui voudrait dire que deux histidines sont impliquées dans la sphère de coordination ou (ii) le changement de coordination de Cu(I) ou/et Cu(II) dans leurs états au repos, se rapprochant du mode de coordination de l'état « in-between », augmentant la vitesse de réarrangement entre les états au repos et « in-between ». Comme il a été montré que Cu(I) est coordiné aux peptides contenant 1 His par l'Asp1, et qu'il en est de même dans l'état « in-between », la seconde hypothèse a été confirmée. Il a donc été proposé qu'une seule histidine participe à la coordination du cuivre dans l'état « in-between ». Pour les peptides contenant une seule His, les modes de coordination du Cu(I) au repos et pendant la production de ROS étant proches, l'état « in-between » est plus peuplé que dans le cas de Aβ, et donc la réaction menant à la formation de HO$^{\bullet}$ est plus rapide.

Ces résultats, informatifs sur le mode de coordination de Cu-Aβ produisant les ROS dans l'état « in-between », ont également conduit à proposer un mécanisme pour le transfert d'électron menant à la formation de ROS. Ce mécanisme est illustré dans la Figure V.B-4 avec la réduction du dioxygène mais peut également être appliqué à la réduction de l'anion superoxyde ou du peroxyde d'hydrogène.

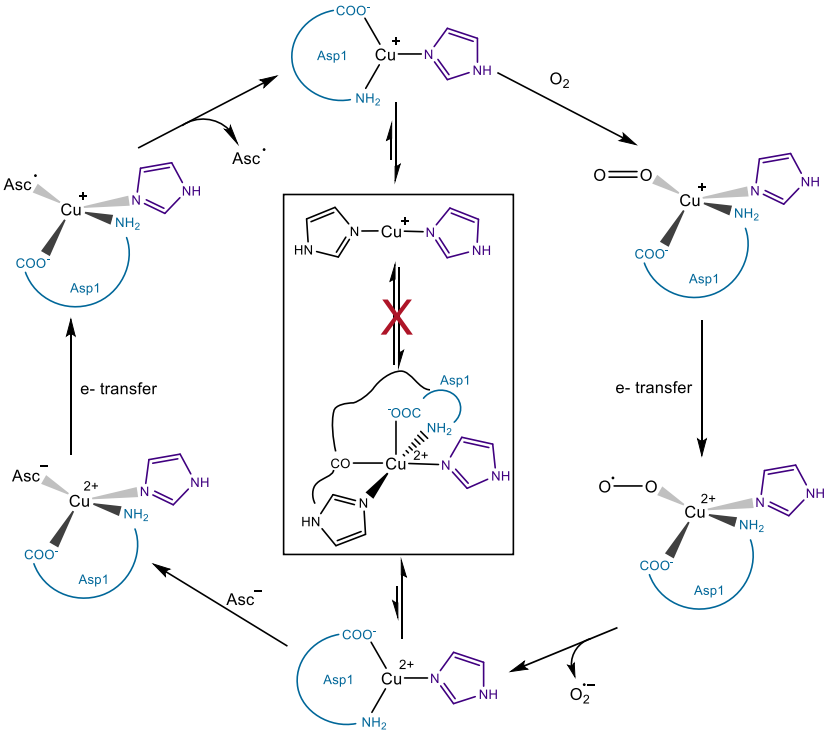

Figure V.B-4: Mécanisme proposé des transferts électroniques entre l'ascorbate et le complexe Cu(II)-Aβ et entre le peroxyde d'hydrogène et le complexe Cu(I)-Aβ, réalisés par le passage vers des modes de coordination du complexe Cu-Aβ transitoires appelés états « in-between ». L'amine terminale et le groupe carboxylate de l'Asp1 sont indiqués en bleu et le motif imidazole de l'His impliquée dans l'état IB est indiqué en violet.

V.C. Supporting Information

Identification of key structural features of the elusive Cu-Aβ complex involved in oxidative stress in Alzheimer's Disease

Clémence Cheignon, Megan Jones, Elena Atrián-Blasco, Isabelle Kieffer, Peter Faller, Fabrice Collin and Christelle Hureau

Supporting Information

Experimental section

EPR measurements

EPR spectra were recorded on a Bruker Elexsys E500 spectrometer equipped with a continuous flow cryostat (Oxford). Analysis was performed with aqueous solution containing 10% of glycerol, ^{65}Cu (450 µM) and peptide (500 µM, $A\beta_7$, H6A-H13A-$A\beta_{16}$, H6A-H14A-$A\beta_{16}$, D7H-$A\beta_{16}$, D1E-$A\beta_{16}$, D1N-$A\beta_{16}$ or $A\beta_{16}$). pH was adjusted with H_2SO_4 (1 M) and NaOH (1 M). Experimental parameters were set as following: T = 120 K, ν = 9.5 GHz, microwave power = 20.5 mW, Amplitude modulation = 5.0 G, Modulation frequency = 100 kHz.

Cu K-edge X-ray Absorption Data Collection and Measurement

The copper-containing Aβ solutions were injected into sample holders in between two windows made of Kapton tape (3M, cat. #1205; Minneapolis, MN) and quickly frozen in liquid nitrogen. All samples were maintained at 10-20 K throughout the data collection using a helium cryostat. Cu K-edge XANES (X-ray absorption near edge structure) spectra were recorded at the BM30B (FAME) beamline of the European Synchrotron Radiation Facility (ESRF, Grenoble, France)[1]. The storage ring was operating in 7/8+1 multibunch filling mode at 6 GeV with a ~ 200 mA current. The beam energy was selected using an Si(220) N_2 cryo-cooled double-crystal monochromator with an experimental resolution close to that theoretically predicted (namely ~ 0.5 eV)[2]. The beam spot on the sample was approximately 300 x 100 μm^2 (H x V, FWHM). The spectra are reported as fluorescence data, which were recorded utilizing a 30-element Ge solid-state fluorescence detector (Canberra). The energy was calibrated with a Cu metallic foil, such that the maximum of the first derivative was set at 8979 eV. Cu data were collected differently in 3 regions: from 8830 to 8960 eV using 5 eV steps and counting 2 s per point, from 8960 to 9020 eV using 0.5 eV steps and counting 3 s per point, and from 9020 to 9300 eV with a k-step of 0.05 $Å^{-1}$ and an increasing counting time of 2 to 10 s per point.

For each sample, three scans were averaged and XANES spectra were background-corrected by a linear regression through the pre-edge region and a polynomial through the post-edge region and normalized to the edge jump. This data treatment was carried out using the software Athena. The beam was moved to a different position on the sample for each scan to avoid potential Cu photoreduction. All spectra were individually inspected prior to data averaging to ensure that sample decomposition in the beam was not occurring.

Cu(I) samples were prepared by direct addition (10 equiv.) of fresh made $Na_2S_2O_4$ stock solution (0.1M) and Cu(I) 10 mM into the sample holder containing the peptide in the presence of 10% glycerol as cryoprotectant and under a continuous flow of N_2. The sample was immediately frozen in liquid nitrogen. In such conditions, no significant pH drift due to the addition of $Na_2S_2O_4$ was measured.

High-Resolution Mass spectrometry

High resolution mass spectrometry (HPLC/HRMS) analysis was performed on a LTQ-Orbitrap XL mass spectrometer (ThermoFisher Scientific, Les Ulis, France) equipped with an electrospray ionization source and coupled to an Ultimate 3000 LC System (Dionex, Voisins-le-Bretonneux, France). The Orbitrap cell was operated in the full-scan mode at a resolution power of 60 000. Sample (10 µL) was injected into the column (Phenomenex, Kinetex RP-C18, 50 × 3 mm, 2.6 µm), whose temperature was maintained at 25°C. Gradient elution was carried out with formic acid 0.1% (mobile phase A) and acetonitrile/water (80/20 v/v) formic acid 0.1% (mobile phase B) at a flow-rate of 500 µL min-1. The mobile phase gradient was programmed with the following time course: 5% mobile phase B at 0 min, held 3 minutes, linear increase to 45% B at 8 min then to 100% B at 9 min, held 2 min, linear decrease to 5% B at 12 min and held 3 min. The mass spectrometer was used as a detector, working in the full scan positive mode between 150 and 1200 Da. Trace chromatograms of Aβ and oxidized species were obtained in QualBrowser software (ThermoScientific), at 6 ppm mass accuracy.

^{1}H NMR spectroscopy

Studies were performed or D_2O. However, for clarity and consistency, we decided to use the notation pH even when the measurements were made in D_2O. The pD was measured using a classical glass electrode according to pD = pH* + 0.4, and the apparent pH value was adjusted according equation pH = (pD − 0.32)/1.044,[3] or equivalently according equation pH = 0.929pH* + 0.41,[4] to be in ionization conditions equivalent to those in H_2O.

Stock solutions of $A\beta_7$ and H6A-H13A were prepared by dissolving the powder in D_2O. H6A-H13A concentration was then determined by UV-visible absorption of tyrosine Tyr10 considered as free tyrosine (ε(276)-ε(296) = 1410 $M^{-1}cm^{-1}$) and $A\beta_7$ concentration was determined by UV-visible absorption of phenylalanine Phe4 considered as free phenylalanine (ε(258)-ε(280) = 195 $M^{-1}cm^{-1}$).

Cu(I) addition to $A\beta_7$ or H6A-H13A was carried out as follow: 1 equivalent of Cu(II) was added to a 0.5 mM solution of peptide in 0.2 M phosphate buffer in D_2O. The buffer pH was adjusted to 7.3 using NaOD and D_2SO_4. 2 equivalents per Cu ion of 0.1 M freshly prepared dithionite solution in D_2O were added under Ar atmosphere to the Cu(II)-Aβ solution in a NMR sealed tube.

The ^{1}H NMR experiments were recorded on a Bruker Avance 500 spectrometer equipped with a 5 mm triple resonance inverse Z-gradient probe (TBI 1H, 31P, BB). The presaturation of the water signal was achieved with a zqpr sequence (Bruker). ^{1}H NMR experiments are performed at 298K.

HO• scavenging monitoring: test of equivalents

The experiment was performed following the procedure of a coumarin-3-carboxylic acid (CCA) assay previously described. CCA was used as a probe to detect HO• as it reacts with CCA to form the 7-hydroxycoumarin-3-carboxylic acid (7-OH-CCA), which is fluorescent at 450 nm upon excitation at 390 nm. The intensity of the fluorescence signal is proportional to the number of 7-OH-CCA molecules formed, which in turn is proportional to the HO• radicals released. Phosphate buffer was used, after treatment with Chelex,

as HEPES buffer can react with HO radicals. The fluorescence experiments were performed on a microplate reader FLUOstar OPTIMA (BMG Labtech). An automatic injector was used to add ascorbate (500 µM) at cycle 5 into the wells containing phosphate buffered solutions (50 mM, pH 7.4) solutions with CCA (500 µM), Cu^{2+} (50 µM) and the different tested peptides and mutants ($A\beta_{16}$; $A\beta_{16}$ double mutants: H6AH13A, H6AH14A; $A\beta_7$) at peptide:Cu ratios of 1.2, 1.5 and 2. Each one of the conditions was repeated at least 3 times to minimize errors.

The gradient for each condition was calculated for the first 360 seconds after the injection of ascorbate, and the plateau from an average of the fluorescence emission during the last 210 seconds. All the gradient/plateau values for the double mutants and $A\beta_7$ were normalized to those obtained for $A\beta_{16}$ to check there is no a significant difference between using 1.2 or > 1.2 equivalents of peptide.

Cu(I) coordination investigated by XANES spectroscopy

The N-terminal modification, or the addition or removal of 1 His residue on the Aβ sequence does not impact the Cu(I) binding mode, as shown in Figures S1 and S2. The XANES signatures of the Cu(I) complexes with modified peptides are similar to the XANES signature of Cu(I)-Aβ. As Cu(I) binds to 2 His residues, these results were expected.

When the Aβ peptide has only 1 His residue left on its sequence, the Cu(I) binding mode differs from the one of Cu(I)-Aβ. Figure S3 shows that $A\beta_7$-Cu(I) and (H6A-H13A)-Cu(I) complexes have similar Cu XANES signatures that are different from Cu(I)-$A\beta_{16}$ and Cu(I) in buffer signatures. The decrease of intensity of the pre-edge peak around 8980 eV indicates an increase of the number of ligands compared with Cu(I)-$A\beta_{16}$ (2 His residues as ligands). This has been previously addressed for Cu(I)-$A\beta_7$.[5]

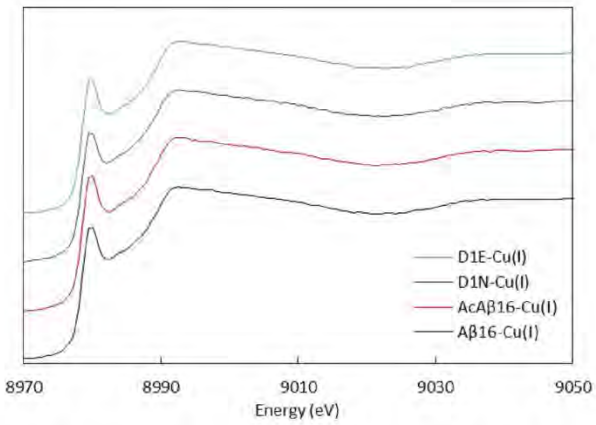

Figure S1: Cu XANES K-edge X-ray absorption spectra of $A\beta_{16}$-Cu(I) (black curve), $AcA\beta_{16}$-Cu(I) (red curve), D1N-Cu(I) (purple curve) and D1E-Cu(I) (blue curve) at pH 7.1.

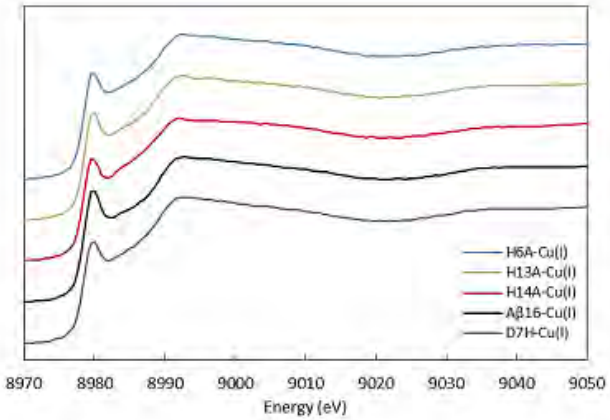

Figure S2: Cu XANES K-edge X-ray absorption spectra of $A\beta_{16}$-Cu(I) (black curve), H14A-Cu(I) (red curve), H13A-Cu(I) (green curve), D7H-Cu(I) (purple curve) and H6A-Cu(I) (blue curve) at pH 7.1.

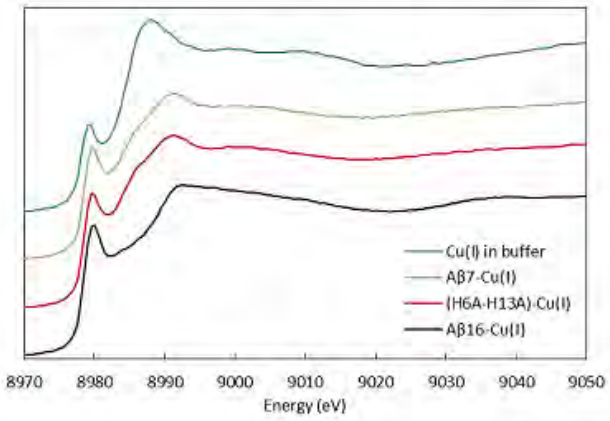

Figure S3: Cu XANES K-edge X-ray absorption spectra of $A\beta_{16}$-Cu(I) (black curve), (H6A-H13A)-Cu(I) (red curve), $A\beta_{7}$-Cu(I) (green curve) and Cu(I) in buffer (blue curve) at pH 7.1.

Cu(II) coordination investigated by EPR spectroscopy

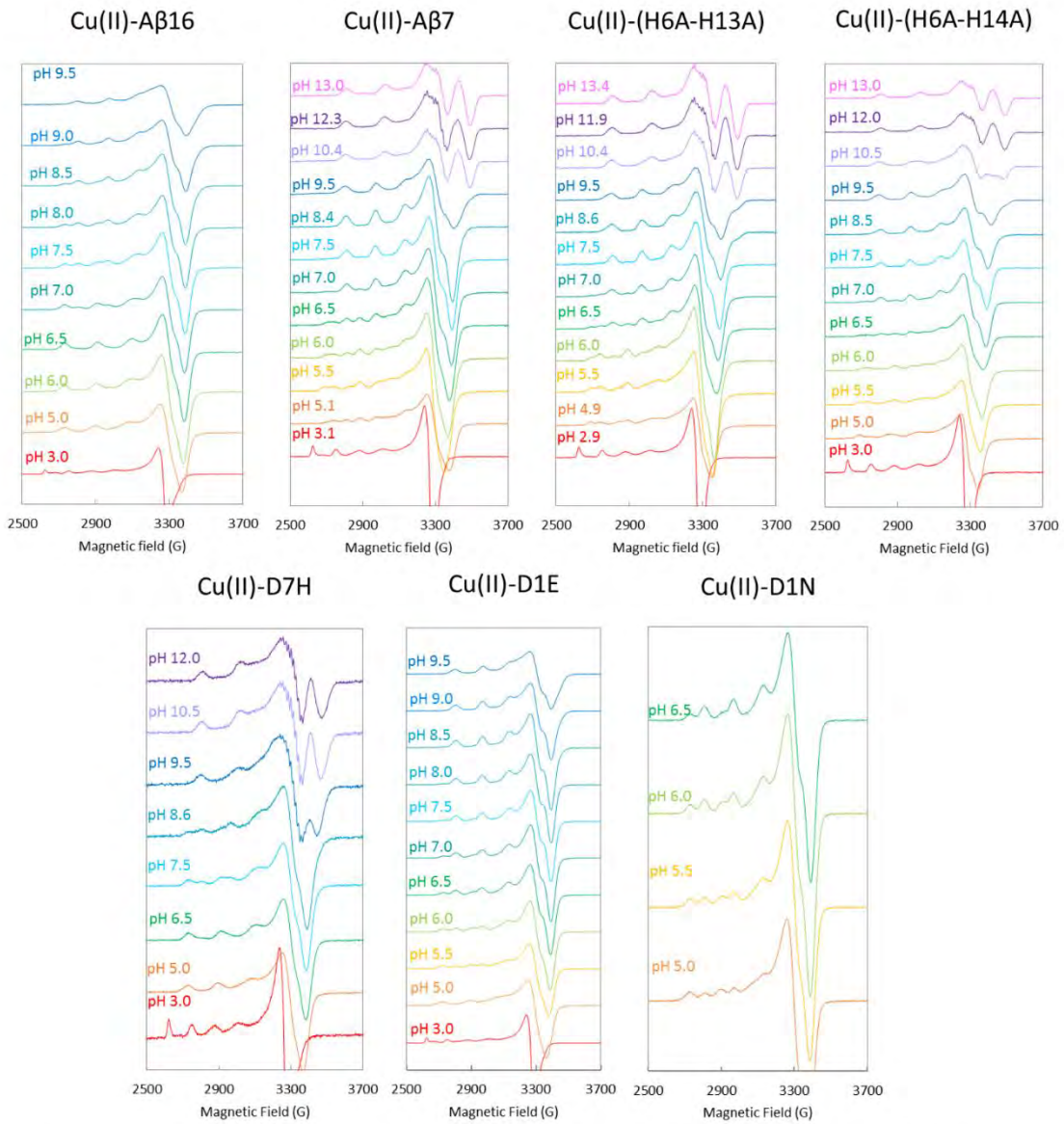

Figure S4 : EPR spectra of ^{65}Cu(II) coordinated to $A\beta_{16}$, $A\beta_7$, H6A-H13A, H6A-H14A, D7H, D1E or D1N at different pH. Aqueous solution of ^{65}Cu(II) (0.45 mM), peptide (0.5 mM) with 10 % of glycerol.

The EPR parameters shown in Table S1 have been calculated from the EPR spectra of Figure S4 for each ^{65}Cu(II)-peptide complex. The pKa(I/II) value and the $g_{//}$ and $\mathcal{A}_{//}$ values of components I et II of Cu(II)-$A\beta_{16}$ obtained are similar to the literature.[6] The same results are obtained with D7H, meaning that the addition of one His residue in the sequence does not have any consequence on the coordination mode of Cu(II).

For the $A\beta_7$, H6A-H13 and H6A-H14A peptides which have only one His residue, the Cu(II) ion is bound to them as a component II, as shown by the $g_{//}$ and $\mathcal{A}_{//}$ values close to the Cu-$A\beta_{16}$ component II. It was expected as only one His residue is involved in the coordination sphere of the component II.

EPR parameters obtained for D1N are also in line with the literature [7] and are very similar to those obtained with D1E. Thus, as well as D1N mutation, the mutation of Asp1 by a Glu residue only leads to a decrease of the pKa(I/II) value from 7.8 to 6.0.

Table S1: EPR parameters of components I and II of $^{65}Cu(II)$-peptides complexes along with the pKa values of components I and II and their equatorial binding mode.

Peptide	Component	$g_{//}$	$\mathcal{A}_{//}$ (10^{-4} cm^{-1})	pKa (I/II)	Equatorial binding mode
$A\beta_{16}$	I	2.27	181	7.8	NH_2 (D1), CO (D1-A2), N_{im} (H6), N_{im} (H13 or H14)
	II	2.23	158		NH_2 (D1), N^- (D1-A2), CO (A2-E3), N_{im}
$A\beta_7$	II	2.22	158	Major species from pH 6	NH_2 (D1), N^- (D1-A2), CO (A2-E3), N_{im}
H6A-H13A	II	2.22	162		
H6A-H14A	II	2.23	164		
D7H	I	2.27	181	7.8	NH_2 (D1), CO (D1-A2), N_{im} (H6), N_{im}
	II	2.24	151		NH_2 (D1), N^- (D1-A2), CO (A2-E3), N_{im}
D1E	I	2.28	184	6.0	NH_2 (E1), CO (E1-A2), N_{im} (H6), N_{im} (H13 or H14)
	II	2.23	163		NH_2 (E1), N- (E1-A2), CO (A2-E3), N_{im}
D1N	I	2.28	181	6.0	NH_2 (N1), CO (N1-A2), N_{im} (H6), N_{im} (H13 or H14)
	II	2.23	157		NH_2 (N1), N- (N1-A2), CO (A2-E3), N_{im}

Parallel spin Hamiltonian parameters ($g_{//}$ and $\mathcal{A}_{//}$) were obtained directly from the experimental spectra and were calculated from the second and the third hyperfine lines in order to remove second-order effects. $\mathcal{A}_{//}$ parameters are calculated for ^{63}Cu isotop for comparison with the litterature, by using the ratio $g_n(^{65}Cu)/\ g_n(^{63}Cu) = 1.07$ for comparison with the litterature. pKa values are estimated from EPR spectra with an uncertainty of ±0.3 pH unit.

^{1}H NMR of 1-His peptides with Cu(I)

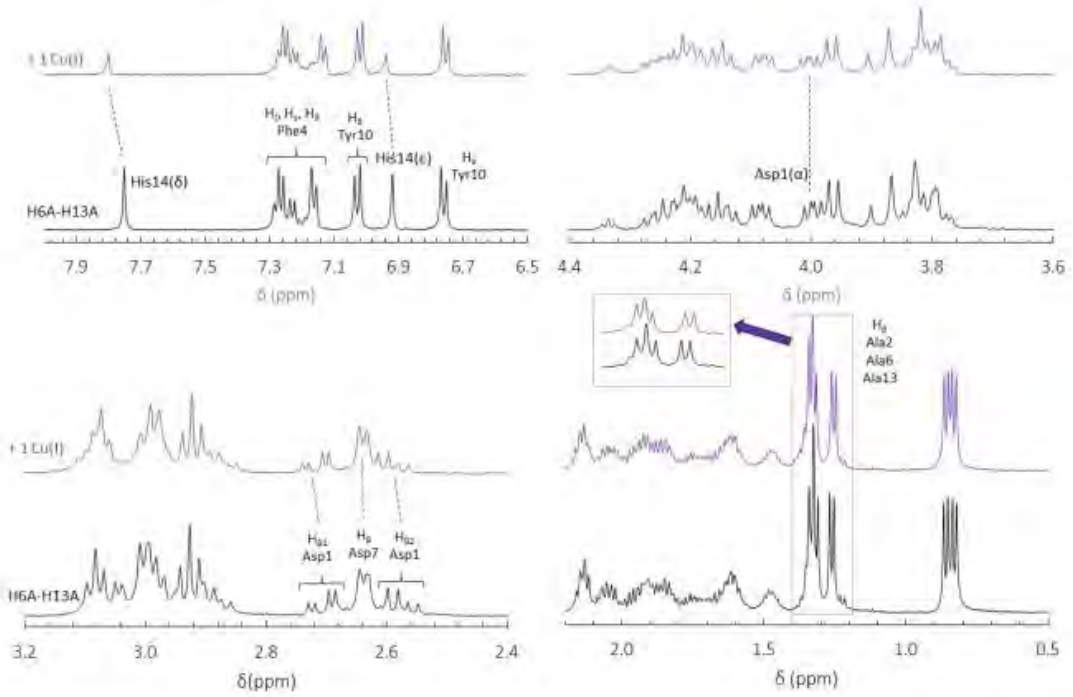

Figure S5: ^{1}H NMR spectra of H6A-H13A (black curve) and H6A-H13A with 1 equivalent of Cu(I) (purple curve) at pH 7.3. The chemical shifts of protons observed with the addition of Cu(I) are indicated with dotted lines. All chemical shifts were referenced at 0.00 ppm relative to internal TSP.

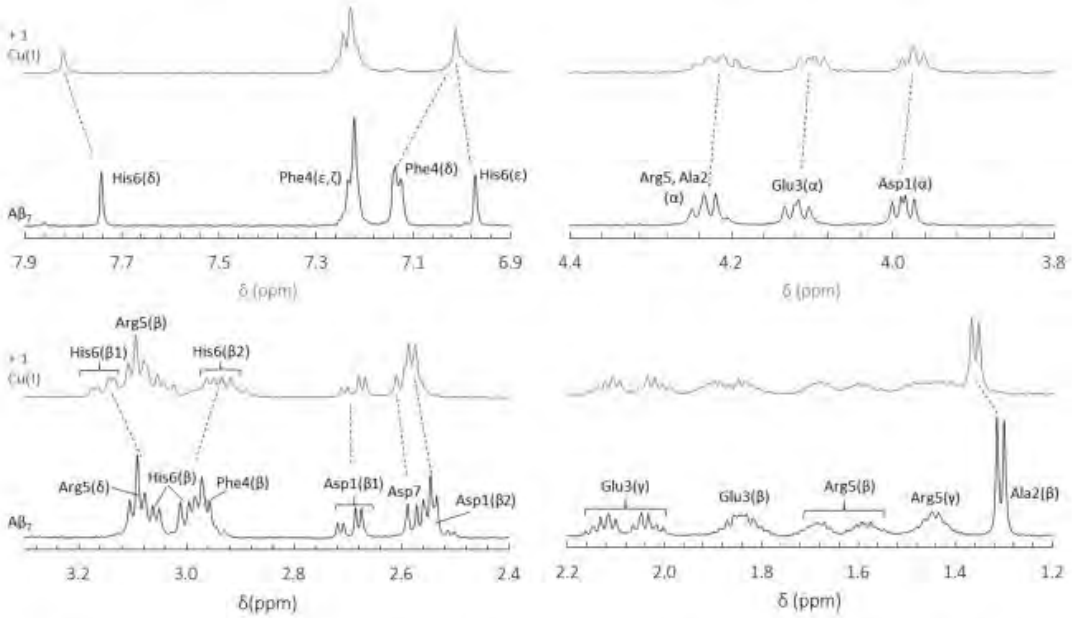

Figure S6: ^{1}H NMR spectra of Aβ$_7$ (black curve) and Aβ$_7$ with 1 equivalent of Cu(I) (purple curve) at pH 7.3. The chemical shifts of protons observed with the addition of Cu(I) are indicated with dotted lines. All chemical shifts were referenced at 0.00 ppm relative to internal TSP.

Aβ7: a special case

The Cu(I) metal ion binding with amino acid residues modifies the electron density of the protons, and results in a chemical shift of the protons close to the Cu(I). As an example, in Figure S6, the H_δ, H_ε and H_β protons of His6, present at about 7.75, 6.97 and 3.04 ppm, are strongly shifted. Thus, His6 residue of Aβ7 is involved in Cu(I) binding.

Both Hα (around 4.23 ppm) and H_β (around 1.30 ppm) protons of Ala2 are also strongly shifted with the addition of Cu(I). As the chemical shift of Ala protons is very sensitive to the chemical environment, and since Ala2 residue cannot bind metal ions, it is expected that an amino acid residue close to Ala2 is bound to Cu(I) ion. Except H_α of Glu3 which is shifted (around 4.12 ppm), the other protons are not really impacted by the addition of Cu(I). Thus, it is unlikely that Glu3 is a Cu(I) ligand, and neither Arg5 residue as its protons (at 1.44, 1.60, 1.68 and 3.10 ppm) are not shifted in the presence of Cu(I). For Asp1, H_α and $H_{\beta2}$ are also impacted by Cu(I) addition (3.98 and 2.56 ppm). Asp1 has a terminal amine group, Cu(I) is probably coordinated to the N-terminal NH_2 of Asp1. This is in line with the higher affinity of Cu(I) for nitrogen atom than for oxygen atom. However, the $H_{\beta1}$ peak (around 2.68 ppm) being not shifted, the carboxylate group of Asp1 seems to not be involved in the coordination sphere of Cu(I). These results are supported by the ^{1}H NMR spectra of Aβ16 in which the Asp1 and Ala2 protons are not shifted in the presence of Cu(I) (See Figure 4).

The carboxylate group of Asp7 in Aβ7 is also proposed to be involved in Cu(I) coordination. The two H_β protons, whose chemical shift is close to the one of Asp1 $H_{\beta2}$ proton (around 2.56 ppm), are also strongly shifted. For Phe4, although its H_ε and H_ζ protons keep the same chemical shift in the presence of Cu(I) (at 7.22 ppm), H_δ (7.13 ppm) and H_β (2.97 ppm) peaks shift and get wider with the addition of Cu(I). This was also observed with Aβ16 (Figure 4) and is probably linked to the reorganization of the peptide 3D structure due to the coordination of Aβ with the Cu(I).

^{1}H NMR experiments on Aβ7 with Cu(I) confirm the increase of the number of ligands for Cu(I) in the Aβ7 peptide that was previously shown by Cu(I) K-edge XANES.[5] The proposed ligands for Cu(I)-Aβ7 coordination are the terminal NH_2 of Asp1, a N atom of the imidazole ring of His6 and the carboxylate group of Asp7. Thus, unlike H6A-H13A and H6A-H14A, the closeness of His6 (a ligand of Cu(I)) with Asp7 leads to the coordination of the carboxylate group of Asp7 instead of the one of Asp1 in the case of Aβ7.

Metal-catalyzed ROS production by Cu ion with modified Aβ peptides

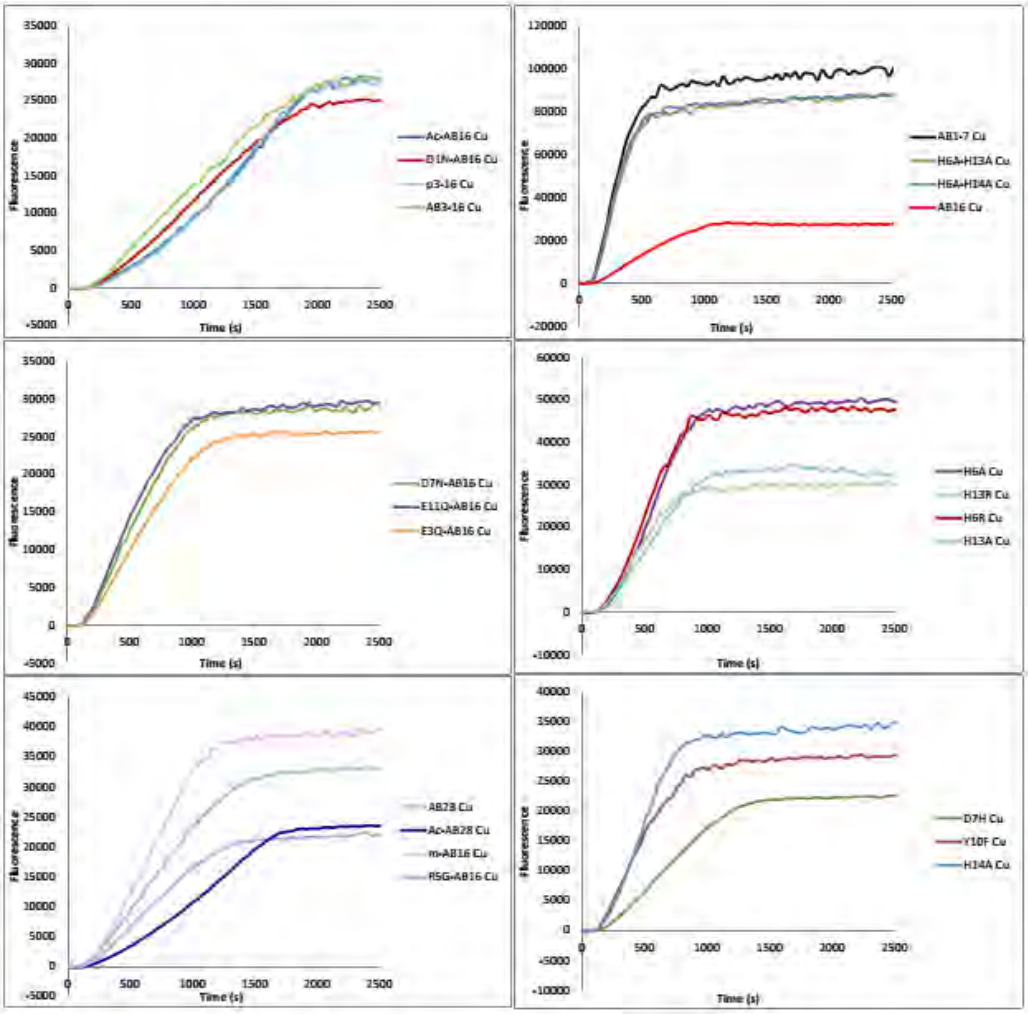

Figure S7: Fluorescence curves of ROS production. Fluorescence of the 7-OH-CCA (λ_{ex} = 395 nm, λ_{em} = 452 nm) as a function of the time, showing the scavenging kinetics of HO• produced by Cu^{2+} (50μM), ascorbate (500μM) and peptide (60μM) in phosphate-buffered solution (pH 7.4, 50 mM) with CCA (500 μM). The curves of the 22 peptides with copper are represented.

Gradient and fluorescence at the plateau values inform on the rate of 7-OH-CCA formation and on the quantity of 7-OH-CCA formed, respectively. However, they cannot be directly linked to the rate and quantity of HO• produced by the Cu-Aβ system. Indeed, the total amount of ROS produced by Cu-Aβ in the presence of ascorbate only depends on ascorbate and dioxygen concentrations, the process being catalytic.
Thus, the same ascorbate concentration should lead to the same total fluorescence at the plateau (after HO• has been trapped by CCA). But this is not the case, since for His-Ala single mutants and D7H, the value of fluorescence at the plateau is stronger and weaker than the one obtained for $Aβ_{16}$, respectively (Figure 7b, main text). As shown previously, Aβ is also a target for the hydroxyl radicals and the coordination of copper influences the HO• release.[8] The analysis of the trend obtained for the His mutants clearly shows that higher the number of His, lower the value at the plateau. This is confirmed by High-Resolution Mass Spectrometry (LC-HRMS) experiments showing that ratio of N-terminal oxidation vs. the other oxidations decreases when increasing the number of His in the peptide sequence (Figure S7, Tables S2 and S3). Thus, the total amount of HO• released by the Cu-Aβ system is dependent on the peptide nature (number of potential targets for HO• and spatial arrangement of the peptide when coordinated to the copper ion). This has also an influence on the gradient-values obtained in the fluorescence curves, meaning on the HO• exiting the system per time

unit. Thus, the relative gradient to plateau ratio was calculated in order to evaluate the intrinsic rate of HO• release (i.e. independent of the HO• by the peptide) (Figure 7c, main text).

Detection of oxidation on native and modified Aβ peptides after metal-catalyzed ROS production by High-Resolution Mass Spectrometry

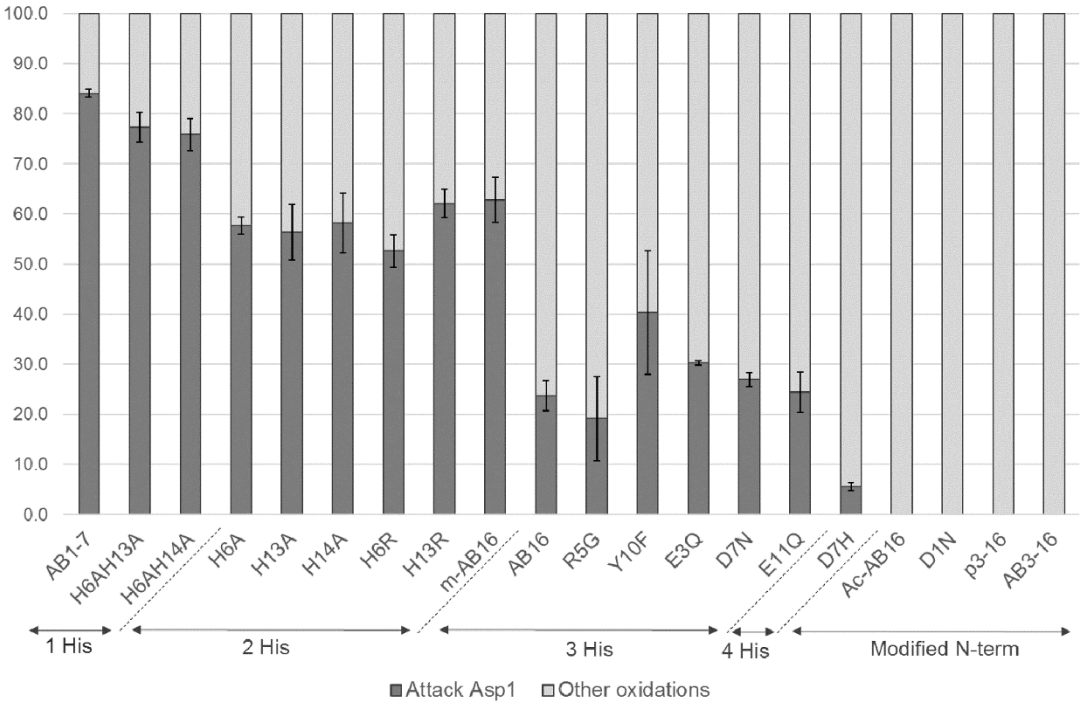

Figure S8: Relative proportions (in percent, + standard deviation) of the specific oxidations on Asp1 and the non-specific oxidations detected for the native and modified Aβ peptides under focus, after oxidation in the presence of copper and ascorbate. Operating conditions are similar as for fluorescence study. Specific oxidations on Asp1 are indicated in dark grey while the other oxidations are in light grey. The nature of the oxidations are listed in Table S2 and the different proportions of each oxidation are indicated in Table S3.

Table S2: abbreviation used for the oxidation products of Aβ, as previously identified.[8]

Specific of Asp1	**dd**	Decarboxylation/deamination of Asp1, leading to a mass loss of 45 Da
	ox	Oxidative fragmentation of Asp1, leading to a mass loss of 89 Da
Not specific	**+14**	Formal addition of one atomic oxygen, followed by a dehydrogenation
	+16	Formal addition of one atomic oxygen

Table S3: Relative proportions (in percent, + standard deviation) of the oxidation products detected for the native and modified Aβ peptides under focus, after oxidation in the presence of copper and ascorbate. Operating conditions are similar as for fluorescence study.

Peptide	Non ox		dd*		ox*		+16/+32		+14/+28	
AB1-7	4.1	*(2.4)*	15.7	*(1.2)*	64.9	*(1.8)*	10.8	*(0.4)*	4.5	*(0.6)*
H6AH13A	2.3	*(0.6)*	13.2	*(0.8)*	62.4	*(3.1)*	18.9	*(2.3)*	3.2	*(0.5)*
H6AH14A	0.9	*(0.3)*	12.0	*(0.8)*	63.2	*(3.3)*	20.7	*(2.7)*	3.3	*(0.5)*
H6A	0.5	*(0.1)*	11.3	*(1.5)*	46.1	*(2.9)*	27.8	*(2.1)*	14.4	*(0.7)*
H13A	4.7	*(4.2)*	18.0	*(1.8)*	35.9	*(8.9)*	28.5	*(5.3)*	12.8	*(1.9)*
H14A	1.9	*(1.7)*	14.7	*(2.7)*	42.5	*(9.4)*	27.4	*(6.5)*	13.5	*(1.5)*
H6R	0.4	*(0.4)*	15.2	*(4.4)*	37.2	*(2.3)*	35.9	*(2.3)*	11.3	*(5.3)*
H13R	3.5	*(2)*	15.6	*(3.1)*	44.3	*(2.7)*	26.1	*(2.3)*	10.5	*(5.3)*
m-AB16	11.3	*(3.3)*	16.4	*(8.2)*	39.4	*(3.7)*	24.6	*(3.4)*	8.3	*(0.8)*
AB16	2.9	*(3.4)*	3.5	*(2)*	19.5	*(3.8)*	44.8	*(4.4)*	29.2	*(7.9)*
R5G	23.4	*(14.7)*	1.7	*(1.1)*	14.0	*(8.2)*	48.3	*(1.3)*	12.6	*(5)*
Y10F	0.3	*(0.3)*	17.3	*(8.6)*	23.0	*(4)*	30.5	*(9)*	29.0	*(3.3)*
E3Q	5.5	*(3.2)*	5.1	*(0.6)*	23.5	*(1.2)*	46.4	*(3.5)*	19.5	*(2.6)*
D7N	4.9	*(3)*	4.7	*(1.2)*	20.9	*(0.8)*	50.9	*(2.4)*	18.6	*(1.8)*
E11Q	6.2	*(3.5)*	3.3	*(1.2)*	19.6	*(2.1)*	54.2	*(5.7)*	16.8	*(2.4)*
D7H	0.7	*(0.4)*	0.2	*(0.4)*	4.7	*(0.2)*	46.0	*(18)*	48.4	*(18.4)*
Ac-AB16	6.4	*(2.5)*	*nd*		*nd*		68.0	*(3.9)*	25.6	*(1.4)*
D1N	4.6	*(2.2)*	*nd*		*nd*		66.6	*(2.1)*	28.8	*(2.9)*
p3-16	2.2	*(2.1)*	*nd*		*nd*		66.6	*(2.5)*	31.2	*(3.5)*
AB3-16	0.4	*(0.3)*	*nd*		*nd*		57.2	*(5)*	42.4	*(5)*

nd = not detected

** includes [dd, dd+14 and dd+16] or [ox, ox+14 and ox+16], i.e. primary and secondary oxidation products (re-oxidation of a primary oxidized Aβ).*

HO• scavenging monitoring: test of equivalents

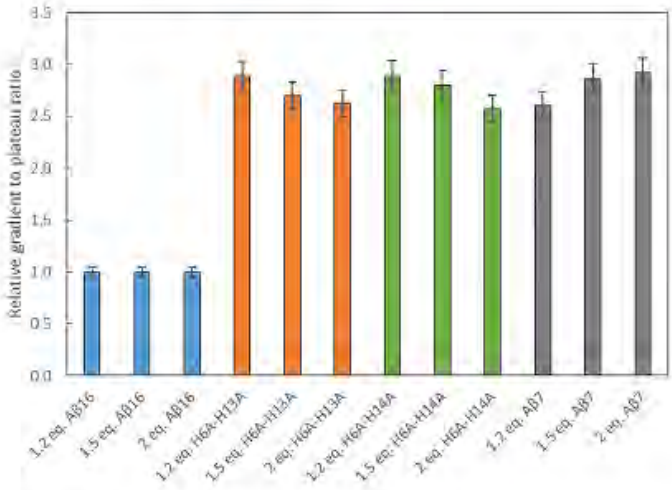

Figure S9: HO• scavenging by CCA. Gradient to plateau ratio of 7-OH-CCA fluorescence resulting from oxidation of CCA 500 µM in the presence of ascorbate 500 µM, Cu(II) 50 µM and native or modified Aβ peptides (1.2, 1.5 or 2 equivalents for 1 Cu). Phosphate-buffered (50 mM) solutions at pH 7.4.

For each peptide, similar relative HO• production rates are obtained with 1.2, 1.5 and 2 equivalents of peptide by Cu ion. The results show that the higher HO• production rate obtained with the 1-His peptides ($A\beta_7$, H6A-H13A and H6A-H14A) is not due to a contribution of free copper.

Ascorbate consumption by Cu ion with modified Aβ peptides at different pH.

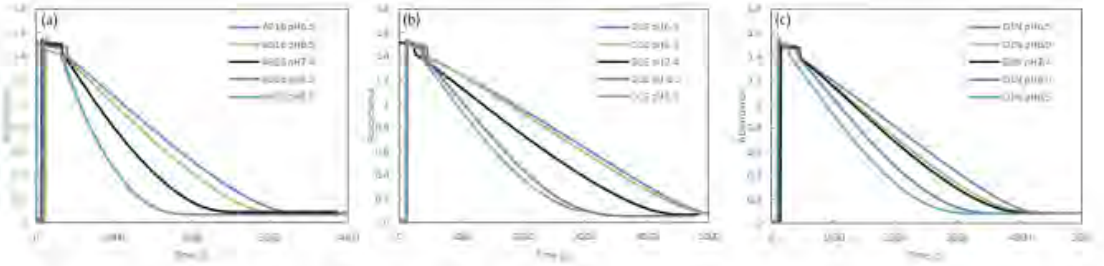

Figure S10: UV-Visible curves of ascorbate oxidation. Absorbance at 265 nm of ascorbate (100 µM) as a function of the time by Cu (10 µM) bound to $A\beta_{16}$ (a), D1E-Aβ16 (b) or D1N-Aβ16 (c) (20 µM) in HEPES buffered solution (pH 6.5, 7.0, or 7.4) or POPSO buffered solution (pH 8.0 or 8.5).

Determination of the pKa value of the NH_2(Asp1) of $A\beta_{16}$ in the presence of Cu(I) by ^1H NMR

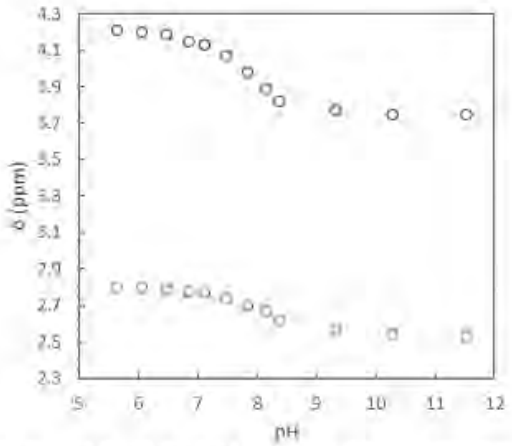

Figure S11: Chemical shifts of the H_α and $H_{\beta1}$ of the Asp1 residue of $A\beta_{16}$ as a function of pH, in the presence of Cu(I). **pKa value: 7.8.**

References

1. O. Proux, X. Biquard, E. Lahera, J. Menthonnex, A. Prat, O. Ulrich, Y. Soldo, P. Trévisson, G. Kapoujyan and G. Perroux, *Phys. Scr.*, 2005, **2005**, 970.
2. O. Proux, V. Nassif, A. Prat, O. Ulrich, E. Lahera, X. Biquard, J.-J. Menthonnex and J.-L. Hazemann, *Journal of synchrotron radiation*, 2006, **13**, 59-68.
3. R. Delgado, J. F. Da Silva, M. Amorim, M. Cabral, S. Chaves and J. Costa, *Anal. Chim. Acta*, 1991, **245**, 271-282.
4. A. Krężel and W. Bal, *J. Inorg. Biochem.*, 2004, **98**, 161-166.
5. C. Cheignon, P. Faller, D. Testemale, C. Hureau and F. Collin, *Metallomics*, 2016, **8**, 1081-1089.
6. C. Hureau, *Coord. Chem. Rev.*, 2012, **256**, 2164-2174.
7. B. Alies, H. Eury, C. Bijani, L. Rechignat, P. Faller and C. Hureau, *Inorg. Chem.*, 2011, **50**, 11192-11201.
8. L.-E. Cassagnes, V. Hervé, F. Nepveu, C. Hureau, P. Faller and F. Collin, *Angew. Chem. Int. Ed.*, 2013, **52**, 11110-11113.

References

[1] V. Balland, C. Hureau and J.-M. Saveant, *Proceedings of the National Academy of Sciences of the United States of America* **2010**, *107*, 17113-17118.

[2] P. Faller, C. Hureau, P. Dorlet, P. Hellwig, Y. Coppel, F. Collin and B. Alies, *Coordination Chemistry Reviews* **2012**, *256*, 2381-2396.

[3] L.-E. Cassagnes, V. Hervé, F. Nepveu, C. Hureau, P. Faller and F. Collin, *Angewandte Chemie International Edition* **2013**, *52*, 11110-11113.

[4] B. Alies, H. Eury, C. Bijani, L. Rechignat, P. Faller and C. Hureau, *Inorganic Chemistry* **2011**, *50*, 11192-11201.

[5] T. Kowalik-Jankowska, M. Ruta, K. Wiśniewska and L. Łankiewicz, *Journal of Inorganic Biochemistry* **2003**, *95*, 270-282.

[6] C. Cheignon, P. Faller, D. Testemale, C. Hureau and F. Collin, *Metallomics* **2016**, *8*, 1081-1089.

Chapter VI

Chapter VI: Pro versus antioxidant properties of Ascorbate

The chapter focuses on the study of the prooxidant and antioxidant properties of the ascorbate anion, in the context of Alzheimer's Disease (AD). The chapter is composed of a communication published in the journal *Dalton Transactions* in August 2016 [1] along with a summary of the article, written in French (requirement of the doctoral school). The supporting information related to the communication is situated at the end of the chapter (Section VI.C).

VI.A. Communication

Dalton Transactions

COMMUNICATION

View Article Online
View Journal | View Issue

Cite this: *Dalton Trans.*, 2016, **45**, 12627

Received 17th May 2016,
Accepted 23rd May 2016

DOI: 10.1039/c6dt01979j

www.rsc.org/dalton

Is ascorbate Dr Jekyll or Mr Hyde in the Cu(Aβ) mediated oxidative stress linked to Alzheimer's disease?†

Clémence Cheignon,[a,b,c] Fabrice Collin,[a,b,c] Peter Faller*‡[a,b] and Christelle Hureau*[a,b]

Evaluation of the pro *versus* antioxidant activity of ascorbate regarding Cu(Aβ) induced reactive oxygen species production in the context of Alzheimer's disease shows that a protective activity can only be observed at high ascorbate concentration for exogenous molecules but not for the amyloid-β peptide itself.

The misregulation of reactive oxygen species (ROS) leading to oxidative stress is observed in multiple diseases, including neurodegenerative disorders like Alzheimer's or Parkinson's disease. Therefore, there is strong interest in the effect of antioxidants as they could have potential therapeutic benefits.[1] There are different families of antioxidants depending on their mode of action (sacrificial or catalytic scavengers of ROS produced, inhibitors of ROS production). Sacrificial scavengers work by capturing ROS and other free radical species *via* reduction or addition reactions.[2] Ascorbate belongs to this family. It is a main physiological reducing agent present at a high concentration, in particular in the brain (up to 10 mM in neurons).[3] It can reduce radicals and convert them into non-radicals, like for instance $HO^{\bullet}$ to HO^{-}, or $O_2^{\bullet -}$ to H_2O_2. This is part of its antioxidant activity but transferring an electron to a non-radical species can also produce radicals. This happens when an electron is transferred to O_2 or H_2O_2, leading to $O_2^{\bullet -}$ or to the very reactive $HO^{\bullet}$ radical. However, these reactions are not efficient,[4] unless they are catalyzed. This can be performed by redox active metal ions like Cu(I/II) and Fe(II/III) which can catalyze very efficiently the transfer of a single electron. This is for instance the case in the well-known Fenton reaction leading to the formation of $HO^{\bullet}$ from dioxygen and a reducing agent like ascorbate. Actually, redox active metal ions, mainly Fe(II/III), Cu(I/II) and Mn(II/III) play a crucial role *in vivo* that essentially depends on their coordination chemistry. This is illustrated by the role of Cu ions that can be catalytic scavengers of $O_2^{\bullet -}$ when bound inside superoxide dismutase (SOD) or are involved in the catalytic production of ROS when loosely bound (Scheme 1).[4]

In the case of the reaction of loosely bound Cu ions with ascorbate and dioxygen, it is known that the concentration of ascorbate has an important impact on the production of $HO^{\bullet}$. In general, it was concluded that low concentrations of ascorbate are required for prooxidant conditions, while high concentrations are needed for antioxidant conditions.[5] Thus there is a "cross-over" point, *i.e.* an ascorbate concentration at which the prooxidant ability of ascorbate is maximal. Such a value depends on the experimental conditions.[5] This has been supported by experiments in different systems *in vitro* and *in cellulo*.[6] *In vivo*, the prooxidant activity of ascorbate seems to be limited to conditions where Fe and Cu are aberrantly coordinated and hence able to catalyze the Fenton type reaction.[7]

In Alzheimer's disease (AD), Cu ions are found in high concentrations (0.4 mM) in amyloid plaques, a hallmark of the disease.[8] Cu is bound to the amyloid-β (Aβ) peptide in the extracellular plaques themselves but its coordination to the monomeric soluble form of Aβ is also proposed,[9] as the Cu

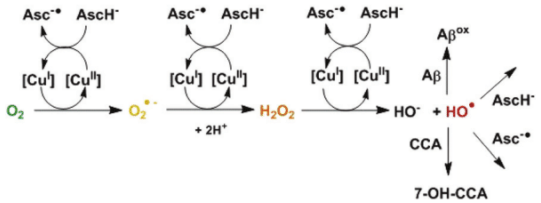

Scheme 1 Mechanism of $HO^{\bullet}$ production from ascorbate and dioxygen catalyzed by copper. $HO^{\bullet}$ can then react with different compounds, with CCA to form the fluorescent 7-OH-CCA, or with ascorbate/ascorbyl or with Aβ in the case of Cu bound to Aβ. [Cu] corresponds to free or Aβ-bound Cu.

[a]*LCC (Laboratoire de Chimie de Coordination), CNRS UPR 8241, 205 route de Narbonne, 31062 Toulouse Cedex 09, France.*
E-mail: christelle.hureau@lcc-toulouse.fr
[b]*Université de Toulouse; UPS, INPT, 31077 Toulouse, France*
[c]*UMR 152 Pharma Dev, Université de Toulouse, IRD, UPS, France*

† Electronic supplementary information (ESI) available: Materials and methods, conditions for $HO^{\bullet}$ detection using CCA, and LC-MS quantification of the oxidized peptide. See DOI: 10.1039/c6dt01979j

‡ Current address: Institut de Chimie (UMR 7177), 4 rue B. Pascal, F-67000 Strasbourg, France. E-mail: pfaller@unistra.fr

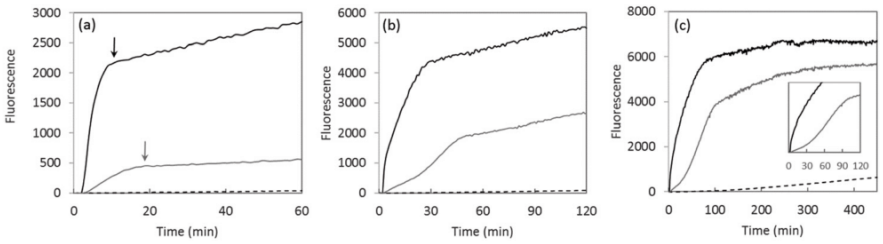

Fig. 1 Time dependence of HO• production measured by 7-OH-CCA fluorescence assay ($\lambda_{excitation}$ = 390 nm and $\lambda_{emission}$ = 450 nm) for Cu (black curves), $A\beta_{16}$ (dotted curves) and Cu-$A\beta_{16}$ (grey curves) with ascorbate ((a) 0.5 mM, (b) 1 mM and (c) 5 mM). Phosphate-buffered solution (50 mM, pH 7.4) of CCA (0.5 mM), Cu (50 μM), either $A\beta_{16}$ (60 μM) or no peptide. Experiments with only ascorbate give similar curves to $A\beta_{16}$ with ascorbate (dotted curves). Arrows indicate the completion of ascorbate consumption as measured independently (Fig. S7†).

concentration can reach up to 10 μM in certain synaptic clefts.[10,11] The coordination sites of Cu(II) and Cu(I) lie in the first 16 amino acids of the 40 to 42 amino-acid residue peptide. They have been extensively studied and are well characterized (Fig. S1 and S2†), in relation to their redox ability.[9] *In vitro*, Cu(Aβ) is able to catalyze the production of ROS in the presence of ascorbate, and it was proposed that these ROS can contribute to the oxidative stress observed in AD.[12,13]

In the present work, we have investigated the impact of Cu coordination to the Aβ peptide on modulation of the pro *versus* antioxidant properties of ascorbate. This is of interest with regard to therapeutic approaches in AD based on oxidative stress regulation. Coumarin-3-carboxylate (CCA) was used as a prototypical target mimicking the biological ones, to detect the deleterious radical HO•. CCA reacts with HO• and forms the fluorescent adduct 7-hydroxycoumarin-3-carboxylate (7-OH-CCA), which shows emission at 450 nm upon excitation at 390 nm. While the detection of HO• by CCA was reported to be sensitive and specific,[14] there are some parameters to be considered in order to have a quantitative detection (at a particular pH, see the ESI for details: Fig. S3–S6†).

In Fig. 1, black lines show the time dependence of Cu-induced formation of 7-OH-CCA in line with similar literature data.[15–18] Two main phases were observed: (i) a first fast process with an exponential growth profile and (ii) a second slow process with an almost linear increase. The origin of the latter one is not known, but it seems to be independent of the Cu-catalyzed HO• production from ascorbate and O_2 and thus irrelevant for the present study. Indeed, completion of the first process almost coincides with total ascorbate consumption (Fig. S7†) and thus there is not much ascorbate available when the second process occurs. Note that unless specified all the experiments described in the paper were performed with the C-terminally truncated peptide encompassing the first 16 amino-acid residues that correctly reproduce the binding properties of the full-length peptide.[9]

In the presence of 1.2 equivalents of $A\beta_{16}$, the curves are different (Fig. 1, grey curves). The first phase takes more time, indicating that the formation of 7-OH-CCA is slower, in line with the lower catalytic activity of Cu($A\beta_{16}$) with respect to ROS formation, described already in the past.[15–17] Also the plateau reached during the second phase is lower compared to the one obtained in the presence of Cu only. This is in line with the observation that HO• reacts with the peptide Aβ itself thus precluding its reaction with CCA as previously observed.[18–21] Indeed, the plateau corresponds to the part of HO• able to react with CCA, *i.e.* it reflects the part of HO• that would be able to damage biomolecules other than Aβ or ascorbate, like proteins, lipids or nucleic acids in a biological environment. In line with this comment, it is worth noting that the higher the ascorbate over the $A\beta_{16}$ ratio, the closer the plateau obtained for free Cu and Cu(Aβ) species. At a high concentration of ascorbate, the first phase is more complex in the presence of a peptide with a sigmoid-like trend in line with (i) the oxidation of the $A\beta_{16}$ peptide and (ii) the subsequent release of free Cu (inset in Fig. 1). This was verified by measuring the level of intact peptide by LC-MS (Fig. S8 and Table S1†).§ Indeed the peptide was degraded at the end of the reaction. The degradation degree depends on the ascorbate concentration, but is complete above 1 mM (Fig. S9†).

In order to determine the pro *versus* antioxidant regime of ascorbate with both free Cu and Cu($A\beta_{16}$), the ascorbate dependence of the 7-OH-CCA formation was measured and compared. Fig. 2¶ shows the initial rate (calculated over the first five minutes) of the 7-OH-CCA formation at different ascorbate concentrations for Cu and Cu($A\beta_{16}$). The initial rate can be

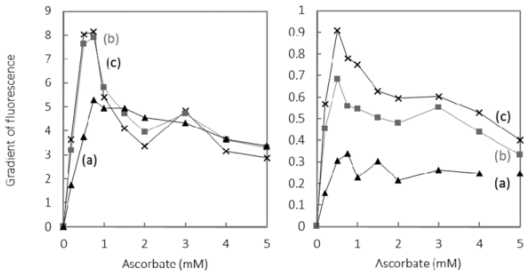

Fig. 2 Initial kinetics of 7-OH-CCA fluorescence at 450 nm, reflecting the scavenging of HO• by CCA. Phosphate-buffered solution (50 mM, pH 7.4) of CCA (0.5 mM) with Cu (left panel, (a) 10 μM, (b) 50 μM, (c) 100 μM), or Cu-$A\beta_{16}$ (right panel, (a) 10–12 μM, (b) 50–60 μM, (c) 100–120 μM) and ascorbate (concentration between 0 and 5 mM).

considered as the most relevant reaction under steady state conditions of ascorbate and oxygen supposed to occur *in vivo*.

For free Cu, the shapes are similar for the three different Cu concentrations used and all show a very marked ascorbate concentration dependence. At low ascorbate concentration the initial rate of 7-OH-CCA formation increases with the ascorbate concentration. The maximal rate, which has previously been called the cross-over point,[5] is observed around 0.7 mM in ascorbate. At higher ascorbate concentrations the initial rate of 7-OH-CCA formation decreases continuously, supporting an antioxidant property from 0.7 mM. This dependence can be explained due to the double effect of ascorbate: on one side, it promotes the production of HO$^\bullet$ that further reacts with CCA (pro-oxidant part, Scheme 1) and on the other hand it scavenges HO$^\bullet$ (antioxidant part).[5] In the absence of ascorbate, no HO$^\bullet$ is produced, as ascorbate is needed as an electron source to reduce dioxygen to HO$^\bullet$. At low concentration, HO$^\bullet$ trapped by CCA increases with ascorbate concentrations, because ascorbate fuels the formation of HO$^\bullet$, and does not scavenge HO$^\bullet$ efficiently. At higher ascorbate concentrations, the initial rate does not increase anymore, because the ascorbate is no more the limiting species and the scavenging ability becomes more and more efficient. For these reasons, the initial rate of 7-OH-CCA formation decreases.

In the presence of Aβ_{16}, *i.e.* when HO$^\bullet$ production is catalyzed by Cu(Aβ_{16}), the overall dependence is similar, with a cross-over point at 0.7 mM of ascorbate (Fig. 2, right panel). In general, the initial Cu(Aβ_{16}) induced formation of 7-OH-CCA formation is slower than without a peptide, in line with the more sluggish Cu(I/II) redox process of Cu when bound to Aβ.[22–24] Note that only the very first points of the 7-OH-CCA formation curves were taken into account to avoid any issue due to the release of Cu at high ascorbate concentrations (inset in Fig. 1). The rate of 7-OH-CCA formation is dependent on the Cu(Aβ_{16}) concentration. This is in line with the slower rate of HO$^\bullet$ formation in the presence of Aβ_{16}. The same trends were observed for the longer peptide encompassing the first 28 amino-acid residues and the full-length peptide (Fig. S10†).

Finally, the total amounts of 7-OH-CCA produced were measured. For doing this, the reaction was stopped after the total consumption of ascorbate (arrows in Fig. 1), and the intensities of the plateau were compared (Fig. 3) as a function of the initial ascorbate concentration and the Cu (resp. Cu(Aβ)) concentration.

For free Cu, the ascorbate concentration dependence follows a sort of saturation curve. Again this can be explained by the two properties of ascorbate that fuels the HO$^\bullet$ production and scavenges them. At low concentration the formation of 7-OH-CCA increases steadily, as under this condition the former property prevails. At increasing concentrations the scavenging ability progressively counter-balances the formation of HO$^\bullet$ and the highest ascorbate concentrations have no more effect on 7-OH-CCA formation. Note that a plateau is reached (and not the same shape curve as previously) because cumulative amounts of 7-OH-CCA (and not amounts of 7-OH-CCA at a given time) are measured in this case.

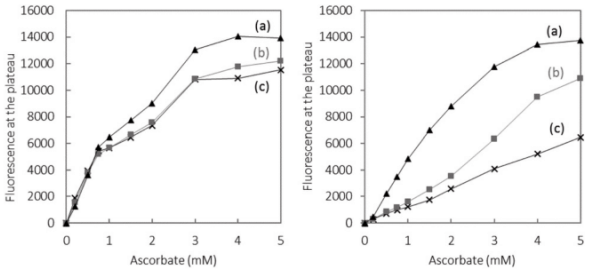

Fig. 3 Metal-catalyzed oxidation of CCA by HO$^\bullet$. Phosphate-buffered solution (50 mM, pH 7.4) of CCA (0.5 mM) with Cu (left panel, (a) 10 μM, (b) 50 μM, (c) 100 μM), or Cu-Aβ_{16} (right panel, (a) 10–12 μM, (b) 50–60 μM, (c) 100–120 μM) and ascorbate (concentration between 0 and 5 mM). At the end of the ascorbate oxidation, POPSO buffer (pH 9.0, 0.4 M) is added to adjust the pH at 8.5. The fluorescence of 7-OH-CCA ($\lambda_{excitation}$ = 390 nm and $\lambda_{emission}$ = 450 nm) is then measured.

In the presence of Aβ a similar shape is obtained, but with much lower intensities. This is assigned to the scavenging ability of Aβ itself, which increases with the Cu(Aβ) concentration.

To probe the ability of ascorbate to protect the Aβ peptide, we have compared the degradation of the peptide after the same amount of HO$^\bullet$ was produced, but at different initial ascorbate concentrations, *i.e.* (i) at the end of the reaction with 1 mM ascorbate and (ii) after consumption of 1 mM ascorbate with the initial concentration of ascorbate at 10 mM (Fig. S11†). This should yield the same amount of HO$^\bullet$ produced, but in the second sample much more ascorbate was present to exert the antioxidant effect. Even under this condition, no rescue in Aβ degradation was observed (Table S2†). This indicated that although ascorbate can scavenge HO$^\bullet$ before it reacts with CCA, it is much less efficient in intercepting HO$^\bullet$ when reacting with the Aβ peptide itself. This could be explained by the fact that Aβ is linked to Cu ions and hence HO$^\bullet$ are produced in the vicinity of the peptide. In contrast, CCA is not bound to the metal centre and has to encounter HO$^\bullet$ by diffusion.

In the present communication, we have reported that ascorbate can have a pro- or an antioxidant effect concerning the initial rates of HO$^\bullet$ attack on biological targets, here modelled by the CCA compound. The approach proposed here in the AD context with Cu(Aβ) species as the ROS production catalyst, could apply to any other chemical system able to form ROS. This includes other Cu-amyloidogenic peptide species, as encountered in Parkinson's disease, prion diseases, *etc.*[25] In the present case, the "cross-over" point, *i.e.* the ascorbate concentration at which the rate of HO$^\bullet$ formation is maximal, was observed at about 0.7 mM for a range of 10–100 μM Cu(Aβ). This means that below this concentration, ascorbate fuels the formation of HO$^\bullet$ that mainly reacts with CCA and the Aβ peptide. At higher concentrations, HO$^\bullet$ scavenging by ascorbate becomes more efficient and hence the rate of CCA oxidation slows down. Measuring the initial rate might be the most relevant condition in a more biological environment, as systems tend to maintain a steady state in terms of ascorbate

and dioxygen concentrations. Under such conditions, the "cross-over" point corresponds to the maximal rate of HO$^{\bullet}$ escaping from Cu(Aβ), and hence to maximal damage to biomolecules (proteins, DNA, lipids *etc*.) other than Aβ. At lower or higher ascorbate concentrations, less biomolecule damage would occur but for different reasons (weaker ROS production or higher scavenging activity, respectively). The situation for the Aβ peptide is different. Aβ scavenges the HO$^{\bullet}$ due to its proximity with the place of ROS production and is oxidized regardless of ascorbate concentrations. Even very high ascorbate concentrations were not able to protect Aβ from oxidation, which is likely due to the proximity of the peptide residues to the HO$^{\bullet}$ production site thus making it difficult for ascorbate to intercept the HO$^{\bullet}$. However, our *in vitro* studies could mainly be relevant for the surroundings of Cu(Aβ) complexes and the general situation *in vivo* under AD conditions could be more complex and the local prooxidant activity of ascorbate could be counteracted.[7]

Sacrificial antioxidants have been investigated as therapeutic compounds in several neurodegenerative diseases including AD.[19,26] In contrast to ascorbate, such compounds are mainly HO$^{\bullet}$ scavengers but can hardly induce the formation of ROS. In this context, our data indicate that ascorbate could be a "Dr Jekyll and Mr Hyde"[27] partner: (i) because ascorbate concentrations in the extracellular fluid in the brain are estimated to be 200–400 μM, the prooxidant regime is possible; (ii) in contrast, ascorbate concentrations in neurons are much higher (10 mM) leading to the antioxidant regime.[3] However, even at much higher ascorbate concentration the antioxidant effect is incomplete as CCA can still trap HO$^{\bullet}$. This raises the question whether it is possible to reach high enough ascorbate or other sacrificial anti-oxidant[1] concentration *in vivo*, so that they could completely scavenge HO$^{\bullet}$ produced by Cu(Aβ). Using compounds that can redox silence the Cu bound to Aβ (and hence stop ROS production in general) might be a more efficient strategy. Cu chelating agents that can bind and/or remove Cu ions from Aβ and redox silence them are among such compounds.[28–31] Another possibility would be to use catalytic ROS scavengers, such as SOD mimics.[32,33]

While high ascorbate concentrations could have an antioxidant effect for other biomolecules, they cannot prevent Aβ from oxidative damage. Whether this would be a beneficial or detrimental process depends on the toxicity of the oxidized Aβ, which is not clear yet.

The authors acknowledge L. Debrauwer and E. Jamin for providing the Orbitrap mass spectrometer (MetaToul-AXIOM, INRA, UMR1331 Toxalim, Toulouse, France). F.C. and P. F. thank the ANR – ANR-13-BSV5-0016; C.H. thanks the ERC aLzINK – contract no. 638712 for financial support.

Notes and references

§ For technical reasons, the Aβ28 peptide encompassing the first 28 amino-acid residues has been used in mass spectrometry experiments (see the ESI† for details).

¶ Note that data shown in Fig. 2 and 3 are representative from a series of measurements performed under slightly different conditions, but for which the very same trends were observed.

1 F. Di Domenico, E. Barone, M. Perluigi and D. A. Butterfield, *Expert Rev. Neurother.*, 2015, **15**, 19.
2 H. Sies, *Eur. J. Biochem.*, 1993, **215**, 213.
3 M. E. Rice, *Trends Neurosci.*, 2000, **23**, 209.
4 B. Halliwell, *J. Neurochem.*, 2006, **97**, 1634.
5 G. R. Buettner and B. A. Jurkiewicz, *Radiat. Res.*, 1996, **145**, 532.
6 I. D. Podmore, H. R. Griffiths, K. E. Herbert, N. Mistry, P. Mistry and J. Lunec, *Nature*, 1998, **392**, 559.
7 A. Carr and B. Frei, *FASEB J.*, 1999, **13**, 1007.
8 L. M. Miller, Q. Wang, T. P. Telivala, R. J. Smith, A. Lanzirotti and J. Miklossy, *J. Struct. Biol.*, 2006, **155**, 30.
9 C. Hureau, *Coord. Chem. Rev.*, 2012, **256**, 2164.
10 D. E. Hartter and A. Barnea, *Synapses*, 1988, **2**, 412.
11 J. Kardos, I. Kovács, F. Hajós, M. Kálmán and M. Simonyi, *Neurosci. Lett.*, 1989, **103**, 139.
12 D. J. Bonda, X. Wang, G. Perry, A. Nunomura, M. Tabaton, X. Zhu and M. A. Smith, *Neuropharmacology*, 2010, **59**, 290.
13 D. G. Smith, R. Cappai and K. J. Barnham, *Biochim. Biophys. Acta, Biomembr.*, 2007, **1768**, 1976.
14 Y. Manevich, K. D. Held and J. E. Biaglow, *Radiat. Res.*, 1997, **148**, 580.
15 C. Hureau and P. Faller, *Biochimie*, 2009, **91**, 1212.
16 S. Noël, F. Perez, J. T. Pedersen, B. Alies, S. Ladeira, S. Sayen, E. Guillon, E. Gras and C. Hureau, *J. Inorg. Biochem.*, 2012, **117**, 322.
17 B. Alies, I. Sasaki, O. Proux, S. Sayen, E. Guillon, P. Faller and C. Hureau, *Chem. Commun.*, 2013, **49**, 1214.
18 E. Atrián-Blasco, E. Cerrada, A. Conte-Daban, D. Testemale, P. Faller, M. Laguna and C. Hureau, *Metallomics*, 2015, **7**, 1229.
19 S. Chassaing, F. Collin, P. Dorlet, J. Gout, C. Hureau and P. Faller, *Curr. Top. Med. Chem.*, 2013, **12**, 2573.
20 T. Kowalik-Jankowska, M. Ruta, K. Wiśniewska, L. Łankiewicz and M. Dyba, *J. Inorg. Biochem.*, 2004, **98**, 940.
21 R. C. Nadal, S. E. J. Rigby and J. H. Viles, *Biochemistry*, 2008, **47**, 11653.
22 V. Balland, C. Hureau and J.-M. Saveant, *Proc. Natl. Acad. Sci. U. S. A.*, 2010, **107**, 17113.
23 L.-E. Cassagnes, V. Hervé, F. Nepveu, C. Hureau, P. Faller and F. Collin, *Angew. Chem., Int. Ed.*, 2013, **52**, 11110.
24 L. G. Trujano-Ortiz, F. J. González and L. Quintanar, *Inorg. Chem.*, 2014, **54**, 4.
25 H. Kozlowski, M. Luczkowski, M. Remelli and D. Valensin, *Coord. Chem. Rev.*, 2012, **256**, 2129.
26 T. Persson, B. O. Popescu and A. Cedazo-Minguez, *Oxid. Med. Cell. Longevity*, 2014, 2014.
27 R. L. Stevenson, *Strange case of Dr Jekyll and Mr Hyde*, Longmans, Green, and Co., London, 1886.
28 A. S. Pithadia and M. H. Lim, *Curr. Opin. Chem. Biol.*, 2012, **16**, 67.

29 C. Rodríguez-Rodríguez, M. Telpoukhovskaia and C. Orvig, *Coord. Chem. Rev.*, 2012, **256**, 2308.
30 K. J. Barnham and A. Bush, *Chem. Soc. Rev.*, 2014, **43**, 627.
31 M. G. Savelieff, A. S. DeToma, J. S. Derrick and M. H. Lim, *Acc. Chem. Res.*, 2014, **47**, 2475.
32 I. Batinic-Haberle, A. Tovmasyan, E. R. Roberts, Z. Vujaskovic, K. W. Leong and I. Spasojevic, *Antioxid. Redox Signaling*, 2014, **20**, 2372.
33 I. Batinic-Haberle, S. Reboucas Julio and I. Spasojevic, *Antioxid. Redox Signaling*, 2010, **13**, 877.

VI.B. French summary

Ce chapitre est composé d'une communication publiée dans Dalton Transactions en août 2016.[1] L'article détaille l'étude réalisée sur les propriétés pro- et anti-oxydantes de l'ascorbate dans le contexte de la maladie d'Alzheimer. L'ascorbate est un réducteur présent en grande concentration dans le cerveau humain (jusqu'à 10 mM dans les neurones).[2] Il est classé dans la catégorie des anti-oxydants puisqu'il a la capacité de réagir avec certaines espèces oxydantes telles que les espèces réactives de l'oxygène (ROS), en particulier $O_2^{\bullet -}$ et $HO^{\bullet}$ (Figure VI.B-1, voie verte), limitant ainsi de possibles dommages qui résulteraient de l'oxydation de biomolécules environnantes.

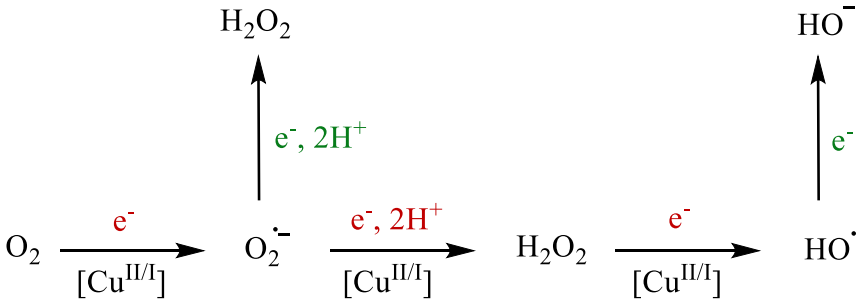

Figure VI.B-1: Effets pro-oxydants de l'ascorbate menant à la production de ROS catalysée par le cuivre (voie rouge) et effets anti-oxydants de l'ascorbate menant à la formation d'espèces non radicalaires (voie verte).

Ses propriétés pro-oxydantes sont en revanche plus méconnues. L'ascorbate étant un excellent réducteur, il peut également participer à la formation des mêmes espèces réactives qu'il combat normalement grâce à ses propriétés anti-oxydantes (Figure VI.B-1, voie rouge). C'est le cas en présence d'ions métalliques redox-actifs tels que les ions cuivre et fer, qui peuvent catalyser des réactions d'oxydo-réduction.

Comme nous l'avons vu précédemment (voir section I.C.2.b), les ions cuivre peuvent catalyser la production de l'anion superoxyde, du peroxyde d'hydrogène et du radical hydroxyle à partir du dioxygène, en présence d'un agent réducteur tel que l'ascorbate. La réaction directe d'oxydo-réduction entre l'ascorbate et le dioxygène n'est pas efficace [3] mais le devient en présence d'un catalyseur tel que le cuivre. L'ascorbate réduit l'ion cuivrique en ion cuivreux, et ce dernier transfère à son tour un électron au dioxygène, formant ainsi l'anion superoxyde. Le cuivre est ensuite à nouveau réduit par l'ascorbate, ce qui entretient le cycle catalytique.

Lorsque le cuivre est coordiné au peptide Aβ, il reste capable de cycler entre ses états d'oxydation Cu(II)-Aβ et Cu(I)-Aβ, le système catalysant ainsi la production de ROS.[4-5] Dans ce cas, l'ascorbate peut donc être considéré comme ayant des propriétés pro-oxydantes.

Les effets pro- et anti-oxydants de l'ascorbate ont été étudiés par spectroscopie de fluorescence, en présence de cuivre libre ou du complexe Cu-Aβ et de dioxygène. L'acide coumarine-3-carboxylique (CCA, Figure VI.B-2a) a été utilisé comme sonde pour la captation du radical hydroxyle. En effet, l'un des produits formés lors de l'oxydation du CCA par $HO^{\bullet}$ est l'acide 7-hydroxycoumarine-3-carboxylique (7-OH-CCA, Figure VI.B-2b), qui possède des propriétés de fluorescence (voir section II.D.2). Le CCA a donc été utilisé comme mime des biomolécules environnantes susceptibles de subir l'attaque de $HO^{\bullet}$. Le pH a dû être contrôlé avec précision pendant l'étude : le pKa de déprotonation du 7-OH-CCA formé est très proche du pH de l'étude (pKa = 7.5, voir informations complémentaires, section VI.C) et seule la forme protonée est fluorescente.

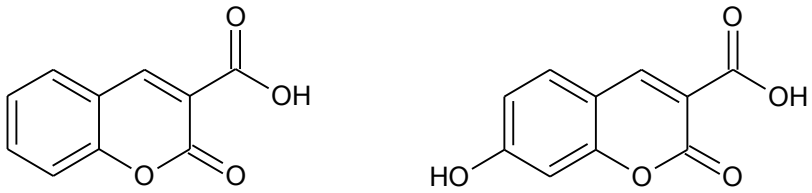

Figure VI.B-2: Structures chimique de l'acide coumarine-3-carboxylique (nommé CCA, panel a) et l'acide 7-hydroxycoumarine-3-carboxylique (nommé 7-OH-CCA, panel b).

L'étude a été réalisée avec Cu et Cu-Aβ, en faisant varier la concentration d'ascorbate. La vitesse de formation du 7-OH-CCA (déduite de la pente initiale de fluorescence) et la quantité totale de 7-OH-CCA formés au cours de la réaction (déduite du plateau de fluorescence à la fin de réaction) ont été extraites des courbes de fluorescence et tracées respectivement en fonction de la concentration d'ascorbate. De ces données, il ressort qu'à faible concentration (inférieur ou égal à 0.7 mM), les propriétés pro-oxydantes de l'ascorbate prédominent : la vitesse initiale de réaction et la quantité de 7-OH-CCA formés augmentent avec la concentration d'ascorbate. Cependant, à plus haute concentration, la vitesse initiale de formation du 7-OH-CCA diminue avec l'augmentation de la concentration d'ascorbate, et la quantité totale de 7-OH-CCA augmente plus faiblement pour les grandes concentrations en ascorbate. Ces résultats mettent en évidence l'effet anti-oxydant de l'ascorbate, prédominant à

haute concentration. Dans ces conditions, il participe toujours à la formation des ROS en réduisant le Cu(II), mais il peut également empêcher les radicaux hydroxyles formés d'oxyder le CCA (et donc les cibles biologiques) en réagissant avec. L'effet pro- *vs* anti-oxydant de l'ascorbate pour les molécules environnantes est donc dépendant de sa concentration.

En présence du peptide Aβ, les mêmes effets sont observés. Cependant, lorsque le cuivre est lié au peptide Aβ, la vitesse initiale de formation de 7-OH-CCA et la quantité totale de 7-OH-CCA formés sont plus faibles qu'avec le cuivre libre, à une concentration d'ascorbate donnée. Comme nous l'avons vu précédemment, le peptide Aβ est une cible pour les radicaux hydroxyles formés. Une partie des $HO^{\bullet}$ réagit donc avec Aβ au lieu du CCA, ce qui entraîne une diminution de la formation de 7-OH-CCA. Cette hypothèse a été corroborée par l'analyse de l'échantillon en fin de la réaction par chromatographie liquide couplée à la spectrométrie de masse haute résolution (LC-HRMS), mettant en évidence l'oxydation du peptide lors de la réaction de production de ROS. La quantité de peptide non-oxydé restant dans l'échantillon diminue avec l'augmentation de la concentration en ascorbate et devient nulle à partir de 1 mM d'ascorbate.

Afin d'évaluer la capacité de l'ascorbate à inhiber l'oxydation du peptide Aβ par $HO^{\bullet}$ à haute concentration comme c'est le cas pour le CCA, la dégradation du peptide a été évaluée après la consommation de 1 mM d'ascorbate, dans des échantillons contenant initialement 1 et 10 mM d'ascorbate. Même en présence de 10 mM d'ascorbate dans le milieu, le pourcentage de peptide non-oxydé retrouvé est quasiment nul. Ces résultats montrent donc que bien que l'ascorbate soit capable d'empêcher les dommages oxydatifs des molécules environnantes, mimées ici par le CCA, il n'a aucun effet sur l'oxydation du peptide Aβ lui-même. Comme le peptide est lié au cuivre lors de la production de ROS, il en est la cible la plus proche (notamment celle des radicaux hydroxyles). L'ajout d'ascorbate en grande quantité ne protège pas le peptide Aβ de l'oxydation. Tous ces résultats sont résumés dans la Figure VI.B-3.

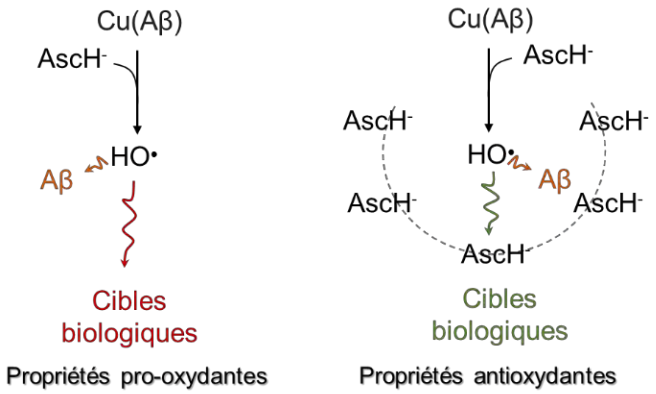

Figure VI.B-3: Représentation schématique des effets pro- et anti-oxydants de l'ascorbate et conséquences sur les cibles biologiques environnantes et sur le peptide Aβ. $AscH^-$ est l'abréviation de l'ascorbate.[1]

L'ascorbate a donc des propriétés anti-oxydantes à l'égard des cibles biologiques (mimées ici par le CCA) lorsqu'il est présent en grande concentration, mais il ne peut cependant inhiber l'oxydation de Aβ. De plus, bien que l'effet anti-oxydant de l'ascorbate soit visible dans cette étude, l'ajout en grande quantité d'ascorbate n'empêche pas totalement l'oxydation des molécules environnantes puisque le CCA piège toujours les $HO^\bullet$. On peut donc se demander s'il est possible d'atteindre une concentration en ascorbate pour laquelle l'effet anti-oxydant sera complet, c'est-à-dire pour laquelle aucun dommage oxydatif ne sera subi par les molécules environnantes. Plus globalement, cette étude tendrait à montrer que l'utilisation d'anti-oxydants sacrificiels (ascorbate ou autres piégeurs de radicaux) comme composés thérapeutiques n'est pas forcément la meilleure stratégie dans le contexte spécifique de la maladie d'Alzheimer.

VI.C. Supporting information

Is ascorbate Dr Jekyll or Mr Hyde in the Cu(Aβ) mediated oxidative stress linked to Alzheimer's Disease?

Clémence Cheignon [a,b,c], Fabrice Collin [a,b,c], Peter Faller [a,b,d*], Christelle Hureau [a,b*]

[a] LCC (Laboratoire de Chimie de Coordination), CNRS UPR 8241, 205 route de Narbonne, 31062 Toulouse Cedex 09 (France). E-mail : christelle.hureau@lcc-toulouse.fr

[b]Université de Toulouse ; UPS, INPT, 31077 Toulouse (France).

[c]UMR 152 Pharma Dev, Université de Toulouse, IRD, UPS, France.

[d]Current adress: Institut de Chimie (UMR 7177), 4 rue B. Pascal, F-67000 Strasbourg, France. E-Mail: pfaller@unistra.fr

Supporting Information

Material and methods

Chemicals

Cu(II) used was from $CuSO_4.5(H_2O)$ and purchased from Sigma. Stock solution of Cu(II) was prepared in milliQ water (18.2 mΩ). Monobasic and dibasic phosphate buffers were bought from Sigma-Aldrich, dissolved in ultrapure water to reach a 0.1 M concentration mixed together to obtain a pH of 7.4. POPSO was bought from Sigma-Aldrich, dissolved in milliQ water to reach a 0.4 M concentration and adjusted to pH 9.0 with NaOH or H_2SO_4. Ascorbate solutions (20 mM and 0.2 M) were freshly prepared few minutes prior to each experimental set by dissolving sodium ascorbate (Aldrich) in milliQ water. A stock solution of coumarin-3-carboxylic acid (CCA) 1 mM (from Sigma) was prepared in phosphate buffer (0.1 M, pH 7.4). A stock solution of 7-hydroxycoumarin-3-carboxylic acid (7-OH-CCA) 1 mM (from Sigma) was prepared in milliQ water.

Peptide

Amyloid beta peptides were bought from GeneCust (Dudelange, Luxembourg), with purity grade > 95%. Stock solution of the $A\beta_{16}$ (sequence DAEFRHDSGYEVHHQK) and $A\beta_{28}$ (sequence DAEFRHDSGYEVHHQKLVFFAEDVGSNK) peptides were prepared by dissolving the powder in milliQ water (resulting pH ~ 2). Peptide concentration was then determined by UV-visible absorption of Tyr10 considered as free tyrosine (at pH 2, $(\varepsilon_{276}-\varepsilon_{296})$ = 1410 $M^{-1}cm^{-1}$). Stock solution of $A\beta_{40}$ peptide (sequence DAEFRHDSGYEVHHQKLVFFAEDVGSNKGAIIGLMVGGVV) was prepared by dissolving the powder in NaOH (50mM) and passing the solution through FPLC to obtain the monomeric fraction. The peptide concentration was then determined in NaOH (50mM) by UV-visible absorption of Tyr10, considered as free tyrosine ($(\varepsilon_{293}-\varepsilon_{360})$=2400 $M^{-1}cm^{-1}$).

Mass spectrometry

High Performance Liquid Chromatography / High Resolution Mass Spectrometry (HPLC/HRMS) analysis was performed on a LTQ-Orbitrap XL mass spectrometer (ThermoFisher Scientific, Les Ulis, France) coupled to an Ultimate 3000 LC System (Dionex, Voisins-le-Bretonneux, France). The Orbitrap cell was operated in the full-scan mode at a resolution power of 60 000. Samples were washed three times with water prior analysis,by using Amicon 3 kDa centrifugal device (Millipore). Samples (10 µL) were then injected onto

the column (Acclaim 120 C18, 50 × 3 mm, 3 µm, ThermoScientific), at room temperature. The gradient elution was carried out with formic acid 0.1% (mobile phase A) and acetonitrile/water (80/20 v/v) formic acid 0.1% (mobile phase B) at a flow-rate of 0.5 mL.min^{-1}. The mobile phase gradient was programmed with the following time course: 5% mobile phase B at 0 min, held 3 minutes, linear increase to 55% B at 8 min, linear increase to 100% of B at 9 min, held 2 min, linear decrease to 5% B at 12 min and held 3 min. The mass spectrometer was used as a detector, working in the full scan positive mode between 150 and 2 000 Da.

Fluorescence

Fluorescence experiments were performed on a multi-plate reader FLUOstar Optima 96-well plate reader system (BMG Labtech). Two automatic injectors were used to add ascorbate solutions into the wells during the experiments. Coumarin-3-carboxylic acid (CCA) was used to detect HO$^{\bullet}$. HO$^{\bullet}$ reacts with CCA to form 7-hydroxy-coumarin-3-carboxylic acid (7-OH-CCA), which is fluorescent at 450 nm upon excitation at 390 nm. Under the conditions used here, the intensity of the fluorescence signal is proportional to the number of 7-OH-CCA molecules formed, which in turn is proportional to the HO$^{\bullet}$ radicals trapped (Figure S1). Ascorbate is added to phosphate buffered (pH 7.4, 50 mM) solutions containing CCA (0.5 mM) and Cu^{II} (10/50/100 µM) with or without 1.2 equivalent of Aβ peptide ($A\beta_{16}$, $A\beta_{28}$ or $A\beta_{40}$). The final concentration of ascorbate in wells is between 0 and 5 mM. Two stock solutions of ascorbate (0,2 M and 20 mM) are used to cover the range of concentrations.

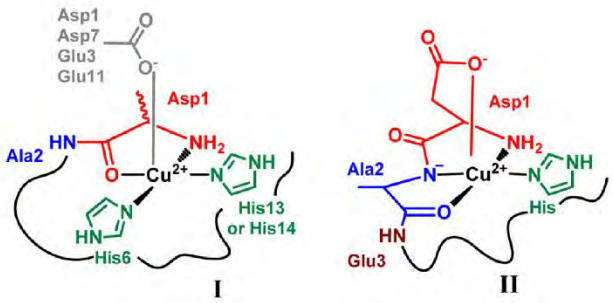

Figure S1: Schematic view of the proposed Cu(II) binding site in Aβ in component I (left) and II (right). pKa (I/II) = 7.8 [6]

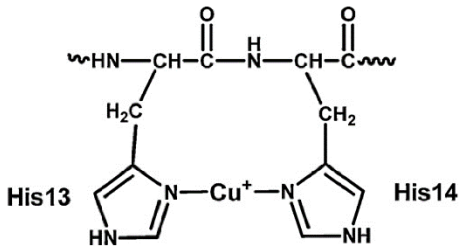

Figure S2: Schematic view of the proposed Cu(I) coordination site in Aβ.[6]

Fluorescent detection of HO• by CCA

Fluorescence emission of 7-OH-CCA is very sensitive to pH as, the hydroxyl-group has a pKa of 7.5 (Figures S2 and S3), and only the deprotonated form emits at 450 nm after excitation at 390 nm. Since the experiment is performed at pH 7.4, i.e. very close to the pKa, the pH has to be strictly stable in order to have accurate results. Because the oxidation of ascorbate releases protons, it is not easy to keep the pH constant even with a high concentrated buffer, this issue being more important at higher ascorbate concentrations. Therefore, we established a new methodology to take into account this possible pH drift: (i) For the gradient measurement (Figure 2 in Full Text), we have verified that the pH drift is negligible even at high ascorbate concentration. This is due to the weak ascorbate consumption during the first minutes of the experiment. (ii) For the plateau measurement (Figure S5 and figure 3 in the Full Text), we have established a new protocol in which the pH was raised at the end of the reaction to pH 8.5, a region where 7-OH-CCA fluorescence is weakly sensitive to pH changes. Additionally, we have also verified that the rate of HO• trapped by CCA was independent of pH in the range of pH 7.0 to 7.4, where 7.0 is the minimal value of final pH obtained after experiment with high ascorbate concentration (Figure S4). Thus, the value of the measured fluorescence is proportional to the HO• trapped at pH 7.4.

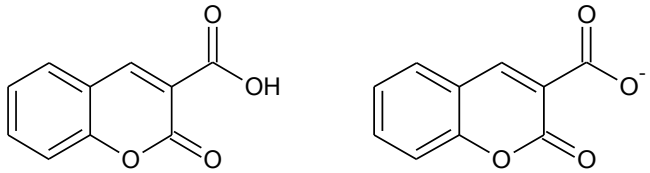

Coumarin-3-carboxylic acid / Coumarin-3-carboxylate (pKa 3.3)

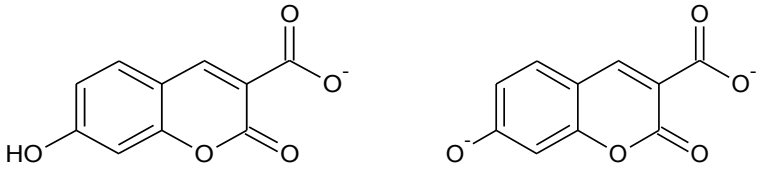

7-hydroxycoumarin-3-carboxylate / 7-oxidocoumarin-3-carboxylate (pKa 7.5)

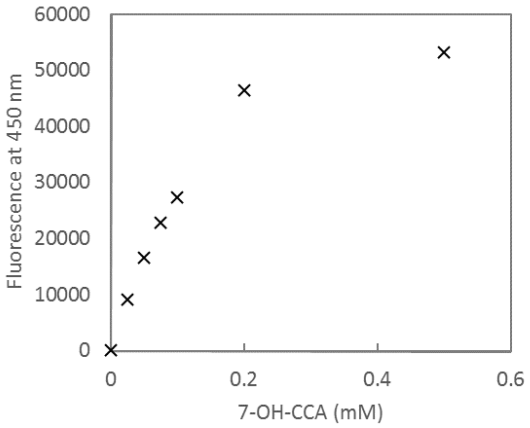

<u>Figure S3:</u> Fluorescence at 450 nm as a function of 7-OH-CCA concentration, after excitation at 390 nm. Phosphate-buffered solution (50 mM, pH 7.4) of 7-OH-CCA (concentration range from 0 to 0.5 mM).

Since the higher fluorescence intensity obtained in the present study (recorded under the very same conditions) is 14000, the fluorescence value is proportional to the 7-OH-CCA and the inner filter effect has not to be taken into account.

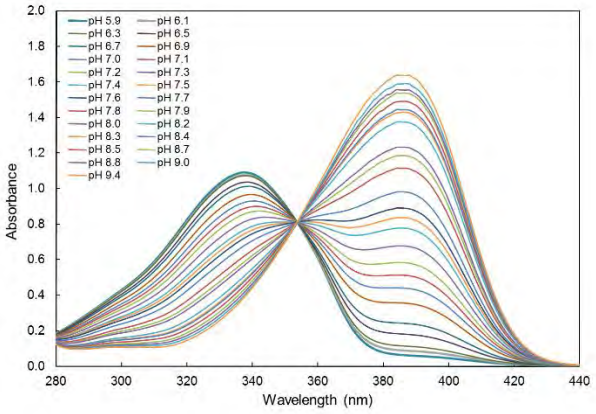

<u>Figure S4:</u> UV-Visible spectra of the 7-OH-CCA (50 µM) in a phosphate buffered solution (50 mM) with pH increased from 5.9 to 9.4 at 25°C.

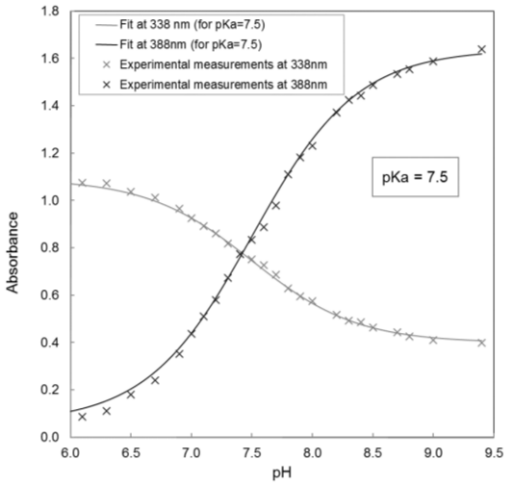

Figure S5: Determination of the pKa of the hydroxyl functional group of the 7-OH-CCA. Absorbance is plotted as a function of the pH of the acidic form absorbing at λ_{max} = 338 nm (grey crosses) and the basic form absorbing at λ_{max} = 388 nm (black crosses).

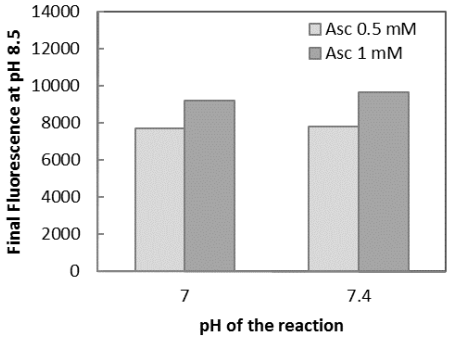

Figure S6: Impact of the pH on the formation of 7-OH-CCA during the metal-catalyzed production of the $HO^{\bullet}$. Reaction of Cu (50 µM), ascorbate (0.5 mM for grey panel and 1 mM for dark panel) in phosphate buffered solution (50 mM, pH 6.5, 7.0, 7.4, 8.0 or 8.5) containing CCA (0.5 mM). At the end of the reaction, the pH is ajusted to 8.5 with POPSO buffer (0.4 M, pH 9.0).

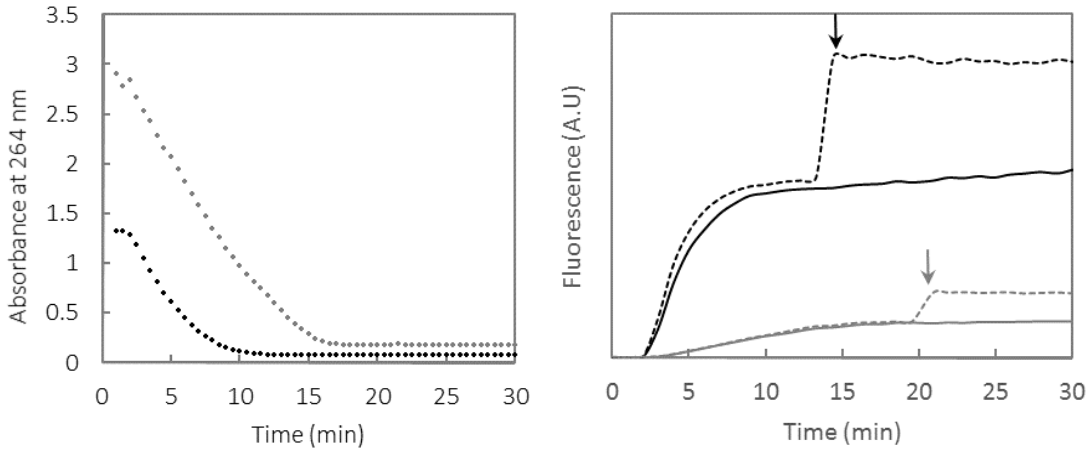

Figure S7: Reaction of Cu (50 µM, black curves) or Cu-Aβ$_{16}$ (50-60 µM, grey curves) with ascorbate (0.5 mM, in phosphate buffered solution, pH 7.4). Left: Ascorbate consumption followed using UV (absorption of ascorbate at λ_{max} = 264 nm) as a function of the time. Right: Fluorescence of the 7-OH-CCA produced by HO$^{\bullet}$ trapping by CCA (0.5 mM) as a function of the time. When ascorbate is fully consumed (see left figure), POPSO buffer is added to increase the pH to 8.5. Arrow indicates the addition of POPSO on dotted curve.

LC-MS Experiments

Table S1: monoisotopic apparent masses (m/z) of mono- and multi-protonated ions of non-oxidized Aβ$_{28}$. m/z values in blue are used for Aβ$_{28}$ detection in HRMS.

Name	Sequence	$[M+H]^+$	$[M+2H]^{2+}$	$[M+3H]^{3+}$	$[M+4H]^{4+}$	$[M+5H]^{5+}$
Aβ$_{28}$	DAEFRHDSGYEVHHQKLVFFAEDVGSNK	3261.5353	1631.27156	1087.85032	816.139694	653.11332

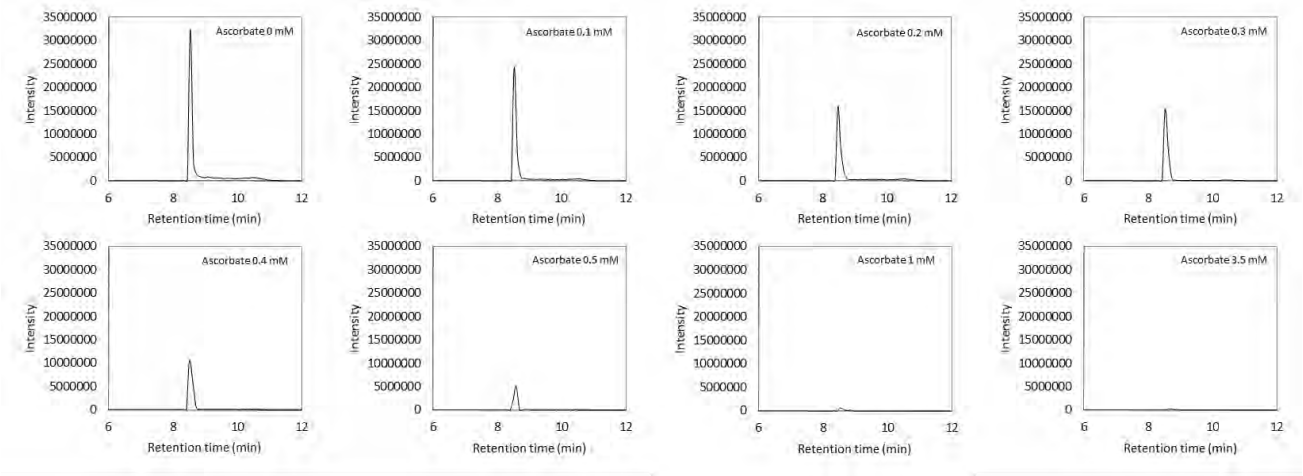

Figure S8: Trace chromatograms of the non-oxidized Aβ$_{28}$ peptide (60 µM) in the presence of Cu^{II} (50 µM) and ascorbate (0, 0.1, 0.2, 0.3, 0.4, 0.5 or 3.5 mM) at the end of the reaction. Mass tolerance set at 5 ppm; m/z ratios used for detection are specified in blue in table S1.

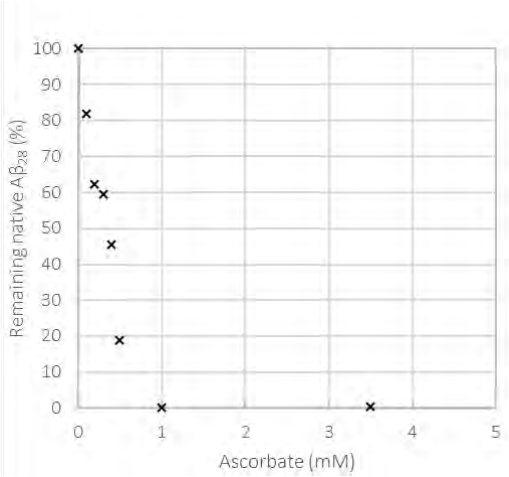

Figure S9: Remaining non-oxidized $A\beta_{28}$ at the end of the ROS production as a function of the ascorbate concentration. Phosphate-buffered solution (50 mM, pH 7.4) of $A\beta_{28}$ (60 µM), Cu^{II} (50 µM) and ascorbate (concentration range from 0 to 3.5 mM) analyzed in HPLC/HRMS. $A\beta_{28}$ peptide is detected with the monoisotopic masses (m/z) given in blue in table S1. Mass tolerance set at 5ppm. Trace chromatograms are given in Figure S8.

Since similar results are obtained whatever the length of the peptide (see Figure S10), the MS experiments were performed with $A\beta_{28}$ instead of $A\beta_{16}$ for technical reason.

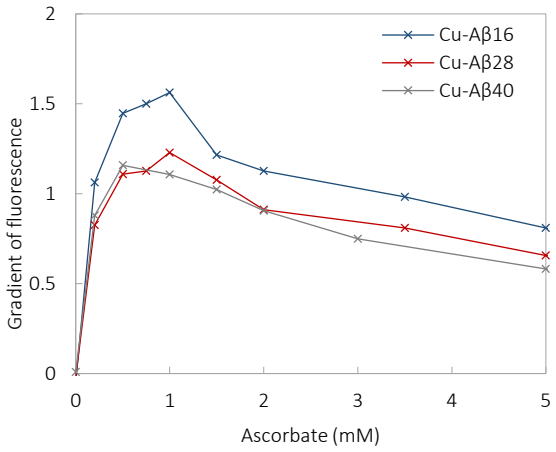

Figure S10: Initial rates of 7-OH-CCA fluorescence at 450 nm, reflecting the scavenging of $HO^{\bullet}$ by CCA. Phosphate-buffered solution (50 mM, pH 7.4) of CCA (0.5 mM), Cu (50 µM),), $A\beta_{16}$, $A\beta_{28}$ or $A\beta_{40}$ (60 µM) and ascorbate (concentration between 0 and 5 mM).

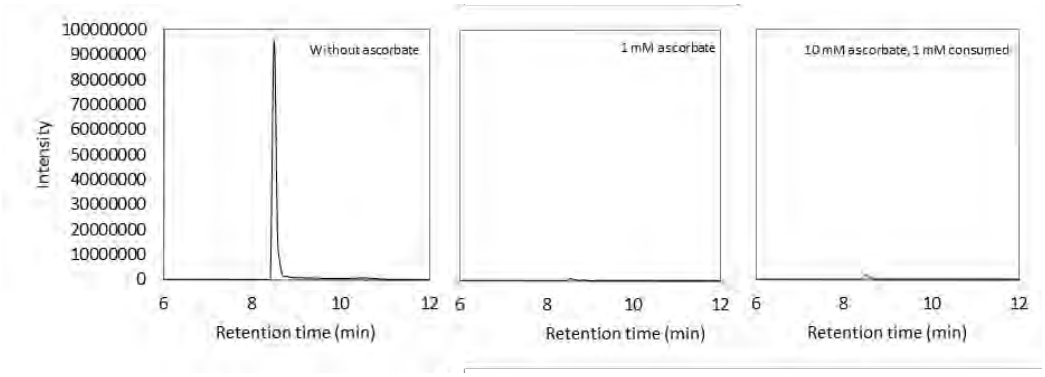

Figure S11: Trace chromatograms of the remaining non-oxidized Aβ$_{28}$ peptide (60 µM) after the addition of Cu^{II} (50 µM) and ascorbate (0 mM, 1 mM or 10 mM with only 1 mM consumed). Mass tolerance set at 5 ppm ; m/z ratios used for detection are specified in blue in table S1.

Table S2: Remaining non-oxidized Aβ$_{28}$ peptide (%) after the addition of Cu^{II} (50 µM) and ascorbate (0 mM, 1 mM or 10 mM with only 1 mM consumed). Percentages are calculated with the peak areas of the chromatograms traces (see Figure S11).

Starting ascorbate (mM)	Consumed ascorbate (mM)	Remaining Aβ$_{28}$ (%)
0	0	100%
1	1	1%
10	1	4%

References

[1] C. Cheignon, F. Collin, P. Faller and C. Hureau, *Dalton Transactions* **2016**, *45*, 12627-12631.

[2] M. E. Rice, *Trends in Neurosciences* **2000**, *23*, 209-216.

[3] B. Halliwell, *Journal of neurochemistry* **2006**, *97*, 1634-1658.

[4] D. G. Smith, R. Cappai and K. J. Barnham, *Biochimica et Biophysica Acta, Biomembranes* **2007**, *1768*, 1976-1990.

[5] D. J. Bonda, X. Wang, G. Perry, A. Nunomura, M. Tabaton, X. Zhu and M. A. Smith, *Neuropharmacology* **2010**, *59*, 290-294.

[6] C. Hureau, *Coordination Chemistry Reviews* **2012**, *256*, 2164-2174.

General conclusion

General conclusion

Les travaux présentés dans ce manuscrit concernent l'oxydation du peptide amyloïde-bêta (Aβ) lors de la production d'espèces réactives de l'oxygène (ROS) catalysées par les ions cuivre. Différents aspects ont été étudiés autour de l'oxydation du peptide Aβ : (i) l'identification des résidus oxydés et les conséquences que peut entraîner cette oxydation quant à la coordination des ions métalliques, l'agrégation du peptide oxydé et la production de ROS par le peptide oxydé en présence de cuivre, (ii) la caractérisation du mode de coordination du complexe Cu-Aβ dans l'état transitoire, appelé état « in-between », responsable de la production de ROS et donc de l'oxydation de Aβ et (iii) les effets à la fois pro- et anti-oxydants de l'ascorbate envers les biomolécules et le peptide Aβ lors de la production de ROS catalysée par le cuivre.

L'étude du peptide après oxydation catalysée par le cuivre a permis d'identifier les principaux acides aminés oxydés : l'aspartate 1 ainsi que les histidines 13 et 14. Ces acides aminés étant impliqués dans les coordinations de Cu(I) et/ou Cu(II), il a été proposé qu'ils soient aussi engagés dans la coordination du cuivre pendant la production de ROS. Etant proches du site de production, cela expliquerait leur oxydation ciblée.

Des oxydations collatérales ont aussi été détectées sur les phénylalanines 19 et 20 et sur la méthionine 35. Ces acides aminés ne sont pas engagés dans la sphère de coordination des ions métalliques (partie N-terminale), mais sont très sensibles aux attaques du radical hydroxyle. Il a été proposé qu'ils soient ciblés par les ROS quittant le système Cu-Aβ, lorsque les premières cibles des radicaux (Asp1, His13 et His14) sont suffisamment endommagées. Ils sont donc plutôt les victimes d'une fuite lors de la production de $HO^{\bullet}$ par le système Aβ-Cu, les radicaux ciblant avant tout les ligands du cuivre.

Nous avons pu montrer que l'oxydation du peptide Aβ a entraîné un changement de coordination des deux ions métalliques Cu(I) et Cu(II) ainsi que de Zn(II). Lorsque le peptide est suffisamment oxydé, ce changement est à l'origine d'une production de ROS plus rapide et d'une quantité plus importante de $HO^{\bullet}$ quittant le système Cu-Aβ. L'oxydation de Aβ peut donc être considéré comme un événement délétère pour le peptide lui-même, mais également pour les biomolécules environnantes pour lesquelles on observe une augmentation des oxydations.

Concernant l'influence de l'oxydation sur l'agrégation du peptide Aβ, les résultats préliminaires ont montré que le peptide oxydé a une faible tendance à agréger et à privilégier la formation de fibres. Cela marque une différence importante avec le peptide non-oxydé qui forme des fibres dans lesquelles il s'arrange en feuillets β. D'autres expériences sont en cours au laboratoire, elles visent à confirmer les premiers résultats obtenus et à mieux comprendre la manière dont le peptide oxydé se comporte en termes d'agrégation.

Par l'étude de la production de ROS catalysée par le cuivre en utilisant différents peptides Aβ modifiés, il a été possible de proposer une sphère de coordination du cuivre avec Aβ dans l'état transitoire « in-between », responsable de la production de ROS. Ainsi, une histidine, l'amine N-terminale et le groupe carboxylate de l'aspartate 1 seraient liés au cuivre dans l'état « in-between ». Le peptide Aβ non-modifié possédant 3 résidus histidine, il est probable qu'ils soient tous trois impliquées dans la sphère de coordination du cuivre en échange dynamique, comme c'est déjà le cas pour les complexes Cu(I)-Aβ et Cu(II)-Aβ dans les états dits « au repos ».

Enfin, les propriétés pro-oxydantes et anti-oxydantes de l'ascorbate ont été étudiées. Antioxydant bien connu du grand public (notamment sous le nom de Vitamine C), l'ascorbate présente un double visage puisqu'il participe également à la production de ROS en transférant un électron au centre métallique, qui peut à son tour réduire l'oxygène moléculaire ou les espèces intermédiaires que constituent les ROS. L'étude a permis de déterminer que son effet dépend de sa concentration. Quelle qu'elle soit, l'ascorbate participe à la production de ROS, mais à forte concentration, il réagit aussi avec les radicaux hydroxyles formés et joue son rôle d'antioxydant vis-à-vis des biomolécules environnantes. Cependant, il n'est pas efficace dans la protection du peptide Aβ. Même à forte concentration dans le milieu, le peptide n'est pas protégé contre les attaques du radical hydroxyle.

Ainsi, il ressort de cette étude que l'Aspartate 1 et les Histidines du peptide Aβ sont des acides aminés clés dans la production de ROS. Impliqués dans la coordination des ions Cu(I) et Cu(II) dans les états au repos, ils le sont également dans l'état transitoire, seul état redox activement impliqué dans la production de ROS. Ils sont les premiers ciblés et leur dégradation entraîne des changements importants quant à la coordination des métaux, l'agrégation et de la production de ROS. L'ascorbate, même présent en grande concentration, ne peut faire bénéficier Aβ de ses propriétés antioxydantes. Le peptide Aβ, en se liant à un ion cuivre,

participe donc à sa propre destruction en contribuant à la production des ROS qui l'endommagent irréversiblement.

L'intérêt de cette étude et des résultats qu'elle a permis d'obtenir réside dans une meilleure connaissance des mécanismes et conséquences de l'activité redox du système Cu-Aβ, à rapprocher du lien existant entre stress oxydant et maladie d'Alzheimer. Des perspectives directes peuvent être envisagées, à plus ou moins long terme. Une meilleure connaissance de l'état redox responsable de la production de ROS peut permettre le développement de stratégies thérapeutiques ciblées et efficaces, pouvant conduire à une réduction des dommages oxydatifs qui seraient en cause dans la neurodégénérescence liée à la maladie. D'autre part, et étant donné sa spécificité, l'oxydation du peptide Aβ peut représenter une piste intéressante dans la recherche de biomarqueurs pour le diagnostic précoce de la maladie d'Alzheimer. Il serait ainsi intéressant de pouvoir purifier le peptide Aβ à partir de matériel biologique (sérum, liquide céphalo-rachidien, …) pour étudier spécifiquement de possibles dégâts dus à l'oxydation. La production d'anticorps spécifiquement dirigés contre le peptide oxydé représenterait alors une avancée intéressante pour une telle étude. Enfin, une meilleure connaissance du système Cu-Aβ devrait permettre aussi de mieux comprendre le fonctionnement d'autres systèmes impliquant des peptides amyloïdogéniques mis en cause dans d'autres pathologies, tels que l'amyline, pour le diabète de type II, et l'alpha-synucléine, pour la maladie de Parkinson.

Annexes

Annex I

High-Resolution Mass Spectrometry data

Table 1: Monoisotopic apparent masses (m/z) of mono- and multi-protonated ions of Aβ40, Aβ28, Aβ16 and the tryptic peptides (Aβ1-5, Aβ6-16, Aβ17-28 and Aβ29-40) as well as their oxidized counterparts.

Name	Sequence	$[M+H]^+$	$[M+2H]^{2+}$	$[M+3H]^{3+}$	$[M+4H]^{4+}$	$[M+5H]^{5+}$
Aβ16	**DAEFRHDSGYEVHHQK**	**1954.8796**	**977.9437**	**652.2984**	**489.4758**	**391.7822**
	D^{dd}AEFRHDSGYEVHHQK	1909.8581	955.4330	637.2913	478.2204	382.7779
	DAEFRHDSGYEV**H**$^{+16}$HQK	1970.8745	985.9412	657.6300	493.4745	394.9812
	DAEFRHDSGYEV**H**$^{+16}$H^{+16}QK	1986.8694	993.9386	662.9617	497.4732	398.1801
	D^{dd}AEFRHDSGYEV**H**$^{+16}$HQK	1925.8530	963.4304	642.6229	482.2191	385.9769
	D^{ox}AEFRHDSGYEVHHQK	1865.8319	933.4199	622.6159	467.2138	373.9726
	D^{ox}AEFRHDSGYEV**H**$^{+16}$HQK	1881.8268	941.4173	627.9475	471.2126	377.1716
Aβ28	**DAEFRHDSGYEVHHQKLVFFAEDVGSNK**	**3261.5353**	**1631.2716**	**1087.8503**	**816.1397**	**653.1133**
	D^{dd}AEFRHDSGYEVHHQKLVFFAEDVGSNK	3216.5138	1608.7608	1072.8432	804.8843	644.1090
	DAEFRHDSGYEV**H**$^{+16}$HQKLVFFAEDVGSNK	3277.5302	1639.2690	1093.1820	820.1384	656.3123
	DAEFRHDSGYEV**H**HQKLVFFAEDVGSNK $^{+32}$	3293.5251	1647.2665	1098.5136	824.1372	659.5113
	D^{dd}AEFRHDSGYEV**H**$^{+16}$HQKLVFFAEDVGSNK	3232.5088	1616.7583	1078.1748	808.8831	647.3080
	D^{ox}AEFRHDSGYEVHHQKLVFFAEDVGSNK	3172.4876	1586.7477	1058.1678	793.8778	635.3038
	D^{ox}AEFRHDSGYEV**H**$^{+16}$HQKLVFFAEDVGSNK	3188.4825	1594.7452	1063.4994	797.8765	638.5028
Aβ40	**DAEFRHDSGYEVHHQKLVFFAEDVGSNKGAIIGLMVGGVV**	**4328.1561**	**2164.5820**	**1443.3906**	**1082.7949**	**866.4375**
	D^{dd}AEFRHDSGYEVHHQKLVFF…	4283.1347	2142.0713	1428.3834	1071.5395	857.4332
	DAEFRHDSGYEV**H**$^{+16}$HQKLVFF…	4344.1511	2172.5794	1448.7222	1086.7936	869.6365
	DAEFRHDSGYEV**H**$^{+16}$H^{+16}QKLVFF…	4360.1460	2180.5769	1454.0539	1090.7924	872.8355
	D^{dd}AEFRHDSGYEV**H**$^{+16}$HQKLVFF…	4299.1296	2150.0687	1433.7151	1075.5383	860.6322
	D^{ox}AEFRHDSGYEVHHQKLVFF…	4239.1085	2120.0581	1413.7080	1060.5330	848.6280
	D^{ox}AEFRHDSGYEV**H**$^{+16}$HQKLVFF…	4255.1034	2128.0556	1419.0397	1064.5317	851.8269
	DAEF**R**^{p}HDSGYEVHHQ**K**^{p}LVFF…	4387.1483	2194.0781	1463.0547	1097.5429	878.2359
Aβ1-5	**DAEFR**	**637.2945**	**319.1512**	**213.1034**	**160.0795**	**128.2652**
	DAEFR+16	653.2895	327.1486	218.4350	164.0782	131.4642
	DAEFRdd	592.2731	296.6405	198.0962	148.8241	119.2609
	DAEFRox	548.2469	274.6273	183.4208	137.8176	110.4556
	DAEFR+32	669.2844	335.1461	223.7667	168.0770	134.6631
	DAEFR$_{dd}$+16	608.2680	304.6379	203.4279	152.8229	122.4599
	DAEFR$_{ox}$+16	564.2418	282.6248	188.7525	141.8163	113.6546
Aβ6-16	**HDSGYEVHHQK**	**1336.6034**	**668.8056**	**446.2064**	**334.9067**	**268.1269**
	HDSGYEVHHQK+14	1350.5827	675.7953	450.8661	338.4015	270.9228
	HDSGYEVHHQK+16	1352.5983	676.8031	451.5380	338.9055	271.3259
	HDSGYEVHHQK+32	1368.5932	684.8005	456.8696	342.9042	274.5249
	HDSGYEVHHQK(diTyr)	2670.1834	1335.5956	890.7330	668.3017	534.8429
Aβ17-28	**LVFFAEDVGSNK**	**1325.6741**	**663.3410**	**442.5633**	**332.1744**	**265.9411**
	LVFFAEDVGSNK+16	1341.6690	671.3384	447.8949	336.1731	269.1401
	LVFFAEDVGSNK+14	1339.6534	670.3306	447.2230	335.6692	268.7369
	LVFFAEDVGSNK+32	1357.6639	679.3359	453.2265	340.1719	272.3390
Aβ29-40	**GAIIGLMVGGVV**	**1085.6392**	**543.3235**	**362.5516**	**272.1657**	**217.9341**
	GAIIGLMVGGVV+16	1101.6342	551.3210	367.8833	276.1644	221.1331
	GAIIGLMVGGVV+32	1117.6291	559.3184	373.2149	280.1631	224.3321

Annex II

^{1}H NMR data

Table 2: ^{1}H NMR chemical shifts of Aβ$_{28}$ at pH 7.4.[1]

All the ^{1}H signals were assigned on the basis of chemical shifts by using ^{1}H-^{1}H TOCSY and ^{1}H-^{1}H NOESY experiments for Aβ28 (500µM) in 10 mM phosphate buffer pH 7.4, 90/10 H_2O/D_2O at 10°C. All chemical shifts were referenced at 0.00 ppm relative to internal TSP.

Résidu	HN	Hα	Hβ	Hγ	Hδ	Hε
Asp1		4.13	2.68-2.80			
Ala2		4.29	1.36-1.37			
Glu3	8.52	4.20	1.83-1.92	2.17-2.19		
Phe4	8.35	4.56	3.01		7.16	7.25
Arg5	8.19	4.27	1.62-1.74	1.49	3.12	
His6		4.54	3.05-3.10		7.88	7.03
Asp7	8.40	4.62	2.66			
Ser8	8.46	4.37	3.87-3.91			
Gly9	8.59	3.88-3.94				
Tyr10	8.01	4.52	2.94-3.03		7.06	6.78
Glu11	8.44	4.18	1.89-1.92	2.12-2.21		
Val12	8.13	3.94	1.95	0.78-0.87		
His13		4.53	3.04		7.83	6.94
His14		4.59	3.01-3.08		7.85	6.96
Gln15	8.44	4.26	1.97-2.06	2.32		
Lys16	8.44	4.27	1.67-1.74	1.37	1.44	2.97
Leu17	8.31	4.32	1.57-1.61	1.45	0.85-0.91	
Val18	8.04	4.02	1.90	0.75-0.83		
Phe19	8.31	4.58	2.91-2.99		7.30	7.17
Phe20	8.27	4.57	2.94-3.09		7.32	7.24
Ala21	8.29	4.22	1.36-1.37			
Glu22	8.42	4.21	1.92-2.04	2.27		
Asp23	8.48	4.65	2.63-2.74			
Val24	8.20	4.15	2.19	0.96		
Gly25	8.59	3.98				
Ser26	8.22	4.46	3.88			
Asn27	8.54	4.74	2.77-2.85			
Lys28	7.96	4.16	1.71-1.83	1.39	1.66	2.99

[1] H. Eury in *Etude de l'intéraction de la thioflavine T et de complexes de ru (ii) avec le peptide amyloïde bêta dans le cadre de la maladie d'alzheimer*, *Vol.* **2013**.

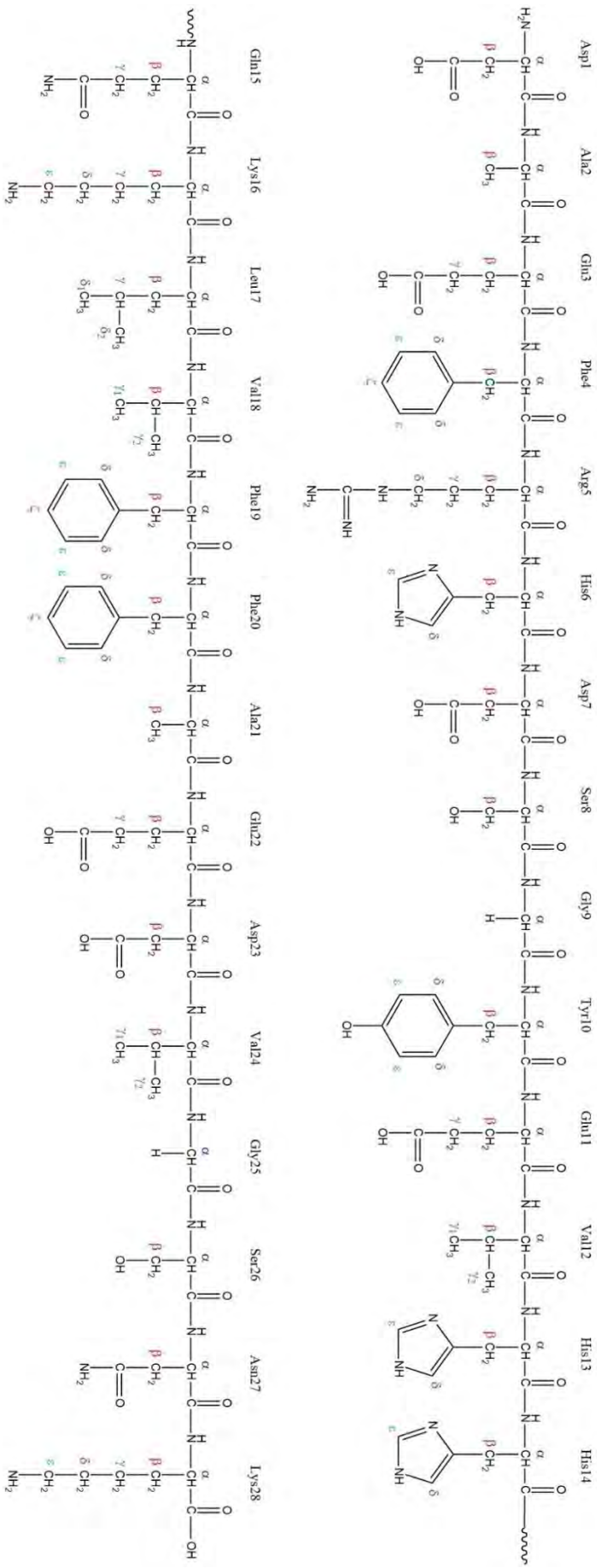

Figure 1: Chemical structure of $A\beta_{28}$ sequence along with the atom identifiers of each amino acid residue.

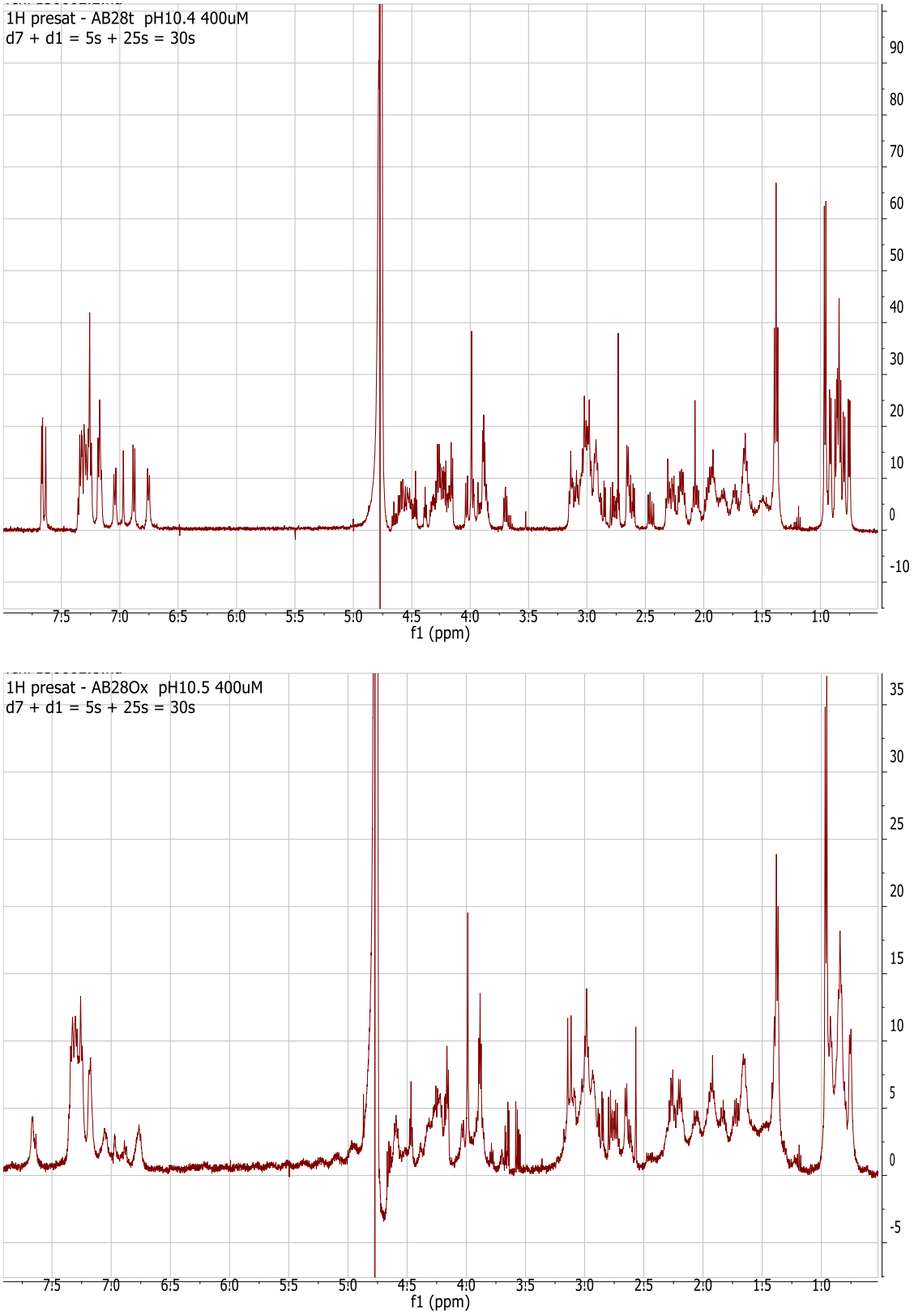

Figure 2: 1H NMR spectra of $A\beta_{28}$ (top) and $A\beta_{28}ox$ (bottom) at 400 µM, pH 10.5.

Annex III

Linear combination fitting of XANES Zn-Aβ$_{28}$ox spectrum with different Zn-peptide complexes

```
      LCF fit of Zn-AB28ox 2016 as flattened mu(E) from 9644.58 to 9764.58

      Fit included 149 data points and 2 variables, and approximately 61.303
measurements
      Weights sum to 1: yes
      Weights forced between 0 and 1: yes
      Overall e0 shift used: no
      Noise added to data: 0
      R-factor = 0.0004887
      Chi-square = 0.01424
      Reduced chi-square = 0.0000968

      .  standard       weight      e0
      ========================================================
      .  Zn-Ab28        0.443 (0.016)  0.000 (0.000)
      .  Zn-H13A        0.224 (0.018)  0.000 (0.000)
      .  Zn-(H6A-H14A)  0.333 (0.028)  0.000 (0.000)

      .     sum ........... 1.000
```

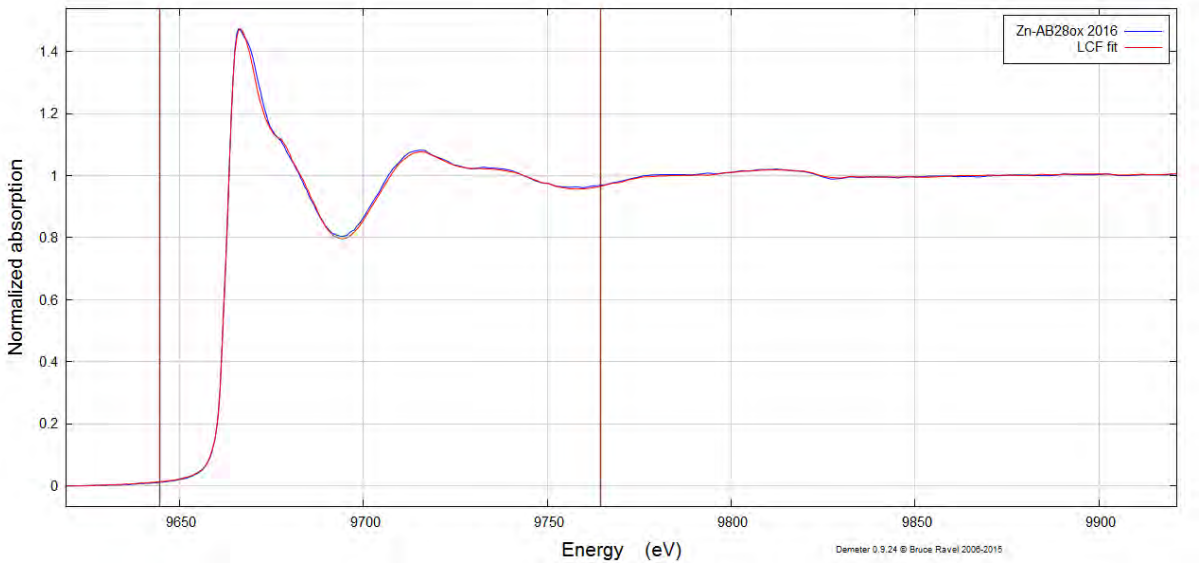

Figure 3: Linear Combination Fitting of Aβ$_{28}$-Zn, H13A-Zn and (H6A-H14A)-Zn to reproduce Aβox-Zn spectrum. Quantitative results of linear combination fitting (top) and the resulting XANES spectra with 44% of Aβ$_{28}$-Zn, 22% of H13A-Zn and 33% of (H6A-H14A)-Zn (red curve) compared to Aβox-Zn XANES spectrum (blue curve).

```
      LCF fit of Zn-AB28ox 2016 as flattened mu(E) from 9644.58 to 9764.58

      Fit included 149 data points and 2 variables, and approximately 61.303
measurements
      Weights sum to 1: yes
      Weights forced between 0 and 1: yes
      Overall e0 shift used: no
      Noise added to data: 0
      R-factor = 0.0009376
      Chi-square = 0.02731
      Reduced chi-square = 0.0001858

      .  standard       weight      e0
      ============================================================
      .  Zn-Ab28        0.446 (0.039)  0.000 (0.000)
      .  Zn-D1N         0.118 (0.033)  0.000 (0.000)
      .  Zn-(H6A-H14A)  0.436 (0.053)  0.000 (0.000)

      .     sum ........... 1.000
```

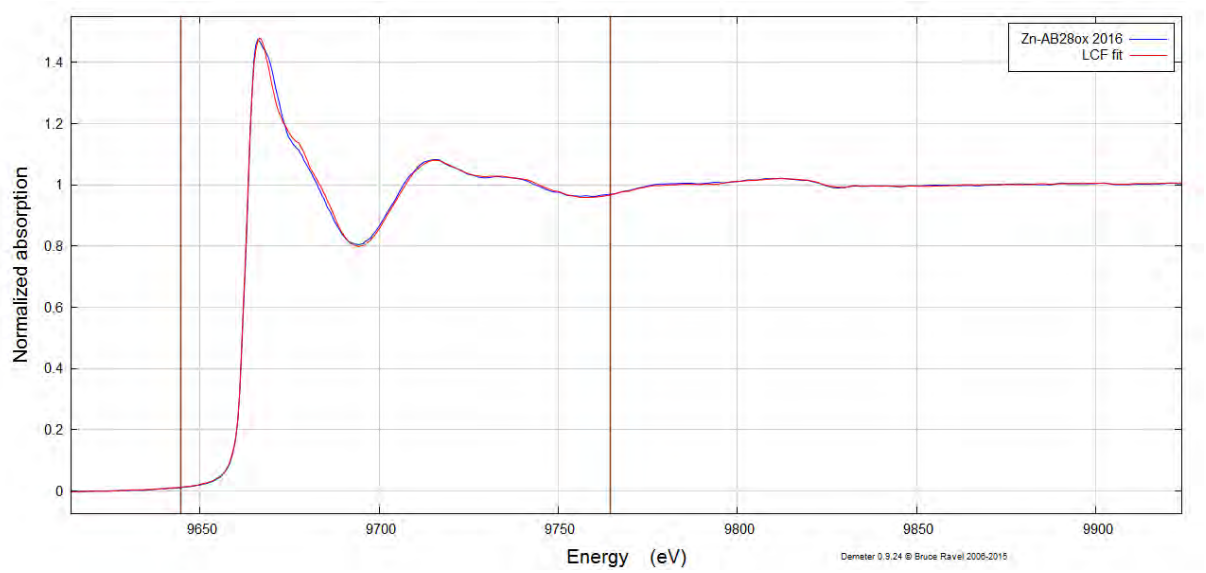

Figure 4: Linear Combination Fitting of $A\beta_{28}$-Zn, D1N-Zn and (H6A-H14A)-Zn to reproduce Aβox-Zn spectrum. Quantitative results of linear combination fitting (top) and the resulting XANES spectra with 45% of $A\beta_{28}$-Zn, 12% of D1N-Zn and 44% of (H6A-H14A)-Zn (red curve) compared to Aβox-Zn XANES spectrum (blue curve).

```
      LCF fit of Zn-AB28ox 2016 as flattened mu(E) from 9644.58 to 9764.58

      Fit included 149 data points and 2 variables, and approximately 61.303
measurements
      Weights sum to 1: yes
      Weights forced between 0 and 1: yes
      Overall e0 shift used: no
      Noise added to data: 0
      R-factor = 0.0016980
      Chi-square = 0.04946
      Reduced chi-square = 0.0003365

      .  standard       weight      e0
      ============================================================
      .  Zn-D1N         0.385 (0.034)  0.000 (0.000)
      .  Zn-H13A        0.119 (0.046)  0.000 (0.000)
      .  Zn-(H6A-H14A)  0.496 (0.059)  0.000 (0.000)

      .     sum ........... 1.000
```

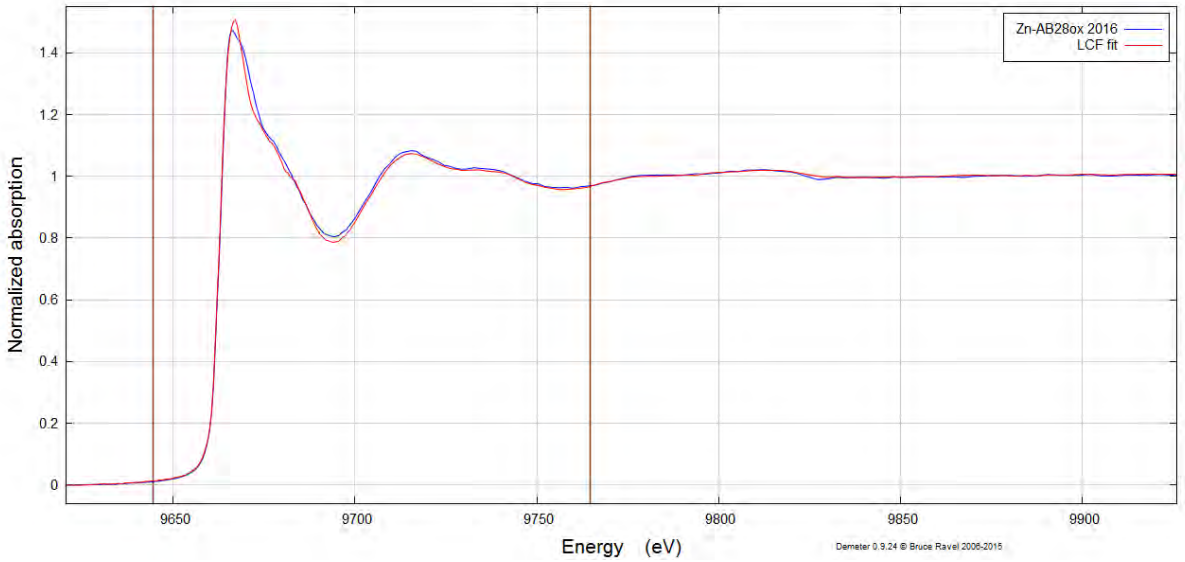

Figure 5: Linear Combination Fitting of D1N-Zn, H13A-Zn and (H6A-H14A)-Zn to reproduce Aβox-Zn spectrum. Quantitative results of linear combination fitting (top) and the resulting XANES spectra with 38% of D1N-Zn, 12% of H13A-Zn and 50% of (H6A-H14A)-Zn (red curve) compared to Aβox-Zn XANES spectrum (blue curve).

Résumé

Résumé

Le cerveau humain est un organe très surprenant. Alors qu'il ne pèse que 2 % du poids total du corps et qu'il est constitué majoritairement d'eau (75%), il assure les fonctions cognitives et motrices du corps et traite les informations provenant de la vue, de l'ouïe, de l'odorat, du toucher et du goût. Il est l'une des parties du corps dont l'activité métabolique est la plus intense, et utilise au repos, à lui tout seul, 20% de l'oxygène consommé par l'organisme entier. Il est constitué de 100 milliards de neurones qui communiquent entre eux grâce aux neurotransmetteurs, messagers chimiques qui traversent les synapses. Le cerveau étant un organe extrêmement complexe et multitâche, les origines biologiques et chimiques de ses nombreuses fonctions ne sont pas encore toutes parfaitement connues.

De nombreuses pathologies sont liées à un dysfonctionnement métabolique du cerveau, mais pour la plupart, leur étiologie est inconnue. C'est le cas des maladies neurodégénératives, ou démences, qui touchent actuellement plus de 45 millions de personnes à travers le monde. En raison de l'augmentation de l'espérance de vie liée aux avancées de la médecine, le nombre de personnes atteintes de démence ne fait que s'accroître. Parmi les différentes maladies neurodégénératives, la maladie d'Alzheimer, découverte il y a plus d'un siècle, est la plus répandue. Bien que la cause de son développement soit encore inconnue à l'heure actuelle, deux types de lésions cérébrales sont observés chez les patients : (i) les enchevêtrements neurofibrillaires, ayant pour origine l'hyperphosphorylation de la protéine Tau et (ii) la formation de plaques amyloïdes extracellulaires. Les recherches scientifiques sont donc principalement dirigées vers l'étude de ces deux caractéristiques de la maladie, que ce soit d'un point de vue mécanistique, pour comprendre l'étiologie de la maladie, ou d'un point de vue thérapeutique, pour tenter de trouver un médicament efficace.

Dans ce cadre global, le travail présenté ici s'est focalisé sur la problématique des plaques amyloïdes – appelées aussi plaques séniles – et plus précisément sur son composant principal, le peptide amyloïde-bêta (Aβ). Aβ est un peptide composé de 40 à 42 acides aminés, naturellement présent sous forme monomérique dans le cerveau. Dans le cas de la maladie d'Alzheimer, il est retrouvé sous forme agrégée dans les plaques amyloïdes. Ces dernières peuvent être formées dans l'espace inter-synaptique et empêcher le bon fonctionnement des neurones en obstruant le passage des neurotransmetteurs entre les synapses de deux cellules

nerveuses. Un lien entre maladie d'Alzheimer et stress oxydant a également été démontré. En plus de sa capacité d'agrégation dans des conditions spécifiques à la maladie d'Alzheimer, Aβ est également à l'origine de la production d'espèces réactives de l'oxygène (ROS) car il est capable de chélater des ions métalliques ayant des propriétés oxydo-réductrices, ions cuivre ou fer par exemple. En présence d'un agent réducteur tel que l'ascorbate, naturellement présent dans le cerveau à des concentrations pouvant être localement importantes, le complexe Cu-Aβ formé peut catalyser la production de l'anion superoxyde ($O_2^{\bullet -}$), du peroxyde d'hydrogène (H_2O_2) et du radical hydroxyle ($HO^{\bullet}$) à partir du dioxygène (Figure 1). Ces ROS, et plus spécifiquement le radical hydroxyle, sont des espèces oxydantes réactives qui peuvent endommager les biomolécules environnantes (lipides, protéines, ADN). Lors de la production de ROS, le peptide Aβ, lié au cuivre, subit également des attaques oxydantes.

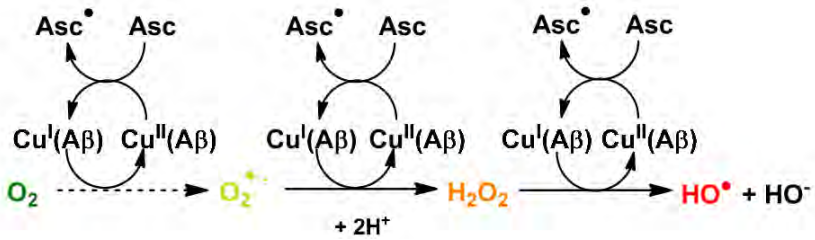

Figure 1 : Production d'espèces réactives de l'oxygène (ROS) catalysée par le complexe Cu-Aβ en présence d'ascorbate (Asc). L'anion superoxyde ($O_2^{\bullet -}$), le peroxyde d'hydrogène (H_2O_2) et le radical hydroxyle ($HO^{\bullet}$) sont formés à partir du dioxygène.

Nous nous sommes tout d'abord intéressé à l'oxydation du peptide amyloïde-β lors de la production de ROS catalysée par le complexe Cu-Aβ (chapitre III). Les dommages oxydatifs subis par le peptide Aβ ont été étudiés par spectrométrie de masse haute résolution ainsi que par spectrométrie de masse en tandem. La combinaison des deux techniques a permis d'identifier 6 acides aminés oxydés ainsi que la nature des produits d'oxydation obtenus (Figure 2). L'aspartate 1, les histidines 13 et 14, les phénylalanines 19 et 20 ainsi que la méthionine 35 sont des cibles pour les ROS lors de leur production catalysée par le complexe Cu-Aβ.

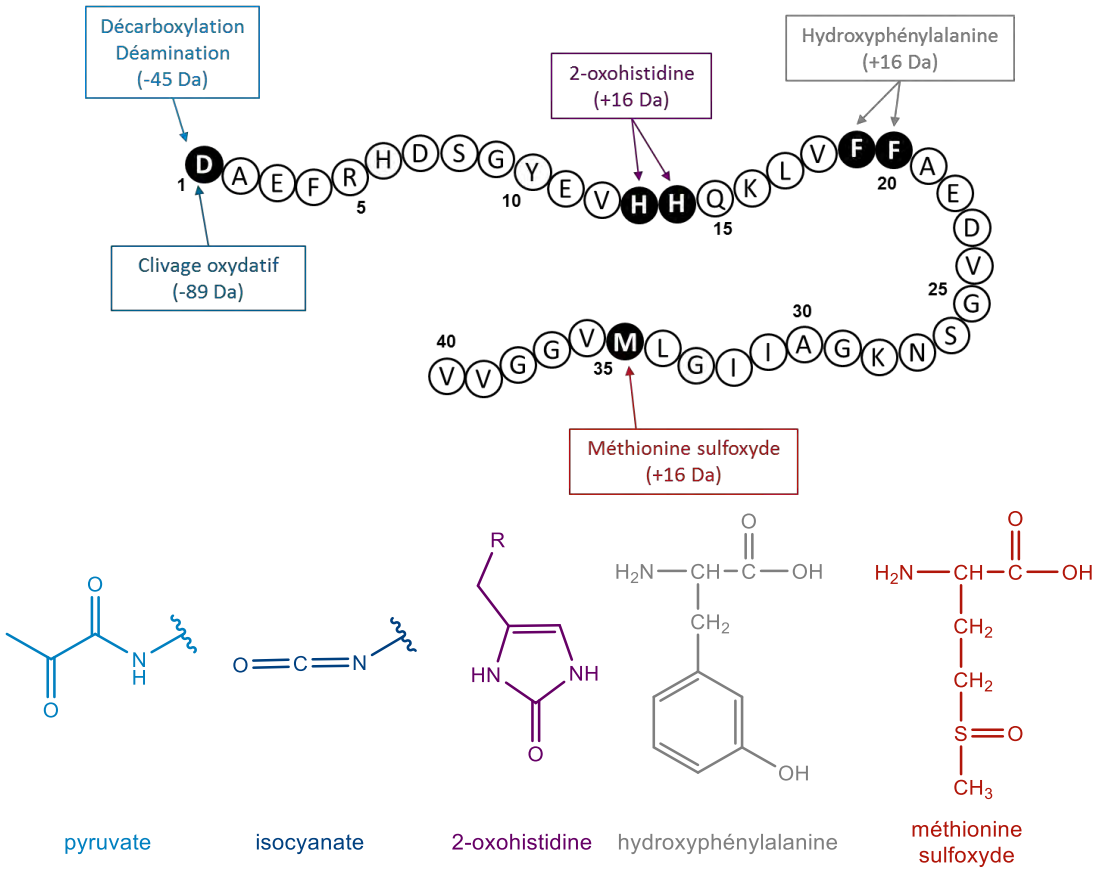

Figure 2 : Séquence peptidique de Aβ$_{40}$ avec les acides aminés oxydés (cercles noirs) détectés ainsi que la nature de l'oxydation et le changement de masse (en Da) et structure chimique des acides aminés oxydés. La 3-hydroxyphenylalanine est montrée comme exemple de produit d'oxydation de la phénylalanine, mais les 2- et 4-hydroxyphenylalanines pourraient également être formés.

Nous avons également étudié la cinétique d'oxydation des acides aminés par spectrométrie de masse haute résolution, afin de déterminer s'il y avait des cibles privilégiées pour les ROS parmi ces 6 acides aminés retrouvés oxydés. La figure 3 montre les courbes d'évolution de l'oxydation au cours du temps pour les 4 peptides obtenus après la digestion trypsique du peptide Aβ$_{40}$. L'oxydation de Asp1 et des histidines a lieu dès le début de la réaction de production de ROS et semble s'arrêter au bout de 8 min (figures 3a et 3b). Au contraire, l'oxydation des phénylalanines n'a lieu qu'au bout de quelques minutes, après la phase de latence observée sur la courbe (figure 3c). La quantité de phénylalanine oxydée ne cesse de s'accroitre pendant le reste de la réaction. Pour la Met35 (figure 3d), aucune conclusion ne peut être faite, l'ascorbate présent lors de la réaction ayant la capacité de réduire la méthionine oxydée en méthionine, ce qui a pour conséquence de biaiser les résultats.

Les résultats ainsi obtenus ont permis d'identifier Asp1, His13 et His14 comme cibles privilégiées des ROS car ils subissent des dommages oxydatifs dès le début de la réaction alors que les phénylalanines, cibles secondaires, sont oxydées après un temps de latence.

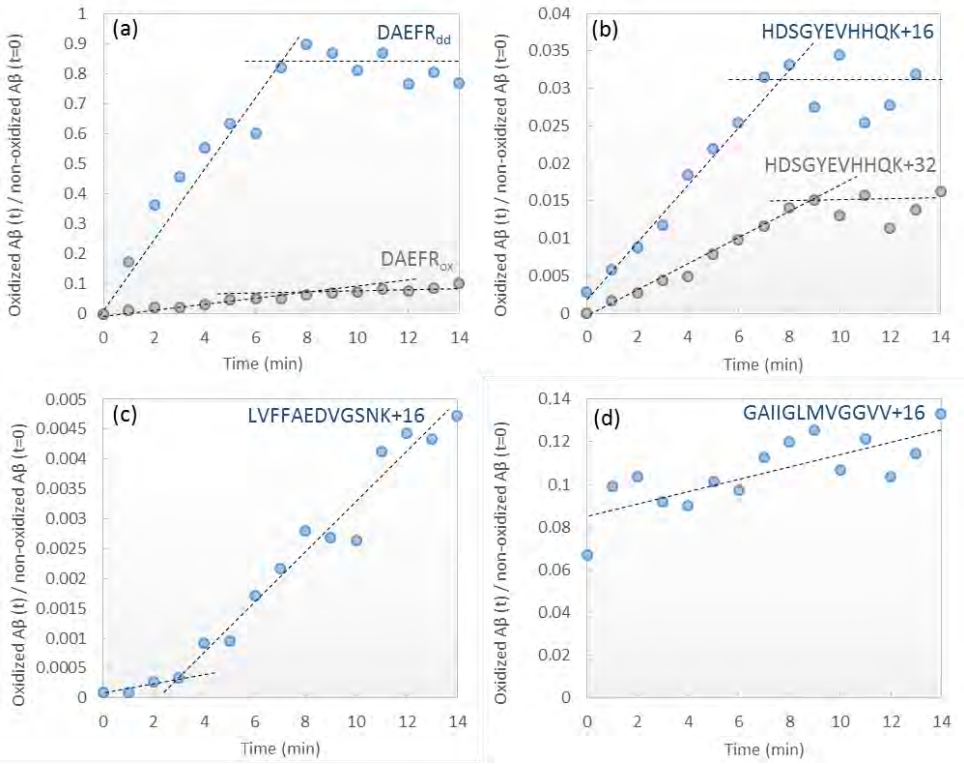

Figure 3 : Oxydation des peptides obtenus après digestion trypsique de $A\beta_{40}$ en fonction du temps. Ratio des aires entre le peptide trypsique de $A\beta_{40}$ oxydé et son equivalent non-oxydé (contrôle, t=0) en fonction du temps de réaction. (a) Décarboxylation et déamination de Asp1 ($DAEFR_{dd}$) et clivage oxydatif de Asp1 ($DAEFR_{ox}$); (b) oxydation de His13/His14 (HDSGYEVHHQK+16 et +32); (c) oxydation de Phe19/20 (LVFFAEDVGSNK+16); (d) oxydation de Met35 (GAIIGLMVGGVV+16).

Les acides aminés Asp1, His13 et His14 ont donc été identifiés comme les cibles préférentielles du radical hydroxyle. Ils sont tous trois connus pour être impliqués dans la sphère de coordination de Cu(II) et /ou Cu(I) à pH physiologique, comme le montre la figure 4.

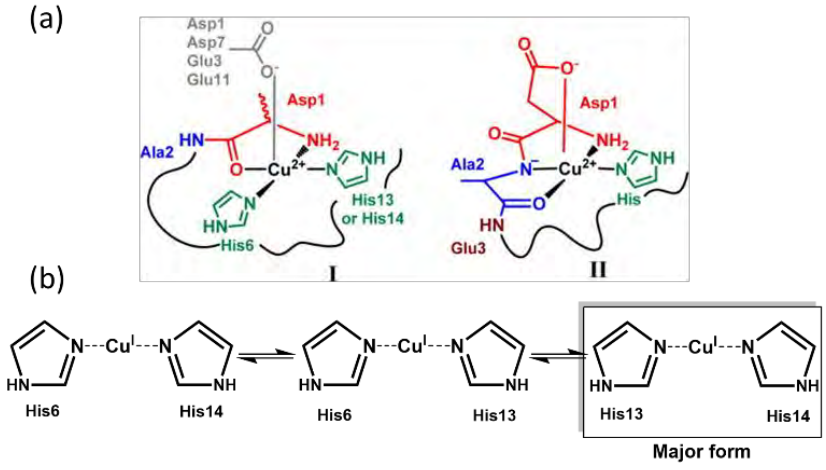

Figure 4 : Modes de coordination du peptide Aβ avec les ions Cu(II) (panel a) et Cu(I) (panel b) à pH physiologique.

Ces acides aminés étant coordinés au cuivre et donc proches du site de production des ROS, ils sont les premières cibles pour ceux-ci.

Les dommages oxydatifs subis par le peptide Aβ ayant mené à une importante modification chimique de la séquence (voir figure 2), les conséquences de l'oxydation du peptide Aβ sur les événements supposés liés à la maladie d'Alzheimer (production des espèces réactives de l'oxygène (ROS), coordination avec les ions métalliques Cu(I), Cu(II) et Zn(II) et processus d'agrégation) ont été étudiées dans le chapitre IV.

Le peptide a été oxydé en présence de Cu et d'ascorbate, menant à un mélange nommé Aβox, contenant 20 % de Aβ non-oxydé et 80 % de diverses espèces oxydées, dont les principales oxydations sont ciblées sur l'Asp1, les His13 et His14. Le mode de coordination de Aβox avec Cu(I) et Cu(II) a été étudié par comparaison avec deux peptides Aβ commerciaux modifiés dont le comportement vis-à-vis de la coordination du cuivre permet de mimer les oxydations sur les acides aminés de Aβox. Le peptide tronqué $A\beta_7$ ne contient qu'un seul résidu His, il est utilisé pour mimer la double oxydation sur les His13 et His14. Le peptide possédant une amine N-terminale acétylée (peptide nommé AcAβ) est quant à lui utilisé pour mimer l'oxydation sur Asp1, car l'ajout du groupement acétyle empêche la coordination du cuivre à l'amine terminale.

Le mode de coordination de Cu(I) avec Aβox a été étudié par absorption des rayons X (XANES) en comparant la signature du complexe Cu(I)-Aβox avec celles de Cu(I) lié au peptide non-oxydé Aβ ou lié au peptide tronqué $A\beta_7$ (Figure 5). Il a été trouvé que la signature de Cu(I)-Aβox est intermédiaire entre celles de Cu(I)-Aβ et de Cu(I)-$A\beta_7$. Une combinaison linéaire des signatures XANES a montré qu'environ 40 % de Cu(I) était coordiné à Aβox de la même manière que Cu(I)-$A\beta_7$, ce qui signifierait qu'environ 40 % des espèces oxydées ont subi des dommages sur deux résidus histidine.

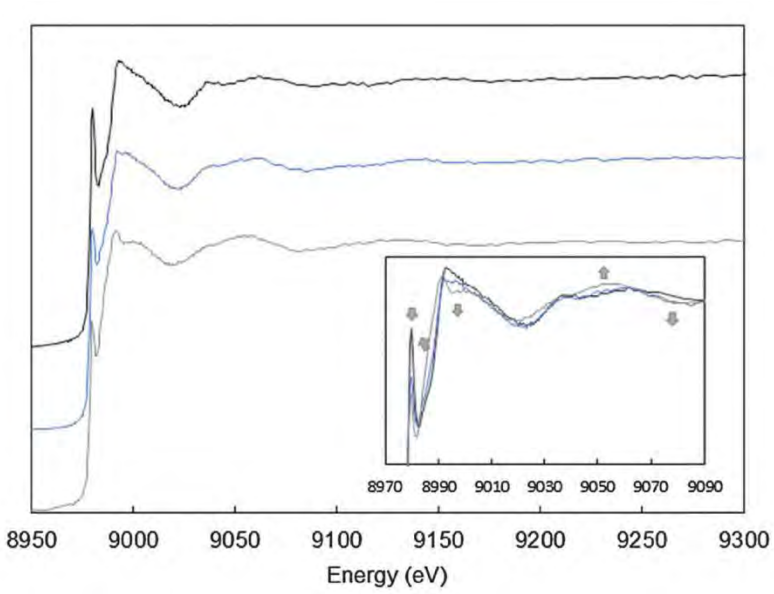

Figure 5 : Spectre XANES au seuil du Cu de Aβ-Cu(I) (courbe noire), Aβox-Cu(I) (courbe bleue) et Aβ7-Cu(I) (courbe grise). Les flèches indiquent l'évolution de la signature de Aβox-Cu(I) comparée à celle de Aβ-Cu(I).

La coordination de Aβox avec Cu(II) a été étudiée par résonance paramagnétique électronique (RPE) en comparant la signature RPE du complexe Cu(II)-Aβox avec celles des complexes Cu(II)-Aβ et Cu(II)-AcAβ (Figure 6).

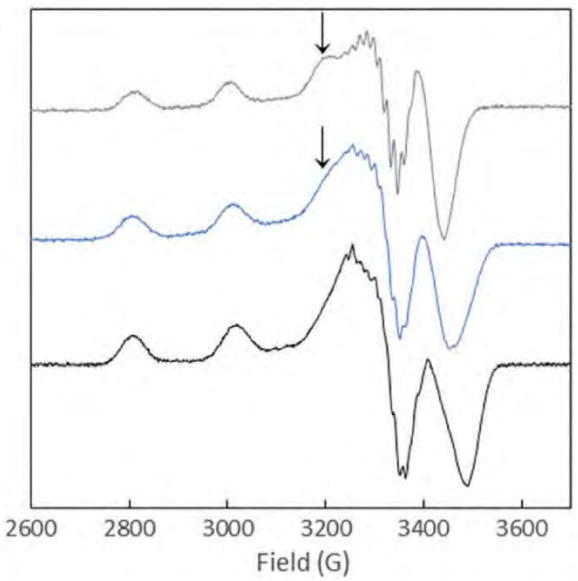

Figure 6 : Spectres RPE de Cu(II)-Aβox (courbe bleue), Cu(II)-Aβ (courbe noire) et Cu(II)-AcAβ (courbe grise) à pH 12,5.

De la même manière que pour Cu(I), il a été déduit grâce à une combinaison linéaire des spectres RPE qu'environ 40 % de Cu(II) est coordiné à Aβox de la même manière qu'AcAβ (pas de coordination de l'amine terminale). Il a pu être déduit qu'environ 40 % des espèces oxydées dans l'échantillon de Aβox ont subi des dommages oxydatifs sur Asp1. Par ailleurs,

nous avons montré que les deux modes de coordination de Cu(I) et de Cu(II) sont fortement impactés par l'oxydation du peptide Aβ, avec comme conséquence directe un probable changement quant à la production de ROS.

La production de ROS par le complexe Cu-Aβox a été étudiée en suivant (1) la consommation d'ascorbate en fonction du temps par spectroscopie UV-Visible, et (2) la production de l'acide 7-hydroxycoumarine-3-carboxylique (7-OH-CCA), un produit fluorescent issu de la réaction de l'acide coumarine-3-carboxylique (CCA) avec le radical hydroxyle, par spectroscopie de fluorescence. Le suivi cinétique de la fluorescence du 7-OH-CCA lors de la production de ROS donne une indication sur la vitesse et la quantité de $HO^{\bullet}$ piégés par le CCA, et donc sur la quantité de $HO^{\bullet}$ s'échappant du complexe Cu-Aβ et pouvant ainsi oxyder les molécules environnantes. Comme une partie des radicaux réagit avec Aβ, la cible la plus proche du site de production de $HO^{\bullet}$, on ne peut pas directement lier l'intensité de fluorescence à la quantité de $HO^{\bullet}$ générés par le système Cu-Aβ/ascorbate/O_2.

La comparaison des courbes de la consommation d'ascorbate par les complexes Cu-Aβ et Cu-Aβox a montré que le cuivre lié au peptide oxydé produit des ROS plus rapidement que celui lié au peptide non-oxydé. Le cuivre lié au peptide oxydé présente donc une activité catalytique plus importante.

Le suivi cinétique de la captation de $HO^{\bullet}$ par CCA a également montré que le complexe Cu-Aβox laisse échapper plus de radicaux que Cu-Aβ. En première approche, ce résultat peut être expliqué par le fait que le peptide est oxydé et qu'il y a donc moins de cibles potentielles sur Aβox pour les radicaux hydroxyles. Cela est en accord avec l'arrêt de l'oxydation de Asp1 et de His13 et His14 observé au cours de l'oxydation catalysée par le cuivre (voir figure 3). Il faut cependant prendre également en compte le changement de coordination de Aβox avec le cuivre.

Les études précédentes ont été réalisées avec Aβox, elles donnent des informations sur l'impact de l'oxydation de Aβ à la fin de la réaction. Afin de comprendre comment l'oxydation de Aβ impacte la libération de radicaux hydroxyles dans le milieu, la quantité de $HO^{\bullet}$ captés par le CCA (formant le 7-OH-CCA) a été étudiée à différentes étapes d'oxydation du peptide Aβ. Pour ce faire, ascorbate et peroxyde d'hydrogène ont été ajoutés en faible quantité 8 fois

consécutivement à une solution contenant le complexe Cu-peptide, en suivant pour chaque ajout la cinétique de formation du 7-OH-CCA.

Pour cette étude, plusieurs peptides modifiés ont été utilisés : les peptides AcAβ et $A\beta_7$, déjà utilisés dans les études précédentes, mais également le peptide mutant D7H qui a un résidu histidine supplémentaire dans sa séquence peptidique. La quantité de $HO^{\bullet}$ produits par Cu-$A\beta_7$ et piégés par le CCA reste constante quel que soit le nombre d'ajouts de réactifs (ascorbate et peroxyde d'hydrogène) et se rapproche de celle du cuivre libre. Pour Cu-Aβ, la quantité de $HO^{\bullet}$ piégés est presque 5 fois plus faible que pour Cu-$A\beta_7$, mais elle augmente brusquement au $4^{ème}$ ajout de réactifs. Un résultat similaire est observé pour Cu-AcAβ, et le même phénomène est visible pour Cu-D7H au bout du $5^{ème}$ ajout de réactifs.

Ce phénomène peut être lié à un changement de coordination du cuivre lorsque le peptide est suffisamment oxydé. Cette hypothèse est corroborée par l'augmentation de la quantité de $HO^{\bullet}$ piégés qui a lieu pour un ajout supplémentaire de réactifs avec D7H : ayant un résidu histidine en plus dans sa séquence, il a donc un ligand supplémentaire pour le cuivre et une cible de plus à oxyder. En doublant la concentration de Aβ par rapport à celle du cuivre, on n'observe plus de rupture dans l'augmentation de la quantité de $HO^{\bullet}$ piégés au cours des 8 ajouts d'ascorbate et de H_2O_2. Dans ces conditions, seule la moitié du peptide est coordinée au cuivre. Durant l'oxydation, lorsque le peptide est suffisamment oxydé pour induire un changement du mode de coordination, il est probable que le cuivre lié au peptide oxydé soit chélaté par un autre peptide non-oxydé présent dans le milieu, et garde donc le même comportement que Cu-Aβ quant à la production de ROS. Cela tend à montrer que l'affinité du cuivre pour le peptide oxydé est moindre que pour le peptide non-oxydé.

En replaçant cette étude dans un contexte plus biologique, l'oxydation du peptide Aβ en présence de cuivre et d'ascorbate induit un processus qui conduirait *in fine* à un stress oxydant plus délétère pour les molécules environnantes, en particulier à cause d'une augmentation de la vitesse de production des ROS et d'une quantité plus importante de radicaux $HO^{\bullet}$ libérés par le système (Figure 7).

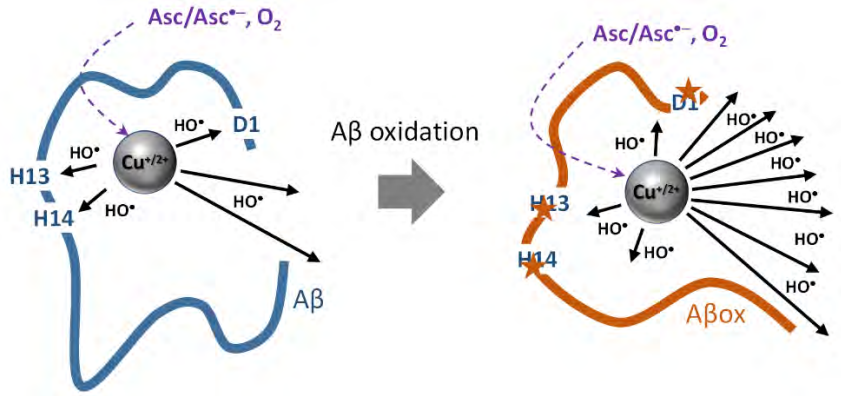

Figure 7 : Vue schématique de l'attaque oxydante du radical hydroxyle sur le peptide Aβ lors de la production d'espèces réactives de l'oxygène.

L'étude du mode de coordination du peptide Aβox avec l'ion Zn(II) a également été réalisée, en comparant les signatures XANES du complexe Zn-Aβox avec celles du Zn(II) coordinés aux peptides mutants mimant l'oxydation de Aβ. La signature XANES de Zn-Aβox diffère de celle de Zn-Aβ, montrant que l'oxydation de Aβ impacte également la coordination du zinc. Cependant, aucune information plus précise n'a pu être obtenue, les signatures XANES du Zn avec les différents peptides étant larges, elle ne permettent pas de faire des combinaisons linéaires pouvant reproduire précisément la signature de Zn-Aβox.

Les conséquences de l'oxydation de Aβ sur le processus d'agrégation du peptide ont été étudiées par spectroscopie de fluorescence ainsi que par microscopie électronique à transmission (TEM). Le peptide Aβ a la capacité de former des fibres amyloïdes composées de structures en feuillets β. Ce sont ces fibres amyloïdes qui constituent les plaques séniles, lésions caractéristiques de la maladie d'Alzheimer. La Thioflavine T (ThT), sonde fluorescente dont l'intensité de fluorescence est exaltée de manière spécifique au contact de structures en feuillets β telles que les fibres amyloïdes, est utilisée pour suivre la cinétique de formation des fibres.

Le processus d'agrégation a été suivi en fonction du temps, pour le peptide $A\beta_{40}$ et pour le peptide $A\beta_{40}$ oxydé. Le panel du haut de la figure 8 montre que, contrairement au peptide $A\beta_{40}$, le peptide oxydé ne forme pas de structures en feuillets β, aucune fluorescence n'étant détectée au cours du temps. Ces résultats sont confirmés par les images obtenues par microscopie (TEM) après le processus d'agrégation (Figure 8). En effet, pour $A\beta_{40}$, des agrégats de type fibrillaires sont observés alors que dans le cas de Aβ oxydé, on ne détecte pas de fibres, mais des agrégats de type amorphes.

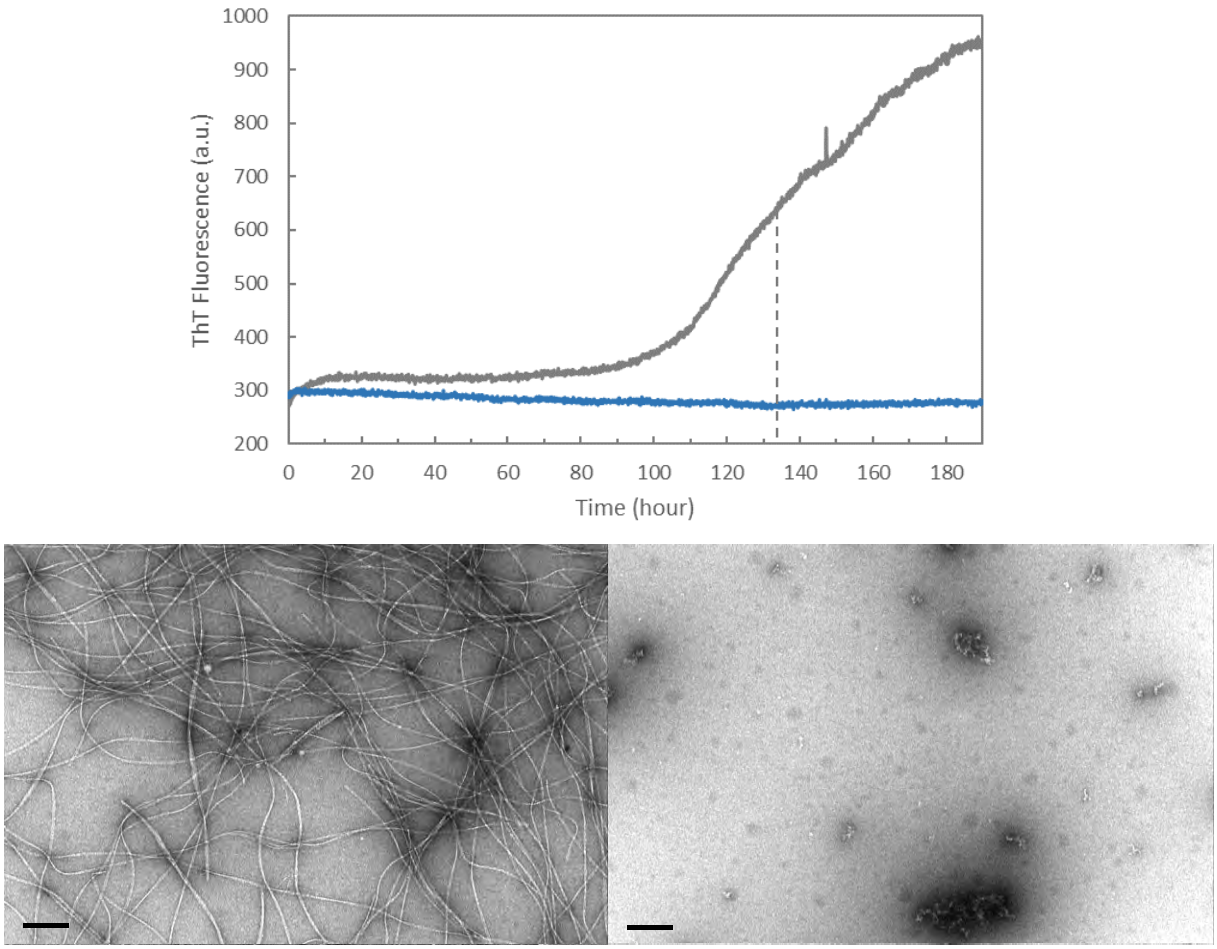

Figure 8 : (Panel du haut) formation des feuillets β pendant l'agrégation de Aβ$_{40}$ (courbe grise) et de Aβ$_{40}$ox (courbe bleue). Fluorescence de la ThT en fonction du temps. (Panel du bas) images par microscopie électronique à transmission (TEM) de Aβ$_{40}$ (à gauche) et Aβ$_{40}$ox (à droite) après 200 h d'incubation at 37°C.

Les résultats montrent donc que l'oxydation de Aβ a un impact important sur la morphologie des agrégats formés. Cependant, ces résultats sont préliminaires et des études plus approfondies devront être menées afin de pouvoir déterminer quelle(s) oxydation(s) impacte(nt) le processus d'agrégation.

Dans le chapitre V, nous nous sommes focalisé sur la réaction de production de ROS. Lors cette réaction, catalysée par le complexe Cu-Aβ, un état de coordination redox compétent et transitoire, appelé état « in-between » permet le transfert électronique menant à la production des ROS. Les géométries des modes de coordination des ions Cu(I) et Cu(II) avec le peptide Aβ étant très éloignées dans les états au repos, le passage par l'état « in-between » est nécessaire pour que le cuivre cycle entre ses états d'oxydation +1 et +2 (figure 9). Cet état « in-between » est caractérisé par des modes de coordination des ions Cu(I) et Cu(II) supposés plus proches

voire similaires, permettant le transfert électronique avec une énergie de réarrangement entre les deux modes de coordination bien plus faible que dans le cas des états au repos. Cet état fugace étant très peu peuplé (de l'ordre de 0,1 %), la caractérisation directe de son mode de coordination par les techniques spectroscopiques traditionnelles n'est pas possible.

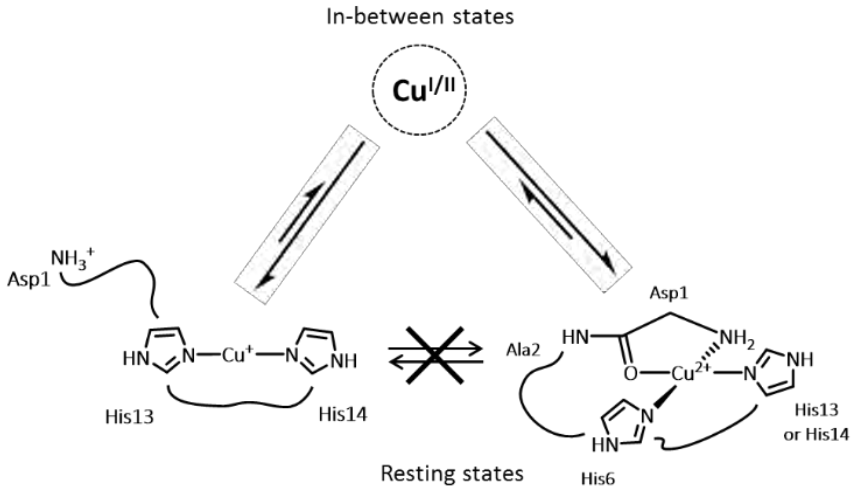

Figure 9 : Vue schématique de l'équilibre entre les états "resting" (au repos) et "in-between" du complexe Cu-Aβ pendant la production de ROS.

La détection des principales oxydations subies par le peptide Aβ durant la production de ROS par spectrométrie de masse (MS) a mené à la proposition de 3 principaux ligands du cuivre dans l'état « in-between ». L'aspartate situé en première position, et les histidines situées en position 13 et 14, qui sont impliqués dans la coordination de Cu(I) ou/et de Cu(II) au repos, sont les principaux acides aminés retrouvés oxydés après la production de ROS. Il est donc proposé que ces 3 acides aminés soient également les ligands du cuivre dans l'état « in-between » qui est responsable de la production de ROS. La figure 10 schématise les réarrangements entre les états au repos, appelés états « resting », et les états « in-between », ainsi que les transferts électroniques entre Cu(II)-Aβ et l'ascorbate et entre Cu(I)-Aβ et le peroxyde d'hydrogène.

Comme le cuivre a un mode de coordination avec le peptide Aβ impliquant des acides aminés spécifiques, la mutation de ces derniers entraîne un changement du mode de coordination. Les modes de coordination de Cu(I) et Cu(II) dans les états au repos ont été étudiés avec de nombreux mutants de Aβ.

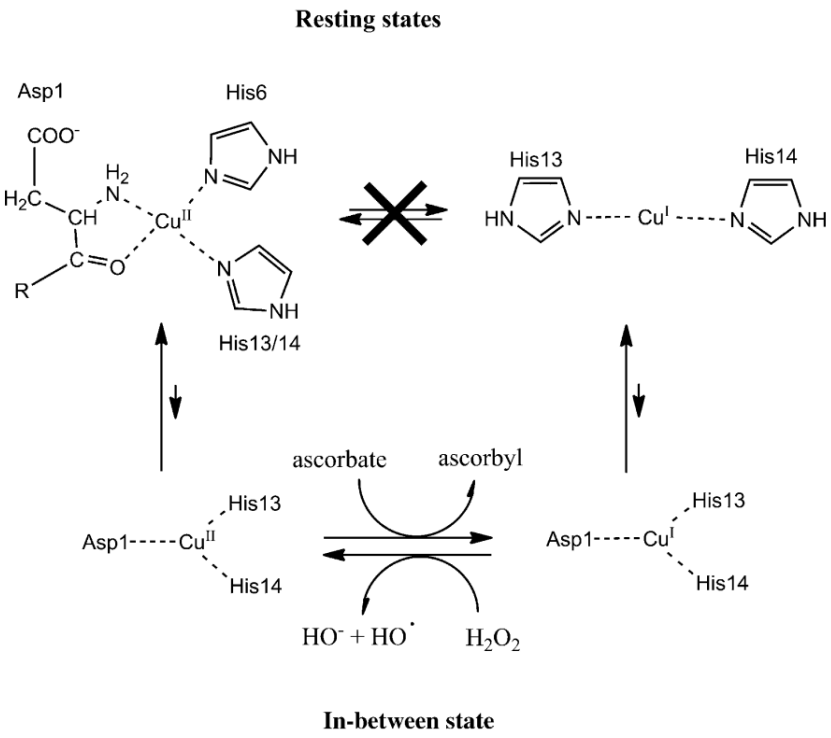

Figure 10 : Représentation schématique des modes de coordination de Cu(II)-Aβ et Cu(I)-Aβ au repos (resting states) et la proposition de mode de coordination de Cu(I/II)-Aβ dans l'état « in-between ».

Pour Cu(II), la non-disponibilité de l'amine terminale de l'Asp1 (*via* l'utilisation d'un peptide avec une acétylation de l'amine N-terminale) entraîne un profond changement de coordination. Pour Cu(I), la présence d'une seule histidine dans la séquence (*via* la mutation de deux histidines par des alanines) a également un impact sur le mode de coordination. De la même manière, la mutation d'un acide aminé impliqué dans la sphère de coordination du cuivre dans l'état « in-between » devrait induire une variation dans la production des ROS, puisque c'est cet état qui est responsable du transfert électronique.

La production de ROS par le cuivre avec les différents peptides modifiés a été suivie par la fluorescence de l'acide 7-hydroxycoumarine-3-carboxylique (7-OH-CCA), produit par le piégeage des radicaux hydroxyles ($HO^{\bullet}$) par l'acide coumarine-3-carboxylique (CCA). Le blocage de l'amine terminale ainsi que la mutation de l'Asp1 menant à un changement de la chaîne latérale contenant le groupe carboxylate de l'Asp1 ont fortement diminué la vitesse de production de $HO^{\bullet}$. Il a donc été déduit qu'à la fois l'amine terminale et l'oxygène du groupe carboxylate de l'Asp1 sont engagés dans la coordination du cuivre dans l'état « in-between ». Il a également été montré que le nombre d'histidines présents dans la séquence peptidique a un impact sur la vitesse de production des radicaux hydroxyles. Moins il y a d'histidines, plus les

HO• sont produits rapidement. Cet effet est accru lorsque la séquence peptidique ne contient qu'une seule histidine.

Le mode de coordination du Cu(I) avec les peptides ne possédant qu'une histidine, a été étudié par RMN du proton. Il a été montré que Cu(I) est coordiné par l'amine N-terminale de l'Asp1, le cycle imidazole de l'His et un groupe carboxylate. Toutes ces informations ont permis la proposition d'un mode de coordination unique des ions Cu(I) et Cu(II) avec le peptide Aβ dans l'état « in-between », responsable de la formation de ROS. L'ion métallique serait lié à l'amine N-terminale et au groupe carboxylate de l'Asp1, ainsi qu'à une histidine (voir figure 11). La séquence de Aβ comprenant 3 histidines, celles-ci sont supposées être en échange dynamique, comme cela est le cas dans les états au repos.

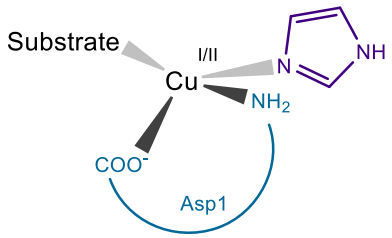

Figure 11 : Représentation schématique du mode de coordination proposé de Cu(I/II)-Aβ dans l'état « in-between » lors de la production de ROS en présence d'un substrat.

La modification de la chaine latérale de l'aspartate 1 et l'indisponibilité de l'amine N-terminale du peptide ont tous les deux menés à une forte diminution de la vitesse de production de HO•. De plus, une étude de la consommation d'ascorbate à plusieurs pH par les différents peptides modifiés en N-terminal a confirmé que les deux groupements de l'Asp1 sont bien impliqués dans la coordination du cuivre dans l'état transitoire qui conduit à la formation des ROS.

La forte augmentation de la vitesse de production des radicaux hydroxyles par le cuivre lié à un peptide n'ayant qu'une histidine (tel que $A\beta_7$) pouvait avoir deux origines : (i) la modification du mode de coordination du cuivre dans l'état « in-between », ce qui voudrait dire que deux histidines sont impliquées dans la sphère de coordination ou (ii) le changement de coordination de Cu(I) ou/et Cu(II) dans leurs états au repos, se rapprochant du mode de coordination de l'état « in-between », augmentant la vitesse de réarrangement entre les états au repos et « in-between ». Comme il a été montré que Cu(I) est coordiné aux peptides contenant 1 His par l'Asp1, et qu'il en est de même dans l'état « in-between », la seconde hypothèse a été

confirmée. Il a donc été proposé qu'une seule histidine participe à la coordination du cuivre dans l'état « in-between ». Pour les peptides contenant une seule His, les modes de coordination du Cu(I) au repos et pendant la production de ROS étant proches, l'état « in-between » est plus peuplé que dans le cas de Aβ, et donc la réaction menant à la formation de HO• est plus rapide.

Ces résultats, informatifs sur le mode de coordination de Cu-Aβ produisant les ROS dans l'état « in-between », ont également conduit à proposer un mécanisme pour le transfert d'électron menant à la formation de ROS. Ce mécanisme est illustré dans la figure 12 avec la réduction du dioxygène mais peut également être appliqué à la réduction de l'anion superoxyde ou du peroxyde d'hydrogène.

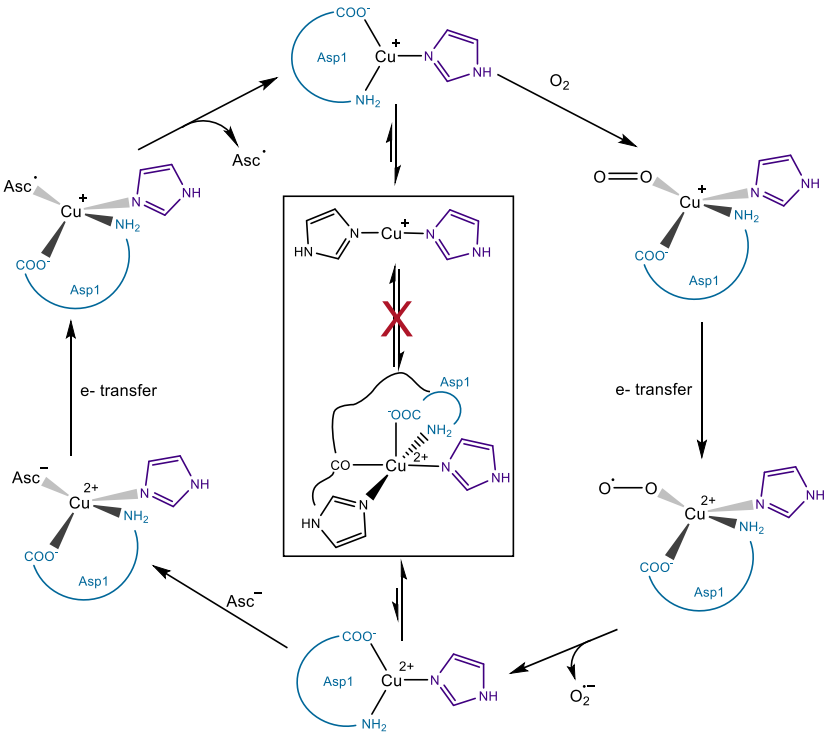

Figure 12 : Mécanisme proposé des transferts électroniques entre l'ascorbate (Asc-) et le complexe Cu(II)-Aβ et entre le dioxygène et le complexe Cu(I)-Aβ, réalisés par le passage vers des modes de coordination du complexe Cu-Aβ transitoires appelés états « in-between ». L'amine terminale et le groupe carboxylate de l'Asp1 sont indiqués en bleu et le motif imidazole de l'His impliquée dans l'état in-between est indiqué en violet. Asc• représente le radical ascorbyl.

Enfin, dans le chapitre VI, nous avons réalisé une étude sur les propriétés pro- et anti-oxydantes de l'ascorbate dans le contexte de la maladie d'Alzheimer. L'ascorbate est un réducteur présent en grande concentration dans le cerveau humain (jusqu'à 10 mM dans les neurones). Il est classé dans la catégorie des anti-oxydants puisqu'il a la capacité de réagir avec

certaines espèces oxydantes telles que les espèces réactives de l'oxygène (ROS), en particulier $O_2^{\bullet -}$ et $HO^{\bullet}$ (figure 13, voie verte), limitant ainsi de possibles dommages qui résulteraient de l'oxydation de biomolécules environnantes.

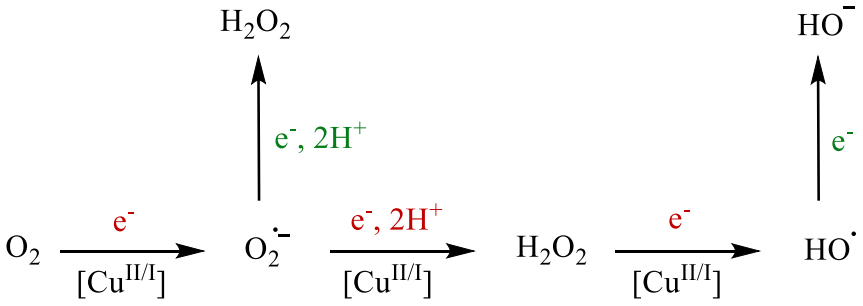

Figure 13 : Effets pro-oxydants de l'ascorbate menant à la production de ROS catalysée par le cuivre (voie rouge) et effets anti-oxydants de l'ascorbate menant à la formation d'espèces non radicalaires (voie verte).

Ses propriétés pro-oxydantes sont en revanche plus méconnues. L'ascorbate étant un excellent réducteur, il peut également participer à la formation des mêmes espèces réactives qu'il combat normalement grâce à ses propriétés anti-oxydantes (figure 13, voie rouge). C'est le cas en présence d'ions métalliques redox-actifs tels que les ions cuivre et fer, qui peuvent catalyser des réactions d'oxydo-réduction.

Comme nous l'avons vu précédemment (voir figure 1), les ions cuivre peuvent catalyser la production de l'anion superoxyde, du peroxyde d'hydrogène et du radical hydroxyle à partir du dioxygène, en présence d'un agent réducteur tel que l'ascorbate. La réaction directe d'oxydo-réduction entre l'ascorbate et le dioxygène n'est pas efficace mais le devient en présence d'un catalyseur tel que le cuivre. L'ascorbate réduit l'ion cuivrique en ion cuivreux, et ce dernier transfère à son tour un électron au dioxygène, formant ainsi l'anion superoxyde. Le cuivre est ensuite à nouveau réduit par l'ascorbate, ce qui entretient le cycle catalytique. Lorsque le cuivre est coordiné au peptide Aβ, il reste capable de cycler entre ses états d'oxydation Cu(II)-Aβ et Cu(I)-Aβ, le système catalysant ainsi la production de ROS. Dans ce cas, l'ascorbate peut donc être considéré comme ayant des propriétés pro-oxydantes.

Les effets pro- et anti-oxydants de l'ascorbate ont été étudiés par spectroscopie de fluorescence, en présence de cuivre libre ou du complexe Cu-Aβ et de dioxygène. L'acide coumarine-3-carboxylique (CCA, figure 14a) a été utilisé comme sonde pour la captation du radical hydroxyle. En effet, l'un des produits formés lors de l'oxydation du CCA par $HO^{\bullet}$ est

l'acide 7-hydroxycoumarine-3-carboxylique (7-OH-CCA, figure 14b), qui possède des propriétés de fluorescence. Le CCA a donc été utilisé comme mime des biomolécules environnantes susceptibles de subir l'attaque de $HO^{\bullet}$. Le pH a dû être contrôlé avec précision pendant l'étude : le pKa de déprotonation du 7-OH-CCA formé est très proche du pH de l'étude (pKa = 7.5) et seule la forme protonée est fluorescente.

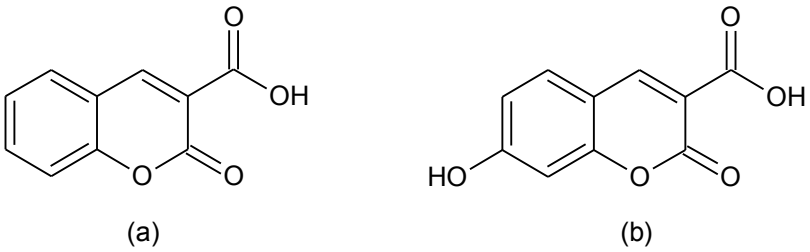

Figure 14 : Structures chimique de l'acide coumarine-3-carboxylique (nommé CCA, panel a) et l'acide 7-hydroxycoumarine-3-carboxylique (nommé 7-OH-CCA, panel b).

L'étude a été réalisée avec Cu et Cu-Aβ, en faisant varier la concentration d'ascorbate. La vitesse de formation du 7-OH-CCA (déduite de la pente initiale de fluorescence) et la quantité totale de 7-OH-CCA formés au cours de la réaction (déduite du plateau de fluorescence à la fin de réaction) ont été extraites des courbes de fluorescence et tracées respectivement en fonction de la concentration d'ascorbate. De ces données, il ressort qu'à faible concentration (inférieur ou égal à 0.7 mM), les propriétés pro-oxydantes de l'ascorbate prédominent : la vitesse initiale de réaction et la quantité de 7-OH-CCA formés augmentent avec la concentration d'ascorbate. Cependant, à plus haute concentration, la vitesse initiale de formation du 7-OH-CCA diminue avec l'augmentation de la concentration d'ascorbate, et la quantité totale de 7-OH-CCA augmente plus faiblement pour les grandes concentrations en ascorbate. Ces résultats mettent en évidence l'effet anti-oxydant de l'ascorbate, prédominant à haute concentration. Dans ces conditions, il participe toujours à la formation des ROS en réduisant le Cu(II), mais il peut également empêcher les radicaux hydroxyles formés d'oxyder le CCA (et donc les cibles biologiques) en réagissant avec. L'effet pro- *vs* anti-oxydant de l'ascorbate pour les molécules environnantes est donc dépendant de sa concentration.

En présence du peptide Aβ, les mêmes effets sont observés. Cependant, lorsque le cuivre est lié au peptide Aβ, la vitesse initiale de formation de 7-OH-CCA et la quantité totale de 7-OH-CCA formés sont plus faibles qu'avec le cuivre libre, à une concentration d'ascorbate donnée. Comme nous l'avons vu précédemment, le peptide Aβ est une cible pour les radicaux

hydroxyles formés. Une partie des HO• réagit donc avec Aβ au lieu du CCA, ce qui entraîne une diminution de la formation de 7-OH-CCA. Cette hypothèse a été corroborée par l'analyse de l'échantillon en fin de réaction par chromatographie liquide couplée à la spectrométrie de masse haute résolution (LC-HRMS), mettant en évidence l'oxydation du peptide lors de la réaction de production de ROS. La quantité de peptide non-oxydé restant dans l'échantillon diminue avec l'augmentation de la concentration en ascorbate et devient nulle à partir de 1 mM d'ascorbate.

Afin d'évaluer la capacité de l'ascorbate à inhiber l'oxydation du peptide Aβ par HO• à haute concentration comme c'est le cas pour le CCA, la dégradation du peptide a été évaluée après la consommation de 1 mM d'ascorbate, dans des échantillons contenant initialement 1 et 10 mM d'ascorbate. Même en présence de 10 mM d'ascorbate dans le milieu, le pourcentage de peptide non-oxydé retrouvé est quasiment nul. Ces résultats montrent donc que bien que l'ascorbate soit capable d'empêcher les dommages oxydatifs des molécules environnantes, mimées ici par le CCA, il n'a aucun effet sur l'oxydation du peptide Aβ lui-même. Comme le peptide est lié au cuivre lors de la production de ROS, il en est la cible la plus proche (notamment celle des radicaux hydroxyles). L'ajout d'ascorbate en grande quantité ne protège pas le peptide Aβ de l'oxydation. Tous ces résultats sont résumés dans la figure 15.

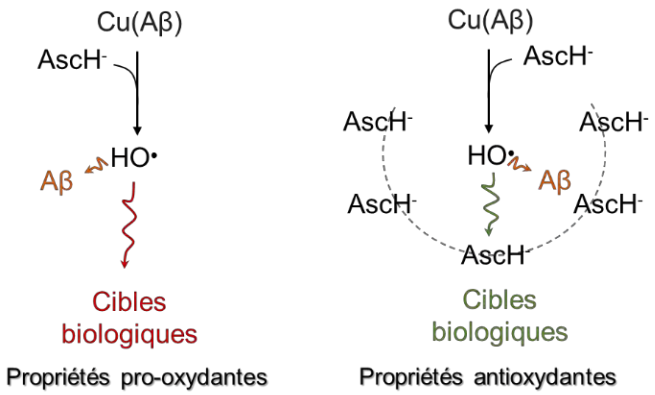

Figure 15 : Représentation schématique des effets pro- et anti-oxydants de l'ascorbate et conséquences sur les cibles biologiques environnantes et sur le peptide Aβ. $AscH^-$ est l'abréviation de l'ascorbate.

L'ascorbate a donc des propriétés anti-oxydantes à l'égard des cibles biologiques (mimées ici par le CCA) lorsqu'il est présent en grande concentration, mais il ne peut cependant inhiber l'oxydation de Aβ. De plus, bien que l'effet anti-oxydant de l'ascorbate soit visible dans cette étude, l'ajout en grande quantité d'ascorbate n'empêche pas totalement l'oxydation des molécules environnantes puisque le CCA piège toujours les $HO^{\bullet}$. On peut donc se demander s'il est possible d'atteindre une concentration en ascorbate pour laquelle l'effet anti-oxydant sera complet, c'est-à-dire pour laquelle aucun dommage oxydatif ne sera subi par les molécules environnantes. Plus globalement, cette étude tendrait à montrer que l'utilisation d'anti-oxydants sacrificiels (ascorbate ou autres piégeurs de radicaux) comme composés thérapeutiques n'est pas forcément la meilleure stratégie dans le contexte spécifique de la maladie d'Alzheimer.

En conclusion, les travaux présentés dans ce manuscrit englobent différents aspects autour de l'oxydation du peptide amyloïde-bêta (Aβ) lors de la production de ROS catalysées par les ions cuivre : (i) l'identification des résidus oxydés et les conséquences que peut entraîner cette oxydation quant à la coordination des ions métalliques, l'agrégation du peptide oxydé et la production de ROS par le peptide oxydé en présence de cuivre, (ii) la caractérisation du mode de coordination du complexe Cu-Aβ dans l'état transitoire, appelé état « in-between », responsable de la production de ROS et donc de l'oxydation de Aβ et (iii) les effets à la fois pro- et anti-oxydants de l'ascorbate envers les biomolécules et le peptide Aβ lors de la production de ROS catalysée par le cuivre.

L'étude du peptide après oxydation catalysée par le cuivre a permis d'identifier les principaux acides aminés oxydés : l'aspartate 1 ainsi que les histidines 13 et 14. Ces acides aminés étant impliqués dans les coordinations de Cu(I) et/ou Cu(II), il a été proposé qu'ils soient aussi engagés dans la coordination du cuivre pendant la production de ROS. Etant proches du site de production, cela expliquerait leur oxydation ciblée.

Des oxydations collatérales ont aussi été détectées sur les phénylalanines 19 et 20 et sur la méthionine 35. Ces acides aminés ne sont pas engagés dans la sphère de coordination des ions métalliques (partie N-terminale), mais sont très sensibles aux attaques du radical hydroxyle. Il a été proposé qu'ils soient ciblés par les ROS quittant le système Cu-Aβ, lorsque les premières cibles des radicaux (Asp1, His13 et His14) sont suffisamment endommagées. Ils sont donc plutôt les victimes d'une fuite lors de la production de $HO^{\bullet}$ par le système Aβ-Cu, les radicaux ciblant avant tout les ligands du cuivre.

Nous avons pu montrer que l'oxydation du peptide Aβ a entraîné un changement de coordination des deux ions métalliques Cu(I) et Cu(II) ainsi que de Zn(II). Lorsque le peptide est suffisamment oxydé, ce changement est à l'origine d'une production de ROS plus rapide et d'une quantité plus importante de HO• quittant le système Cu-Aβ. L'oxydation de Aβ peut donc être considéré comme un événement délétère pour le peptide lui-même, mais également pour les biomolécules environnantes pour lesquelles on observe une augmentation des oxydations.

Concernant l'influence de l'oxydation sur l'agrégation du peptide Aβ, les résultats préliminaires ont montré que le peptide oxydé a une faible tendance à agréger et à privilégier la formation de fibres. Cela marque une différence importante avec le peptide non-oxydé qui forme des fibres dans lesquelles il s'arrange en feuillets β. D'autres expériences sont en cours au laboratoire, elles visent à confirmer les premiers résultats obtenus et à mieux comprendre la manière dont le peptide oxydé se comporte en termes d'agrégation.

Par l'étude de la production de ROS catalysée par le cuivre en utilisant différents peptides Aβ modifiés, il a été possible de proposer une sphère de coordination du cuivre avec Aβ dans l'état transitoire « in-between », responsable de la production de ROS. Ainsi, une histidine, l'amine N-terminale et le groupe carboxylate de l'aspartate 1 seraient liés au cuivre dans l'état « in-between ». Le peptide Aβ non-modifié possédant 3 résidus histidine, il est probable qu'ils soient tous trois impliquées dans la sphère de coordination du cuivre en échange dynamique, comme c'est déjà le cas pour les complexes Cu(I)-Aβ et Cu(II)-Aβ dans les états dits « au repos ».

Enfin, les propriétés pro-oxydantes et anti-oxydantes de l'ascorbate ont été étudiées. Antioxydant bien connu du grand public (notamment sous le nom de Vitamine C), l'ascorbate présente un double visage puisqu'il participe également à la production de ROS en transférant un électron au centre métallique, qui peut à son tour réduire l'oxygène moléculaire ou les espèces intermédiaires que constituent les ROS. L'étude a permis de déterminer que son effet dépend de sa concentration. Quelle qu'elle soit, l'ascorbate participe à la production de ROS, mais à forte concentration, il réagit aussi avec les radicaux hydroxyles formés et joue son rôle d'antioxydant vis-à-vis des biomolécules environnantes. Cependant, il n'est pas efficace dans la protection du peptide Aβ. Même à forte concentration dans le milieu, le peptide n'est pas protégé contre les attaques du radical hydroxyle.

Ainsi, il ressort de cette étude que l'Aspartate 1 et les Histidines du peptide Aβ sont des acides aminés clés dans la production de ROS. Impliqués dans la coordination des ions Cu(I) et Cu(II) dans les états au repos, ils le sont également dans l'état transitoire, seul état redox activement impliqué dans la production de ROS. Ils sont les premiers ciblés et leur dégradation entraîne des changements importants quant à la coordination des métaux, l'agrégation et la production de ROS. L'ascorbate, même présent en grande concentration, ne peut faire bénéficier Aβ de ses propriétés antioxydantes. Le peptide Aβ, en se liant à un ion cuivre, participe donc à sa propre destruction en contribuant à la production des ROS qui l'endommagent irréversiblement.

L'intérêt de cette étude et des résultats qu'elle a permis d'obtenir réside dans une meilleure connaissance des mécanismes et conséquences de l'activité redox du système Cu-Aβ, à rapprocher du lien existant entre stress oxydant et maladie d'Alzheimer. Des perspectives directes peuvent être envisagées, à plus ou moins long terme. Une meilleure connaissance de l'état redox responsable de la production de ROS peut permettre le développement de stratégies thérapeutiques ciblées et efficaces, pouvant conduire à une réduction des dommages oxydatifs qui seraient en cause dans la neurodégénérescence liée à la maladie. D'autre part, et étant donné sa spécificité, l'oxydation du peptide Aβ peut représenter une piste intéressante dans la recherche de biomarqueurs pour le diagnostic précoce de la maladie d'Alzheimer. Il serait ainsi intéressant de pouvoir purifier le peptide Aβ à partir de matériel biologique (sérum, liquide céphalo-rachidien, …) pour étudier spécifiquement de possibles dégâts dus à l'oxydation. La production d'anticorps spécifiquement dirigés contre le peptide oxydé représenterait alors une avancée intéressante pour une telle étude. Enfin, une meilleure connaissance du système Cu-Aβ devrait permettre aussi de mieux comprendre le fonctionnement d'autres systèmes impliquant des peptides amyloïdogéniques mis en cause dans d'autres pathologies, tels que l'amyline, pour le diabète de type II, et l'alpha-synucléine, pour la maladie de Parkinson.

Résumé

La maladie d'Alzheimer (MA) est la forme la plus fréquente de démence chez les personnes âgées. L'une de ses caractéristiques est la formation extracellulaire de plaques séniles dans le cerveau des malades, composées du peptide Amyloïde-β (Aβ) sous forme agrégée et d'ions métalliques tels que le cuivre. Le peptide Aβ forme un complexe avec les ions cuivre, capable de catalyser la formation d'espèces réactives de l'oxygène (ERO), en présence d'un réducteur tel que l'ascorbate. Ces espèces oxydantes sont délétères pour les molécules environnantes, ainsi que pour le peptide Aβ lui-même. Etant proche du site de production des ERO, Aβ est une cible privilégiée, notamment pour le radical hydroxyle $HO^{\bullet}$. L'objectif de ce travail a été d'étudier la réaction de production des ERO par le système Aβ/Cu/ascorbate, de caractériser les dommages oxydatifs subis par Aβ et d'évaluer les conséquences de l'oxydation de Aβ sur la production des ERO, la coordination des ions métalliques et l'agrégation. Différentes techniques spectroscopiques ont été utilisées, notamment la spectrométrie de masse (MS), la spectroscopie de fluorescence, la résonnance paramagnétique électronique (RPE) et l'absorption de rayons X (XANES).

Les sites d'oxydation du peptide Aβ ont été étudiés par spectrométrie de masse (MS et MS/MS). Grâce à l'utilisation des outils de la protéomique et de la spectrométrie de masse à haute-résolution (HRMS), les acides aminés oxydés du peptide Aβ ont été identifiés. Ainsi, Asp1, His13 et His14 sont les cibles privilégiées de l'attaque de $HO^{\bullet}$. Ce résultat était attendu puisque ces résidus sont impliqués dans la coordination du cuivre, par l'intermédiaire duquel les ERO sont directement générées.

L'impact de l'oxydation du peptide sur la coordination des ions métalliques Cu(II), Cu(I) et Zn(II), la production de ERO ainsi que sur l'agrégation du peptide a été étudié. Les résultats ont montré que l'oxydation du peptide induit un changement de coordination du Zn(II) ainsi que des deux états d'oxydation du cuivre, menant à une augmentation de la production de ERO. De plus, l'oxydation de Aβ a également un impact sur l'agrégation, ne privilégiant pas la formation de fibrilles.

Le mode de coordination du complexe Cu-Aβ lors de la production des ERO a été déduit de l'étude d'une série de peptides Aβ comprenant un ou plusieurs acides aminés mutés. L'hypothèse proposant que les acides aminés oxydés sont ceux liés au cuivre lors de la production des ERO (Asp1, His13 et 14) a été renforcée, la mutation de Asp1 ou des deux His13 et 14 ayant un impact direct sur la production des ERO.

Enfin, les effets pro- et anti-oxydants de l'ascorbate ont été étudiés, montrant que, sur le système Cu-Aβ, l'ascorbate n'exerce ses propriétés anti-oxydantes qu'à forte concentration pour les molécules environnantes, mais qu'il n'a aucun effet protecteur sur le peptide Aβ lui-même.

Abstract

Alzheimer's Disease (AD) is the most frequent for of dementia in the elderly. A hallmark of AD is the extracellular formation of senile plaques in the brain of AD subjects, composed of the Amyloid-β peptide (Aβ) under aggregated form with metal ions such as copper ions. Aβ can form a complex with copper ions, able to catalyze reactive oxygen species (ROS) formation in the presence of a reducing agent such as ascorbate. These oxidative species can oxidize the surrounding molecules and the Aβ peptide itself. Being close to the production site of ROS, Aβ is the preferential target, especially for the hydroxyl radical $HO^{\bullet}$. The aim of this work was to study the ROS production by the Aβ/Cu/ascorbate system, to characterize the oxidation undergone by Aβ and to evaluate the consequences of Aβ oxidation on ROS production, metal ions coordination and aggregation. Several spectroscopic techniques have been used, in particular mass spectrometry (MS), fluorescence spectroscopy, electron paramagnetic resonance (EPR) and X-Ray absorption spectroscopy (XANES).

The oxidation sites of Aβ have been studied by mass spectrometry (MS and MS/MS). Thanks to the use of proteomic tools and high-resolution mass spectrometry (HRMS), the oxidized amino acid residues have been identified. Asp1, His 13 and His14 have been found to be the preferential targets for $HO^{\bullet}$ on Aβ. This result was expected as these residues are involved in copper coordination, from which the ROS are generated.

The impact of Aβ oxidation on Cu(II), Cu(I) and Zn(II) on metal ions coordination, on ROS production and on Aβ aggregation has been studied. Results have shown that Aβ oxidation induces a change of coordination of Zn(II) as well as Cu(II) and Cu(I), leading to an increase of ROS production. Moreover, Aβ oxidation has also an impact on aggregation, as it does not favor fibrils formation.

The Cu-Aβ binding mode during ROS production has been deduced from the study of a series of mutated Aβ peptides. The hypothesis, in which the amino acid residues bound to Cu during the ROS production are the oxidized one (Asp1, His 13 and His14) has been corroborated by the results of this study, the mutation of Asp1 or the two His having an impact on ROS production.

Finally, the pro- and antioxidants effects of ascorbate have been investigated, showing that, on the Cu-Aβ system, ascorbate only has antioxidant properties at high concentration for surrounding molecules, but does not exhibit any protecting effect on Aβ itself.